Structural Evolution of the Gold-rich Ashanti Belt, SW Ghana

Stephane Perrouty

▶ To cite this version:

HAL Id: tel-00772832
https://theses.hal.science/tel-00772832

Submitted on 11 Jan 2013

THÈSE

En vue de l'obtention du

DOCTORAT DE L'UNIVERSITÉ DE TOULOUSE

Délivré par *Université Toulouse III – Paul Sabatier*
Discipline ou spécialité : *Sciences de la Terre et des Planètes Solides*

Présentée et soutenue par Stéphane Perrouty

Le *Mardi 19 Juin 2012*

Titre : *Évolution Structurale de la Ceinture Minéralisée d'Ashanti, SO Ghana*

JURY

Pr. Jean-Luc Bouchez   (Président du Jury)
Pr. Campbell T. McCuaig   (Rapporteur)
Pr. Olivier Vanderhaeghe   (Rapporteur)
Dr. Guillaume Martelet   (Examinateur)
Dr. Mark W. Jessell   (Directeur de Thèse)
Dr. Laurent Aillères   (Directeur de Thèse)
Dr. Lenka Baratoux   (Directrice de Thèse)

Remerciements

Les travaux de thèse présentés au cours de cet ouvrage ne furent rendus possibles que grâce à la généreuse contribution de nombreux organismes et de personnes que je me devais de remercier en ces premières pages.

Abstract

The Paleoproterozoic Ashanti Belt hosts numerous world class gold deposits such as the Obuasi deposit (60 million ounces) and the Tarkwa deposit (40 million ounces). Characterising the regional structural and magmatic evolution provides new insight into the geotectonic context forming these deposits. In this work, we build a new geologic and structural map of the area using field observations and airborne geophysical data. This new map and series of geophysically constrained cross-sections allowed construction of a three-dimensional model of Birimian geology. The three-dimensional model highlights possible relationships between the location of deposits, metabasalt layers and major shear zones. Both structural and geochemical analyses have helped to clarify the geological evolution of the Ashanti belt during the Eburnean Orogeny.

The Eburnean Orogeny in southwest Ghana is separated by two broad phases of deformation and magmatism. The first, the Eoeburnean (2190 – 2140 Ma), formed strong isoclinal F1 folds that deformed the Sefwi Group metavolcanic rocks in the southeast of the Ashanti Belt. Simultaneously an early mineralisation event related to F1 folding occurred in the vicinity of Wassa mine. The Eoeburnean phase developed subduction-related calc-alkaline magmatism producing TTGs enriched in heavy rare earth elements. Kumasi group deposition (2150 – 2125 Ma) followed D2 extension, facilitating Kumasi and Akyem basin formation with regional structures such as the Ashanti Fault.

The second Eburnean phase (2130 – 2070 Ma) is characterised by Tarkwa Group sedimentation and paleoplacer formation at the beginning of D3 NW-SE shortening. D3 events formed major folds in the sedimentary basins of Kumasi, Akyem and Tarkwa. Regional scale sinistral shearing reactivated the Ashanti Fault during D4, resulting in a remobilisation and concentration of gold. F4 folds accommodating shearing induced displacement were formed at Obuasi and Wassa. Later deformation events (D5 – D6) do not significantly affect regional geological geometry. Several granite and granodiorite intrusions, depleted in heavy rare earth elements, were formed during D3 to D6 by partial melting of previously thickened lower crust.

Résumé de la thèse

La ceinture Paléoprotérozoïque d'Ashanti, au sud-ouest du Ghana, est l'hôte de nombreux gisements d'or, de classe mondiale, tels les gisements d'Obuasi (60 million d'onces) et de Tarkwa (40 millions d'onces). La caractérisation de l'évolution structurale et magmatique régionale permet d'éclaircir le contexte géotectonique de formation de ces gisements et ainsi fournir des pistes pour de futures explorations. Ainsi, au cours de ces travaux de thèse, a été réalisée une nouvelle carte géologique et structurale de la région, en accord avec les observations de terrains et les données de géophysique aéroportée. Cette carte et une série de coupes géologiques ont permis la construction d'un modèle tridimensionnel de la géologie Birimienne et la mise en évidence de possibles relations entre la localisation des minéralisations et la présence d'unités de métabasaltes à proximité des zones de cisaillement majeures. Les analyses structurales et géochimiques ont permis de clarifier l'évolution géologique de la ceinture d'Ashanti au cours de l'Orogénèse Éburnéenne.

L'Orogénèse Éburnéenne au sud-ouest du Ghana se divise en deux phases de déformation et de magmatisme. La première phase, Éoéburnéenne (2190 – 2140 Ma), développa un intense plissement isoclinal (D1) des roches à dominance métavolcanique du groupe de Sefwi, au sud-est de la ceinture d'Ashanti. Dans un même temps, une minéralisation précoce associée aux plis F1 apparut à la mine de Wassa. La phase Éoéburnéenne se caractérise également par un magmatisme calco-alcalin de zone de subduction avec la production de TTGs enrichis en terres rares lourdes. La sédimentation du groupe de Kumasi (2150 – 2125 Ma) est liée à une phase d'extension (D2) contrôlant la formation des bassins de Kumasi et d'Akyem par l'activation des failles majeures comme la Faille d'Ashanti.

La seconde phase, Éburnéenne (2130 – 2070 Ma), est marquée par la sédimentation du groupe de Tarkwa et des paléoplacers, associés au début d'un raccourcissement NW-SE (D3). Cette déformation forma les plis majeurs dans les bassins métasédimentaires de Kumasi, Akyem et Tarkwa. La déformation suivante (D4) développa des zones de cisaillement d'échelle régionale et réactiva la faille d'Ashanti en cisaillement sénestre, résultant en une remobilisation et une concentration des minéralisations en or. Des plis F4, accommodant la déformation, apparurent localement à Obuasi et à Wassa. Les déformations tardives (D5, D6) eurent peu d'impact sur la géométrie régionale. Pendant ces déformations (D3 à D6), d'abondantes intrusions de granites et granodiorites appauvris en terres rares lourdes se mirent en place, suite à la fusion de la base de la croûte, épaissie par l'orogénèse.

Sommaire

Introduction

Introduction

1.1 <u>Le Ghana</u>

Le Ghana, autrefois appelé Côte de l'Or, est un pays démocratique d'Afrique occidentale subéquatoriale d'environ 238000 km². Avec la totalité du territoire située à moins de 800 m d'altitude, sa topographie ne présente aucun relief majeur. La population approche les 25 millions d'habitants, principalement regroupés autour des principales agglomérations : Accra, la capitale, au sud-est du pays sur la côte Atlantique, Kumasi, au centre-ouest et Tamale, au nord (Fig. 1).

Le climat et la végétation sont très variables du nord au sud du pays. La partie sud du Ghana possède un climat de type subéquatorial marqué par deux saisons des pluies : de mars à juillet et de septembre à novembre. L'harmattan, vent d'origine subsaharienne, est omniprésent durant la saison sèche. L'humidité ambiante est élevée (toujours supérieure à 60 %) et les températures moyennes varient entre 25 et 30°C. Ces conditions climatiques favorisent l'altération des sols et la croissance d'une végétation abondante, de type équatorial.

Le Ghana exporte principalement quatre ressources majeures que sont le cacao, l'or, le bois et la bauxite. De récentes exploitations de pétrole dans le golfe de Guinée, ainsi que la production de diamants alluviaux, contribuent aussi à l'économie. À elle seule, l'industrie minière de l'or représente plus de 5 % du produit intérieur brut du Ghana, avec près de 80 tonnes produites par an (Bermúdez-Lugo, 2009). L'essentiel des gisements d'or se situe dans les terrains Paléoprotérozoïques du craton Ouest Africain, au sud-ouest du pays.

L'industrie de l'or ghanéen, l'une des plus anciennes au monde, a évolué pendant plus de 2500 ans. Durant plusieurs siècles, l'or du Ghana fut utilisé dans le cadre d'échanges commerciaux avec les peuples d'Afrique du Nord. L'essentiel de la production était alors réalisé selon des méthodes artisanales (Hilson, 2002), toujours utilisées de nos jours par certains orpailleurs. L'arrivée des Européens au 15e siècle contribua à l'expansion significative du marché de l'or en Afrique de l'Ouest et, en particulier, au Ghana, plaque tournante du commerce d'or et d'esclaves (Buah, 1998). Pour cela, de nombreux forts de défense et d'échanges furent construits sur la côte, dont celui d'Elmina, construit en 1482 par les portugais. Les arrivées des Hollandais à la fin du 16e et surtout des Anglais au 17e siècle développèrent la production minière, et un début d'industrialisation s'installa dès la fin du 19e siècle. Les principaux

gisements tels Tarkwa et Obuasi commencèrent alors à être exploités à grande échelle par les premières compagnies minières, motivant ainsi l'exploration géologique de la région d'Ashanti, au sud-ouest du pays. Une première cartographie des terrains du bassin de Tarkwa fut ainsi publiée dès 1904 par le service géologique de la Côte de l'Or (Whitelaw, 1904). Celle-ci fut affinée et étendue par la suite, en plusieurs étapes, pour aboutir à une cartographie complète du Ghana, révisée en 2009 par Agyei Duodu et al.
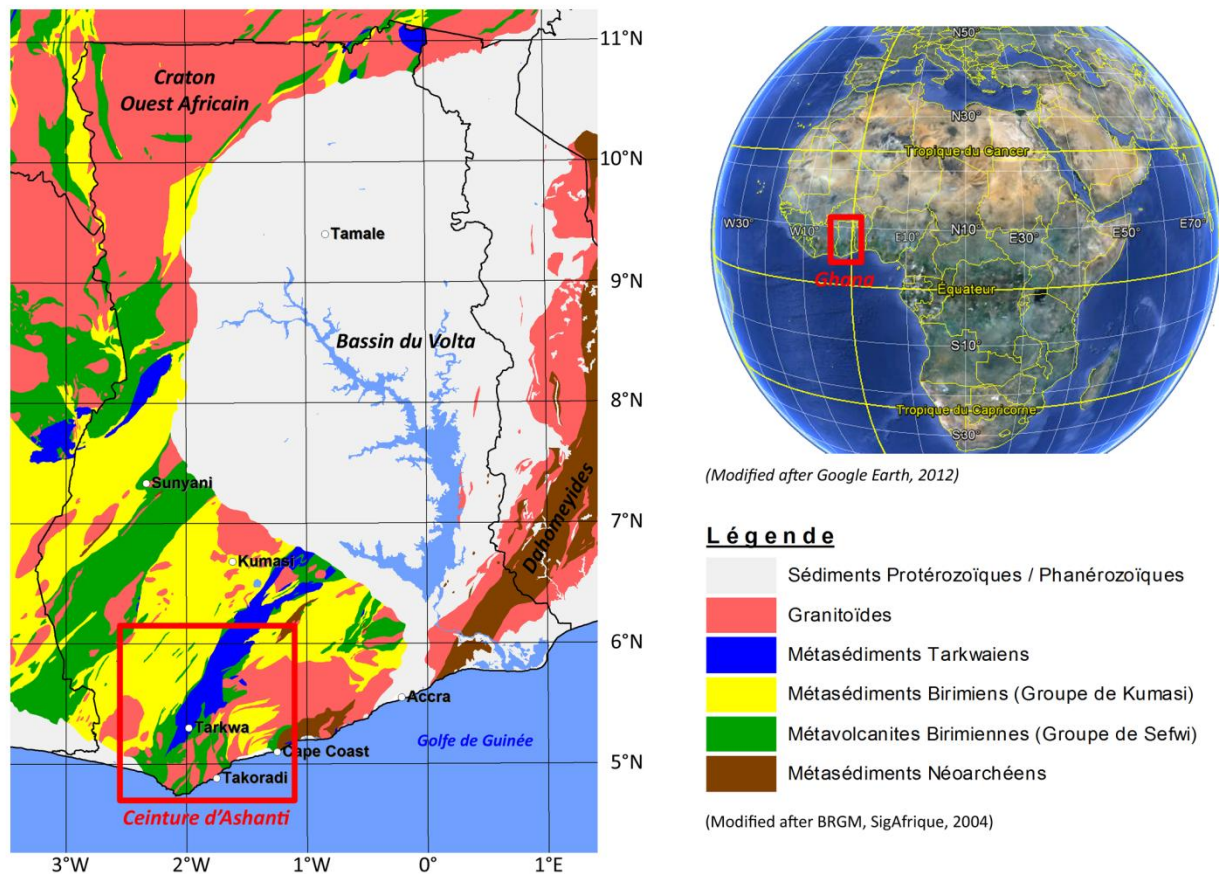
Figure 1   *Carte géologique simplifiée du Ghana (d'après BRGM, SigAfrique, 2004), avec la localisation de la zone d'étude (cadre rouge) ainsi que des principales agglomérations. Le fond de carte utilisé correspond au modèle numérique de terrain SRTM. L'image de droite est une projection de l'Afrique avec la localisation de la zone d'étude (d'après Google Earth, 2012).*

1.2 La géologie du Ghana

La géologie du Ghana se divise en trois ensembles principaux : la chaîne de suture Panafricaine au sud-est, le bassin du Volta dans sa partie nord-est, et le craton Ouest Africain pour le reste du territoire (Agyei Duodu et al., 2009). Ces trois ensembles témoignent de deux évènements tectoniques bien distincts dans l'évolution géologique ghanéenne et ouest-africaine

(Bonhomme, 1962) : L'Orogénèse Éburnéenne, d'âge Paléoprotérozoïque (2.1 Ga) et l'Orogénèse Panafricaine, d'âge Néoprotérozoïque (≈ 0.6 Ga).

1.2.1 *Le craton Ouest Africain*

Le craton LéoMan, formé de terrains Archéens et Paléoprotérozoïques, constitue la majeure partie de l'Afrique de l'Ouest. Il est limité au sud et à l'ouest par la marge Atlantique et par les bassins sédimentaires associés, au nord par la chaîne de l'Atlas et à l'est par la suture Panafricaine (Ennih et Liégeois, 2008). De nombreux bassins sédimentaires (Taoudeni, Volta) d'âges Néoprotérozoïques à Paléozoïques recouvrent certaines parties du craton sur plusieurs kilomètres d'épaisseur.

Ce craton est composé d'un noyau Archéen dans sa partie sud-ouest, contre lequel se juxtaposent des séries de ceintures de roches vertes Paléoprotérozoïques. Ces ceintures alternent avec des bassins formés de métasédiments, au Ghana, ou de granitoïdes, au Mali et au Burkina Faso (Metelka et al., 2011). Au sud-ouest du Ghana, quatre ceintures (Bui, Sefwi, Ashanti et Kibi-Winneba) sont séparées par trois bassins sédimentaires (Sunyani, Kumasi et Akyem, aussi appelé bassin de Cape Coast, Agyei Duodu et al., 2009). Ces ceintures de roches vertes et les bassins associés ont été formés puis déformés en relation avec l'Orogénèse Éburnéenne (Bonhomme, 1962).

En Amérique du Sud, le craton Guyanais est considéré comme un homologue du craton Ouest Africain, duquel il fut séparé par l'ouverture de l'océan Atlantique (Caen-Vachette, 1988). Cependant, des études récentes de paléomagnétisme suggèrent que ces deux cratons, assemblés autour de 2000 Ma, pourraient avoir vécu une histoire antérieure bien différente (Nomade et al., 2003). Le craton São Luís (Klein et al., 2005, 2008), au nord du Brésil, constitue un petit fragment de la partie sud ghanéenne du craton d'Afrique de l'Ouest. Il est principalement composé de granitoïdes d'âges et composition similaires à ceux du sud-ouest du Ghana.

1.2.2 *Le bassin du Volta*

Le bassin du Volta recouvre la partie ghanéenne du craton Ouest Africain et est bordé à l'est par la chaîne des Dahomeyides (Fig. 1). Il se compose d'environ 5 km de sédiments d'âge Néoprotérozoïque à Paléozoïque subdivisés en trois groupes (Kalsbeek et al., 2008) : le groupe de Kwahu-Morago (ou Bombouaka), avec des sédiments déposés entre 1000 et 950 Ma (Agyei Duodu et al., 2009), le groupe de Oti-Pendjari (635 Ma – 542 Ma) et le groupe d'Obosum, d'âge Cambrien (542 Ma - 488 Ma). La présence d'un important volume de zircons détritiques datés

entre 2200 et 2000 Ma indique qu'une majeure partie des sédiments du bassin de Volta dérive de l'érosion du craton Ouest Africain (Kalsbeek et al., 2008).

Selon Trompette (1994), les deux groupes sédimentaires basaux (Bombouaka et Oti) pourraient être interprétés comme des dépôts de marge passive reliés à l'ouverture d'un océan Panafricain. Sa fermeture aurait entrainé la formation de la chaîne des Dahomeyides et en conséquence, des dépôts de molasses syn-orogéniques du groupe d'Obosum.

1.2.3 *La suture Panafricaine*

La chaîne des Dahomeyides, au sud-est du Ghana, représente une partie de la zone de suture Panafricaine (Fig. 1). Cette chaîne, aussi appelée Trans-Saharienne ou Trans-Brésilienne, correspond à l'assemblage final du supercontinent Gondwana au Néoprotérozoïque (Trompette, 1980, 1994). Elle s'étend sur plus de 2000 km de long pour 100 km de large, marquant la limite orientale du craton Ouest Africain. Cette chaîne se compose d'une succession de nappes déplacées d'est en ouest lors de la collision entre le bloc Paléoprotérozoïque d'Afrique de l'Ouest et les assemblages protérozoïques du Togo, Benin et Nigéria (Attoh et al., 1997). Le métamorphisme et les intrusions associées à l'Orogénèse Panafricaine lui donnent des âges aux alentours de 600 Ma (Attoh et al., 2007).

1.3 La ceinture d'Ashanti

Parmi les ceintures de roches vertes du sud-ouest du Ghana, la ceinture d'Ashanti est l'une des plus remarquables pour la variété de ses lithologies, pour sa complexité structurale et pour son intérêt économique majeur dans la région. C'est en effet l'une des ceintures les plus riches en gisements métalliques, principalement d'or et de manganèse, en Afrique de l'Ouest. Les unités stratigraphiques « Birimien » et « Tarkwaien » regroupent l'essentiel des roches observées à l'échelle du craton Ouest Africain et forment également la ceinture d'Ashanti et ses bassins périphériques. Au cours de l'Orogénèse Éburnéenne, les déformations et les nombreuses intrusions de granitoïdes ont contribuées à la mise en place des structures et des minéralisations observées.

Figure 2   *Les lithologies du sud-ouest du Ghana : (a) métabasaltes Birimiens, groupe de Sefwi, (b) métavolcanosédiments Birimiens, groupe de Sefwi, (c) métaconglomérats Tarkwaiens, (d) quartzites Tarkwaiennes, avec une stratification entrecroisée marquée par des lits de magnétite, (e) phyllites Tarkwaiennes, (f) granitoïde Éburnéen, (g) dolérite (dyke), (h) sédiments phanérozoïques.*

Figure 3   *Altération de la surface : (a) couche organique de sol, (b) niveau B2, à pisolithes, (c) niveau B3, zone tachetée, (d) niveau B4, saprolite. L'épaisseur totale de ce profil d'altération approche 15 m.*

1.3.1 *Le Birimien*

Le Birimien se compose de roches métavolcaniques et métasédimentaires (Fig. 2). Une première description de cette unité stratigraphique majeure fut réalisée par Kitson (1918) dans la rivière Birim située à 80 km à l'est de la ceinture d'Ashanti. Les géologues du début du 20e siècle tels Kitson (1928), Whitelaw (1929) et Junner (1935, 1940) ont divisés le Birimien du Ghana en deux sous-groupes : un Birimien Supérieur formé par les métavolcanites et un Birimien Inférieur formé par les métasédiments. Leur stratigraphie fut ensuite conservée dans les études de Hastings (1982), Ntiamoah-Agyakwa (1979), Kesse (1985) et Milési et al. (1992). D'autres études ont pourtant souligné les incohérences de cette stratigraphie : Leube et al. (1990) et Eisenlohr (1992) ont suggéré que les roches métavolcaniques et métasédimentaires du Birimien pourraient avoir été synchrones. Finalement, ce débat fut interrompu par les premières datations absolues, suggérant des métasédiments plus jeunes que les métavolcanites (analyses Sm/Nd, Taylor et al., 1992). Cette nouvelle stratigraphie fut confirmée par des datations U/Pb sur zircons donnant des âges variant entre 2142 ± 24 Ma et 2266 ± 2 Ma pour les métavolcanites (U/Pb sur zircons, Adadey et al., 2009, Loh et al., 1999) et inférieurs à 2154 ± 2 Ma pour les métasédiments du bassin de Kumasi (U/Pb sur zircon détritiques, Oberthür et al., 1998). Récemment, Adadey et al. (2009) proposent une nouvelle stratigraphie du Birimien avec un groupe de Sefwi (2195-2170 Ma), composé de micaschistes et de métavolcanites et un groupe de Kumasi, déposé après 2150 Ma et formé par des métasédiments.

1.3.1.1 Le groupe de Sefwi

Selon Adadey et al. (2009), le groupe de Sefwi se compose principalement de métabasaltes, métaandésites, métagabbros et de micaschistes qui alternent avec des niveaux de phyllites et de métasédiments volcanoclastiques. Ce groupe occupe les parties sud et sud-est de la ceinture d'Ashanti et se prolonge probablement sous les sédiments du bassin de Tarkwa.

La carte géologique du Ghana (Agyei Duodu et al., 2009) indique trois ensembles majeurs de roches métavolcaniques qui affleurent le long de la côte, à Dixcove (plage de Butre), Cape Three Point et Axim. Selon Loh et al. (1999) les métabasaltes en coussins observés à Dixcove (à l'est) seraient à la base de la stratigraphie du groupe de Sefwi et par conséquent plus anciens que les métabasaltes et métaandésites d'Axim (à l'ouest). Une autre hypothèse, proposée par Sylvester et Attoh (1992) et réutilisée dans les études de Dampare et al. (2008) et Attoh et al. (2006), considère un groupe de Sefwi formé d'une unique série volcanique avec près de 3500 m de basaltes massifs recouvrant un socle de gabbros et de roches ultrabasiques.

L'étude géochimique, par Dampare et al (2008), des métabasaltes et métaandésites des secteurs de Cape Three Point et d'Axim ont mis en évidence deux types de métavolcanites, de composition et de sources différentes, évoluant d'est en ouest. Leurs basaltes de type I, échantillonnés dans la région de Cape Three Point, présentent une composition en majorité tholéiitique issue de la fusion d'un manteau appauvri, avec des caractéristiques géochimiques proches de celles des basaltes de dorsales océaniques. D'après Dampare et al. (2008), les métabasaltes et métaandésites du secteur d'Axim représenteraient un second type de métavolcanites (type II), de composition calco-alcaline, formées le long d'arcs volcaniques dans un contexte de subduction. La présence de rhyolites dans le secteur d'Axim, mentionnées par Loh et al. (1999), illustre toute une série de cristallisation fractionnée dans le secteur d'Axim allant des basaltes aux rhyolites.

Au nord-ouest de Cape Three Point, Loh et al. (1999) et Agyei Duodu et al. (2009) ont cartographié une bande de roches ultrabasiques (péridotite, pyroxénite, harzburgite et dunite). Selon Attoh et al. (2006), ces roches correspondraient à une série ophiolitique mise en place au tout début de l'histoire Éoéburnéenne. La présence de sédiments volcanoclastiques, de basaltes en coussins et de roches ultrabasiques indiquerait que le groupe de Sefwi pourrait consister en un fragment d'une croûte océanique ou d'un plateau océanique d'âge pré-Éoéburnéen (> 2190 Ma).

1.3.1.2 Le groupe de Kumasi

Les bassins d'Akyem et de Kumasi, situés de part et d'autre de la ceinture d'Ashanti, consistent en une alternance entre des niveaux de phyllites, de métasédiments volcanoclastiques et de rares lits d'andésites (Adadey et al., 2009). L'analyse géochimique des métasédiments du bassin d'Akyem (Birim Diamondfield, Asiedu et al., 2004) et du bassin de Kumasi (la région de Konongo, Asiedu et al., 2009) indique une concentration en éléments ferromagnésiens plus importante que la moyenne de la croûte Paléoprotérozoïque, ce qui suggère une source dominée par des roches basiques. Asiedu et al. (2004) proposent que les sédiments du groupe de Kumasi dérivent de l'altération d'un socle métavolcanique (groupe de Sefwi) et de granitoïdes.

1.3.2 *Le Tarkwaien*

Le groupe de Tarkwa (Kitson, 1928, Whitelaw, 1929, Junner, 1940) est une succession de quatre unités métasédimentaires (Fig. 2) : Le groupe de Kawere, à la base des sédiments Tarkwaien, est composé de conglomérats et de grès. Son épaisseur varie entre 250 m et 700 m. Il est recouvert par les 600 m de la formation de Banket consistant en des lits de conglomérats en alternance avec des grès. Ces derniers présentent une stratification entrecroisée marquée par de

fins niveaux de magnétite. Les conglomérats sont principalement composés de galets de quartz (> 90%) et de roches basiques Birimiennes (Hirdes et Nunoo, 1994). Ils hébergent le gisement d'or alluvial de Tarkwa. La série du Tarkwaien se continue par 400 m de phyllites (Tarkwa Phyllites) puis par les quartzites du groupe de Huni, entrecoupés de quelques niveaux de phyllites sur plus de 1300 m.

L'âge des dépôts sédimentaires du bassin de Tarkwa est peu connu. Les datations U/Pb et Pb/Pb, sur zircons détritiques, de Davis et al. (1994) et Hirdes et Nunoo (1994) indiquent un âge maximum de dépôt de 2132 ± 2,8 Ma pour le groupe de Kawere et de 2132,6 ± 3,4 Ma pour la formation de Banket. Cependant, ces âges sont contradictoires avec la présence de zircons détritiques plus jeunes identifiés dans l'étude de Pigois et al. (2003). La formation de sills de métagabbros / dolérites à 2102 ± 13 Ma (U/Pb sur zircon, Adadey et al., 2009) et des intrusions de granitoïdes à 2097 ± 2 Ma (U/Pb sur zircon, Oberthür et al., 1998) délimitent la fin de la sédimentation du groupe de Tarkwa. Bien qu'aucune analyse géochimique n'ait encore été publiée sur les sédiments du bassin de Tarkwa, il est généralement admis qu'ils dérivent de l'érosion des métavolcanites du groupe de Sefwi et des granitoïdes associés (Kesse, 1985).

1.3.3 *Les granitoïdes*

Tous les groupes précédemment décrits ont été pénétrés par des granitoïdes (Fig. 2) au cours de l'Orogénèse Éburnéenne. Ces intrusions se sont déroulées en deux phases au sud-ouest du Ghana : entre 2190 - 2150 Ma (phase Éoéburnéenne) et 2130 - 2000 Ma (phase Éburnéenne). Le craton São Luís, en Amérique du Sud, semble avoir une évolution magmatique similaire (Klein et al., 2005, 2008). La plupart des plutons correspond à des TTG (Tonalite, Trondhjemite, Granodiorite) bien que certaines intrusions soient très basiques, comme le gabbro de Mpohor, ou très acides, comme le granite d'Anibel. Mauer (1990) et Loh et al. (1999) ont classifié ces granitoïdes en deux catégories selon leur mise en place dans la ceinture métavolcanique d'Ashanti (G2 ou belt-type) ou dans les bassins sédimentaires environnants (G1 ou basin-type).

Les trois principales intrusions dans la partie sud de la ceinture sont les plutons de Prince's Town, Dixcove et de Sekondi (Ketan). Leurs datations U/Pb sur zircon donnent respectivement des âges à 2158,9 ± 3,6 Ma (Attoh et al., 2006), 2171 ± 2 Ma (Hirdes et al., 1992) et 2174 ± 2 Ma (Oberthür et al., 1998) pour ces trois plutons. De type-I, leur composition est relativement basique (tonalites). Dampare et al. (2008), proposent qu'une fusion partielle de métabasaltes dans un contexte d'arc volcanique est à la source de ces granitoïdes. Au contraire, pour Mauer (1990), ils proviennent de la fusion partielle du manteau.

Les granitoïdes de type bassin affleurent principalement dans les bassins d'Akyem et de Kumasi. Ils ont une composition de granodiorite et granite, souvent riches en feldspath potassique pour les plus jeunes intrusions. Leurs caractéristiques de type-S (Loh et al., 1999) indiquent une formation in situ par fusion partielle des métasédiments ou une contamination lors de la mise en place (Mauer, 1990). Les âges des granitoïdes des bassins s'échelonnent de 2136 ± 19 Ma (âge U/Pb sur zircon, Adadey et al., 2009) à 1973 ± 75 Ma (âge Pb/Pb sur roche totale, Taylor et al., 1992).

1.3.4 *Les dykes de dolérite*

De nombreux dykes de dolérite (Fig. 2) parcourent le Craton Ouest Africain sur plusieurs centaines de kilomètres pour moins de 200 m d'épaisseur. Ils recoupent l'ensemble de structures et lithologies Éburnéennes. Ces dykes sont clairement visibles sur les cartes magnétiques ainsi que sur la nouvelle carte du Ghana (Agyei Duodu et al., 2009). Deux principales familles, orientées N-S et ENE-OSO existent au sud-ouest du Ghana. Plus au nord, les dykes sont recouverts par le bassin du Volta, ce qui indique un âge de mise en place avant 950 Ma (Kalsbeek et al., 2008).

Des sills et dykes de dolérite (ou métagabbros) datés à 2102 ± 13 Ma (U/Pb sur zircon, Adadey et al., 2009) dans le bassin de Tarkwa furent déformés lors de la phase Éburnéenne et, de ce fait, ne présentent aucun lien avec les dykes d'échelle régionale.

1.3.5 *Les sédiments Phanérozoïques* :

Les terrains consolidés les plus récents au sud de la ceinture d'Ashanti correspondent à des grès et marnes phanérozoïques (Fig. 2). Ceux-ci affleurent le long de la côte du golfe de Guinée, principalement entre Cape Coast et Takoradi, mais aussi à l'ouest d'Axim. Loh et al. (1999) ont référencé deux groupes principaux avec des âges qui s'étendent du Dévonien au Carbonifère (416 Ma à 299 Ma, Crow, 1952, Mensah, 1973, Chaloner et al., 1974, Baer and Riegel, 1980) et au Crétacé (145 Ma à 65 Ma, Tevendale, 1950).

1.3.6 *Les latérites*

Au sud-ouest du Ghana, le terme « latérite » désigne la couche d'altération météorique séparant le sol du saprolite et de la roche fraîche (Fig. 3). Les conditions climatiques chaudes et humides favorisent sa formation (Bourman, 1993). Les latérites se composent de plusieurs niveaux correspondant à des degrés d'altération différents pour une épaisseur totale variant entre 5 et 15 m environ selon les situations. Le premier niveau, d'une épaisseur d'environ 0,5 m,

correspond à la couche organique du sol (Hong et al., 2009). Le second niveau, aussi appelé B2, est caractérisé par la présence de nodules de fer (pisolithes) dans une matrice argileuse, sur une épaisseur de l'ordre de 1,5 m. Le niveau suivant, B3, correspond à la zone tachetée (3 m). Enfin, le B4, appelé saprolite correspond à la partie la moins altérée de la latérite. Son épaisseur est difficile à estimer en raison d'une transition progressive jusqu'à la roche fraîche.

Les latérites sont un réel problème sur le terrain. Elles sont omniprésentes au sud-ouest du Ghana, excepté au fond de certains cours d'eau, sur la côte et, bien sûr, dans les sites miniers. L'épaisseur de latérite reste relativement constante, au contraire de celle du saprolite qui varie fortement en fonction de la lithologie concernée. Ainsi, les affleurements de granitoïde sont plus fréquents que ceux de métasédiment et de métavolcanite. La lithologie initiale, de même que les structurales principales (S0, S1), commencent à être identifiables à partir du B2, tandis que les structures secondaires ne sont visibles que dans les parties les moins altérées du saprolite.

1.3.7 *L'évolution géotectonique*

Plusieurs auteurs comme Allibone et al. (2002a), Feybesse et al. (2006) ou De Kock et al. (2011) suggèrent une évolution tectonique en deux phases. La première (Éoéburnéenne, 2190 - 2150 Ma) développe un volcanisme et un magmatisme associés à la formation du groupe de Sefwi. Elle se termine par l'ouverture du bassin de Kumasi. Pour ces auteurs, la seconde phase (Orogénèse Éburnéenne, 2125 Ma - 1980 Ma) correspond à une tectonique transpressive senestre dans un contexte de raccourcissement NO-SE (Feybesse et al., 2006). Les déformations associées affectent à la fois les groupes Birimien et Tarkwaien avec le développement de plis ouverts à isoclinaux et de failles subverticales. Ces failles, notamment la faille d'Ashanti, subirent ensuite un mouvement cisaillant sénestre, contemporain du développement d'une nouvelle génération de plis et d'abondantes minéralisations en or (Allibone et al., 2002a). L'Orogénèse Éburnéenne se termine par les déformations tardives observées dans la région de Damang (Tunks et al., 2004).

1.3.8 *Le métamorphisme*

Les groupes stratigraphiques Birimien et Tarkwaien sont affectés par un métamorphisme régional dont l'intensité ne dépasse pas le faciès des schistes verts. Les études sur assemblage amphibole / plagioclase suggèrent des conditions maximales de température et de pression autour de 500-650°C, 5-6 kbar (John et al. 1999) et 520°C, 5,4 kbar (Schmidt Mumm et al., 1997). Ce maximum métamorphique est estimé à 2092 ± 3 Ma (U/Pb sur titanite métamorphique, Oberthür et al., 1998).

La présence de grenats dans la mine de manganèse de Nsuta (Nyame et al., 1998, Kleinschrot et al., 1993, 1994), de grenat et de staurotide autour de la mine d'or de Damang (Pigois et al., 2003), suggèrent des conditions environnementales similaires pour leur formation, bien que les grenats riches en manganèse puissent être stables à de plus basses pressions et températures (Mahar et al., 2004).

1.3.9 *Les minéralisations en or*

La ceinture d'Ashanti, au sud-ouest du Ghana, est réputée pour son intérêt économique majeur en Afrique de l'Ouest. De nombreuses mines d'or d'échelle mondiale parsèment la région, avec notamment, les gisements géants d'Obuasi (hydrothermal, 60 millions d'onces) et de Tarkwa (placer, 40 millions d'onces).

1.3.9.1 Les gisements Birimiens

Les minéralisations portées par les lithologies Birimiennes sont d'origine hydrothermale. La plupart des gisements sont localisés le long de la faille d'Ashanti et des autres zones de cisaillement majeures ou le long du contact entre le socle Birimien et le bassin de Tarkwa.

Oberthür et al. (1994, 1997), Blenkinsop et al. (1994) et Allibone et al. (2002a) montrèrent que les minéralisations principales dans la mine d'Obuasi sont associées à la réactivation en cisaillement senestre (D4) de la faille d'Ashanti. Ces cisaillements sont contemporains de l'altération en carbonates des basaltes et des phyllites graphitiques présents le long de la faille d'Ashanti (Mumin and Fleet, 1995). Ceci s'applique également aux mines de Bogoso et Prestea où Mumin et al. (1994) observent que la minéralisation en or résulte d'une remobilisation de particules d'or antérieures. De nombreux sulfures, notamment de l'arsénopyrite, sont associés aux minéralisations Birimiennes de la ceinture d'Ashanti (Milési et al., 1991).

1.3.9.2 Les gisements Tarkwaien

Deux styles de minéralisations en or affectent le groupe de Tarkwa, représentés par les gisements de types Damang et Tarkwa. Le gisement de Damang résulte de minéralisations hydrothermales localisées le long du contact entre les métasédiments Tarkwaien et le socle Birimien. L'or y est associé à de la pyrite formée à proximité des fractures ou incluses dans des veines de quartz correspondant aux dernières phases de déformation de l'Orogénèse Éburnéenne (Tunks et al. 2004). Un âge de 2063 ± 9 Ma fut obtenu par datations U/Pb sur xénotimes hydrothermaux (Pigois et al., 2003).

Le gisement d'or de Tarkwa est localisé dans la formation de Banket et consiste en des dépôts alluviaux (placers). Les particules d'or sont associées aux niveaux conglomératiques riches en hématite, au fond de paléo-chenaux. La présence de galets ainsi que les concentrations variables d'or suivant la stratigraphie illustrent l'origine sédimentaire de ce gisement (Sestini 1973).

1.4 Problématiques

Bien que la ceinture d'Ashanti fût grandement étudiée au cours du 20ᵉ siècle comme en témoignent les nombreuses études précédemment citées, de nombreuses interrogations persistent. Les études menées le long de cette thèse auront pour objectif principal d'éclaircir certains de ces points et ainsi contribuer à une compréhension plus globale de l'évolution Paléoprotérozoïque du sud-ouest du Ghana, et, dans une moindre mesure de celle du craton Ouest Africain.

1.4.1 *Les déformations antérieures au bassin de Kumasi*

Allibone et al. (2002a) et Feybesse et al. (2006) proposent un évènement de magmatisme et métamorphisme précédant la sédimentation dans les bassins de Kumasi et de Tarkwa, mais restent vagues sur son contexte tectonique et sur les déformations qui lui sont associées. Pourtant, la compréhension de la situation géologique Éoéburnéenne est fondamentale pour l'interprétation géotectonique des structures observées dans les différentes mines et leurs corrélations régionales. Ainsi, l'origine de plusieurs failles secondaires actives lors de la phase Éburnéenne, comme celles décrites par Allibone et al. (2002a) à la mine d'Obuasi, pourrait être liée à la géométrie antérieure du socle Birimien, formée par le groupe de Sefwi.

1.4.2 *Le contexte de formation du bassin de Tarkwa*

Le bassin de Tarkwa recouvre les métavolcanites du groupe de Sefwi tout le long de la ceinture d'Ashanti. Son âge et le contexte de sa formation ne sont pas complètement identifiés. En accord avec les études précédentes de Davis et al. (1994) et Hirdes et Nunoo (1994), Pigois et al. (2003) proposent un âge maximal de 2133 Ma ± 4 Ma (U/Pb) alors qu'un tiers de leurs zircons détritiques sont plus jeunes. De même, l'âge minimal, déterminé par une possible intrusion de granitoïdes à 2097 ± 2 Ma (U/Pb sur zircon, Oberthür et al., 1998) reste incertain en l'absence d'observations claires du contact entre les métasédiments Tarkwaien et cette intrusion.

Allibone et al. (2002a) ont suggéré que la sédimentation du bassin de Tarkwa s'était produite avant les déformations Éburnéennes majeures et, en conséquence, avant les

minéralisations d'Obuasi. À l'opposé, Leube et al. (1990) proposent que l'essentiel des déformations Birimiennes et des minéralisations en or soient antérieures au bassin de Tarkwa. Pour eux, les plis observés dans les métasédiments Tarkwaiens correspondent à de la déformation gravitaire tardive. Pour Ledru et al. (1994), le bassin de Tarkwa se développa en réponse à la déformation qui eu lieu pendant les étapes finales de l'Orogénèse Éburnéenne. L'hypothèse d'une formation du groupe de Tarkwa au début du raccourcissement fut émise par Feybesse et al. (2006) et Adadey et al. (2009). Ces derniers montrèrent qu'une première déformation affecta le groupe de Kumasi avant la formation du groupe de Tarkwa. Ces deux bassins sédimentaires ont ensuite été affectés conjointement par la majeure partie des déformations Éburnéennes.

1.4.3 *La source de l'or alluvial du groupe de Tarkwa*

Le bassin de Tarkwa est l'hôte de plusieurs gisements d'or alluvial. Avant les premières estimations de l'âge des métasédiments Tarkwaiens, l'or contenu dans ces gisements était considéré comme étant dérivé des dépôts hydrothermaux Birimiens tels que ceux localisés le long de la faille d'Ashanti (Kesse, 1985). Cela semblait en accord avec les analyses d'inclusions fluides dans les galets de quartz des unités conglomératiques, suggérant des conditions d'homogénéisation similaires à celles des veines de quartz observées dans les gisements hydrothermaux de la faille d'Ashanti (Klemd et al., 1993). Toutefois, quelques auteurs comme Milési et al. (1991) observèrent quelques contradictions comme, par exemple, l'absence de trace d'arsénopyrite associée à l'or dans les conglomérats Tarkwaiens, alors que celle-ci est pourtant observée en abondance dans les gisements Birimiens de Prestea, Bogoso et Obuasi.

Les études structurales récentes (Milési et al., 1992, Allibone et al., 2002a, 2002b) montrent clairement que les gisements d'or de la faille d'Ashanti sont postérieurs à la formation du bassin de Tarkwa. En conséquence, l'or alluvial ne peut en aucun cas provenir de ces gisements. Ceci suggère un évènement de minéralisation plus ancien, non-référencé, peut-être contemporain du magmatisme Éoéburnéen et des possibles déformations associées.

1.4.4 *L'évolution du magmatisme*

Les granitoïdes du sud-ouest du Ghana furent classés par Mauer (1990) et Loh et al (1999) en deux groupes suivant leur localisation dans la ceinture métavolcanique ou dans les bassins métasédimentaires. Cependant, cette classification ne prend pas en compte les âges de ces granitoïdes, qui indiquent deux séquences de magmatisme séparées par plusieurs dizaines de millions d'années : Éoéburnéen et Éburnéen (De Kock et al., 2011). Les études de Klein et al.

(2005, 2008) sur le craton São Luís, au nord du Brésil, semblent pourtant mettre en évidence un changement de la composition en éléments traces entre les granitoïdes de ces deux phases. La faible superficie couverte par ce petit fragment du craton d'Afrique de l'Ouest limite toutefois les interprétations.

Au Ghana, bien que de nombreuses analyses géochimiques des granitoïdes aient été conduites (John et al., 1999, Yao et Robb, 2000, Dampare et al., 2005, Adadey et al., 2009), les sources et l'évolution du magmatisme restent peu interprétées. Pourtant, les phases de magmatisme pourraient avoir joué un rôle non négligeable dans la genèse et le transport des fluides minéralisateurs, deux des paramètres clés pour la formation d'un gisement.

1.5 <u>Structure de la thèse</u>

Les études précédentes menées sur la ceinture d'Ashanti soulèvent quatre interrogations majeures pour la compréhension de l'évolution Éburnéenne de la ceinture d'Ashanti et la formation des abondants gisements d'or. Pour répondre à ces questions, nous commencerons par la révision de la carte régionale du sud de la ceinture d'Ashanti et réinterprèterons l'évolution géotectonique de la région, via l'analyse de nouvelles données de terrains et des levés de géophysique aéroportée. Cette première étude mettra en évidence une phase de déformation précoce, n'affectant que le groupe de Sefwi, et caractérisée par des plis isoclinaux d'échelle kilométrique au sud-est de la ceinture d'Ashanti, formés sous l'effet d'un raccourcissement N-S. Nous réinterprèterons également les âges U/Pb de Pigois et al. (2003) pour préciser l'âge des sédiments Tarkwaiens et discuter leur contexte tectonique.

Dans un second temps, nous nous intéresserons plus particulièrement à la mine de Wassa, située en terrains Birimiens et dont les minéralisations seraient très précoces par rapport aux déformations principales, selon les géologues de la compagnie minière Golden Star exploitant le site (Bourassa, 2003). Ce travail fournira une première carte et analyse structurale du secteur de Wassa et montrera que l'or contenu dans ce gisement a effectivement une origine plus ancienne que tous les autres gisements connus en terrains Birimiens. Cette étude démontrera donc l'existence de gisements d'or formés avant les métasédiments du bassin de Tarkwa, possibles sources de l'or des gisements alluviaux.

Dans une troisième partie, nous interprèterons les résultats d'analyses géochimiques des granitoïdes, dans le but de mieux cerner les processus magmatiques ayant cours durant les phases Éoéburnéenne et Éburnéenne. Ces analyses seront complétées par des datations U/Pb sur zircon

et permettront de discriminer deux tendances de compositions, en fonction de l'âge des granitoïdes. Ainsi, il sera proposé que les intrusions Éoéburnéennes proviennent de la fusion partielle du manteau en contexte de subduction. Les granitoïdes Éburnéens pourraient, eux, trouver leur source à la base d'une croûte préalablement épaissie.

Finalement, nous terminerons cette étude par une cartographie 3D de la région basée sur les interprétations précédentes et sur les données géophysiques. Les modèles ainsi établis, puis inversés, donneront un meilleur aperçu des volumes occupés par chaque unité stratigraphique ainsi qu'une estimation des imprécisions entre notre vision de la géologie de la ceinture d'Ashanti, les limites de la modélisation et les contraintes géophysiques. La modélisation 3D permettra également une cartographie du socle Birimien sous le bassin de Tarkwa et la mise en évidence de possibles corrélations entre des unités métavolcaniques du groupe de Sefwi et les emplacements des minéralisations en or au sud-est de la ceinture d'Ashanti.

Chapitre I

Chapitre I

Revised Eburnean geodynamic evolution of the gold-rich southern Ashanti Belt, Ghana, with new field and geophysical evidence of pre-Tarkwaian deformations

Abstract

Integration of regional geophysical datasets and detailed field observations provides new insights into the Paleoproterozoic structural evolution of southwestern Ghana. The study area is dominated by three metavolcanic and metasedimentary packages known as the Sefwi Group, the Kumasi Group (Birimian) and the Tarkwa Group (Tarkwaian) that were intruded by abundant TTG granitoids during the Eoeburnean and Eburnean phases of an event termed the "Eburnean Orogeny". This study identifies an Eoeburnean (pre-Tarkwaian) deformation event (D1) that produced significant deformation in the Sefwi Group metavolcanics. D1 is associated with N-S shortening manifested as regional scale folding in the southern Ashanti Belt. D1 synorogenic granitoids were intruded between 2187 Ma and 2158 Ma under greenschist metamorphic condition. Syn-D1 gold mineralisation associated with quartz veining could be the original source of Tarkwaian paleo-placers and/or remobilised gold concentrations along major shear zones.

D2 represents an extensional phase associated with the Kumasi Group sedimentation (2154 – 2125 Ma) which could be related to activation of major structures such as the Ashanti Fault as low angle detachments that controlled the deposition of the Kumasi Group and the opening of the Kumasi and Akyem Basin. The Tarkwa Group (2107 – 2097 Ma) unconformably overlies the Birimian Supergroups and was deposited in response to D3 shortening. D3 resulted in the inversion of syn-D2 detachments faults within the Ashanti Belt. NW-SE D3 shortening produced regional scale folding within the Birimian and the Tarkwaian metasediments. D4 deformation corresponds with sinistral reactivation of D3 thrust faults, and is locally associated with macro-scale folding at Obuasi and Wassa gold mines. By the end of D4, the regional scale architecture was built and was only slightly modified by the two last events. D5 postdates the Eburnean metamorphic peak and corresponds to open recumbent folds associated with a subhorizontal crenulation cleavage. D6 is present as a subvertical crenulation cleavage and reverse faults associated with NE-SW shortening.

2.1 Introduction

The Ashanti greenstone belt in the Western Region of Ghana hosts numerous hydrothermal gold deposits (e.g. Obuasi, 60 Moz) and older placer deposits (e.g. Tarkwa, 41 Moz) that were created and deformed during the Eburnean Orogeny (Bonhomme, 1962). The presence of massive gold placers that predate all known hydrothermal deposits, suggests an early phase of gold mineralisation and synchronous deformation in the Ashanti Belt. Characterising this early event is essential for understanding the tectonic evolution and geological context for gold mineralisation in the southwest Ghana. This region is composed primarily of paleoproterozoic metavolcanic and metasedimentary rocks that are divided into the Birimian Supergroup (Sefwi and Kumasi Groups) and the Tarkwa Group, that are both intruded by abundant granitoids (Fig. I-1).

Allibone et al. (2002a) separated the Paleoproterozoic Eburnean Orogeny into two distinct phases known as Eburnean I and II. Their Eburnean I event predates the deposition of Tarkwaian sediments and is associated with a major period of magmatism and metamorphism in the Sefwi Group basement. Their Eburnean II event is associated with significant post-Tarkwaian deformation that affected both the Birimian Supergroup and overlying Tarkwaian sediments. This second phase of the Eburnean Orogeny is relatively well known in the study area and is described at the mine scale (Blenkinsop et al., 1994, in Obuasi; Allibone et al., 2002a, in Obuasi and, 2002b, in Bogoso; Kutu, 2003, in Konongo; Tunks et al., 2004, in Damang) and at a regional scale (Eisenlohr, 1992; Milési et al., 1992; Ledru et al., 1994; Barritt and Kuma, 1998; Feybesse et al., 2006).

Eburnean I events have been described along the West African Craton and called Eoeburnean in northern Ghana (De Kock et al., 2011) or Tangaean in Burkina Faso (Tshibubudze et al., 2009; Hein, 2010), but are relatively poorly resolved in southwestern Ghana. This study presents an integrated interpretation based on new field data, geophysical surveys and previous structural studies and maps (Loh et al., 1999, Agyei Duodu et al., 2009) that provides a new structural context to the Eoeburnean phase and clarifies the subsequent tectonic evolution of the Ashanti greenstone belt.

2.2 Geological setting

The southern part of the West African Craton, known as the Leo-Man craton, is composed of an Archean nucleus that is tectonically juxtaposed against Paleoproterozoic granitoid-greenstone assemblages to the north and east (Fig. I-1). In southwest Ghana, four NE-SW greenstone belts occur, known as the Bui, Sefwi, Ashanti and Kibi-Winneba belts from west to east, respectively. These belts are separated by three sedimentary basins namely the Sunyani, the Kumasi and the Akyem Basins (or Cape Coast Basin, Agyei Duodu et al., 2009). These greenstone belts and dividing sedimentary basins were formed and deformed during the Eburnean Orogeny (Bonhomme, 1962).
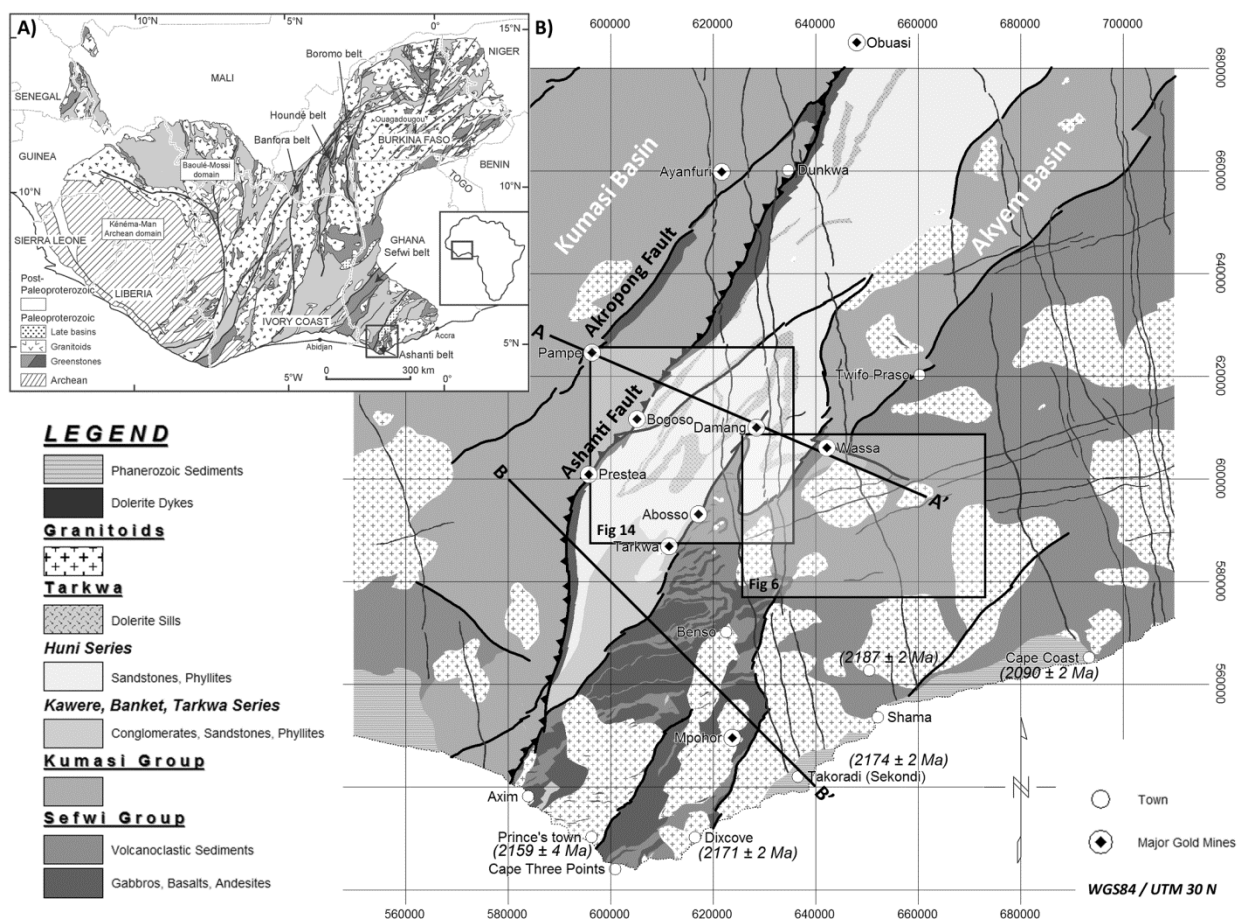
Figure I-1   (*A*) *The West African Craton (modified after Milési et al., 2004, BRGM SIGAfrique) is composed of an Archean nucleus in the southwest bounded by series of paleoproterozoic greenstone belts and voluminous granitoids in the northwest to the east. (B) Simplified geology map of the Ashanti Belt (modified after Agyei Duodu et al., 2009) showing the locations of Figures I-6, I-14 and I-16 (AA' and BB').*

	Regional Interpretation (This Study)	In Birimian Obuasi / Bogoso (Allibone et al., 2002a, b)	In Tarkwaian Damang (Tunks et al., 2004)	Regional (Eisenlhor et al., 1992)	Regional (Feybesse et al., 2006) (Milesi et al., 1992)
Eoeburnean 2187 - 2158 Ma	Sefwi Group volcanism and sedimentation **D1, N-S shortening** Regional scale folding in the Sefwi Group Possible gold mineralization	Volcanism Granitoids intrusion Regional metamorphism		Birimian sediments and volcanics penecontemporaneous Plutonism (Dixcove type granitoids) Onset of deformation in a "foreland thrust" and Tarkwaian deposition	Magmatic accretion Plutonism Birimian sedimentation
	D2, Extension Phase (2154 - 2125 Ma) Kumasi Group sedimentation	D1 S1 parallel to bedding Flat-lying bedding parallel shearing			
Eburnean 2125 - 2000 ? Ma	**Tarkwa Basin Formation (2107 - 2097 Ma)** **D3, NW-SE shortening** Km scale folds in Birimian and Tarkwaian S3 subvertical crenulation cleavage NE-SE Thrust faults (Ashanti, Damang, ...) Peak of green schist metamorphism (≈ 2090 Ma)	D2, NW-SE shortening Isoclinal folds with axial surface parallel to the regional faults and shear zones Ashanti thrust fault D3 Low dip axial surface fold at Obuasi S3 crenulation cleavage overprinting S2 Final stage of D2 ?	D1, NW-SE shortening Km scale folds (with subvertical axial surface (S1)) Damang thrust fault	D1, NW-SE shortening S1 (NE-SE) subvertical and subparallel to bedding in both Birimian and Tarkwaian Regional folds (tight to isoclinal) D2, Continuing compression S2 (NE-SE) fabrics overprint S1 foliation S2 is defined by aligned muscovite and elongate recrystallised quartz grains Metamorphism Synorogenic plutonism (Cape-Coast type granitoids)	D1, NW - SE shortening Thrust faults Tarkwaian sediments deposition (Syn D1) Metamorphism (6 kbar / 550 - 650 °C) D2/D3, NW-SE shortening Tarkwaian folds Strike-slip faults and shearing Gold mineralizations Metamorphism (2 - 3 kbar / 200 - 300 °C)
	D4, NNW-SSE shortening Sinistral shear reactivation of D3 thrust S4 crenulation cleavage ENE-WSW Greenschist retrograde metamorphism Remobilization and concentration of gold along the shear zones and at the base of Tarkwa Basin	D4, NNW-SSE shortening Hm scale fold at Obuasi D5 or syn-D4 Sinistral strike-slip faults and shearing Gold mineralization	D2, NNW-SSE shortening Thrust faults and minor folds		
	D5 Recumbant folds (< m) Subhorizontal crenulation cleavage Last pyrite/gold mineralization associated with quartz vein **D6, NE-SW shortening** Low amplitude folds + crenulation cleavage ≈ N320 / 70 (RH) Reverse faults oriented NW-SE		D3, ESE-WNW shortening Folds with shallowly dipping axial surfaces and mineralized quartz veins, post-dating the peak of metamorphism D4 Faults oriented NW-SE	K-rich plutonism (cross-cutting all previous structures)	Late plutonism

Table I-1   *Comparison between the tectonic evolution presented in this work with other recent studies in southwestern Ghana.*
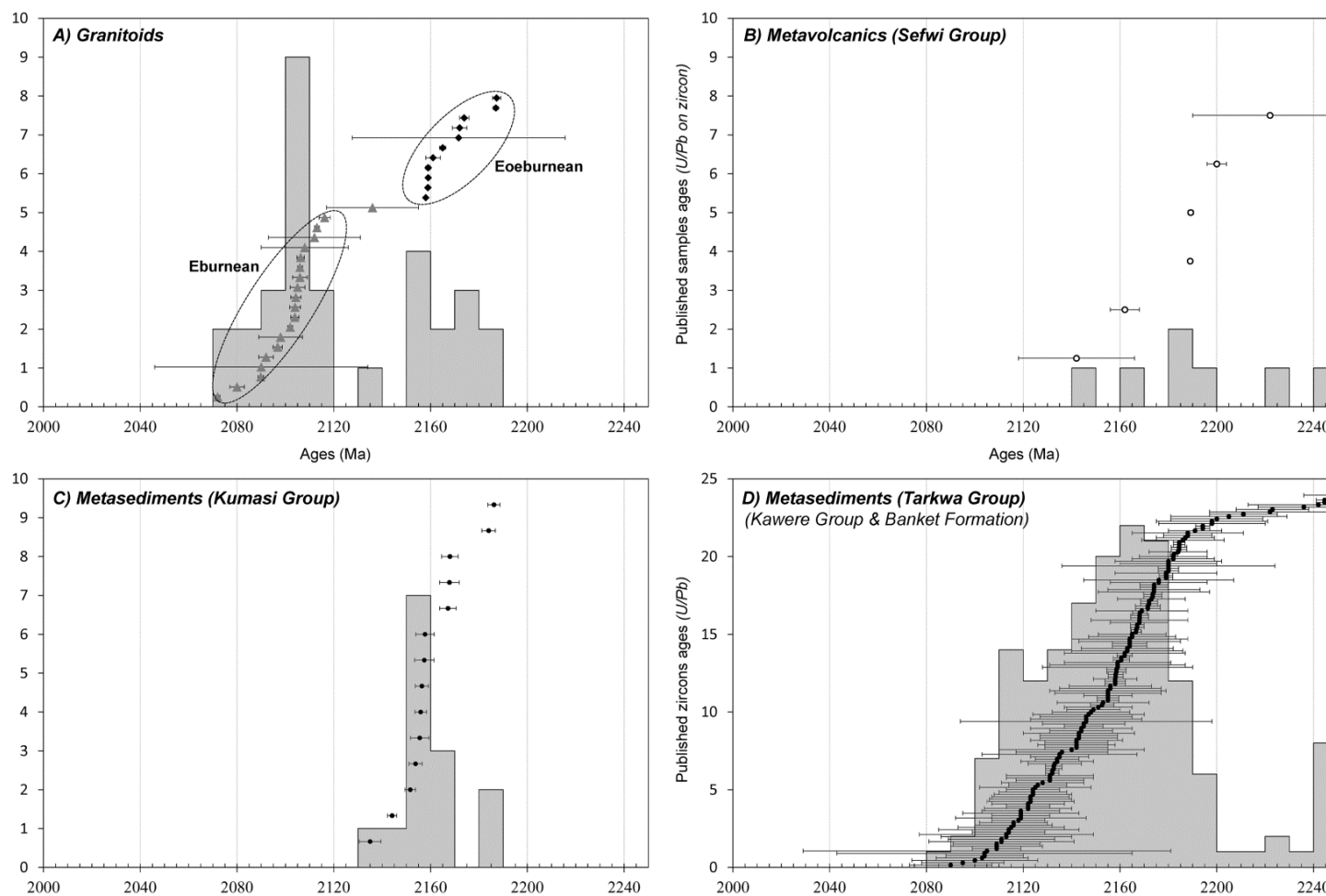
Figure I-2   *Compilation of histograms presenting radiometric age data and the number of zircons / samples for the three main stratigraphic sequences and on granitoids in the study area (after Taylor et al., 1992; Hirdes et al. 1992; Davis et al., 1994; Oberthür et al., 1998, Loh et al., 1999; Pigois et al., 2003; Attoh et al., 2006; Feybesse et al., 2006; Adadey et al., 2009; Agyei Duodu et al., 2009). The age distribution in granitoids shows two distinct peaks that correspond to the Eoeburnean and Eburnean phases. Dots represent dated samples for igneous rocks or detrital zircons ages for sedimentary rocks and their associated error bars.*

2.2.1 *Eburnean Orogeny*

Feybesse et al. (2006) proposed an early Eburnean phase between 2135 Ma and 2100 Ma corresponding to magmatic accretion and plutonism that terminated with development of the Kumasi Basin. The synchronous Eburnean Orogeny (2130-1980 Ma) corresponds to thrust tectonism dominated by sinistral transcurrent deformation in the Ashanti Belt. Allibone et al. (2002a) suggests an alternative two phase Eburnean evolution, divided into the Eburnean I (2200-2150 Ma) and Eburnean II (2116-2088 Ma), that are separated by deposition of the Birimian and Tarkwaian units. In northern Ghana De Kock et al. (2011) called these two phases Eoeburnean and Eburnean, respectively. This nomenclature is referred to in the text, based on the correlation with published zircon geochronology (Fig. I-2A).

Allibone et al. (2002a) suggest that the Eburnean I (Eoeburnean) event was associated with a period of magmatism and metamorphism responsible for the Sefwi Group metavolcanics and TTG granitoid emplacement (Table I-1) that correlates with the pre-Eburnean of Feybesse et al. (2006).

The second phase of the Eburnean Orogeny affects both the Tarkwa Group and the Birimian Supergroup. The Eburnean II (Eburnean) event is associated with major NW-SE shortening (D2 of Allibone et al., 2002(a), 2002(b); D1 of Tunks et al., 2004) that developed major thrust faults - including the Ashanti Fault - along with isoclinal folds in Birimian metasediments and regional scale open folds in the Tarkwaian sediments. These features are overprinted by thrusts that were reactivated during a phase of sinistral transpression that utilised the existing thrust architecture (D2 of Tunks et al., 2004; D3 of Milési et al., 1992; D3 of Feybesse et al., 2006). At the Obuasi mine, 100 m scale folds described by Allibone et al. (2002a) may have developed during (his D4-D5) shearing. This phase of the Eburnean Orogeny is associated with most of the hydrothermal gold deposits in the region. Late Eburnean deformation has been observed in the Damang mine, where it is characterised by very open folding and minor brittle faulting (Tunks et al. 2004). The D3 of Tunks et al. (2004) corresponds to ESE-WNW shortening associated with folds, quartz veins and a shallow dipping crenulation cleavage that overprints D2 reactivated thrust faults. In Damang, Tunks et al. (2004) observed a conjugate system of faults that strike NW-SE and cross-cut all previous structures. These features may correlate with more regionally extensive NW-SE faults recognised in existing maps of southwestern Ghana.

The relationship and timing between Eburnean deformation and Tarkwaian deposition are contentious and not fully understood. Allibone et al. (2002a) suggested Tarkwaian sedimentation

occurred before major Eburnean deformation and mineralisation. Leube et al. (1990) played down the significance of post-Tarkwaian deformation suggesting "tension-related folding by gravity" (Stage V of Leube et al., 1990, page 157) was responsible for Tarkwaian structures, requiring earlier events to have controlled the regional structural architecture and the distribution of gold mineralisation. Other workers propose an intermediate position with Feybesse et al. (2006) suggesting Tarkwaian sedimentation developed in response to Eburnean shortening following a phase of tectonic accretion and magmatism. Further, Ledru et al. (1994) considered the Tarkwa Basin to have initiated as a foreland basin during the final stages of the Eburnean Orogeny.

2.2.2 *Birimian series*

The Birimian series was first described by Kitson (1918) in the Birim River (around 80 km east of the Ashanti Belt). Since this early interpretation, the Birimian stratigraphic column has been revised significantly, including more than one complete reversal. Before the application of absolute geochronology, workers described an Upper Birimian composed by metavolcanics on top of a Lower Birimian corresponding to metasediments (Kitson, 1928; Whitelaw, 1929; Junner, 1935, 1940; Hastings, 1982; Ntiamoah-Agyakwa, 1979; Kesse, 1985; Milési et al., 1992). Leube et al. (1990) and Eisenlohr (1992) suggested that Birimian metavolcanics and metasediments were synchronous. Sm/Nd analyses conducted by Taylor et al. (1992) required a reversal of the stratigraphy with the younger metasediments overlying the older metavolcanics. This relationship was confirmed by Loh et al. (1999) with U/Pb zircon ages varying between 2162 ± 6 Ma and 2266 ± 2 Ma for the metavolcanics. Detrital zircons in the metasediments indicate the initiation of their deposition around 2154 ± 2 Ma in the Obuasi mine (Oberthür et al., 1998). Similar ages have been found in the Kumasi Basin (northwest of the Ashanti Belt) by Davis et al. (1994). Adadey et al. (2009) proposed a new stratigraphy of the Birimian Supergroup with the Sefwi Group (2195-2170 Ma) composed of micaschists and metavolcanics and the Kumasi Group, deposited after 2150 Ma, with metasediments and intercalated andesitic beds dated at 2142 ± 24 Ma (U/Pb on zircon). The Kumasi Group was intruded by the late sedimentary Suhuma granodiorite at 2136 ± 19 Ma (U/Pb on zircon, Adadey et al., 2009).

Tarkwaian Unit		Thickness			
		Whitelaw, 1929	Junner, 1940	Kesse, 1985	Pigois et al., 2003
Huni sandstones	Dompin quartzites	1000 ft (300 m)	4500 ft (1370 m)	1370 m	> 1300 m
	Dompin phyllites	500 ft (150 m)			
	Huni sandstones	1500 ft (450 m)			
Dolerite sills		-	600 ft (180 m)	-	< 200 m
Tarkwa phyllites		800 - 1000 ft (240 - 300 m)	600 ft (180 m)	120 - 400 m	120 - 400 m
Banket Group	Sandstones	2100 ft (640 m)	500 - 600 ft (150 - 180 m)	100 - 180 m	150 - 600 m
	Mineralized conglomerates		100 - 300 ft (30 - 90 m)	20 - 90 m	
	Sandstones		1000 ft (300 m)	150 - 350 m	
Kawere Group	Conglomerates levels interbedded with sandstones and phyllites	-	-	250 - 700 m	250 - 700 m

Table I-2 *Division of Tarkwaian sedimentary sequences and estimated thicknesses.*

2.2.3 *Tarkwaian series*

The Tarkwa Group (Kitson, 1928) is a succession of four sedimentary units (Whitelaw, 1929; Junner, 1940; Kesse, 1985, Pigois et al., 2003) (Table I-2). The Kawere Group, at the base of the Tarkwaian sediments is composed of conglomerates and sandstones. Its thickness varies between 250 m and 700 m and is stratigraphically overlain by the Banket Formation made up of conglomerates with interbedded local cross-bedded sandstones layers. The conglomerates are principally composed of Birimian quartz pebbles (> 90%) and volcanic clasts (Hirdes and Nunoo, 1994) that host the Tarkwa Placer deposit. Gold within the conglomerate forms a zone that is less than 100 m thick, while the maximum thickness of the Banket sequence is estimated to be 600 m. Approximately 400 m of Tarkwa Phyllites overly the Banket sequence. The uppermost unit of the Tarkwa Group is the Huni Sandstone, comprised of alternating beds of quartzite and phyllite intruded by minor dolerite sills that form a package up to 1300 m thick (Pigois et al., 2003).

U/Pb and Pb/Pb dating of a few detrital zircons provide a maximum depositional age of 2132 ± 2.8 Ma for the Kawere formation and 2132.6 ± 3.4 Ma for the Banket formation (Davis et al., 1994, Hirdes and Nunoo, 1994). These ages agree with the study by Pigois et al. (2003), that yielded maximum depositional age of 2133 ± 4 Ma from 71 concordant zircons from the Banket Formation. However 39 of their zircons are younger and contradict this value. According to all

concordant zircons histogram (161 grains) and their uncertainties (Fig. I-2D), a reasonable estimation for the start of the Tarkwaian sedimentation could be as young as 2107 Ma although two zircons may be younger at 2090 ± 17 Ma and at 2095 ± 17 Ma (Pigois et al., 2003). Tarkwaian deposition is also constrained by intrusions of metagabbro sills within the Tarkwaian series at 2102 ± 13 Ma (Adadey et al., 2009) and by granitoids at 2097 ± 2 Ma (Oberthür et al., 1998).

2.2.4 *Granitoids*

Abundant granites and granitoids intruded the Birimian and Tarkwaian units during the Paleoproterozoic. Eburnean plutonism in southwest Ghana can be divided into two phases between 2180-2150 Ma (Eoeburnean) and 2130-2070 Ma (Eburnean) that is supported by the current database of U/Pb and Pb/Pb zircon ages (Fig. I-2A). Most of the granitoids intruded during both phases correspond to typical tonalite-trondhjemite-granodiorite (TTG) suites. However, in the southern part of the Ashanti Belt, intrusions within the Mpohor complex have granodioritic, dioritic and gabbroic compositions. Along with this compositional heterogeneity, granitic rocks in the southern Ashanti Belt also appear to have been emplaced under different tectonic regimes. The Sekondi granodiorite on the eastern margin of the southern Ashanti Belt exhibits a magmatic foliation (Loh et al., 1999), suggesting syntectonic emplacement at around 2174 ± 2 Ma (U/Pb on zircon, Oberthür et al., 1998). In contrast, tonalites at Dixcove and Prince's Town are unfoliated and were dated at 2171 ± 2 Ma (Hirdes et al., 1992) and 2159 ± 2 Ma (Attoh et al., 2006).

Granitoids from the Eburnean phase sometimes show a magmatic mineral alignment (biotite and/or feldspar) but are generally unfoliated. Late Eburnean granitoids are often K-feldspar rich and are mainly found in the Akyem, Kumasi and southern Sunyani basins where they cross-cut all major regional structures.

Similar ages and characteristics have been observed in granitoid intrusions in the small fragment of the Ghanaian craton in northern Brazil (the Sao Luis Craton, Klein et al., 2005, 2008). This fragment covers a small area mostly composed by granitoids. As a consequence, correlation between the Ghanain and the Sao Luis cratons can only be performed via granitoid ages and geochemistry analyses.

2.2.5 *Dolerite dykes*

Dolerite dykes are abundant across the West African craton where they cross-cut Archean and Paleoproterozoic basement. In southwestern Ghana these dykes are well defined in magnetic

data where they are characterised by strong magnetic susceptibility and remanence. The recently compiled regional 1M map of Ghana (Agyei Duodu et al., 2009) shows two families of dykes that are oriented N-S and ENE-WSW that are generally less than 100 m in thickness. In the northern Ashanti Belt these dykes are overlain by the Volta basin. Dolerite dykes are observed to cross-cut undeformed K-feldspar rich granites that formed during the late Eburnean, and are overlain by Volta basin sediments with a maximum depositional age of 950 Ma (Kalsbeek et al., 2008). These relationships constrain dyke emplacement to between 2000 Ma and 950 Ma. In contrast some older dolerite / gabbro dykes and sills were deformed during the Eburnean Orogeny and are dated at 2102 ± 13 Ma (U/Pb on zircon, Adadey et al., 2009).

2.2.6 *Phanerozoic series*

The youngest lithologies in the study area correspond to Phanerozoic sandstones and shales. These can be found along the coast, mainly between Cape Coast and Takoradi but also to the west of Axim. Loh et al. (1999) distinguished two groups with ages ranging from Devonian to Carboniferous (Crow, 1952, Mensah, 1973; Chaloner et al., 1974; Baer and Riegel, 1980) and Cretaceous (Tevendale, 1950).

2.2.7 *Metamorphism*

With the exception of some late Eburnean granitoids, dolerite dykes and Phanerozoic sediments, all other lithologies have undergone metamorphism that generally does not exceed upper greenschist facies. Studies on amphibole/plagioclase assemblages suggest the peak temperature and pressure was 500-650°C and 5-6 kbar (John et al. 1999), dated at 2092 ± 3 Ma (Oberthür et al.,1998). These results are similar to those obtained by Schmidt Mumm et al. (1997) who estimated peak metamorphic conditions along the Ashanti Fault system to 520°C and 5.4 kbar. These conditions are in agreement with the occurrence of garnet in the Nsuta manganese deposit (Nyame et al. 1998; Kleinschrot et al. 1993, 1994) and garnet-staurolite assemblages at the Damang gold mine (Pigois et al., 2003), although these manganese-rich garnet assemblages can be stable to lower pressure and temperature conditions (Mahar et al., 2004). Occurrences of kyanite and sillimanite assemblages have also been reported from the Bonsa diamond field (Kesse, 1985).

	Gold Deposits	Host Rock	Structural Context	Pressure	Temperature	P-T Reference
B i r i m i a n	*Obuasi*	Phyllites, Volcanoclastics, Basalts	Shear zones related fractures	> 0.8 kbar	145 / 340 °C	Bowell et al., 1990
	(60 Moz)	(Kumasi / Sefwi / Tarkwa groups contacts)	(Ashanti and Akropong faults)	1 - 2.2 kbar	215 / 405 °C	Schwartz et al., 1992
			Late D3 to Syn-D4			
		Eburnean Granodiorites - Tonalites	Sheared plutons margins	1 - 3 kbar	180 - 350 °C	Yao et al., 2000
			Late D3 to Syn-D4			
	Bogoso	Phyllites, Basalts	Graphitic shear zone (Ashanti Fault)	1 - 2 kbar	140 - 340 °C	Mumin et al., 1995, 1996
	(4 Moz)	(Sefwi Group / Kumasi Group contact)	Late D3 to Syn-D4			
	Prestea	Phyllites, Basalts	Graphitic shear zone (Ashanti Fault)	1 - 2 kbar	220 - 390 °C	Mumin et al., 1995, 1996
	(11 Moz)	(Kumasi / Sefwi / Tarkwa groups contacts)	Late D3 to Syn-D4	2 - 4 kbar	290 - 323 °C	SchmidtMumm et al., 1997
	Ayanfuri	Eburnean Tonalites	Shear zone (Akropong Fault)	1 - 2.2 kbar	278 - 334 °C	SchmidtMumm et al., 1997
	(1 Moz)		Late D3 to Syn-D4	0.7 - 2.9 kbar	220 - 280 °C	Wille et al., 2004
				0.9 - 3 kbar	209 - 330 °C	Yao et al., 2001
	Mpohor	Eoeburnean ? Gabbros, Granodiorites	Late shear zone and felsic dyke intrusion	1.1 - 3 kbar	197 - 320 °C	Yao et al., 2001
	(2 Moz)		D5 ? or D6 ?			
T a r k w a i a n	*Abosso - Damang*	Sandstones, Phyllites, Dolerites	Late Eburnean quartz veins, fault-related	1 - 2.2 kbar	153 - 278 °C	SchmidtMumm et al., 1997
	(8 Moz)	(Sefwi Group / Tarkwa Group contact)	D5 ?, 2063 ± 9 Ma (U/Pb on hydrothermal xenotime, Pigois et al., 2003)			
	Tarkwa	Banket Conglomerates	Tarkwa Group sedimentation	0.5 - 3 kbar	250 - 400 °C	Klemd et al., 1993
	(41 Moz)	(Placer deposit)	Early D3			

Table I-3   *Synthesis of structural and fluid inclusion studies for major gold deposits of southwestern Ghana. P-T data correspond to the homogenization temperature and pressure of aqueous-carbonic inclusions in quartz veins and pebbles.*

2.2.8 *Mineralisation*

The Ashanti Belt of southwest Ghana hosts a gold district that contains a significant number of world class hydrothermal gold deposits and the giant Obuasi deposit that hosts over 60 million ounces of gold. These deposits are spatially associated with the Ashanti Fault and other major shear zones in the Birimian Supergroup or along the contact between the Birimian and Tarkwaian units. The overlying Tarkwa Basin is also host to the Tarkwa paleoplacer that contains over 40 million ounces of gold.

2.2.8.1 Birimian deposits

Deposits found along the Ashanti Fault are associated with arsenopyrite and lesser other sulphides. According to Oberthür et al. (1994, 1997) and Allibone et al. (2002a) the main mineralisation in the Obuasi mine is associated with ductile shearing along the Ashanti Fault. They also described secondary gold mineralisation that developed within quartz veins and carbonate-alteration in basalts. In the Bogoso and Prestea deposits, Mumin et al. (1994) showed that gold mineralisation resulted from the remobilisation of pre-existing gold along the Ashanti Fault. The source of initial gold mineralisation has not been clearly identified.

Birimian mineralisations are often hosted within shear zones that transect sediments, mafics or granitoids (Table I-3, after Bowell et al., 1990; Schwartz et al., 1992; Klemd et al., 1993; Mumin and Fleet, 1995, Mumin et al., 1996; Schmidt Mumm et al., 1997; Yao and Robb, 2000; Yao et al., 2001; Allibone et al., 2002a, 2002b; Griffis et al., 2002; Pigois et al., 2003; Tunks et al., 2004; Wille and Klemd, 2004). Fluid inclusions studies propose low temperature ($\approx 250°C$) and pressure (≈ 2 kbar) homogenisation conditions for fluid trapped in mineralised Birimian quartz veins and pebbles (Schmidt Mumm et al., 1997).

Few radiometric ages have been acquired from the Birimian deposits. Near Ayanfuri, mineralisation is associated with granitoids dated at 2105 ± 3 Ma for the intrusion (U/Pb on zircon, Oberthür et al. 1998) and 2084 ± 2 Ma (Pb/Pb) for rutile/galena crystallisation from hydrothermal fluids (Oberthür et al., 1998).

2.2.8.2 Tarkwaian deposits

Two styles of gold mineralisation are present in the Tarkwa Group. Hydrothermal deposits occur along the contact between the Birimian and Tarkwaian units (e.g. Damang Mine), and paleoplacers occur within the Tarkwa Basin (e.g. Tarkwa Mine). In Damang, gold mineralisation was found to be associated with pyrite in brittle fractures and tensional quartz

veins that are correlated with the last deformation phase of the Eburnean Orogeny (Tunks et al. 2004). The late timing of mineralised structures was supported by a xenotime age of 2063 ± 9 Ma (U/Pb, Pigois et al., 2003). Fluid inclusions within quartz veins associated with mineralisation formed at low temperature (153-278°C) and pressure (1-2.2 kbar) homogenisation conditions in the Abosso-Damang deposits (Schmidt Mumm et al. 1997).

Tarkwaian sediments also host paleoplacers such as the Tarkwa deposit. Gold grade distribution within the deposit is parallel to bedding, supporting a sedimentary origin (Sestini 1973). Gold is generally found within paleochannels, along conglomerates and proximal to hematite rich areas within the Banket formation (Table I-2). Fluid inclusions studies of mineralised quartz pebbles suggest formation under greenschist facies conditions (250-400°C and 0.5-3 kbar, Klemd et al., 1993). These values are similar to those obtained for Kumasi Group quartz veins fluid inclusions along the Ashanti Belt, and may explain why the source of the Tarkwa placer has been initially described as a Birimian type hydrothermal deposit (Klemd et al., 1993, Hünken et al., 1994).

2.3 Data used for mapping

2.3.1 *Field data*

In order to ground truth and constrain the geophysical interpretation, petrophysical, structural and lithological data were collected across the southern Ashanti Belt. These data were then combined with pre-existing observations and outcrop maps from Loh et al. (1999) and company data from explorers within Ghana (BHP and Golden Star).

Despite collecting data from most of the accessible outcrops in the study area, the presence of a thick lateritic blanket restricts the use of traditional mapping and only allowed for the sparse collection of geological data. In general, the weathered cover sequence presents as 6-15 m of laterite underlain by 40 m of saprolite.

In order to complement the previous regional mapping, geophysical data were used to extrapolate the structures between the isolated outcrop observations and petrophysical data were used to constrain the geophysical modelling.
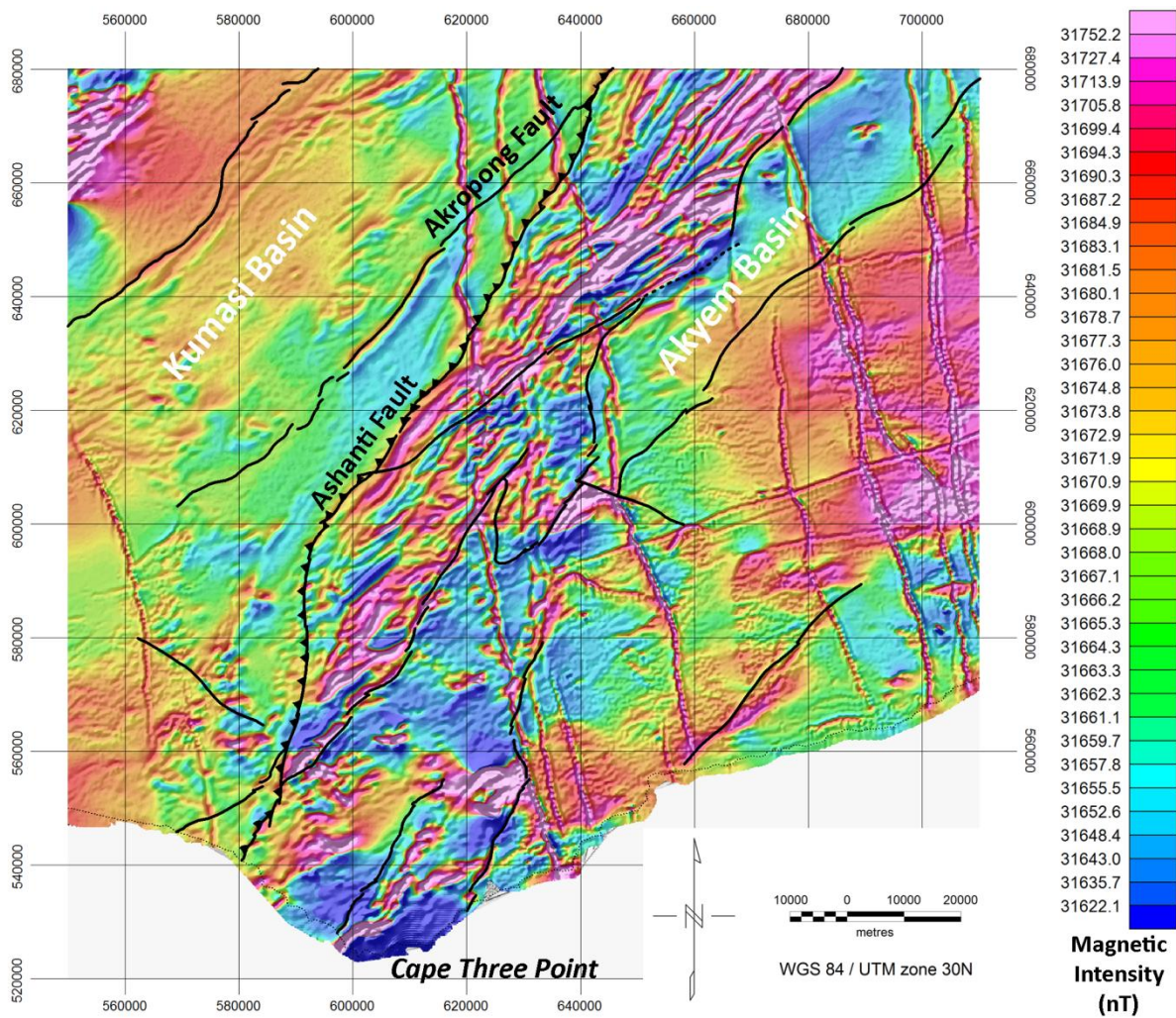
Figure I-3   *The reduced to pole image of the total magnetic intensity draped over the shaded first vertical derivative. The reduced to the pole data was the basis for all subsequent processing and is shown with some of the main significant regional faults. Pixel size is 100m. The colour look up table is histogram equalised.*
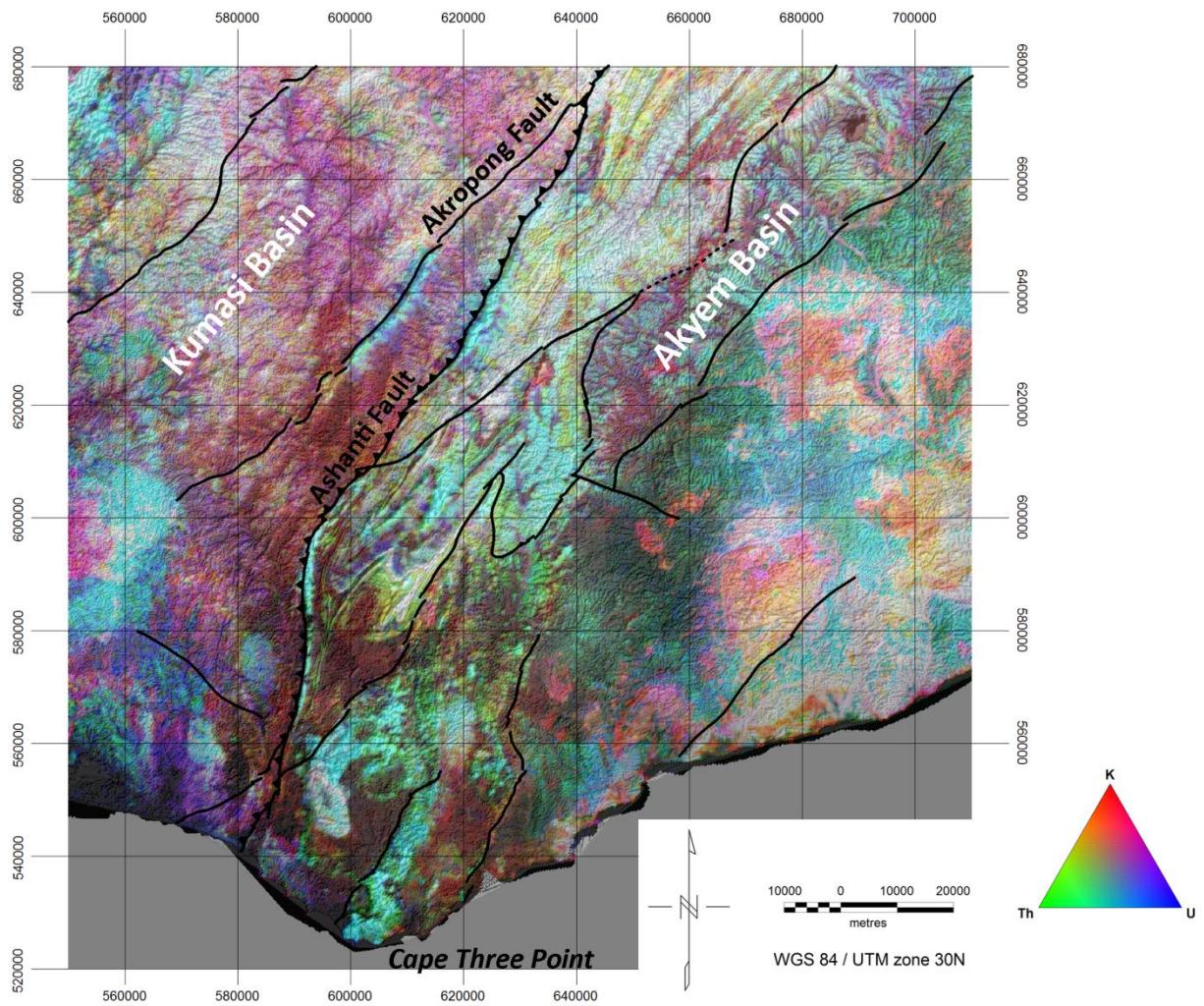
Figure I-4   *Image of the gamma-ray data draped over a shaded digital elevation model. This image shows the relative proportion of potassium, thorium and uranium as an RGB image, and their correlation with the topography. Pixel size is 100 m. U and Th rich areas with high topography correspond to Sefwi Group metavolcanics as around Cape Three Points and proximal to the Ashanti Fault. K-rich granitoids are well defined in the eastern part of the area.*
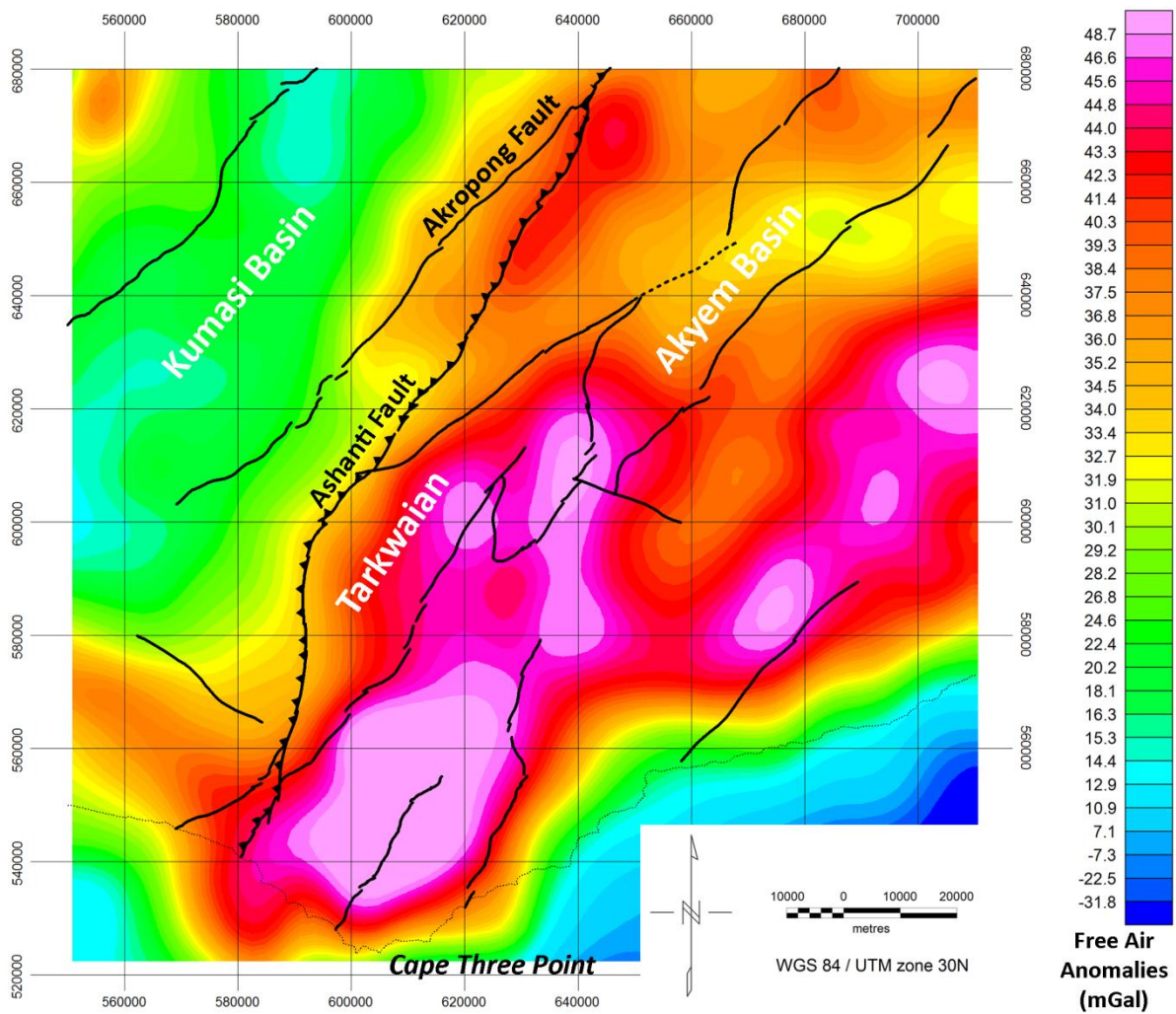
Figure I-5   *Bouguer gravity map over the study area overlain with the regional fault architecture. As a consequence of the low resolution of the grid (5 km per pixels), only long wavelength features are observed, these features are interpreted to be sourced from the major, deep-seated structures.*
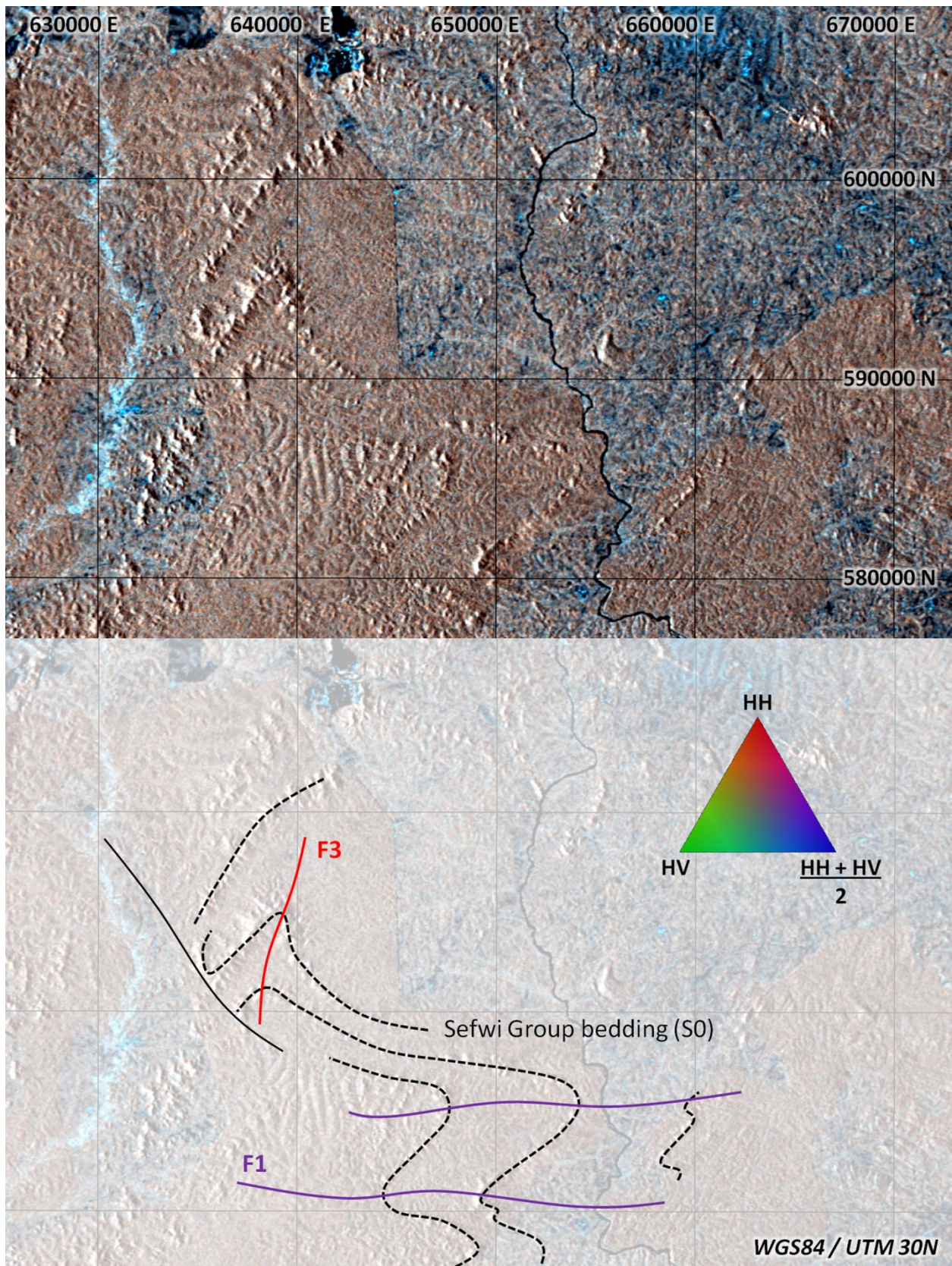
Figure I-6　　*ALOS PALSAR radar image consisting of three colour bands: red = HH radar polarization, blue = HV, and green for the mean of both bands. Sefwi Group bedding highlighted by volcanoclastic layers in this image is folded by E-W trending F1 folds that are refolded by N-S trending F3 folds. See Figure I-1 for location.*

2.3.2 *Processing and interpretation of geophysical data*

Magnetic and radiometric data were acquired between 1994 and 1996 by the Geological Survey of Ghana. The flight altitude of the survey is 80 m above ground, along lines striking 135° and separated by 200 m. The total magnetic intensity (TMI) was gridded with a resolution of 100 m.

2.3.2.1 Aeromagnetic data: The data were reduced to the pole (D = -6.5°, I = -14.5°) (RTP, Fig. I-3) in order to bring anomalies directly over their causative sources. The reduction to the pole was applied without amplitude correction (minor N-S artefacts appears) or with amplitude correction (no artefacts and similar resulting image but different magnetic intensity values). The RTP with amplitude correction was used preferentially for visual interpretation of structures as the absolute values of anomalies are less important than their geometry. Both the RTP and the analytic signal grids (which produce similar images as the RTP, MacLeod et al., 1993) were then filtered to produce further interpretable images that highlighted specific elements of the geology. The first and second vertical derivative and amplitude normalisation (Automatic Gain Control, AGC) and the tilt derivative (Verduzco et al., 2004; Lahti and Karinen, 2010) were also used to highlight structural information (Gunn et al., 1997; Milligan and Gunn, 1997), and upward continuation was applied to highlight the 'deeper' magnetic anomalies.

2.3.2.2 Radiometric (gamma-ray) data: U, Th and K bands have been gridded separately at 100 m resolution. These bands were then combined in a ternary RGB image and draped over a digital elevation model (90 m resolution; Shuttle Radar Topographic Mission, 2000) (Fig. I-4). The combination of radiometric data and the digital elevation model helped delineate lithological domains and structures (Dickson and Scott, 1997).

Due to the relatively subdued topography in the study area (between sea level and 460 m), the variation in elevation corresponds to differential erosion of resistant lithologies. For example, topographic relief along the Ashanti and Akropong faults and near Cape Three Points corresponds to rich Th and U areas. Similar mapping in Burkina Faso (Metelka et al., 2011) shows that these Th and U rich areas correlate with regolith cover. In contrast in SW Ghana these areas correspond to mafic rocks with strong magnetic signatures that are imaged in the aeromagnetic data and confirmed on the field. Using the methodology of Metelka et al. (2011), we help to identify some lithological units and structures by comparison between magnetic, radiometric and topography data (Table I-4).

2.3.2.3 Gravity data have been sourced from the International Gravimetric Bureau (http://bgi.omp.obs-mip.fr/) as Free Air and Bouguer anomalies grids. Fig. I-5 shows the

Bouguer anomaly map calculated using density values of 2.67 g/cm^3 for the Bouguer correction that were gridded at 5 km. These gravity data can only be used to broadly differentiate regional rock packages and image the continuity of the major structures at depth.

2.3.2.4 ALOS PALSAR data (Advanced Land Observing Satellite; Phased Array type L-band Synthetic Aperture Radar) high-resolution data collected in 2009 were used to image structure within lithological packages. Two polarisation channels (HH and HV) (available from-http://www.eorc.jaxa.jp/ALOS/en/) were gridded with a resolution of 50 m. A ternary RGB image was then produced (Fig. I-6), where red, green, blue colours correspond respectively to the HH, HV and (HH+HV/2) polarisations. These radar data are able to image structural details within sedimentary units such as bedding, with better resolution than the combined radiometric and digital elevation model.

2.3.3 *Petrophysics*

Petrophysical data were collected during regional reconnaissance, resulting in a database of over 300 susceptibility measurements of the major lithologies encountered in the Ashanti region. The data provided quantitative information on the magnetic susceptibility of the Birimian and Tarkwaian units and intrusives that were used to constrain the regional magnetic interpretation and subsequent geophysical modelling. These susceptibility data are consistent with common susceptibility range proposed by Clark (1997) and with values measured by Metelka et al. (2011) in Burkina Faso.

The histograms in Fig. I-7 show the range of measured magnetic susceptibilities for the lithologies seen in the study area using a Geofyzika KT-5 Kappameter hand held susceptibility meter. To ensure high quality measurements, some representative samples were re-measured using a Kappabridge KLY-3 magnetic susceptibility meter and no statistically significant differences were found. Natural remanent magnetisation (NRM) of the dolerite dykes was measured using AGICO JR5A spinner magnetometer, mounted within Helmholtz coil systems. Paleomagnetic laboratory experiments were carried out at the GET Magnetism Laboratory (Toulouse).

Density data were acquired for 26 samples taken from all of the outcropping regional units. Calculated values derived from sample weighing in air and water (Table I-5) agree with measurements made by Hasting (1978, unpublished report referenced in Barritt and Kuma, 1998) and with equivalent samples from Burkina Faso (Baratoux et al., 2011).
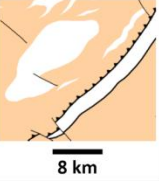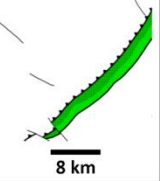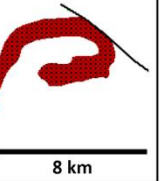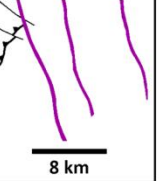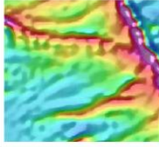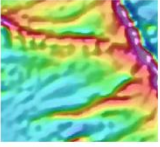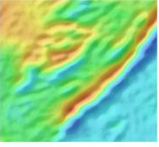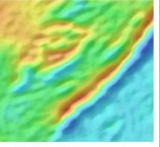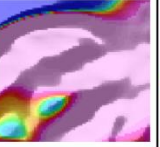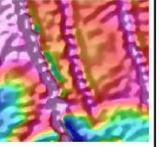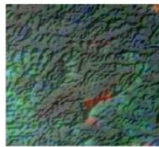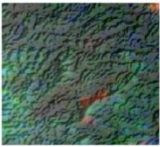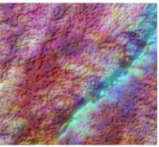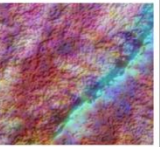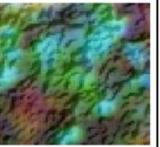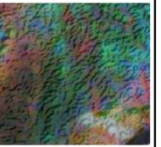
	Birimian					Late Dykes
Lithology	Micaschists	Volcanoclastic metasediments	Phyllites	Metabasalts Metaandesites	Metagabbros	Dolerite (dykes)
Mineralogy	qz, pl, chl, ms, bt, gph, gt	qz, pl, chl, bt	chl, ms, bt, gph, qz, ep	chl, bt, pl, qz, ser, ank, dol, cal	cpx, hbl, pl, chl, bt, qz	ol, opx, cpx, hbl, bt, pl
Susceptibility range (10^{-3} SI)	0.24 - 0.32	0.24 - 0.56	0.06 - 0.60	0.09 - 4.22	0.35 - 24.70	25.13 - 30.90 (+ Remanence)
Sample	GH101B	GH504	GH515	GH503	GH129G	GH370
U (ppm)	1.440	0.460	0.460	0.350	0.310	0.800
Th (ppm)	5.100	1.650	1.030	1.220	0.750	3.120
K_2O (%)	3.150	1.360	1.120	1.130	0.610	1.030
Map	8 km	8 km	8 km	8 km	8 km	8 km
Airborne Magnetic Response	Moderate intensity domains Strong magnetic fabric (parallel to bt. alignment)	Moderate intensity layers	Low intensity domains, uniform	Moderate to high intensity layers	High intensity bodies	High intensity linear features
Airborne Radiometric Response	Medium U High Th Medium K (dark green)	Low U Medium Th Low K (green)	Low U Low Th Medium to high K (red-violet)	Low U, Th, K Often covered by high U, Th regolith (blue-green)	Low U, Th, K Often covered by high U, Th regolith (blue-green)	Low U High Th Low K (green)

Table I-4A
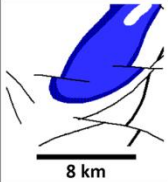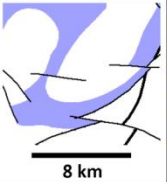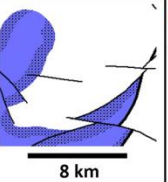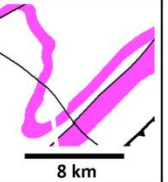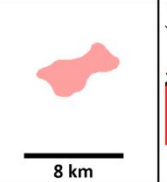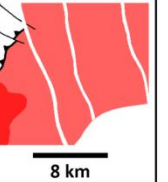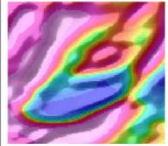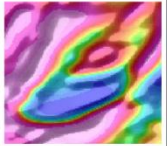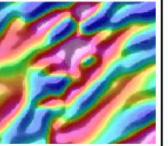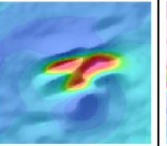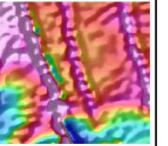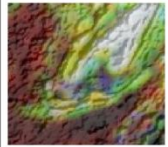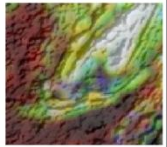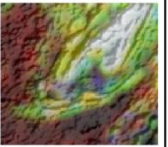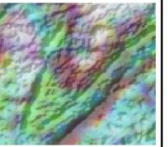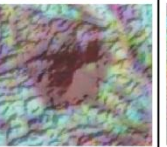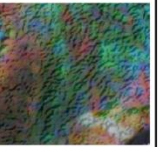
	Tarkwaian			Eburnean Intrusions		Eoeburnean Intrusions
Lithology	Phyllites	Sandstones	Conglomerates	Dolerite (sills)	Granite Granodiorite	Granodiorite Tonalite
Mineralogy	chl, ms, bt, gph, st, gt	qz, mgt, bt	qz, Birimian and Granitoid pebbles	cpx, hbl, pl, chl, bt, gt, cal	bt, ms, qz, pl, kfs	pl, qz, bt, chl, ep
Susceptibility range (10^{-3} SI)	0.08 - 0.16	0.08 - 0.32	0.13 - 13.10	No data	0.06 - 38.00	0.05 - 8.06
Sample	GH397	GH512	No Sample	GH395	GH237	GH507
U (ppm)	4.500	0.880	No data	0.740	0.650	0.110
Th (ppm)	9.290	3.580	No data	2.220	1.510	0.270
K_2O (%)	2.640	1.050	No data	0.140	2.120	0.170
Map	8 km	8 km	8 km	8 km	8 km	8 km
Airborne Magnetic Response	Moderate intensity layers	Low intensity layers	Moderate to high intensity layers	Moderate to low intensity layers	Moderate to high intensity bodies	Low intensity bodies Strong magnetic fabric (parallel to bt. alignment)
Airborne Radiometric Response	High U High Th Medium K (white-yellow)	Medium U High Th Medium K (green - yellow)	Low U Low Th Medium K (dark red)	Medium U High Th Low K (light green)	Low U Low to medium Th Medium K (dark red)	Low U Low to medium Th Low K (dark red-green)

Table I-4B   *Summary table of the lithologies, associated petrophysics properties and geophysical signatures (modified after Metelka et al., 2011). The magnetic image is composed of the RTP draped over the shaded first vertical derivative. The radiometric image is draped over the shaded digital elevation model. Whole rock geochemical analyses were conducted by A.L.S. Mineral Laboratory, Sevilla, Spain. ank. ankerite, bt. biotite, cal. calcite, chl. chlorite, cpx. clinopyroxène, dol. dolomite, ep. epidote, gph. graphite, gt. garnet, hbl. hornblende, mgt. magnetite, ms. muscovite, ol. olivine, opx. orthopyroxene, pl. plagioclase, qz. quartz, ser. sericite, st. staurolite.*
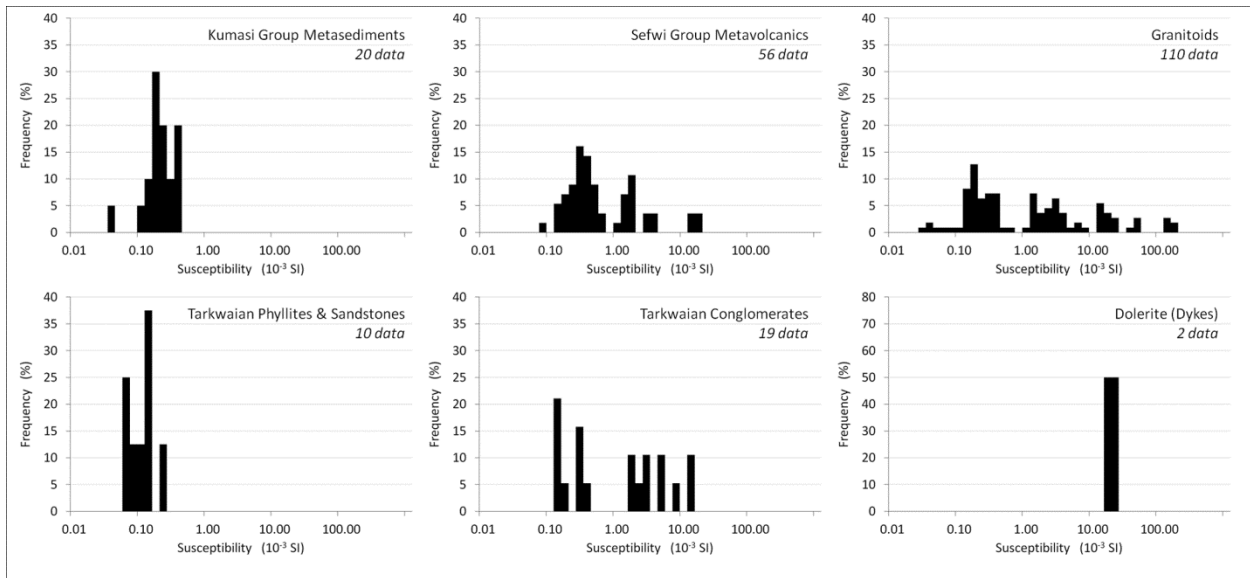
Figure I-7   *Histograms showing the range of measured susceptibility for each rock type found in the area. Several samples were remeasured under laboratory condition to confirm the field based data. The susceptibility of sediments is commonly ten times lower than volcanic rocks. Granitoid susceptibilities are variable with the highest values obtained from dioritic composition. Late doleritic dykes display high magnetic susceptibility values.*

Unit		Density Ranges (g/cc)		
		This Study	(Baratoux et al., 2011)	(Hasting, 1978*)
Dolerite (Sill and Dykes)		2.87 - 2.90	2.92 - 2.93	x
Mpohor Mafic Complex (Gabbro, Diorite)		2.65 - 3.03	x	x
Eburnean granitoids		2.58 - 2.75	2.60 - 3.25	2.41 - 2.76
Eoeburnean granitoids		2.76 - 2.89		
Tarkwaian (Conglomerates, Quartzites, Phyllites)		2.68 - 2.99	2.71 - 2.77	2.45 - 2.84
Kumasi Group (Birimian Phyllites)		2.69	x	2.71 - 2.74
Sefwi Group (Birimian -	Cape Coast Mica Schists)	2.65	x	x
	Volcanoclastics)	2.70 - 2.84	2.66 - 2.99	2.74 - 3.00
	Basalts / Andesites)	2.84 - 2.93	2.72 - 2.97	
	Gabbros)	3.01	3.07 - 3.11	

* Density ranges after Hasting (1978, unpublished report referenced in Barritt and Kuma, 1998)

Table I-5   *Ranges of density values measured on 26 samples of the main lithologies in Ghana (this study) and in Burkina Faso (Baratoux et al., 2011).*

Stratigraphic Column

P H A N E R O Z O I C (< 542 Ma)	> 1000 m	Sandstones and shales	

T A R K W A G R O U P (2107 – 2097 Ma)	> 1300 m	Huni Series Sandstones and phyllites *Cross-bedded stratification* Dolerite (Sills)	2097 ± 2 Ma, Oberthür et al., 1998 (Granitoid intrusion) 2102 ± 13 Ma, Adadey et al., 2009 (Gabbro)
	< 400 m	Tarkwa Phyllites	
	< 600 m	Banket Conglomerates *(Tarkwa Paleoplacer)*	< 2107 Ma (Detrital zircon) Reinterpreted after Pigois et al., 2003
	< 700 m	Kawere Sandstones Kawere Conglomerates	

K U M A S I G R O U P (2154 ~ 2125 Ma)	≈ 1100 m	Phyllites Volcanoclastics	2136 ± 19 Ma, Adadey et al., 2009 (Granitoid intrusion)
	≈ 700 m	Volcanoclastics	2142 ± 24 Ma, Adadey et al., 2009 (Andesitic volcanism)
	≈ 2000 m	Phyllites Volcanoclastics	< 2154 ± 2 Ma, Oberthür et al., 1998 (Detrital zircon)

S E F W I G R O U P (> 2174 Ma)	≈ 600 m	Basalts or Andesites	> 2174 ± 2 Ma, Oberthür et al., 1998 (Syn-tectonic granitoid intrusion)
	≈ 700 m	Volcanoclastics *Syn-sedimentary normal faults*	
	≈ 300 m	Basalts or Andesites	
	≈ 300 m	Phyllites	
	≈ 200 m	Volcanoclastics	
	≈ 400 m	Basalts or Andesites	
	≈ 700 m	Gabbros or Diorites Gabbros or Diorites	
	≈ 600 m	Basalts or Andesites	
	≈ 500 m	Volcanoclastics Mn Sediments	
	≈ 300 m	Basalts or Andesites (with Pillows)	
	≈ 200 m	Volcanoclastics	

Cape Coast Micaschists (> 3200 m)
Volcanoclastics
Volcanoclastics
Volcanoclastics

Figure I-8 *New stratigraphy for the southwest of Ghana based on new data from this study (mapping) and previous studies (Whitelaw, 1929; Junner, 1940; Kesse, 1985; Pigois et al., 2003; Adadey et al., 2009). Unit thicknesses are estimated from the map (Figure I-13). For clarity stratigraphic layers are labelled by their dominant lithology but could be subdivided into several sub-units.*
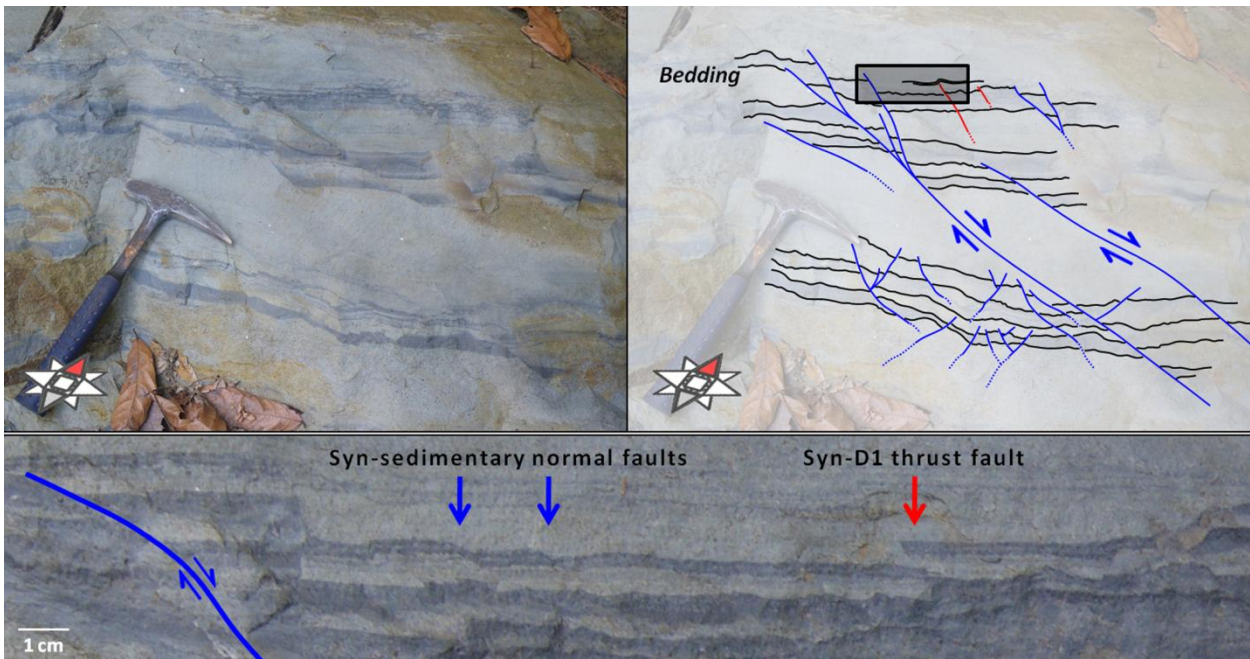
Figure I-9   *Photographs showing syn-sedimentary normal faults within Sefwi Group volcanoclastic sediments. Some of these faults do not affect the youngest layers. Others faults show post-depositional reverse movement that could reflect the start of D1. The compass indicates both the north (in red) and the perspective.*

2.4 Results

2.4.1 *Birimian stratigraphy*

Based on the lithologies encountered in the field, the stratigraphy of the Birimian Supergroup has been redefined in agreement with Adadey et al. (2009) nomenclature. Although individual units could be further subdivided into many thin individual layers, for clarity we have grouped these into the relatively schematic stratigraphy presented in Fig. I-8.

The Sefwi Group is composed of alternating micaschists, metavolcanics and intrusive rocks (Fig. I-8). Micaschists are mainly composed of quartz-muscovite-biotite, rare garnet that dominate the southeast of the Ashanti Belt (Fig. I-1). Metavolcanics consist of basalts (sometimes pillow-lavas, as near Butre village, east of Cape Three Point, Fig. I-1), andesites, gabbros and diorites that are found in the south of the Ashanti Belt proximal to major faults or shear zones. These metavolcanics are locally altered by quartz-sericite-carbonate hydrothermal alteration.

The Kumasi Group contains metasediments, volcanoclastics and phyllites that are locally rich in graphite. This group is found in two major areas corresponding to the Kumasi Basin and to the Akyem Basin (Fig. I-1).

2.4.2 *Structural evolution of the Ashanti Belt*

We have been able to distinguish six discrete deformation events which affected the Ashanti Belt during the Paleoproterozoic Eburnean Orogeny. These six events are defined on the basis of detailed structural analysis at the outcrop scale, and geophysical interpretation at the regional scale. These methods allow the correlation of structure across the study area, and can image overprinting relationships between successive deformation events.

The Sefwi Group represents a "basement" composed by a series of basalts and volcanoclastic sediments intruded by gabbros. To the west of the Benso gold mine, a volcanoclastic unit in the Sefwi Group displays syn-sedimentary normal faulting (Fig. I-9). Two thrust faults observed at this locality (Fig. I-9) may reflect reactivation of these syn-sedimentary normal faults during the early Eoeburnean phase.
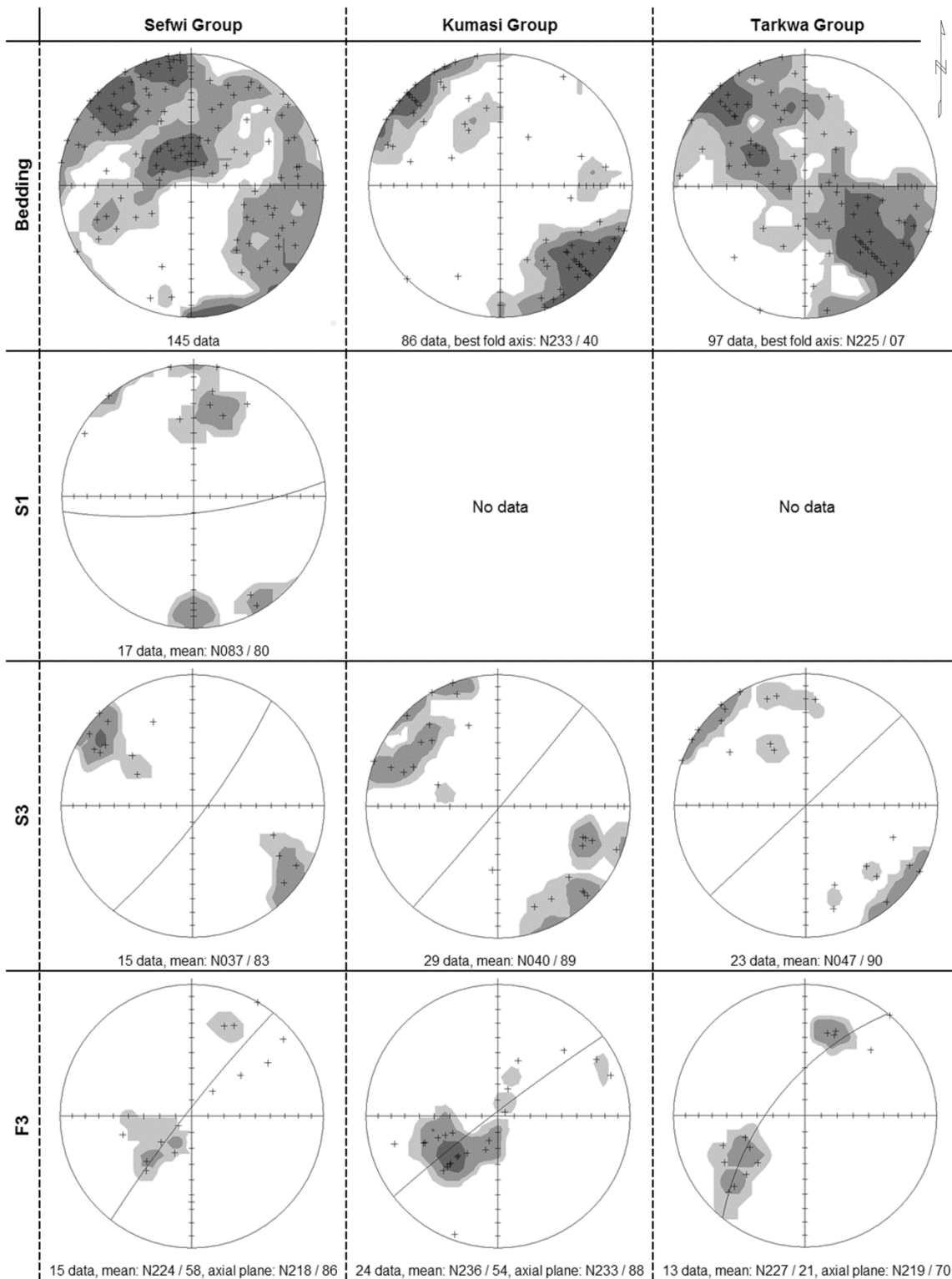
Figure I-10A *Stereo-plot diagrams representing measurement distribution on equal area diagram (lower hemisphere), with density contours, for the three main rocks groups. Distribution of the Kumasi Group and Tarkwaian sediments bedding poles are in good agreement with the F3 folding (and S3 cleavage orientations). In contrast the Sefwi Group bedding poles plots shows a wider dispersion resulting from the interference of multiple fold generations (mostly F1 and F3). Stereo-plots of poles to S1 confirm the presence of the earlier event (D1) affecting only the Sefwi Group.*
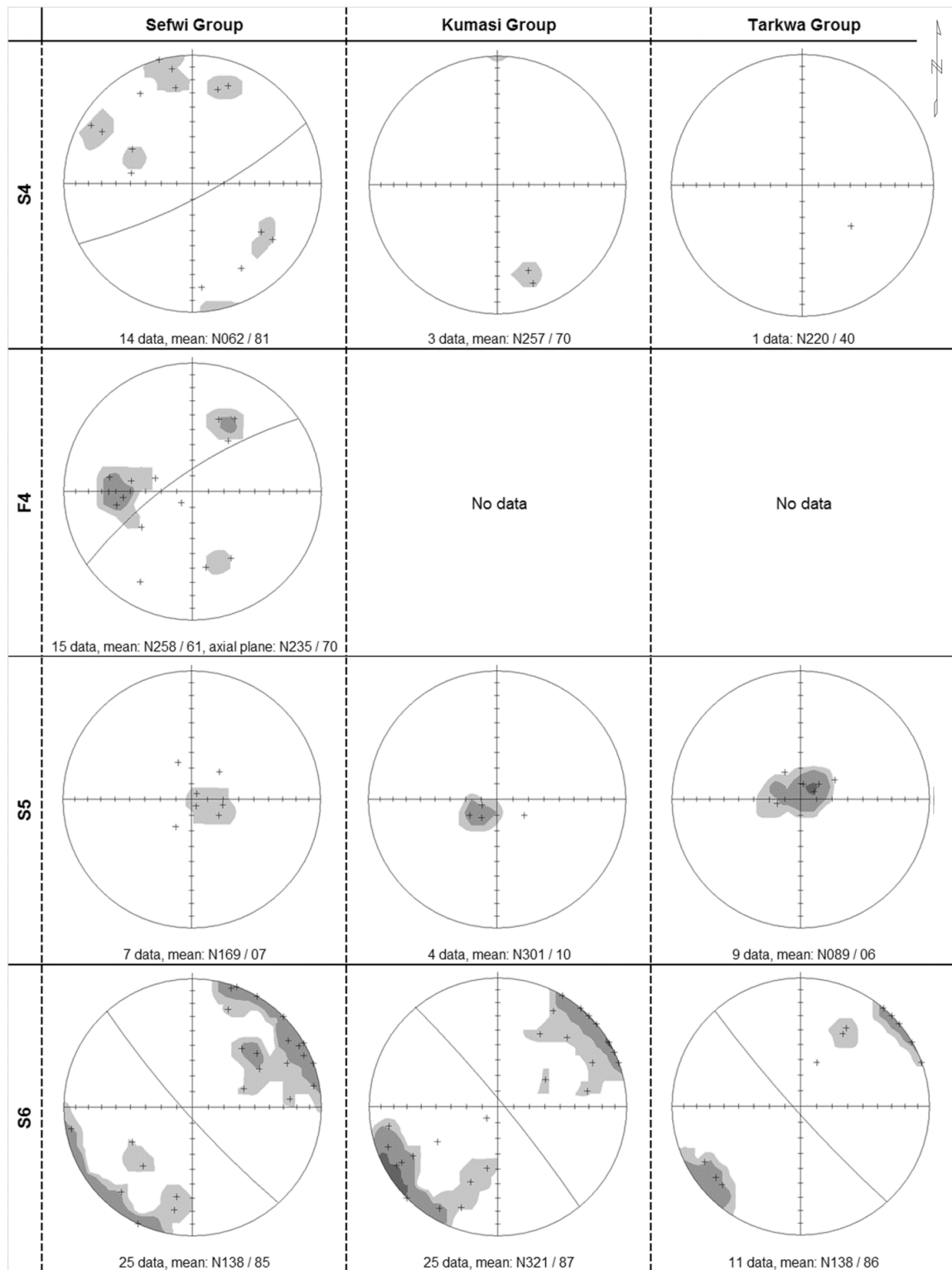
Figure I-10B *Stereo-plot diagrams representing measurement distribution on equal area diagram (lower hemisphere), with density contours, for the three main rocks groups. D4 data are predominantly from the Wassa mine (Sefwi Group), although the S4 cleavage is also observed in the Kumasi Group and in the Tarkwa Group along the Ashanti Fault. S5 is sub-horizontal and consistent across each group. S6 corresponds to subvertical crenulation cleavage striking NW-SE.*

2.4.2.1 *D1 (Eoeburnean)*

Our D1 corresponds to N-S shortening that produced kilometric scale folds within the Sefwi Group. Near Shama village in the SE of the Ashanti Belt, rare field evidence of D1 deformation exists as highly deformed micaschists that alternate with basaltic layers. The relatively competent basalts are strongly boudinaged and define a bedding parallel S1 foliation. In other regions, S1 is oriented approximately E-W (Fig. I-10A) and is defined by the alignment of biotite (Fig. I-11A). Large-scale F1 folds are imaged using high-resolution radar revealing major F1 folds within volcanoclastic units (S0) of the Sefwi Group that are refolded by F3 folds (Fig. I-6).

Two discrete generations of quartz veins and pegmatite intrusions are distinguished. Early veins and intrusions are sub-parallel to bedding and often strongly boudinaged. According to their extension direction (subvertical at the time of formation for veins parallel to bedding), they should have formed pre or syn-D1. Second generation veins and pegmatites cross-cut this composite S0-S1 fabric and were developed during D1. Both generations are refolded during subsequent D3 shortening.

D1 deforms only the Sefwi Group basement, and is not observed in the overlying Kumasi and Tarkwa groups. This relationship suggests that these younger sedimentary packages were deposited after D1 and before subsequent deformation events (D3-D6).

2.4.2.2 *D2*

D2 corresponds to an extensional phase associated with the opening of the Kumasi and Akyem basins into which the Kumasi Group was deposited (Fig. I-1). On the western side of the Ashanti Belt at the Prestea and Bogoso mines, the west-dipping Ashanti Fault marks the contact between Sefwi Group basement and Kumasi Group sediments. The early history of this fault contact is obscured by significant thrust and shear reactivation during D3 and D4.

On the eastern side of the belt, in Damang, the Sefwi/Tarkwa Group contact has been faulted and sheared during later deformation. This sheared contact is represented by a 2 cm thick anastomosed fabric that was probably created during D3/D4 shear reactivation of an original sedimentary contact (erosion surface), or by reactivation of an existing faulted contact that was controlling the development of the Tarkwa Basin in the eastern Ashanti Belt. As a consequence of a strong overprinting of the original sedimentary contacts during Eburnean deformation, the tectonic context of the Tarkwa Group deposition remains unclear.
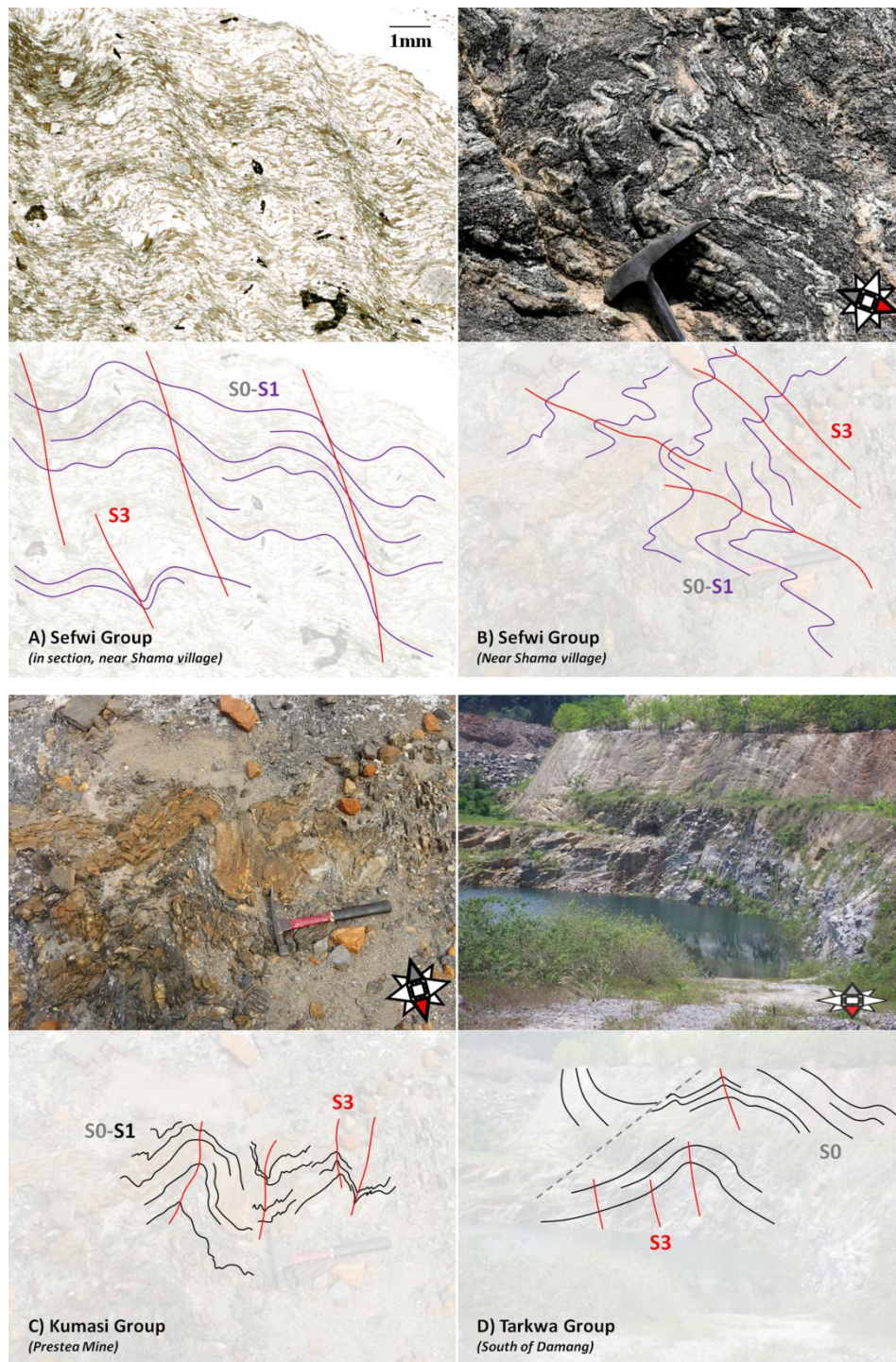
Figure I-11   *Interpreted photographs showing examples of D3 deformation. (A) In the Sefwi Group, the S1 foliation defined by the alignment of biotite is partially transposed along the S3 cleavage. (B) Series of F3 ptygmatic folds at the same location. These F3 are folding a composite S0 / S1 foliation and some quartz veins. (C) On the western side of the belt, F3 folds correspond to the first folding generation affecting the Kumasi Group sediments. (D) Parasitic open folds in the hinge of the Damang anticline in the Tarkwa Group. In all cases, S3 corresponds to a subvertical crenulation cleavage resulting from a NW-SE shortening. The compass indicates both the north (in red) and the perspective.*

63
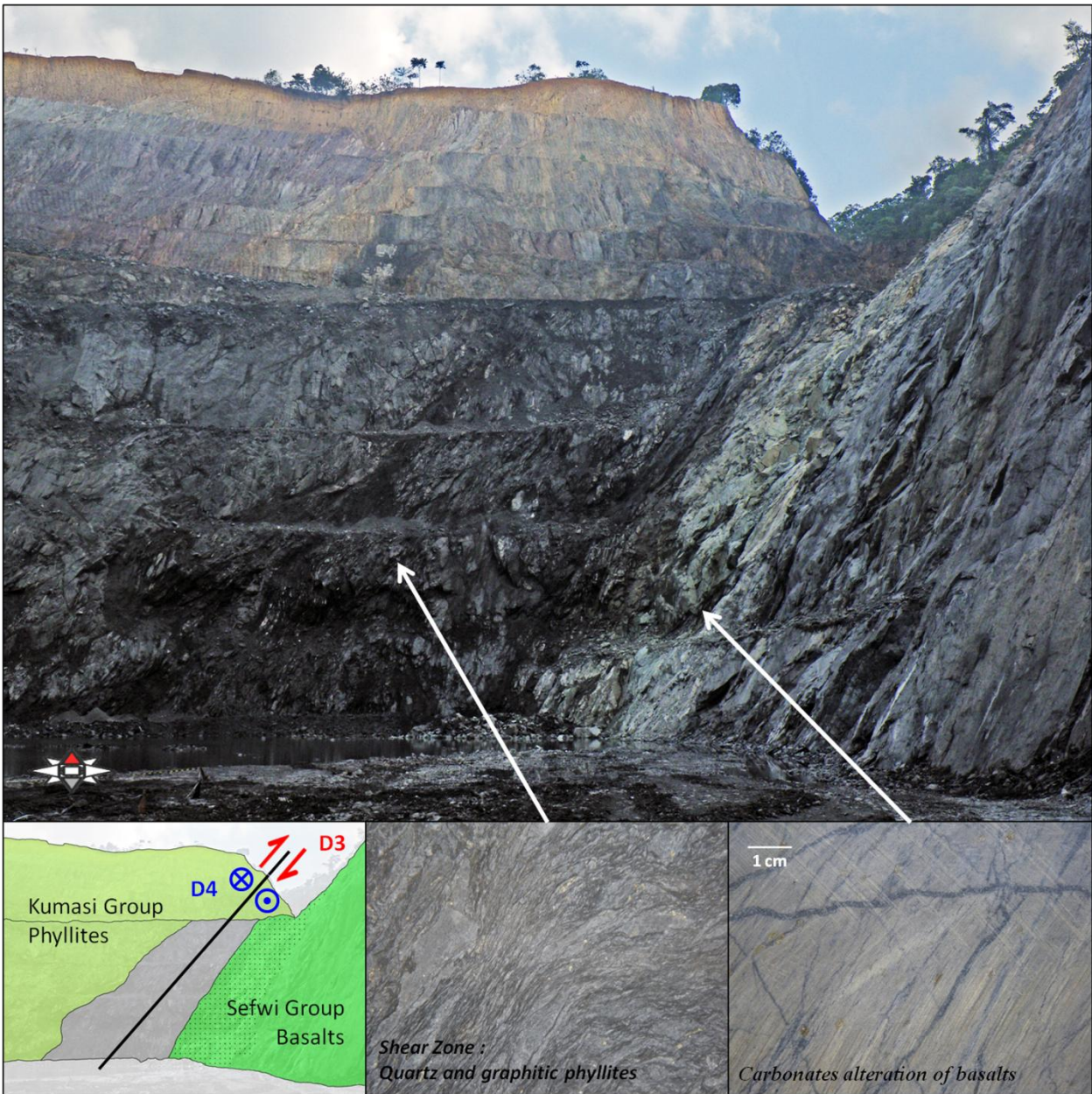
Figure I-12   *Interpreted photographs showing the Ashanti Fault in Buesichem Pit (Bogoso mine). The dark area in the middle corresponds to an approximately 20 m wide shear zone. This major structure separates the Kumasi Group phyllites from the Sefwi Group basalts. This shear zone operated as a thrust during D3 and was reactivated with a sinistral shear movement during D4. In the footwall, carbonatization of the basalts (light green band) is synchronous with gold mineralisation. The compass indicates both the north (in red) and the perspectives view. Photographs of lithologies are not oriented.*

2.4.2.3 D3 (Eburnean)

D3 deformation is conspicuous within both the Birimian and Tarkwaian units in the study area. NW-SE shortening produced km scale folds and a strong sub vertical crenulation cleavage within the Birimian and Tarkwaian units (striking around N040; I-10A). Stereonets of bedding from the Kumasi Group and Tarkwa Group define a single major folding event associated with NW-SE shortening. However, the orientation of bedding within the Sefwi Group reflects the interference between D1 and D3 folds (Fig. I-10A). The overprinting between F1 and F3 fold occurs across the region at multiple scales. In the Sefwi Group near Shama village, a composite S0-S1 foliation is crenulated and partially transposed along the S3 cleavage (Fig. I-11A). Ptygmatic F3 folds are also found where they affect both the S0-S1 and syn-D1 quartz veins and pegmatite intrusions (Fig. I-11B). Radar data images bedding in the Sefwi Group that is folded by E-W trending F1 folds that are refolded by N-S trending F3 folds (Fig. I-6).

The Kumasi Group phyllites in the Prestea, Bogoso and Pampe gold mines host isoclinal F3 folds from cm to m scale (Fig. I-11C) that deform the bedding and a bedding parallel cleavage (S1). Quartz veins that are folded by F3 often show strongly boudinaged fold limbs.

In the Tarkwa Group, D3 is characterised by regional scale folds that deform relatively resistant lithological layers (S0) that are imaged by the combined digital elevation model and radiometric data (Fig. I-4). At the outcrop scale, abundant parasitic F3 folds are observed with increases in frequency and amplitude toward major F3 closures such as the Damang mines anticline (Fig. I-11D). Major F3 folds are often open and low amplitude with NE-SW fold axis (Fig. I-10A). In this region, subvertical S3 cleavages strike NE-SW parallel to the main regional Ashanti thrust fault.

2.4.2.4 D4

In the Bogoso gold mine on the western side of the Ashanti Belt, many small scale shear zones cross-cut F3 folds. Most of these shear zones show sinistral displacements and are interpreted to have formed in response to a later phase of deformation that we identify as D4. Major splays of the Ashanti Fault were also likely reactivated during sinistral shearing associated with D4. At Bogoso, one of these main Ashanti structures is mineralised within a 20 to 30 m thick band of graphitic phyllites and quartz breccias that separate Kumasi Group phyllites from the Sefwi Group basalts (Fig. I-12). At the regional scale, magnetic images show at least two syn-D4 shear zone generations. The first one is oriented N030 and could correspond to the reactivation of D3 thrusts faults, such as the Ashanti Fault. The second is oriented N050 and cross-cuts earlier N030 shears, the F3 folds and the D3 thrusts within the Tarkwa Basin.

In the Wassa gold mine, within the Sefwi Group on the eastern border of the Tarkwaian sediments, a km scale F4 fold and associated parasitic folds overprint D3 faults and folds. F4 folds have only been observed at Wassa, although a subvertical S4 crenulation cleavage was found in many locations on both sides of the Tarkwa Basin. Intersection lineations between S3 and S4 cleavages and F4 folds axis give a plunge approximately 60° toward 260° (Fig. I-10B). These characteristics correspond to a NNW-SSE shortening event that could be compatible with a sinistral shear reactivation of existing D3 regional thrust faults.

2.4.2.5 *D5*

The regional architecture of the Ashanti region was largely built during D1-D4 but has been modified by two subsequent deformation events that are observed to overprint D4 structures within the Sefwi, Kumasi and Tarkwa groups.

D5 is characterised by recumbent folds associated with a subhorizontal crenulation cleavage (Fig. I-10B). These symmetrical open to tight folds have a wavelength varying between 5 m and 1 cm in the outcrops we studied. We note a great variability of amplitude between outcrops, varying with the lithology and orientation of previous structures. F5 folds were mainly observed in Wassa mine, in the NW of the belt (Pampe gold mine) and in the Tarkwaian sediments around Bogoso mine. In Damang mine, many quartz veins were subhorizontal and parallel to the S5 cleavage and formed either during or after D5.

2.4.2.6 *D6*

The final deformation event observed in the study area presents as a subvertical crenulation cleavage (S6) that defines open folds that affects subhorizontal S5 crenulation cleavage. S6 was observed in Tarkwaian sediments, in the Kumasi Group near the Akropong fault and in the Wassa gold mine. S6 is subvertical and NW-SE trending (Fig. I-10B) approximately parallel to a series of reverse faults oriented NW-SE identified from the magnetic data. These faults cross-cut all Paleoproterozoic lithologies and earlier fault and cleavages. They were observed in the field at the Mpohor and Damang gold mines. The absence of observed overprinting of S6, and its relatively constant orientation, suggest that this D6 event was likely the last significant deformation event to affect the area.
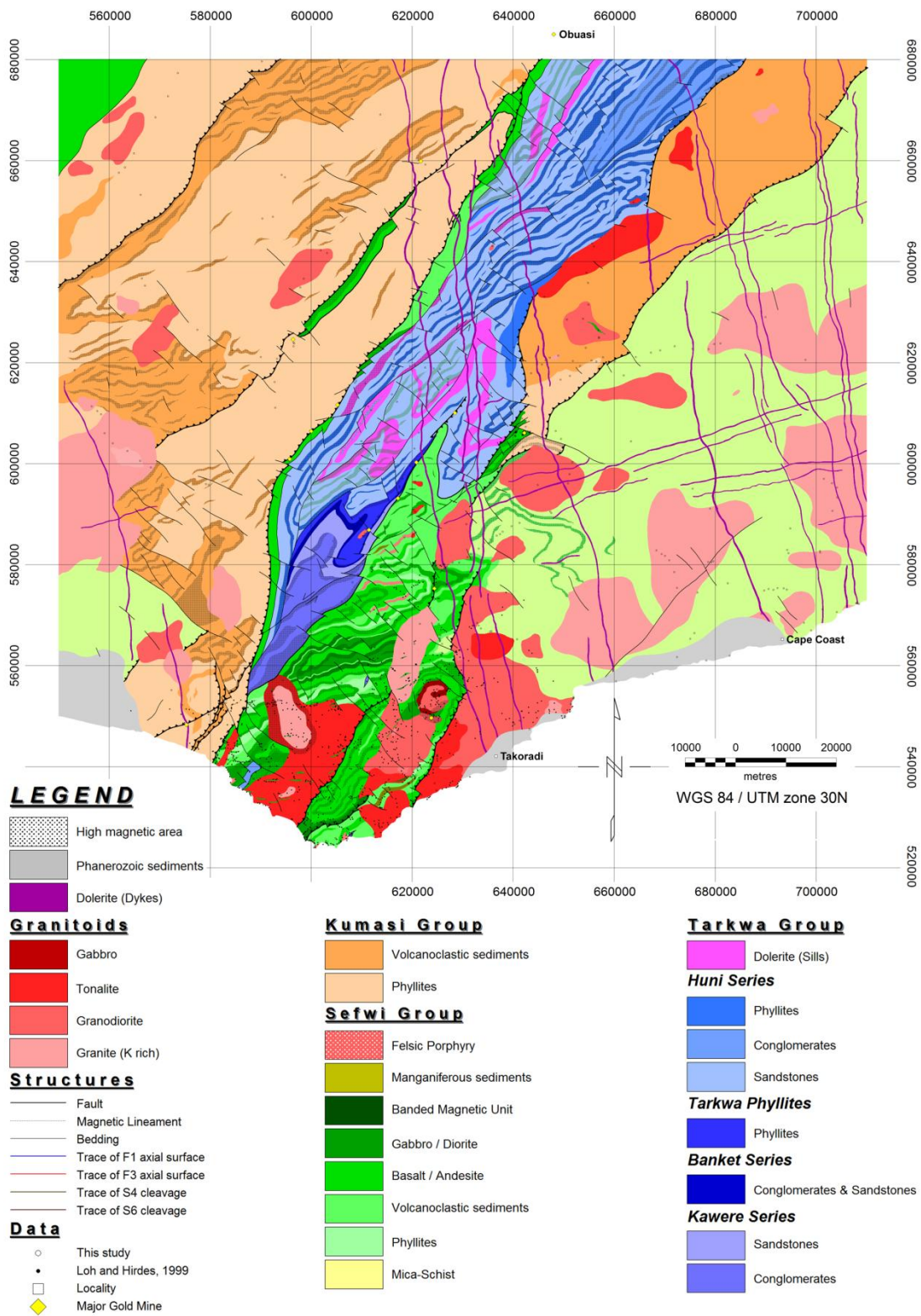
Figure I-13A
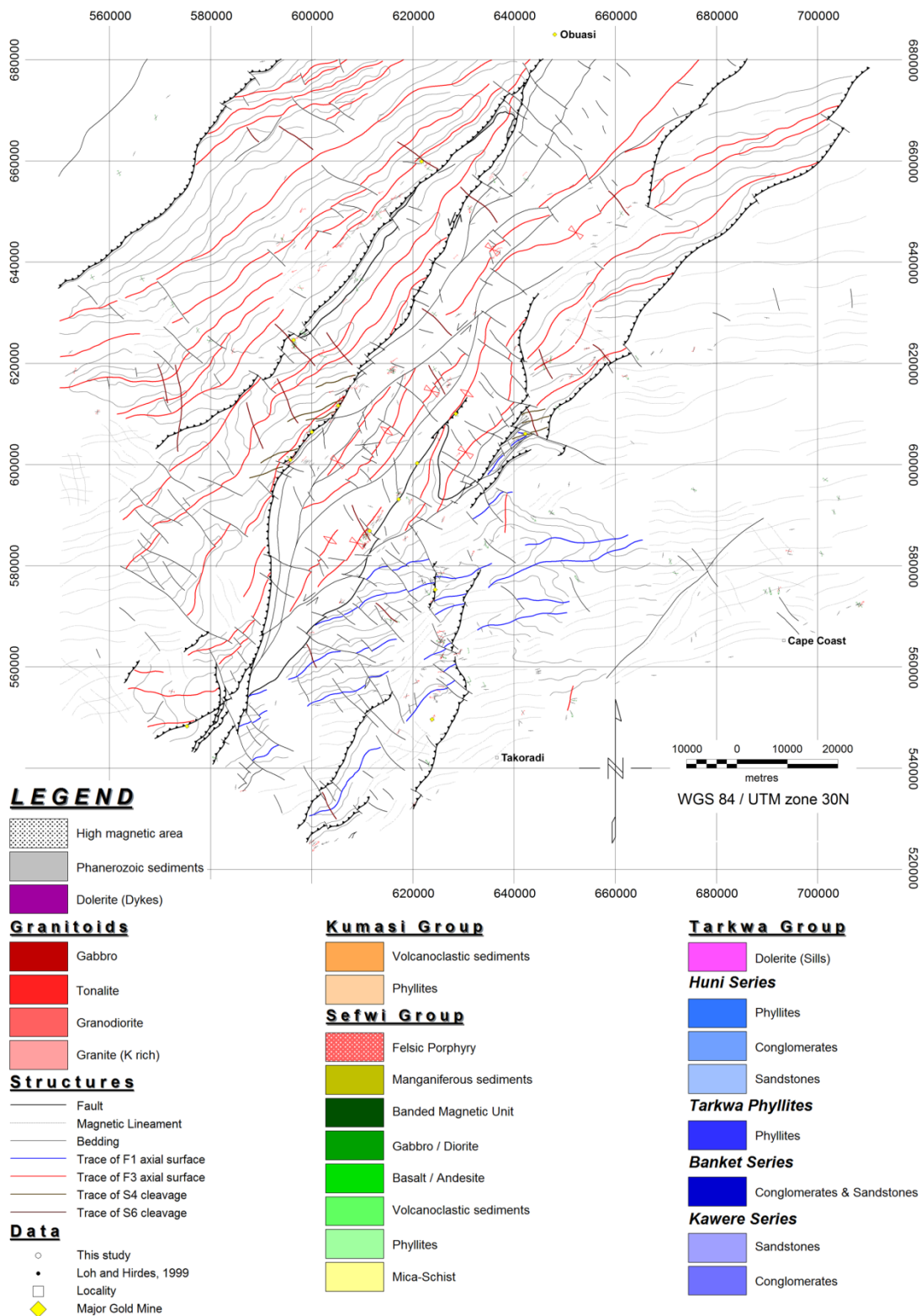
Figure I-13B *New lithological (A) and structural (B) interpretation based on the integration of new field observation, geophysical data and previous work. F1 folds built the regional geometries of the Sefwi Group metavolcanics. F3 folds are dominant in the Kumasi Group and Tarkwa Group sediments. D4 corresponds with a series of sinistral shear zones outlining the edge of the Tarkwaian sequence and cross-cutting it. S4 cleavage planes are oriented NE-SW and are observed around Bogoso/Prestea and Wassa. D5 is a minor event and is not represented as it is a subhorizontal cleavage. D6 is characterized by reverse faults oriented NW-SE.*

68

2.4.3 *Map*

Field observations, combined with geophysical and radar data have allowed the construction of a new structural and geological model of the region (Fig. I-13). This model describes the complex series of deformation events that affected the Sefwi Group basement and overlying Kumasi and Tarkwa groups during the Eburnean Orogeny.

2.4.4 *Sefwi Group D1 structures under the Tarkwa Basin*

During the regional geophysical interpretation several significant differences between features observed in the digital elevation model, radiometric and radar data (which reflect near surface lithologies and structures, Dickson and Scott, 1997) compared to the aeromagnetic data over the Tarkwa Basin were observed. Orientation of regional magnetic trends are inconsistent with observations made in the field (Tarkwaian bedding, S3 cleavage) and features imaged in the radiometric / radar data (e.g. F3 regional folds imaged in the combined radiometric / radar image do not appear in the magnetic data, Fig. I-14).
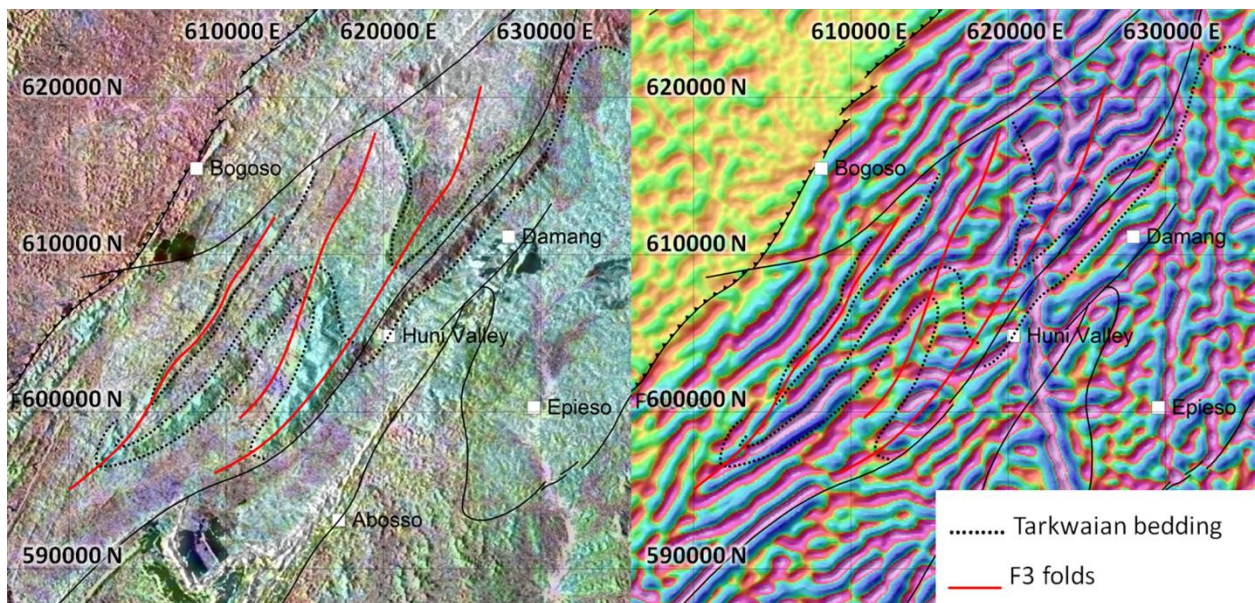
Figure I-14   *Detailed comparison of radiometric (over HH radar polarization) and magnetic data (RTP, first vertical derivative after automatic gain control). The magnetic trends do not correlate with bedding (S0) or S3 orientations observed in the Tarkwa Group that are well imaged in the radiometric data. These trends may correspond to older Sefwi Group lineaments (related to D1) beneath the Tarkwaian sediments. See Figure I-1 for location.*
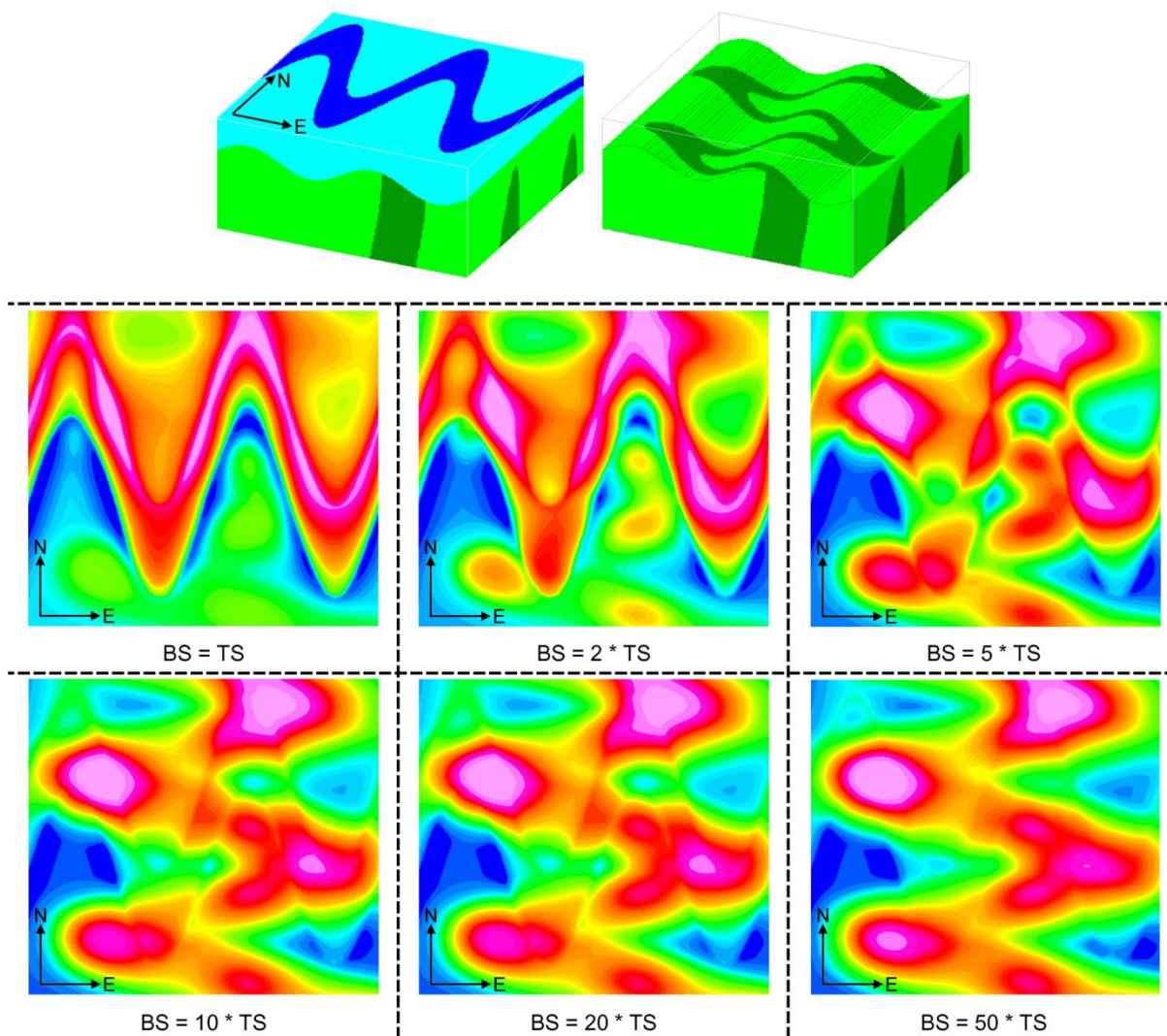
Figure I-15   *Test of susceptibility impact of deep units on magnetic RTP image. These tests were conducted using Noddy software assuming a 3000 m maximum depth for the Tarkwa Basin with various susceptibility contrasts between the Sefwi Group (BS) and the Tarkwa Group (TS) susceptibilities. We note that the Sefwi Group structures (folds in this example) are imaged beneath the Tarkwa Basin when the Sefwi Group is at least 5 times more susceptible than the overlying Tarkwa Basin.*

Previous studies (Table I-2) have estimated the total thickness of Tarkwaian sedimentary layers from 1000 to 3000 m. Assuming a maximum 3000 m depth for the Tarkwa Basin, several tests (Fig. I-15) with various susceptibility contrasts were conducted using Noddy software (Jessell, 1981, 2001, Jessell and Valenta, 1996). The models suggest that in order to image structure in the buried Birimian basement, the Birimian must contain lithologies with approximately 5 times greater susceptibility than the overlying Tarkwa Group. Measurements of magnetic susceptibility within the Tarkwaian sediments show values that are indeed significantly

lower (10 times or more) than the underlying Sefwi Group metavolcanics, with the exception of the few conglomerate layers. It is therefore possible that the magnetic data are not imaging structures within the Tarkwa Group but rather the structures in the underlying relatively magnetic Sefwi Group metasediments and metavolcanics. With this in mind we can interpret trends in the magnetic images as D1 structures in the Sefwi Group that formed prior to the deposition of the Tarkwaian sediments.

2.4.5 *Forward modelling*

Forward-modelled geological cross-sections (Fig. I-16) across the Ashanti Belt and Tarkwa Basin were constructed in order to understand and illustrate the structural relationship between the Birimian and Tarkwaian units produced during D1 and D3 shortening events. These sections are geologically consistent with the regional interpretation and the field observations. Forward-modelling was performed to ensure that geological cross-sections were also geophysically consistent with aeromagnetic, gravity and petrophysical data. Not all features within these models produce a perceptible geophysical contrast but are otherwise in agreement with the geological observations made within the study area.

Modelling was performed using Oasis Montaj GM-SYS software that utilises the algorithm of Talwani et al. (1959) and Talwani and Heirtzler (1964) to calculate the gravity and magnetic response of two-dimensional polygons. Construction of these integrated geological and geophysical models involved creating a traditional geological cross-section that was assigned values of magnetic susceptibility and density. The different fold trends in the Birimian and Tarkwaian units are represented in 2D by different fold wavelengths, amplitudes and positions of fold axes as they occur in the plane of the section. The geophysical response of this model was then calculated and compared to the observed aeromagnetic and gravity anomalies. The geometry and magnetic susceptibility/density values assigned to each rock package were then manipulated within geologically reasonable limits to improve the agreement between the model response and the observed response.

Magnetic susceptibility ranges for the modelled rock packages were based on field and laboratory susceptibility measurements (Fig. I-7). The Kumasi Group metasediments (volcanoclastics and phyllites) show low susceptibility values (less than 10^{-3} SI) an order of magnitude lower than the Sefwi Group metavolcanics rocks (10^{-2} for basalts and gabbros) with anisotropies below 20%. High magnetic susceptibilities were mainly related to hydrothermal magnetite-rich layers within metasediments.

The Tarkwaian quartzite and phyllite display low susceptibilities (around 10^{-4} SI) related to rare detrital magnetite and biotite. However, some sandstone layers showed sedimentary structures that were defined by magnetite grains, resulting in local but important increases in magnetic susceptibility. Anisotropies within these Tarkwaian sediments were up to 56%. Magnetic variability observed within Tarkwaian conglomerates is likely caused by the presence of magnetic pebbles derived from the Sefwi Group metavolcanics rocks or granitoids. An average value of 10^{-3} SI has been used for modelling.

Granitoids displayed large ranges of magnetic susceptibility varying between 10^{-4} SI for the granites and 10^{-1} SI for the diorites. We assumed a mean value of 5×10^{-3} SI in the models. Generally, more mafic units had higher magnetic susceptibilities. Anisotropy maxima are 8% for undeformed granitoids and 23% for the deformed granitoids.

Doleritic dykes correspond to one of the most magnetic lithologies in SW Ghana. They are magnetically isotropic (3%) with an average susceptibility approaching $2*10^{-2}$ SI. These dykes show strong remanent magnetisation of around 3 A/m, with declination of 59° and inclination of -18°.

The dominant magnetic response of the study area is located over the Tarkwa Basin where a complex series of high amplitude ($\approx$100 nT), linear anomalies that trend approximately parallel to the Ashanti Belt are imaged. These anomalies are predominantly produced by magnetic dolerite sills within the Tarkwa Group along with major faults within and along the margins of the Tarkwa Basin that host hydrothermal magnetite. In contrast, faults hosted entirely within the Birimian Supergroup such as the Akropong or the Twifo Praso faults do not produce significant magnetic anomalies. The strongest magnetic anomalies in the region lie to the east of the Tarkwa Basin within highly magnetic Sefwi Group metavolcanics (Fig. I-3). These rocks produce very high amplitude ($\approx$400 nT) broad anomalies over an area of 30 km^2 around Wassa mine. Other dominant magnetic features include NNW trending dolerite dykes that present as high amplitude ($\approx$100 nT) moderately remnant irregular linear anomalies.

The geometry and distribution of the magnetic lithologies were built into the forward-models based on the regional geophysical interpretation (Fig. I-13), field observations, magnetic susceptibility data (Fig. I-7) and gravity data (Table I-5). Significant differences exist between the observed and calculated magnetic anomalies. These differences consist of low amplitude (< 30 nT), short wavelenght anomalies that were not able to be modelled using the previously described magnetic lithologies. Field observations indicate the presence of a 20 m to 80 m thick weathered layer at the surface. This unit corresponds to thick lateritic successions that blanket

most of the study area and contains highly variable magnetic susceptibilities related to the initial lithology and the degree of alteration and weathering. This lateritic horizon was modelled as a 50 m thick homogenous layer. It does not have any influence on the wavelengths at the scale of our modelling but it does reduce the amplitude of near-surface features. Given that we see this layer in the field it would be worse to ignore it altogether, even though we acknowledge that the thickness variations are unknown. Residual magnetic anomalies reflect mostly the variations of susceptibility and thickness within this weathered layer.

Poor gravity coverage over the study area meant these data were only able to broadly constrain the depth of the relatively dense Sefwi Group basement. Density values (Table I-5) used during the gravity modelling spanned the range proposed by Baritt et al. (1998) and Hasting et al. (1982), using 3.0 g/cm^3 for gabbros, 2.9 g/cm^3 for basalts and dolerites, 2.8 g/cm^3 for Eoeburnean granitoids, 2.7 g/cm^3 for both volcanoclastics, phyllites and Eburnean granitoids and 2.65 g/cm^3 for the micaschists. The surficial weathered layer was given a density of 2.6 g/cm^3.

Gravity anomalies are dominantly controlled by the distribution of the relatively dense metavolcanic group (Sefwi Group) and the less dense metasedimentary groups (Kumasi and Tarkwa groups). The small differences between the observed and modelled gravity anomalies are difficult to determine given the model resolution is higher than the gravity data.

2.5 <u>Discussion</u>

2.5.1 *Eoeburnean phase (2187 – 2158 Ma)*

Paleoproterozoic rocks of the southern Ashanti Belt were strongly deformed, mineralised and intruded by granitoids during the "Eburnean Orogeny" (Fig. I-17). Previous interpretations of the regional tectonic evolution (e.g. Allibone et al., 2002a; Feybesse et al., 2006) suggest the Eburnean Orogeny initiated during the first phase of volcanic accretion and subduction that could correlate to D1 deformation. This hypothesis is in agreement with the interpretation of Sefwi Group mafic and ultramafic rocks as an ophiolitic suite (Attoh et al., 2006; Dampare et al., 2008). Our structural interpretation gives this accretionary phase a structural context whereby N-S shortening during D1 produced regional scale E-W trending folds within the Sefwi Group along with the intrusion of syn-tectonic granitoids (Fig. I-13).
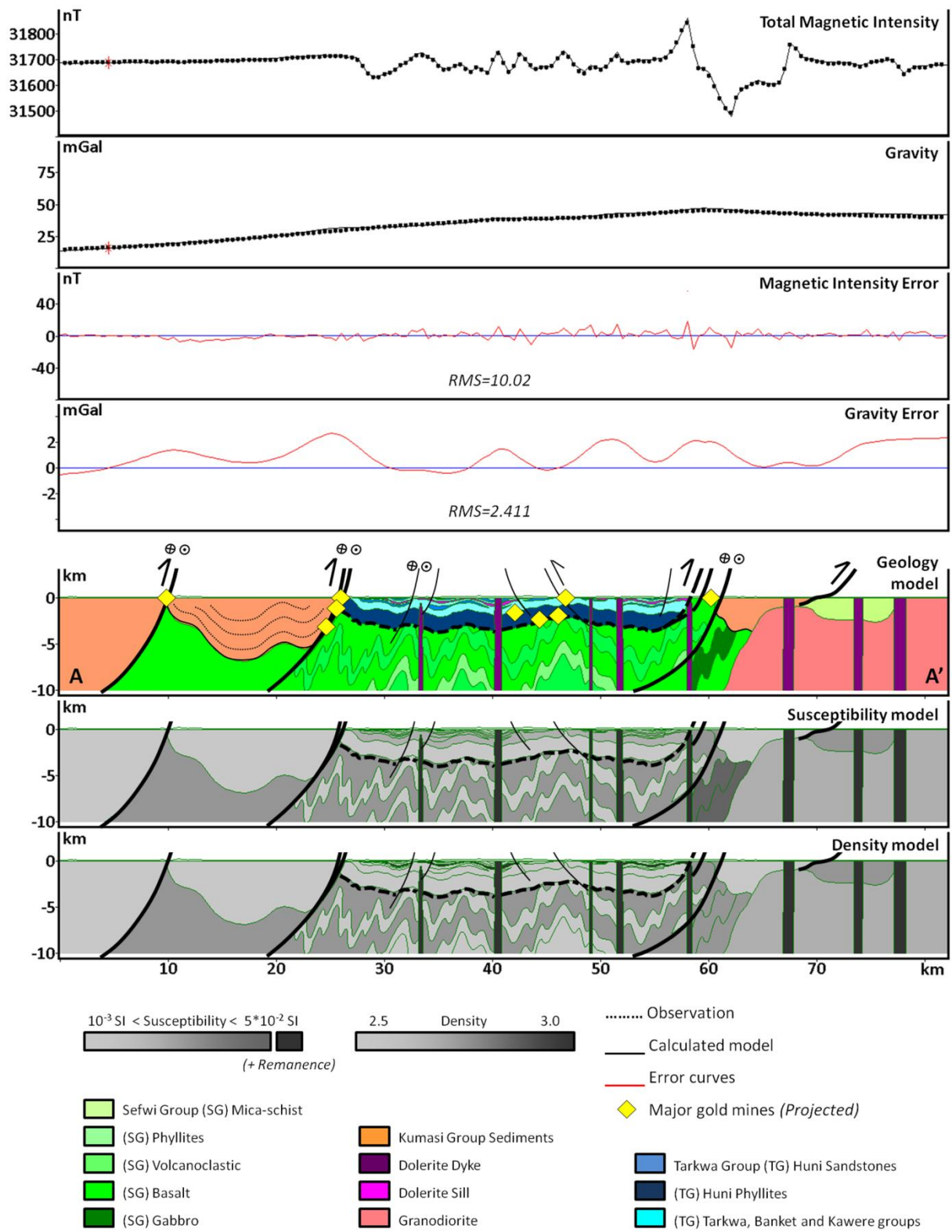
Figure I-16A
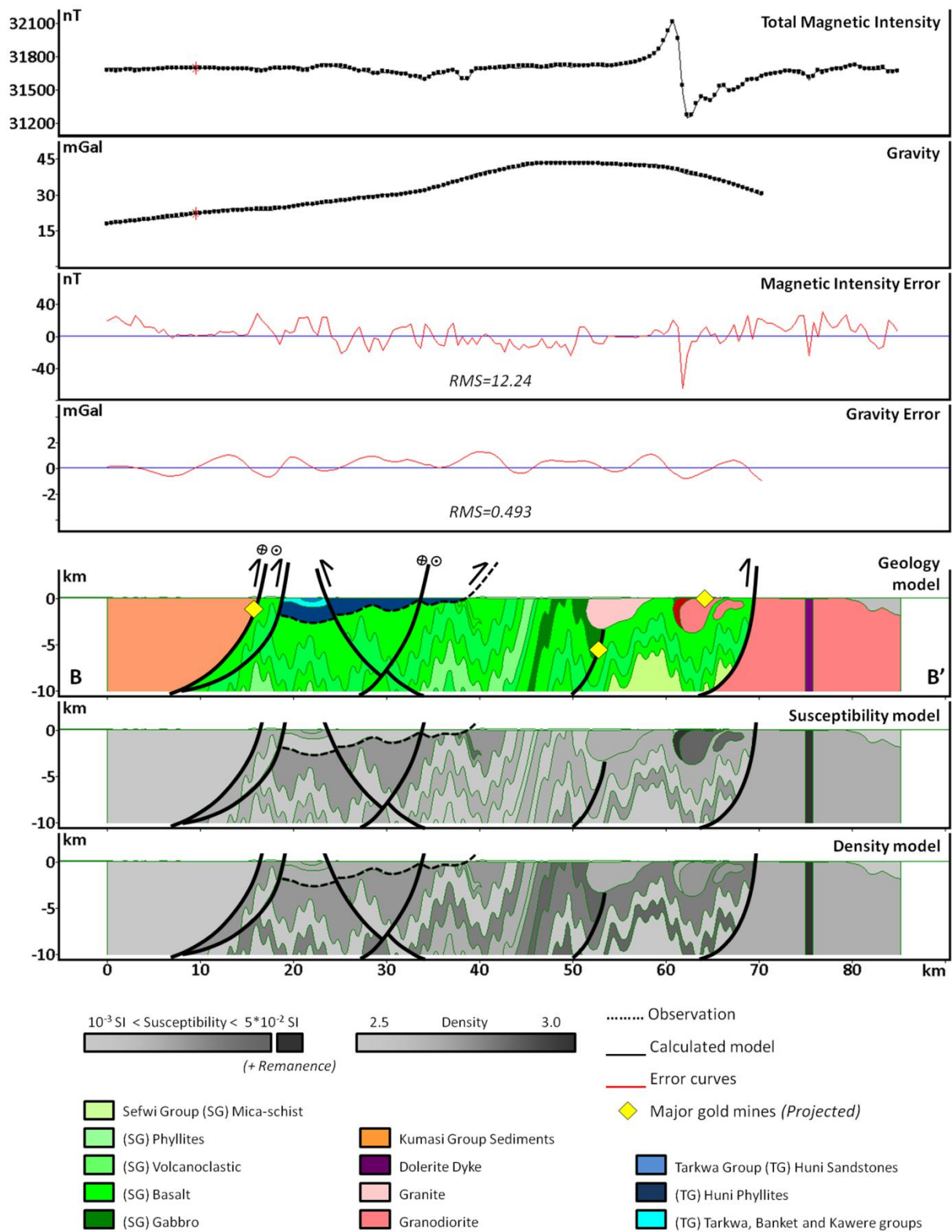
Figure I-16B *Forward-modelled cross-sections across the Ashanti Belt. See Figure I-1 for location of these sections. These models highlight the mineralised Birimian/Tarkwaian contacts. Sefwi Group metavolcanics were highly deformed during the D1 and contrast with the more open syn-D3 folding in the Tarkwa Basin. Kumasi Group sediments on the western side of the Ashanti Fault were also deformed by D3. Major gold deposits have been geometrically projected onto their structural position.*
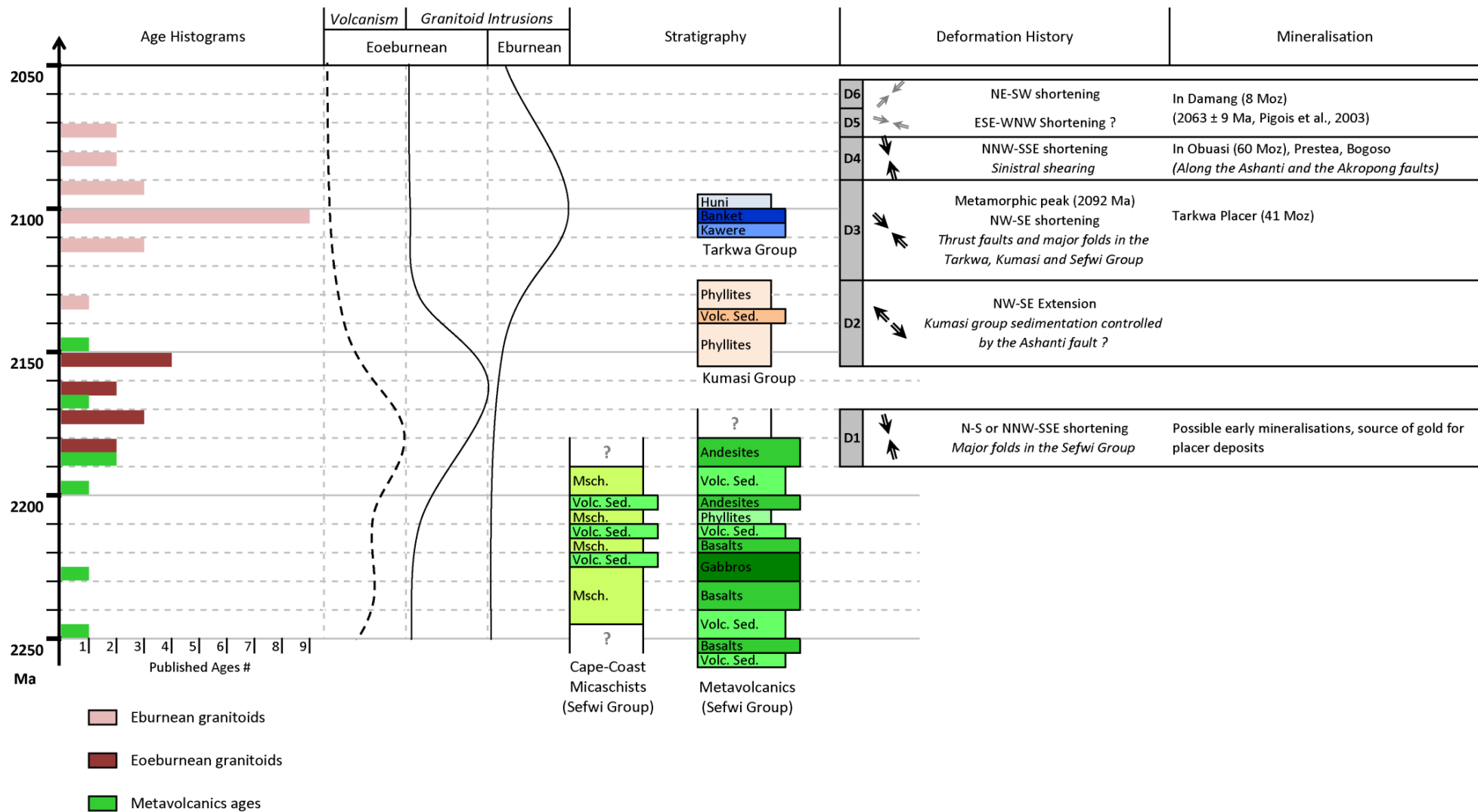
Figure I-17 *Correlations between stratigraphic sequences, magmatism, deformations and mineralisations in southwest Ghana. The Cape Coast micaschists are not constrained by absolute or relative ages.*

D1 occurred across southeastern part of the Ashanti belt (Fig. I-13) and below the Tarkwa Basin (Fig. I-14). In Obuasi, Allibone et al. (2002a) described transfer faults and lineaments oriented E-W that were attributed to their NW-SE D2 shortening (our D3). The Obuasi deposit is mainly hosted within Kumasi Group metasediments. However, minor exposures of metavolcanics indicate the presence of the Sefwi Group basement at shallow depths. It is therefore possible that D1 deformation also affect this basement, developing E-W trending structures under a regional N-S shortening regime. Some existing D1 structures may have been reactivated during D3 (NW-SE shortening) and initiated as transfer faults such as those observed in the Obuasi mine. D1 deformation also explains the presence of the E-W lineaments reported by Allibone et al. (2002a, fig. 5, p. 72).

Deformed granitoids such as those found in Sekondi (Loh et al., 1999), help constrain the timing of this Eoeburnean deformation phase (D1). Linear magnetic anomalies in this granitoid are sub-parallel to the dominant S1 in the Birimian micaschist. Consequently, we suggest that this intrusion, dated at 2174 ± 2 Ma (Oberthür et al., 1998), is contemporaneous with D1. The undeformed Dixcove tonalite suggests that peak D1 deformation occurred before 2171 ± 2 Ma (Hirdes et al., 1992).

2.5.2 *Kumasi Group deposition (2154 – 2125 Ma)*

Eoeburnean tectonism produced magmatism between approximately 2187 and 2158 Ma and deformation that occurred before 2171 Ma. The Eoeburnean event predates deposition of the Kumasi Group sediments, and was only observed within the Sefwi Group basement. This places the deposition and lithification of the Kumasi Group between D1 and D3.

The Kumasi Group within the Kumasi and the Akyem Basins (Fig. I-1) formed under an extensional regime during D2 (Stage 4 of Feybesse et al., 2006), where major faults (e.g. Ashanti, Akropong faults) behaved as primary basin forming structures and possible detachment surfaces prior to reactivation as D3 thrust faults. Direct evidence for an extensional origin for the Ashanti Fault is obscured by the strong overprinting (D3 thrust and D4 strike-slip movement, Allibone et al., 2002a). However, the opening of the Kumasi Basin required the generation of an extensional fault architecture that have been favourably orientated to undergo reactivation during D3 shortening.

The strong magnetic and gravity contrasts across the Ashanti Fault (Fig. I-5, I-16) suggests large amounts of vertical displacement have juxtaposed rocks with contrasting petrophysical properties. The absence of metamorphic gradient across the Ashanti Fault is not

consistent with significant vertical thrust movement during D3 shortening. Consequently, we propose the Ashanti Fault was initiated as a half-graben during D2 deformation. Evidence of a widespread D2 extensional phase has also been identified in northwest Ghana, where De Kock et al. (2011) proposed a significant period of rifting between 2148 Ma and 2125 Ma. This timing is consistent with the deposition of the Kumasi Group between 2154 ± 2 Ma (youngest U/Pb age on zircon found by Oberthür et al., 1998) and 2136 ± 19 Ma (Granitoid intrusion, U/Pb on zircon, Adadey et al., 2009.

Adadey et al. (2009, p. 80) reported an early deformation in the Kumasi Group that was interpreted as pre-diagenetic slumping. This deformation is characterised by rare isoclinal fold-like structures that are coaxial with deformation that affected both the Birimian and Tarkwaian units (our D3). These folds could have resulted from Eburnean D3 deformation that intitiated after the deposition of the Kumasi Group and before the Tarkwaian sedimentation. This hypothesis is also consistent with observations of an early bedding parallel cleavage in the Kumasi Group by Allibone et al. (2002a). This layer parallel fabric is interpreted it as resulting from bedding-parallel shearing (their D1, our D3) during the early Eburnean Orogeny that is absent in the Tarkwa Group.

2.5.3 *Tarkwa Group deposition (2107 – 2097 Ma)*

The Tarkwa Group occurs as a synclinal erosional remnant overlying the metavolcanic Sefwi Group in the Ashanti Belt. The timing and nature of the contact between the Tarkwa Group and the Birimian Supergroup is not clear, but probably represents an unconformity or faulted contact. Both margins of the preserved Tarkwa Basin are represented by major faults. These faults may have been important during the early evolution of the Tarkwa Basin; however, strong reactivation obscures their early history.

The presence of early deformation in the Kumasi Group metasediments is an indicator of the initiation of the Eburnean Orogeny before the Tarkwaian deposition. However, the majority of Eburnean deformation occured after the Tarkwaian deposition and after intrusions of metagabbro sills within the Tarkwa Group at 2102 ± 13 Ma (U/Pb on zircon, Adadey et al., 2009). It is therefore possible that the major D3 transcurrent structures such as the Ashanti Fault initiated before the Tarkwa Group sedimentation. Reactivation of the D2 Ashanti detachment fault with transcurrent movement may occur at the start of Eburnean D3 shortening and would have controlled the Tarkwaian deposition on its western side. Similar faults should exist on the eastern side of the basin, but are not observed due to intense overprinting.

This hypothesis of a Tarkwa Basin bordered by two major transcurrent faults is consistent with the presence of conglomerate and sandstones beds that alternate in the first 1000 meters of the Tarkwa Group. This syn-orogenic molasse and the presence of placer deposits along paleochannels (Sestini, 1973) suggest short transport distances in a shallow water environment that has also been proposed by Baratoux et al. (2011) in Burkina Faso and in the Abitibi or Yilgarn cratons within similar intra-orogenic basins (Eriksson et al., 1994).

2.5.4 *Eburnean phase (2125 – 1980 Ma)*

The post-Tarkwaian Eburnean event is clearly visible and well preserved in the field. D3 deformed the entire crustal pile made up of the Birimian Supergroup and the Tarkwa Group. Regional mapping shows a series of kilometric scale F3 folds in both the Kumasi and Tarkwa groups metasediments related to NW-SE shortening (Fig. I-13). D3 deformation in the Sefwi Group is associated with regional folding of the S1 foliation. An example of this relationship is found at Shama beach, where F3 ptygmatic folds affect bedding and a melt rich S1 foliation (Fig. I-11B). According to Milési et al. (1992) and Feybesse et al. (2006) D3 shortening was responsible for creating many of the major thrust faults as well as regional folding (e.g. the Ashanti and Akropong faults). The distribution of these thrusts is probably related to reactivation of the existing D2 extensional architecture. D3 thrusting along the Ashanti Fault is related to the metamorphic peak (550 °C and 5 kbar; John et al., 1999), dated at 2092 ± 3 Ma (Oberthür et al., 1998). D3 spans from approximately 2125 Ma to over 2092 Ma with major folding occurring after the Tarkwaian deposition at around 2097 Ma.

Observations along the Ashanti Fault zone around Prestea and Bogoso gold mines show an increase in the intensity of F3 folding on the western sides of fault contacts between Kumasi Group phyllites (west) and Tarkwa Group phyllites (east) (Fig. I-12C, I-12D). This asymmetry suggests strain was being preferentially partitioned into the Kumasi Group phyllites. On the other side of the belt, an angular unconformity between the Kumasi and Tarkwa groups sediments is imaged in the geophysical data. This unconformity suggests that Tarkwaian sediments may have been displaced eastward during D3 accommodated by a low angle thrust or decollement at depth.

Our mapping shows syn-D4 shear zones that both bound and cross-cut Tarkwaian sediments. Some of these structures overprint regional F3 folds. D4 structures including the Ashanti and Akropong faults, along with other syn-D3 thrust faults were reactivated via sinistral strike-slip movement during D4 (Allibone et al., 2002b). Two major F4 folds observed in the Wassa and Obuasi gold mines could have been developed during shearing (Allibone et al.,

2002a). By the end of the D4 (NNE-SSW shortening) the regional architecture was created and only weakly modified by successive events. D5 is characterised by small scale recumbent folds, resulting from a WNW -ESE shortening (Tunks et al. 2004). The final D6 event is associated with NW-SE oriented reverse faults identified in the field and in the geophysical data to overprint all earlier generation structures. D4, D5 and D6 deformation occurred approximately from 2092 Ma to 2063 Ma (estimated age of the mineralisation in Damang, Pigois et al., 2003)

Timing of the Eburnean Orogeny plutonism could be constrained by granitoid intrusion at 2136 ± 19 Ma (Adadey et al., 2009) and at 2116 ± 2 Ma (Hirdes et al., 1992) for its beginning, post or syn-sedimentation into the Kumasi Group, pre-sedimentation in the Tarkwa Group. Some undeformed potassium rich granitoid intrusions that overprint all previous structures could be related with the late stages of the Eburnean Orogeny. However, their ages have not been determined precisely yet (1973 ± 75 Ma, Pb/Pb date on whole rock, Taylor et al., 1992 and 1978 ± 37 Ma, Ar/Ar date on amphibole, Feybesse et al. 2006).

2.5.5 *Implications for Au deposits*

2.5.5.1 Timing of gold mineralisation and metamorphism

Gold mineralisation in the southwest of Ghana is divided in to two main hydrothermal events. The first period corresponds to the major gold deposits found along the Ashanti Fault (Prestea, Bogoso, Obuasi, Fig. I-1) and the Akropong fault (Ayanfuri, Pampe, Obuasi, Fig. I-1). Fluid inclusion studies on mineralised quartz veins suggest low temperature and pressure homogenisation conditions for all major deposits. These factors suggest that mineralisation occurred after the metamorphic peak (related to D3) and probably synchronously with D4 shearing (Oberthür et al., 1994, 1997).

The second hydrothermal event is associated with mineralisation along the Sefwi/Tarkwa groups contact on the eastern side of the belt (Abosso-Damang Mine, Fig. I-1) during D6. This mineralisation is dated at 2063 ± 9 Ma (U/Pb on xenotime) by Pigois et al. (2003) and represents the youngest known deposit in the region. The greenschist conditions for its formation are equivalent to the deposits found along the Ashanti Fault.

An additional mineralisation event is required to explain the origin of the Tarkwaian paleoplacer. This placer was developed during Tarkwaian deposition at the start of D3 and has long been considered to be sourced from aforementioned Sefwi Group gold deposits. This correlation is based on similar fluid inclusion chemistry between Tarkwaian quartz pebbles and Birimian (Sefwi Group) quartz veins (Klemd et al., 1993). However, the maximum depositional

age of the Tarkwaian sediments (2107 Ma) and their deformation during D3 is inconsistent, with placer deposits derived from mineralisation hosted in the Sefwi Group that formed during D4-D6 (Milési et al., 1991; Eisenlohr and Hirdes, 1992; Hirdes and Nunoo, 1994). The Tarkwaian paleo-placer therefore needs to be derived from earlier sources of gold.

As shown by our study, the Sefwi Group, in the southeast of the belt, displays strong pre-Tarkwaian deformation associated with significant plutonism. Although no syn-D1 deposits have been described in southwestern Ghana, they may represent early sources of gold that supplied the Tarkwaian Paleoplacer along with gold that was remobilised in shear zones during the Eburnean II orogenic phase. Possible Eoeburnean mineralised quartz veins have been suggested by Sestini (1973) and Kesse (1985). An Eoeburnean gold source is also in agreement with paleoflow indicators that suggest the Banket conglomerates were sourced from Birimian schist and volcano-sedimentary rocks to the east of the Ashanti Belt.

2.5.5.2 Regional distribution of the mines

If we look at the distribution of gold mines in the study area (Fig. I-13, I-16A), several deposits are located at or close to the margin of the Tarkwaian sediments. Prestea, Bogoso and Obuasi on the western side are located along a 500 m thick faulted and sheared area lying the contact (Ashanti Fault). On the eastern side of the belt, the Abosso-Damang deposits appear to lie directly on the Sefwi/Tarkwa groups contact.

In accordance with Feybesse et al. (2006), we suggest that D3 shortening lead to the development of a low angle decollement beneath the Tarkwa Basin that was responsible for transporting the Tarkwa Group to the east. Such a structure would be favourable for gold mineralisation (barrier for fluid flow), and would explain the distribution of many major gold deposits that are located on the margins of the Tarkwaian sediments. Further, gold along this structure would also be a possible source of gold for shear zone hosted deposits remobilised during D4.

2.6 Conclusions

This paper presents a new structural interpretation of the southern Ashanti Belt in southwestern Ghana. Utilising field observations, magnetic, radiometric, gravity and radar data, we distinguish at least 6 distinct deformation events that occurred in two phases (Eoeburnean and Eburnean) during the Paleoproterozoic (Fig. I-17). We also establish a new stratigraphy

(Fig. I-8) for the Birimian Supergroup (Sefwi Group and Kumasi Group). Our map (Fig. I-13) and sections (Fig. I-16) display a series of tight F1 folds that only affected the Sefwi Group basement. This group was overlain by the Kumasi Group during D2 extension and by the Tarkwa Basin that developed at the start of D3 shortening controlled by major transcurrent faults such as the Ashanti Fault.

Significant gold mineralisation may have occurred during both Eoeburnean and Eburnean phases. Quartz veins that formed during the early phase (Eoeburnean) may also represent the source of the gold rich quartz pebbles found in the Tarkwa paleoplacer. We suggest that many hydrothermal gold deposits in the Ashanti region were formed by remobilisation and concentration of syn-D1 gold along D4 shear-zones and the contact zones between the Birimian and Tarkwaian units during the Eburnean Orogeny.

2.7 Résumé du chapitre I

2.7.1 *Introduction*

Ce premier chapitre présente une nouvelle interprétation de l'évolution géodynamique du sud de la ceinture d'Ashanti, via une cartographie détaillée basée sur les observations de terrains et l'interprétation des données géophysiques. Les études de Feybesse et al. (2006) et d'Allibone (2002a) divisent l'Orogénèse Éburnéenne, définie par Bonhomme (1962), en deux phases de déformations (Éoéburnéenne et Éburnéenne, De Kock et al., 2011). Cependant, seule la seconde est décrite à l'échelle régionale. L'un des principaux objectifs de cette première étude sera donc de donner un contexte structural à la phase Éoéburnéenne, puis de préciser l'évolution géotectonique régionale.

2.7.2 *Géologie du sud-ouest Ghana*

Comme cela a été vu précédemment, la géologie du sud-ouest du Ghana se compose de trois unités stratigraphiques (Adadey et al., 2009), formées de roches métavolcaniques et métasédimentaires, qui sont les groupes de Sefwi (Birimien), de Kumasi (Birimien) et de Tarkwa (Tarkwaien). Cette stratigraphie Paléoprotérozoïque fut intensément déformée durant l'Orogénèse Éburnéenne (Bonhomme, 1962) et pénétrée par d'abondantes intrusions de granitoïdes TTGs (Tonalite, Trondhjemite, Granodiorite). La mise en place de dykes de dolérite et d'une couverture sédimentaire le long de la côte, au Protérozoïque et au Phanérozoïque, a achevé de construire la géologie régionale.

2.7.3 *Données géophysiques*

Les données géophysiques utilisées pour la cartographie correspondent à des données magnétiques et radiométriques aéroportées (acquises pour le Service Géologique du Ghana et maillées avec une résolution de 100 m), à des données de gravité (fournies par le Bureau Gravimétrique International, interpolées à 2,5 min d'arc, soit approximativement 4,6 km), à des données d'altimétrie radar (SRTM) et à des données radar (Palsar). Le traitement de ces données a permis la réalisation d'une série d'images interprétables pour l'identification des lithologies et des structures.

2.7.4 *Résultats*

L'interprétation des données géophysiques, couplée avec les observations de terrain ont permis la révision de la carte géologique régionale, avec notamment la mise en évidence de grands plis F1 affectant les roches métavolcaniques au sud-est de la ceinture d'Ashanti. La cartographie a également aidé à définir une nouvelle stratigraphie du groupe de Sefwi. L'étude structurale a montré la présence de six déformations significatives à l'échelle régionale, reliées aux deux phases de l'Orogénèse Éburnéenne.

L'observation des linéaments magnétiques non corrélés aux observations de surface dans le bassin de Tarkwa conduisit à leur interprétation en tant que structures Birimiennes enfouies sous le bassin de Tarkwa. Cette hypothèse fut testée par la réalisation de modèles Noddy (Jessell, 1981, 2001 ; Jessell et Valenta, 1996) suggérant que les structures enfouies sous un bassin sont observables si l'on considère une épaisseur de bassin inférieure à 3000 m pour un contraste de susceptibilité d'au moins 5 fois.

Finalement, la cartographie et les nombreuses données pétrophysiques collectées sur le terrain (susceptibilité magnétique, densité) permirent la construction de deux coupes géologiques en accord avec les données géophysiques.

2.7.5 *Discussion*

Cette étude identifie un premier évènement de déformation (D1), antérieur à la sédimentation des bassins de Kumasi et Tarkwa et donc par conséquent, associé à la phase Éoéburnéenne. Ce D1 se caractérise par un raccourcissement N-S développant une série de plis isoclinaux d'échelle kilométrique dans les roches métavolcaniques du groupe de Sefwi, au sud-est de la ceinture d'Ashanti. Les intrusions de TTGs de la phase Éoéburnéenne furent datés entre 2187 Ma et 2158 Ma. Il a été suggéré que de possibles minéralisations en or formées au cours de

cet évènement D1 pourraient être à la source des paléoplacers du bassin de Tarkwa. Ces minéralisations précoces auraient également pu être remobilisées et concentrées le long de zones de cisaillement majeures lors de la phase Éburnéenne.

La seconde déformation (D2) correspond à une phase d'extension reliée à la sédimentation du groupe de Kumasi (2154 – 2125 Ma). L'activation de structures majeures, comme la Faille d'Ashanti, sous forme de détachements, a pu contrôler la formation des bassins sédimentaires de Kumasi et d'Akyem.

Le début de la phase Éburnéenne (2125 - 1980 Ma), marqué par un raccourcissement NW-SE (D3), eut pour résultat la réactivation inverse de la Faille d'Ashanti, contrôlant, côté est, la formation du groupe de Tarkwa (2107 – 2097 Ma), et, côté ouest, un début de plissement des sédiments du bassin de Kumasi. La poursuite du raccourcissement D3 produisit le développement de plis majeurs dans l'ensemble des unités stratigraphiques Birimiennes et Tarkwaiennes. Le maximum métamorphique estimé autour de 5 kbar, 550°C (Schmidt Mumm et al., 1997, John et al., 1999) et daté à 2092 ± 3 Ma (Oberthür et al. 1998) est corrélé avec la déformation D3.

La déformation D4 (raccourcissement NNW-SSE) permis la réactivation en cisaillement sénestre des failles formées lors de D3 (orientées N30-N40). De nouvelles zones de cisaillement apparurent (orientées N50-N60), recoupant les structures antérieures. Une intense crénulation S4 du clivage S3 se développa sur l'ensemble de la région. L'intégralité des gisements d'or connus le long des failles d'Ashanti (Prestea, Bogoso, Obuasi), d'Akropong (Pampe) et d'Asankragwa se mirent en place pendant les cisaillements D4 (Allibone et al., 2002a).

L'architecture géologique régionale établie à la fin de l'évènement D4 ne fut que légèrement modifiée par les deux déformations postérieures. D5 forma régionalement des plis de faible amplitude (à l'exception du site de Wassa), couchés, et associés à une crénulation sub-horizontale. D6 se caractérise surtout par la formation tardive de très nombreuses failles inverses orientées NW-SE.

Chapitre II

Chapitre II

The tectonic context of the Eoeburnean Wassa gold mine - Implications for relative timing of mineralising events in southwest Ghana

Abstract

The Ashanti greenstone belt in southwest Ghana hosts many hydrothermal gold deposits distinguished by their differing ages and structural contexts. The Wassa gold mine is hosted by the Sefwi group in the eastern part of the SW Ashanti belt. This study investigates the tectonic and hydrothermal evolution of this gold deposit by integrating field and geophysical observations. We believe that Wassa represents the oldest known gold mineralisation in southwest Ghana and discuss implications for the regional evolution of the area.

At least six deformation, associated with gold mineralisation and remobilisation and developed in two phases (Eoeburnean and Eburnean), have been identified in the Wassa mine and at the regional scale. D1 deformation developed a series of isoclinal F1 folds and a strong S0-S1 fabric marked by chlorites, ankerite, rare calcite and gold-bearing elongated and stretched pyrite. Numerous quartz and ankerite veins result from alteration of surrounding metabasalts during D1. Eoeburnean age of this early-D1 mineralisation and local high gold grade suggests that it may be one of the potential sources of gold for the Tarkwa paleoplacer.

The Eburnean orogenic phase starts in the Wassa mine with D3 NW-SE shortening developing both kilometre-scale open folds and non-mineralised QV3 quartz veins in all paleoproterozoic lithologies. D4 corresponds to a NNW-SSE shortening event and is the second most intense deformation in the Wassa mine area with a series of sinistral shear zones controlling large scale folding and a subvertical S4 crenulation cleavage. A kilometre-scale F4 synform centred on the Wassa mine refolds the mineralised isoclinal F1. Late D5 folding and D6 events overprint the D4 structures and are associated with euhedral pyrite, rare chalcopyrite and minor gold remobilisation associated with QV5 quartz veins.

3.1 Introduction

In the West African Craton, a series of paleoproterozoic greenstone belts host numerous hydrothermal gold deposits and rare paleoplacers, particularly in southwest Ghana (Fig. II-1). Hydrothermal Au mineralisations from the southern Ashanti Belt have been relatively well studied including studies on Obuasi (≈ 60 Moz, Blenkinsop et al.,1994; Allibone et al., 2002a); Bogoso-Prestea (≈ 15 Moz, Allibone et al., 2002b); Konongo (≈ 3 Moz, Kutu et al., 2003); and Damang (≈ 8 Moz, Tunks et al., 2004). Mineralisation events for all of these deposits are correlated with the late deformation events of the Eburnean Orogeny (Bonhomme, 1962, Feybesse et al., 2006). In contrast, early Eburnean gold mineralisation has only been mentioned in a few geology reports of recently discovered gold deposits. In the Wassa mine, Bourassa (2003) highlighted the possibility of hydrothermal gold mineralisation associated with early Eburnean quartz vein generation and suggested that this style of mineralisation could be the source of gold for the Tarkwa paleoplacer (≈ 41 Moz, Milesi et al., 1991).

The origin of gold for paleoplacer deposit in southwest Ghana has long been debated (Sestini, 1973; Milési et al., 1991). Before robust age constraints were available (Davis et al., 1994), these paleoplacers were thought to be derived from Birimian type deposits such as those along the Ashanti Fault (e.g. Obuasi). However, authors including Milési et al. (1991) pointed out some inconsistencies with this model: gold rich Tarkwaian conglomerates do not exhibit traces of the arsenopyrite found in the Ashanti fault deposits. These authors proposed that all of the deposits along the Ashanti Fault have been formed post-Tarkwaian during the Eburnean stage (Allibone et al., 2002a). Consequently, pre-Tarkwaian deposits that constitute possible source of gold for the placers remains unrecognised yet.

Investigating the Wassa gold deposit, which seems to be older than other locations in southwest Ghana, could be a great contribution to our understanding of the mineralising events succession and their relationships during the Eburnean Orogeny.

Our objectives here are to characterise the structural evolution of the Wassa mine area, constrained by field and geophysical observations, and to compare the Wassa deformation sequence and gold timing with other deposits in order to put the hydrothermal mineralising sequences into the context of the regional tectonic evolution.

3.2 Geological Setting

3.2.1 *Ashanti Belt*

The Ashanti greenstone belt in southwest Ghana (Fig. II-1) principally consists of three metasedimentary and metavolcanic rock groups known as the Sefwi Group, the Kumasi Group and the Tarkwa Group (Adadey et al., 2009). The Sefwi Group is mainly composed of metabasalts which alternate with metavolcanosedimentary layers, dated as being older than 2162 ± 6 Ma (U/Pb on zircons, Loh et al., 1999). The Kumasi Group corresponds to phyllites and volcanoclastic sediments, deposited in the Kumasi Basin and in the Akyem Basin after 2154 ± 2 Ma (U/Pb on zircons, Oberthür et al., 1998). The Tarkwa Group corresponds to a metasedimentary basin overlying the Birimian Supergroup (Sefwi and Kumasi groups) and deposited between around 2107 Ma (Perrouty et al., 2012, reinterpretation of detrital zircons U/Pb analyses of Pigois et al., 2003) and 2097 ± 2 Ma (granitoid intrusion, U/Pb on zircons, Oberthur et al., 1998). Many tonalite, granodiorite, granite and leucogranite intruded these groups during the Eburnean Orogeny. According to Adadey et al. (2009) and to Perrouty et al. (2012) this plutonism occurred in two stages correlated with deformation events. The first deformation (Eoeburnean, De Kock et al., 2011) affected only the Sefwi metavolcanic Group and was followed by Kumasi Group and Tarkwa Group deposition. The second one (Eburnean) corresponds to the major deformation period around 2092 ± 3 Ma (estimated age for the peak of metamorphism by Oberthür et al., 1998).

Perrouty et al. (2012) described six deformation events in the Ashanti Region. Their nomenclature is used throughout the paper. The D1 event, which correlates with the Eoeburnean phase, is characterised by a north-south shortening developing regional scale folds within the Sefwi Group only. Their D2 correspond to a regional scale extension with the deposition of the Kumasi Group sediments in both the Kumasi Basin and the Akyem Basin, as it was already proposed by Feybesse et al. (2006). D3 and D4 major events affected the Sefwi, Kumasi and Tarkwa groups and were characterised by NW-SE shortening (D3) developing kilometric scale folds and thrust faults, followed by a NNW-SSE shortening (D4) associated with sinistral shear zones that sometimes reactivate the D3 thrust faults such as the Ashanti Fault (Fig. II-1). The D5 and D6 events correspond to minor shortening phase at regional scale with crenulation cleavages and open folds.

Both the Birimian and the Tarkwaian units host Eburnean gold deposits in southwest Ghana. Except for a few paleoplacers in Tarkwaian metasediments (including the Tarkwa gold mine), all the deposits are results of hydrothermal activities and are mainly located close to the

Sefwi / Tarkwa groups contact for the Abosso-Damang deposits and along the Kumasi / Tarkwa groups sheared contact from Konongo to Prestea (Ashanti fault, Fig. II-1). All of these deposits formed under greenschist facies conditions during the last stages of the Eburnean Orogeny (Mumin et al., 1996). In contrast, the Wassa gold deposit is the only known site in southwest Ghana to be hosted entirely within the Sefwi Group and not directly related with the Tarkwa Basin or with a major shear zone.

3.2.3 *The Wassa gold mine*

The Wassa gold deposit is located 40 km northeast of Tarkwa town on the eastern side of the Ashanti Belt near Akyempim village (Fig. II-1). It is mostly a low grade gold deposit (0.5 to 3.0 g/t) that has produced more than one million ounces of gold since industrial mining started in 1998. As a consequence of a strong overprinting of folding events, structural orientations are highly variable within the mine area and are not reported in the following paragraph.

In contrast to the other major deposits in southwest Ghana, no literature has been published including data on the Wassa mine. However, several company reports are available, with descriptions of lithologies and structures (Bourassa 2003; MacCandlish, 2003). The first deformation event (D1) described in these reports consists of rare asymmetrical isoclinal folds associated with a subvertical penetrative foliation. However, MacCandlish (2003) proposed the existence of an older foliation that may be parallel to bedding. For Bourassa (2003) and MacCandlish (2003), the major folding event in the Wassa mine consists of a kilometre-scale tight synformal fold (F4) centred on the mine (Fig. II-2). These authors found numerous parasitic folds in the hinge of this kilometre-scale fold and an associated subvertical crenulation cleavage. Bourassa (2003) identified another event characterised by a flat-lying crenulation cleavage (S5) and shallow plunging open folds. He also correlates this deformation with a major fault zone thrusting the Tarkwaian metasediments over the Sefwi Group on the western side of the Wassa mine. Finally, both authors distinguish late stage Eburnean brittle structures in the Wassa mine represented by a series of east-west faults.
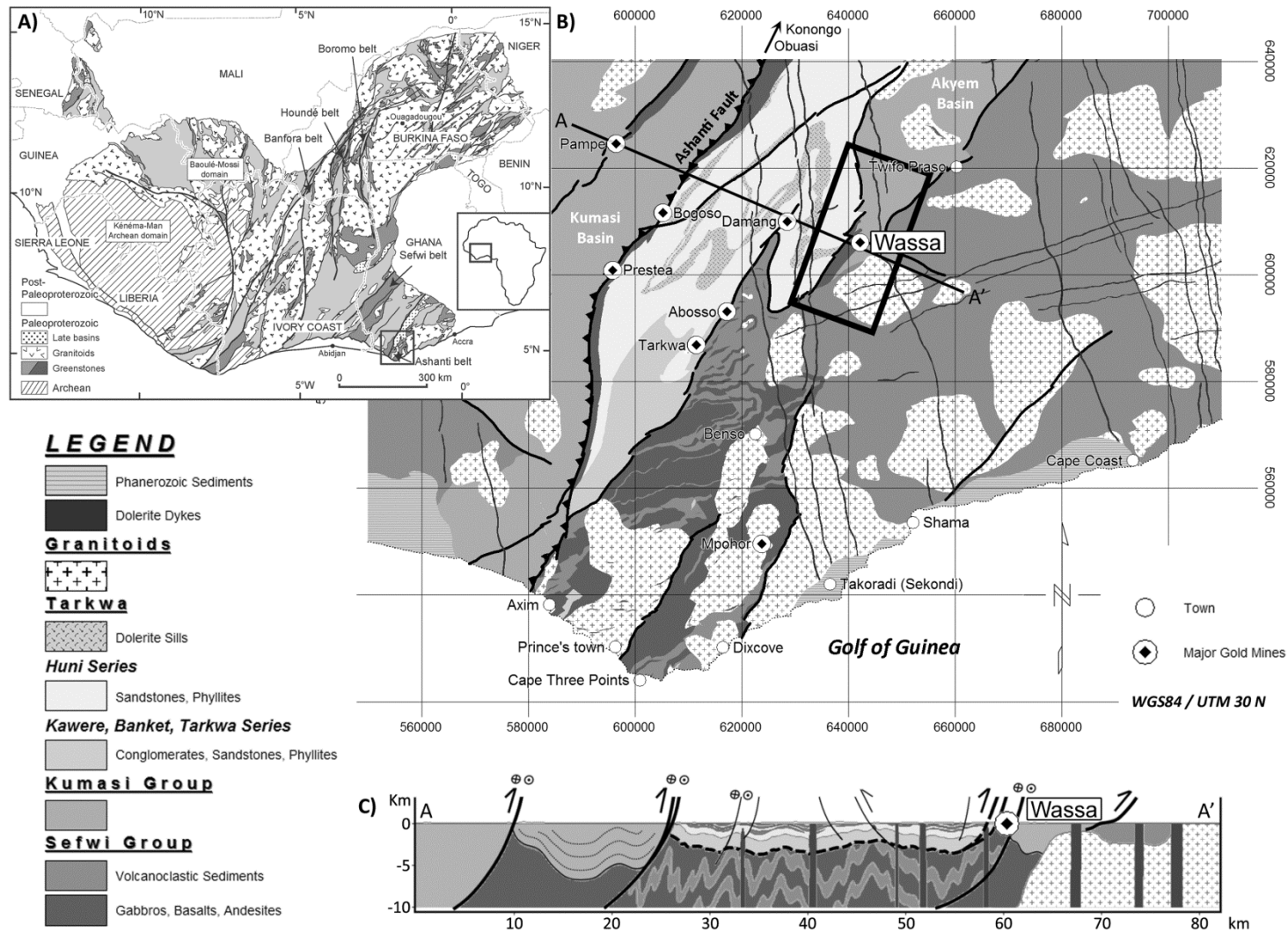
Figure II-1   *Map and section of the southern Ashanti belt. The major hydrothermal gold mines and the Tarkwa paleoplacer are shown. Our study area (black rectangle) is located on the eastern border of the Tarkwa Basin.*
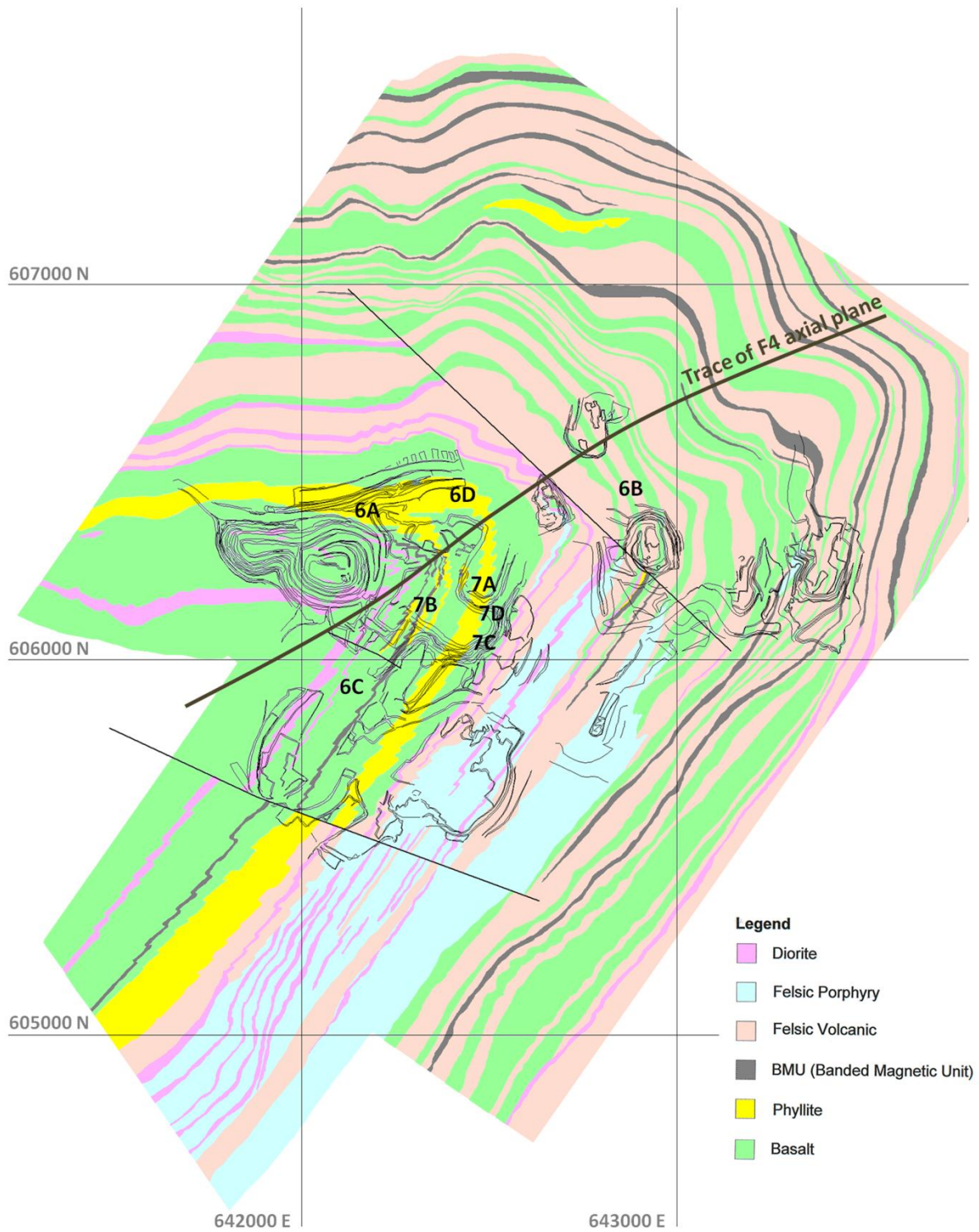
91

Figure II-2   *Geology of the Wassa mine (modified after Bourassa, 2003) draped over pit maps (thin black lines). Projection is WGS84 / UTM zone 30N. All the lithologies have been reoriented along a major F4 fold. Locations of the stereoplots of the S0-S1 fabric shown in Figure II-6 and of the photograph shown in Figure II-7 and are marked.*

Figure II-3   *Photograph showing the five dominant lithologies found in the Wassa mine (after Bourassa, 2003), drillcore samples. Macroscopic differences between the "mafic volcanic", the "felsic volcanic" and the phyllites are mostly a result of variable volume of quartz and ankerite veins (see Figure II-4 for the mineralogy).*
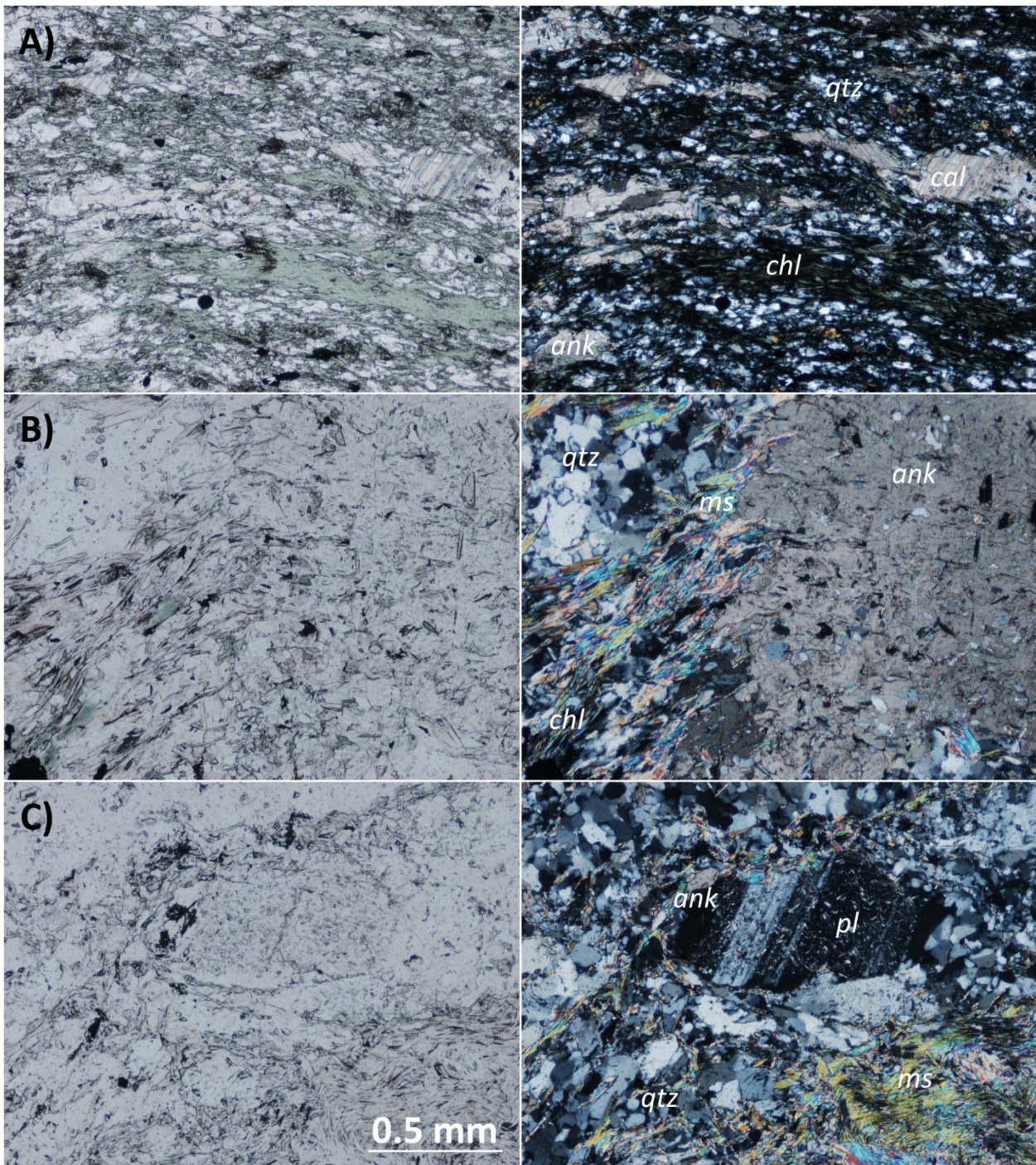
Figure II-4   *Thin-sections photographs of the dominant lithologies sampled in the mine. Plane-polarised light on the left image. Crossed polarised light on the righ image. chl: chlorite, cal: calcite, ank: ankerite, qtz: quartz, pl: plagioclase feldspar, ms: muscovite. A) The "Mafic volcanic, JM013)" show strong chlorite and carbonates alignment that define the S1. The "felsic volcanic (JM017)" and the "phyllites (JM015)" display equivalent mineralogy. B) The "metadiorite (JM016)" shows similar mineral assemblages with large ankerite porphyroblasts up to 2 mm size that are also observed on Figure II-3. C) The "felsic porphyry" contains plagioclase feldspar, quartz, muscovites and rare ankerite.*

These company reports also mention at least three kinds of quartz veins related to different deformation events. According to Bourassa (2003), the first vein generation exhibits a smoky to translucent quartz associated with tourmaline, sericite and sulphides. These veins host the highest gold grade found in the area (≈ 5 g/t, but locally up to 70 g/t). These veins have been deformed by isoclinal F1 folds and are boudinaged in the fold limb. In contrast, the second-generation veins have not been folded by D1 and contain few traces of remobilised gold (MacCandlish, 2003). Bourassa (2003) observed that these veins are mostly located parallel to the subvertical crenulation cleavage associated with the kilometre-scale fold (F4). The third and last quartz veining event corresponds to milky, pinkish quartz veins hosting low gold grades. They are sub-parallel to the horizontal crenulation cleavage and cross-cut all previous folds (Bourassa, 2003).

3.3 Field observations and geochemistry

3.3.1 *Stratigraphy*

Lithologies (Fig. II-3) in the mine area belong to the Sefwi Group and consist of an alternation of "mafic volcanic", "felsic volcanic", "phyllites" and few black shale layers (Bourassa, 2003). Multiple ankerite, calcite and quartz veins subparallel to bedding (or to the S0-S1 fabric) are also observed in these rocks. Eoeburnean intrusions were mapped as "diorite" and "felsic porphyry (granodiorite)" units (Fig. II-2, Fig. II-3). Magnetite enrichment has been observed in some phyllitic layers called the Banded Magnetic Unit (BMU). These layers seem to be bedding parallel and present a variable thickness between 1 to 8 metres (Bourassa, 2003).

In contrast with their macroscopic appearances (Fig. II-3), thin section analysis (Fig. II-4) allowed to distinguish three major lithologies: (1) The "mafic volcanic", "felsic volcanic", and "phyllites" display similar mineral assemblages with variable proportions of quartz, chlorite, ankerite and calcite. (2) The "metadiorite" is characterised by quartz, chlorites, ankerite porphyroblasts and muscovite. (3) The "felsic porphyry" is less affected by metamorphism and hydrothermal alteration and presents quartz, plagioclase feldspar, muscovite and rare ankerite. With the partial exception of the "felsic porphyry", the initial mineralogy of the analysed samples was totally metamorphosed and/or hydrothermally altered.

	Felsic Unit		Mafic Unit	Diorite	Felsic Porphyry		"Phyllites"	Analytical Method
	JM017	JM018	JM013	JM016	JM012	JM012A	JM015	
In wt. %								
SiO2	49.4	47.5	51.7	50.7	69.4	70.1	37.0	ME-ICP06
TiO2	0.54	0.61	0.58	0.48	0.35	0.35	0.60	ME-ICP06
Al2O3	13.70	11.10	12.05	14.70	13.30	13.60	12.95	ME-ICP06
Fe2O3	8.99	10.20	10.25	7.17	2.64	3.02	10.25	ME-ICP06
MnO	0.13	0.17	0.17	0.14	0.04	0.07	0.16	ME-ICP06
MgO	4.70	5.28	6.41	4.07	0.90	1.07	7.21	ME-ICP06
CaO	4.30	6.31	8.58	7.12	2.63	2.97	10.20	ME-ICP06
Na2O	3.76	2.61	1.69	3.54	3.57	4.20	2.02	ME-ICP06
K2O	0.45	0.63	0.03	0.60	2.24	1.71	0.36	ME-ICP06
Cr2O3	0.02	0.02	0.02	0.01	<0.01	<0.01	0.04	ME-ICP06
P2O5	0.15	0.21	0.22	0.23	0.09	0.07	0.12	ME-ICP06
SrO	0.04	0.06	0.04	0.05	0.03	0.03	0.03	ME-ICP06
BaO	0.01	0.02	<0.01	0.02	0.14	0.07	0.01	ME-ICP06
LOI	13.60	16.15	9.44	12.10	4.20	3.10	20.50	OA-GRA05
Tot.	99.8	100.9	101.2	100.9	99.5	100.4	101.5	TOT-ICP06
In ppm								
C	3.62	4.26	1.66	2.91	1.00	0.56	5.28	C-IR07
S	0.25	<0.01	0.46	0.01	0.01	0.01	0.13	S-IR08
V	213	180	255	173	42	51	197	ME-MS81
Cr	120	160	150	70	30	10	280	ME-MS81
Co	40	53	29	28	58	47	46	ME-4ACD81
Ni	27	30	17	42	9	5	139	ME-4ACD81
Cu	89	14	82	13	10	11	39	ME-4ACD81
Zn	80	85	77	66	31	38	92	ME-4ACD81
Ga	13.6	13.0	12.2	15.2	14.7	14.9	14.9	ME-MS81
As	2.1	0.9	25.4	0.3	0.2	0.8	192.0	ME-MS42
Se	0.70	0.40	0.4	0.4	0.3	0.4	0.7	ME-MS42
Rb	14.6	20.9	1.2	20.4	84.5	66.5	9.4	ME-MS81
Sr	380	488	352	474	241	258	303	ME-MS81
Y	13.8	18.3	9.6	12.7	11.8	13.0	16.2	ME-MS81
Zr	51	57	30	60	197	118	41	ME-MS81
Nb	1.8	2.0	1.1	3.3	6.9	6.7	2.0	ME-MS81
Mo	<1	<1	<1	4	<1	<1	<1	ME-4ACD81
Ag	<0.5	<0.5	<0.5	<0.5	<0.5	<0.5	<0.5	ME-4ACD81
Cd	<0.5	<0.5	<0.5	<0.5	<0.5	<0.5	<0.5	ME-4ACD81
Sn	<1	<1	<1	1	1	1	<1	ME-MS81
Sb	0.20	0.07	0.63	0.05	0.13	0.09	0.38	ME-MS42
Te	0.04	<0.01	<0.01	<0.01	<0.01	<0.01	0.04	ME-MS42
Cs	0.91	1.23	0.70	0.87	2.04	1.88	0.56	ME-MS81
Ba	143	176	48	191	1295	609	117	ME-MS81
La	6.8	60.9	9.0	13.3	31.3	28.5	11.0	ME-MS81
Ce	14.3	100.5	18.5	27.0	55.9	51.5	24.6	ME-MS81
Pr	1.90	10.40	2.45	3.42	5.96	5.47	3.30	ME-MS81
Nd	8.0	33.4	10.1	13.1	18.8	17.8	13.2	ME-MS81
Sm	2.03	4.83	2.24	2.78	3.04	3.01	2.80	ME-MS81
Eu	0.69	1.33	0.76	0.89	0.84	0.80	0.95	ME-MS81
Gd	2.30	3.78	2.17	2.69	2.30	2.43	2.78	ME-MS81
Tb	0.36	0.51	0.29	0.37	0.32	0.35	0.42	ME-MS81
Dy	2.38	3.17	1.83	2.35	1.98	2.15	2.81	ME-MS81
Ho	0.51	0.66	0.36	0.45	0.39	0.43	0.59	ME-MS81
Er	1.50	1.89	1.06	1.27	1.18	1.31	1.73	ME-MS81
Tm	0.22	0.27	0.15	0.18	0.18	0.20	0.25	ME-MS81
Yb	1.46	1.78	1.01	1.23	1.24	1.35	1.59	ME-MS81
Lu	0.24	0.28	0.16	0.19	0.21	0.22	0.25	ME-MS81
Hf	1.4	1.6	0.8	1.7	5.4	3.2	1.1	ME-MS81
Ta	0.1	0.1	0.1	0.3	0.6	0.7	0.1	ME-MS81
W	79	139	20	62	316	230	34	ME-MS81
Hg	0.04	0.08	0.017	0.037	0.183	0.131	0.020	ME-MS42
Tl	<0.5	<0.5	<0.5	<0.5	<0.5	<0.5	<0.5	ME-MS81
Pb	7	4	2	5	3	4	3	ME-4ACD81
Bi	0.06	<0.01	0.01	0.01	0.02	0.03	0.05	ME-MS42
Th	0.96	1.18	1.21	1.95	9.29	6.60	0.91	ME-MS81
U	0.40	0.82	0.39	0.70	2.41	1.67	0.25	ME-MS81

Table II-1   *Geochemical analyses of the five dominant lithologies found in the Wassa mine. All samples have been taken from drillcore. The "mafic volcanic", "felsic volcanic", "metadiorite" and "phyllites" display similar whole rock compositions.*
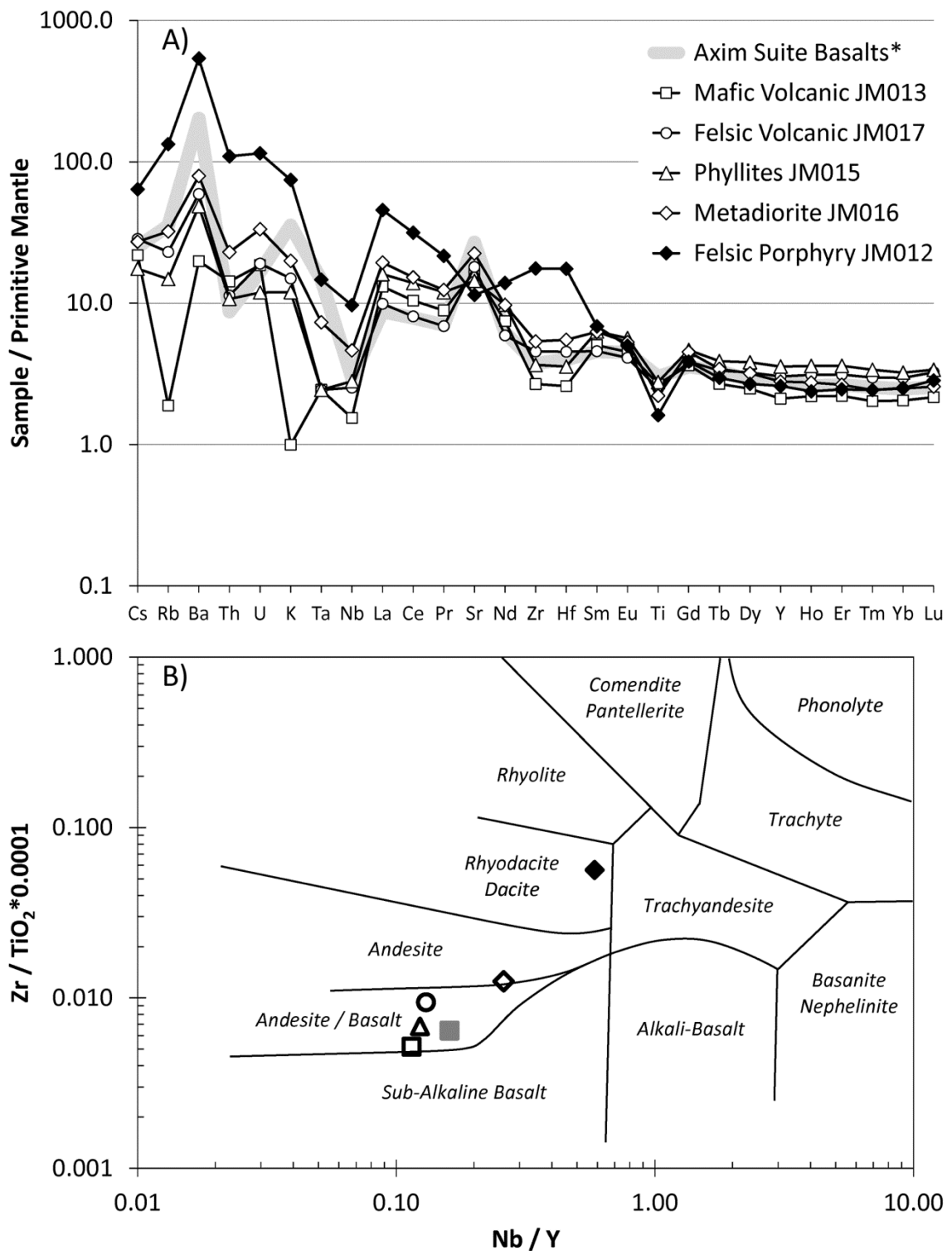
Figure II-5   *A) Extended trace elements profiles normalised to primitive mantle (Sun and McDonough, 1989) of the "five lithologies" observed in the field (Figure II-3). * Average composition of the Axim suite basalts as defined by Dampare et al., 2008. B) Volcanic rock classification using Zr/TiO2 versus Nb/Y ratios (modified after Winchester and Floyd, 1977). With the exception of the "felsic porphyry" intrusive rocks (JM012), all lithologies of the Wassa mine display similar trace element profiles. They correspond to enriched basalt signatures (enriched in light trace elements and depleted in heavy rare earth elements) typical of the type-II basalts of Dampare et al., 2008.*

3.3.2 *Whole rock geochemistry*

Geochemical analyses were conducted on representative samples of the dominant lithologies of the Wassa mine area: the "mafic volcanic" (JM013), the "felsic volcanic" (JM017), the "metadiorite" (JM016), the "felsic porphyry" (JM012) and the "phyllites" (JM015). These samples were sent after pulverising to A.L.S. Mineral laboratory, Sevilla, Spain. Whole rock measurements (Table II-1) were done using ICP-AES for major elements and base metals and using ICP-MS for trace elements and REE. These analyses are characterised by high loss on ignition (LOI, Table II-1) values explained by the presence of carbonates in all rocks.

Major element geochemical analyses indicate that the "mafic volcanic", the "felsic volcanic", the "phyllites" and the "metadiorite" have equivalent major elements (Table II-1) and trace elements whole rock proportions (Fig. II-5A). This geochemistry agrees with thin section observations (Fig. II-4A) that also show similar mineralogy. These samples display extended trace element profile after normalisation to primitive mantle (Sun and McDonough, 1989) corresponding to enriched basalts signature (enriched in light trace elements and depleted in heavy rare earth elements) typical of the Axim Suite type-II basalts of Dampare et al. (2008). Negative Rb and K anomalies for the "mafic volcanic" suggest that they may have been initially less differentiated than the "felsic volcanic" and the "metadiorite". Considering the High Field Strength Elements (HFSE), considered to be less affected by alteration, all of these "lithologies" plot in the andesitic / basaltic domain using the volcanic rock classification of Winchester and Floyd (1977), based on Zr/TiO_2 versus Nb/Y ratios (Fig. II-5B).

In contrast, the "felsic porphyry" (JM012) shows lower LOI, and higher light trace element proportion. Its geochemistry displays high SiO_2, low Fe_2O_3, low MgO, high Na_2O and high K_2O proportions (Table II-1) that agree with its mineralogy corresponding mostly to quartz, plagioclase feldspar and muscovite assemblages (Fig. II-4C). They may correspond to the most differentiated Eoeburnean intrusions (Fig. II-5B) that intruded the mafic lithologies in the Wassa mine.

The initial environment of the Wassa mine may correspond to a package of volcanism-related rocks with basalts more or less mafic, volcano-sedimentary layers and a few diorite intrusions. These rocks have been further intruded by the "felsic porphyry" and entirely recrystallised and modified to metamorphic assemblages by hydrothermal alteration (carbonates, pyrites, quartz) and by veining (quartz, carbonates).

A) S1, north limb
7 data, mean 064/47

B) S1, hinge of F4
3 data, mean 320/82

C) S1, south limb
9 data, mean 218/85

D) S4
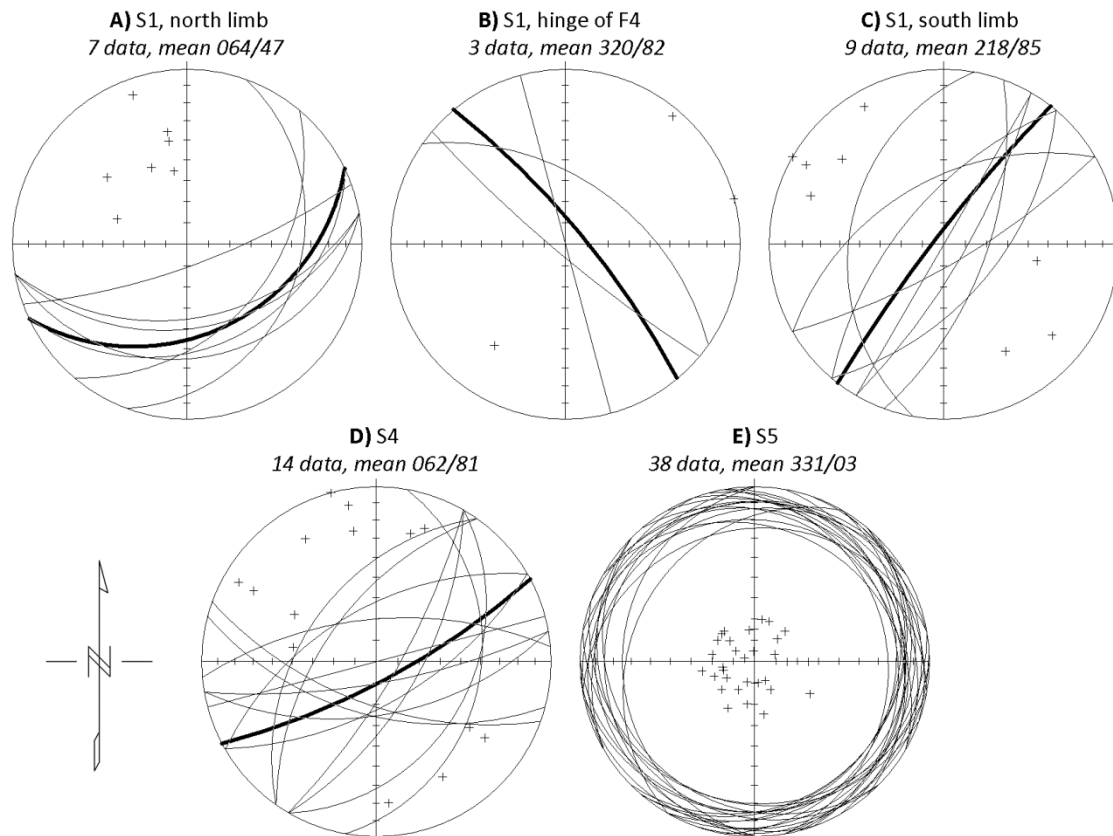*14 data, mean 062/81*

E) S5
38 data, mean 331/03

Figure II-6   *Stereoplots. A,B,C) The S0-S1 foliation orientation varies from the south (N38/subvertical) to the north (N064/47) of the Wassa mine area. These variations define a major fold with a hinge centred on the mine site, related to D4 deformation. D) Axial plane of this F4 correspond to the S4 crenulation cleavage (N062/subvertical). E) The late D5 deformation is characterised by a subhorizontal crenulation cleavage.*
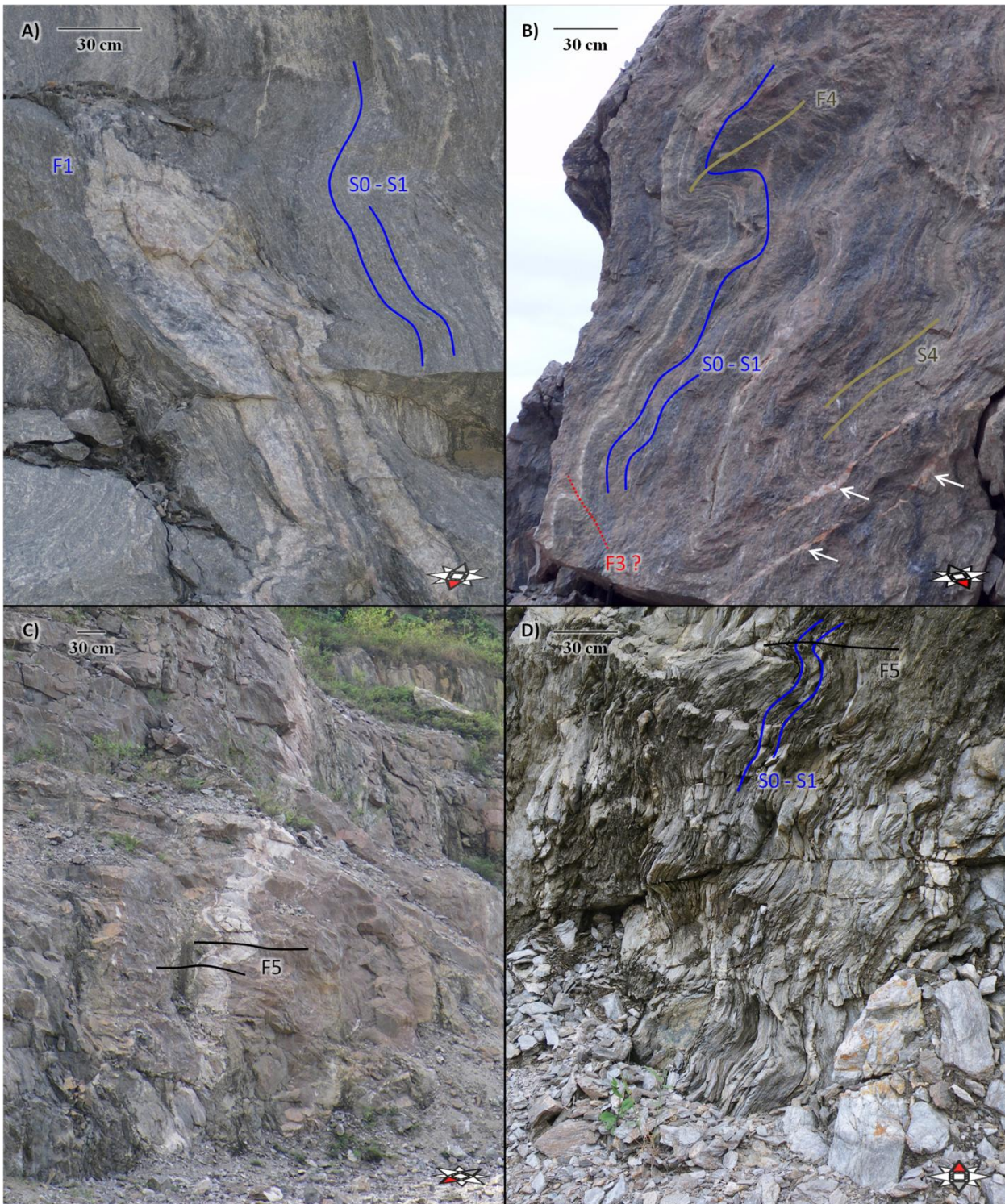
Figure II-7 *Interpreted photographs of Eburnean deformations events found in the Wassa mine. Locations are shown in Figure II-2. A) Metre-scale QV1 quartz vein folded by isoclinal F1. This fold axial plane is parallel to the chlorite alignments that define the S1 cleavage. B) This S0-S1 foliation was significantly deformed by F4 parasitic fold and crenulated by the S4 cleavage. Rare (F3?) folds have also been observed associated with quartz veins (white arrows in the bottom left corner). C) QV4 quartz veins cross-cutting the major F4 folds and deformed by further D5 event. D) F5 open to close recumbent folds. Fractures and QV5 quartz veins were often observed along the axial surface of these folds, with late euhedral pyrite mineralisation.*
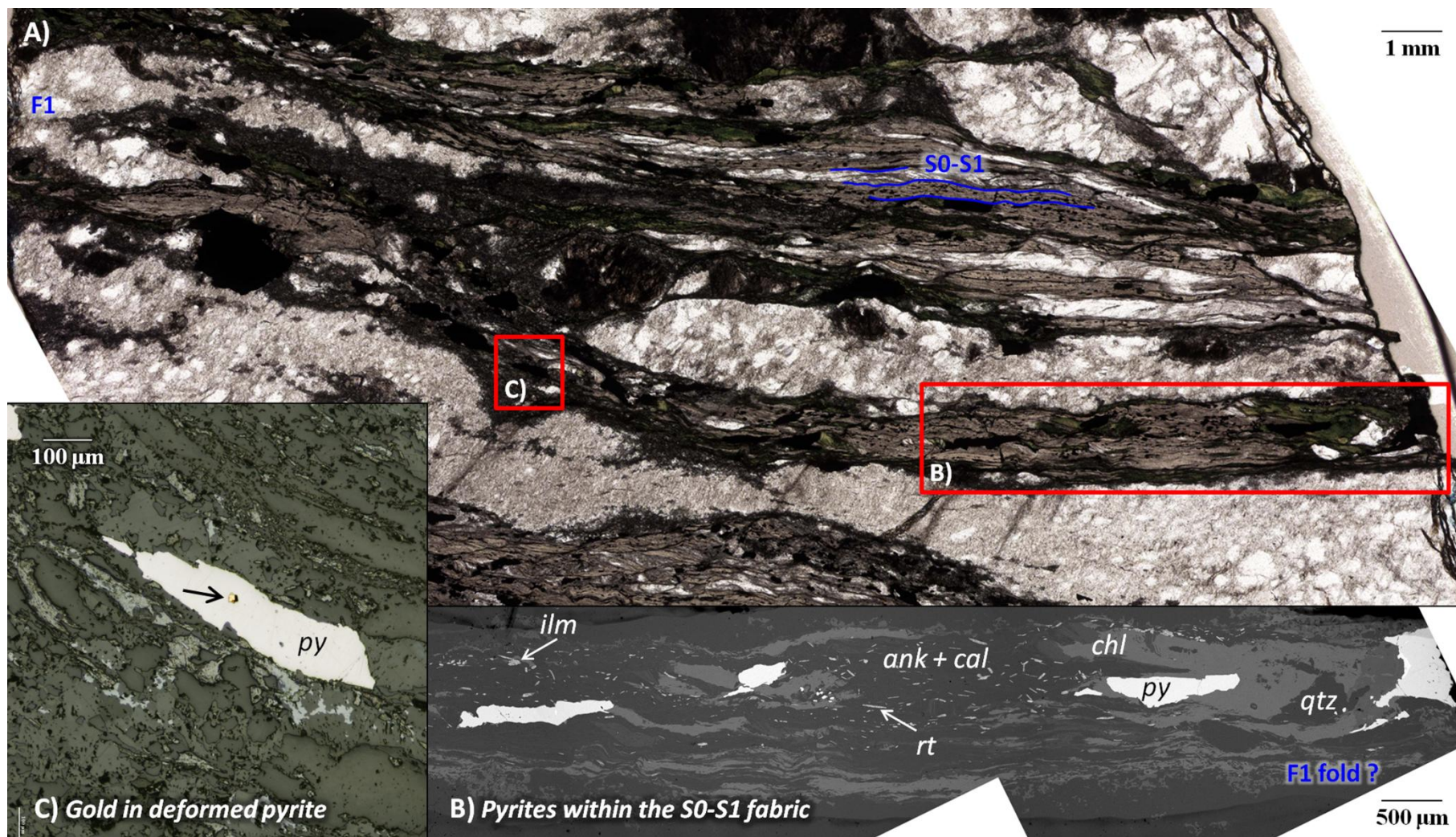
Figure II-8   *Thin-section observations of early-D1 structures, veins and mineralisation. A) Transmitted light photograph of mineralised "mafic volcanic". Chlorite alignment carbonates and quartz-veins defined an S0 foliation folded by small scale F1. B) Scanning Electron Microscope (SEM) mosaic image showing that pyrite are mostly located and deformed within the S0-S1 ductile fabric. C) Reflected light photograph. These pyrites strongly deformed during D1 do not show any fractures and host some visible gold particles.*
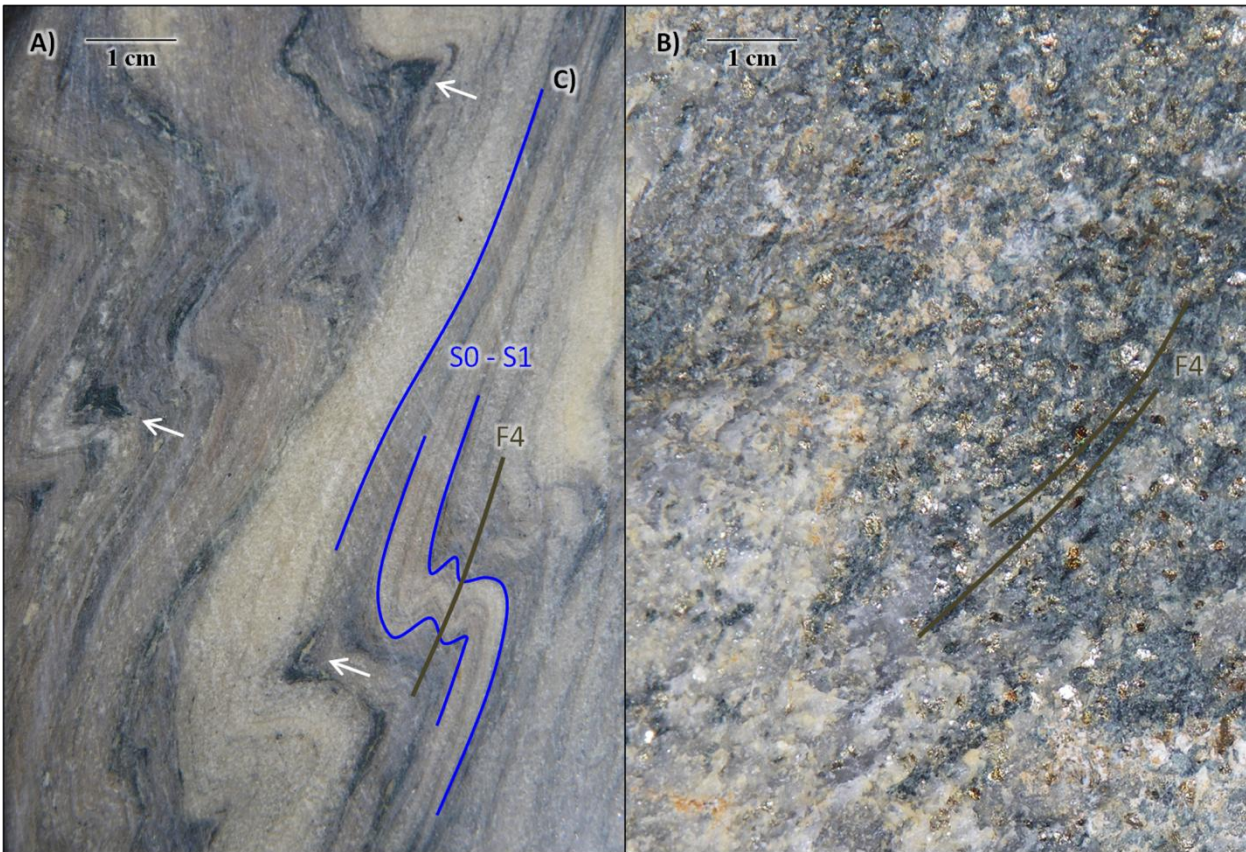
Figure II-9   *A) Drill-core photograph showing small scale parasitic F4 fold with concentration of D1-deformed pyrites in the hinge of the F4 (white arrows). B) Field photograph of euhedral pyrite (up to 0.5 mm size) overprinting the S4 crenulation cleavage. These late pyrite may have been formed during our D5 or D6 events.*
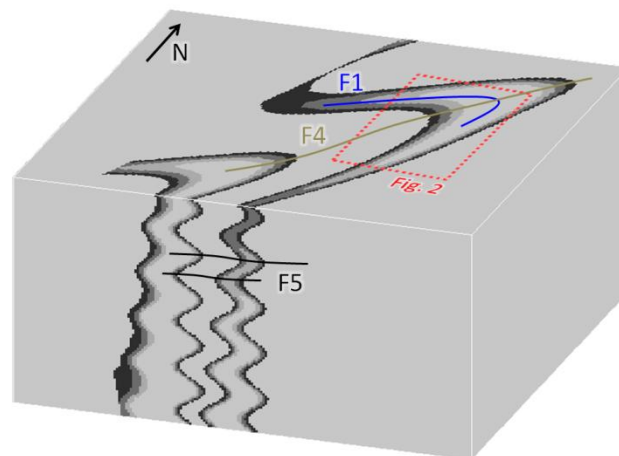
Figure II-10   *Schematic 3D diagram summarizing the three main folding events (D1, D4 and D5) in Wassa mine, using Noddy software (Jessell, 1981, 2001; Jessell and Valenta, 1996). Map shown on Figure II-2 is approximately located on this model. Scaling is not respected considering the F5 meter-size folds.*

3.3.3 *Structural observations*

3.3.3.1 D1 (Eoeburnean)

The observations from the Wassa mine show a main S0-S1 foliation present as a slaty penetrative cleavage in the metavolcanics, phyllites and intrusive bodies (Sefwi Group). An associated lineation is defined by chlorite and magnetite alignments. S0-S1 foliation is subvertical and oriented NE-SW in the south of the Wassa mine whereas it is dipping at around 45° to the SSE in the northwest of the mine (Fig. II-6). The bedding-parallel Banded Magnetic Units (BMU), early-D1 (or pre-D1?) smoky-quartz veins (QV1) and carbonate veins are folded together by isoclinal F1 folds with short wavelengths and high amplitudes at all scales (Fig. II-7A, Fig. II-8). However, bedding is often folded at larger scale than the quartz veins and most of the observed F1 fold hinges are only seen deforming the veins. A strong boudinage of these smoky-quartz veins is also observed, subparallel to the S1 foliations.

Thin-section observations show that chlorite, magnetite, carbonates and pyrite can be used as markers of the S0 (bedding or earlier foliation?). However, these minerals are elongated parallel to the S1 and also folded by F1 (Fig. II-8). As a consequence, they must have been formed at the early stage of the D1 deformation or pre-D1. In particular, the first mineralisation observed in Wassa mine developed pyrites showing ductile deformation, characterised by an elongation parallel to the S1 fabric and by the absence of fractures. These pyrites host visible gold particles (Fig. II-8C) and together form the major gold mineralisation assemblage.

3.3.3.2 D2

Two metasedimentary groups overlay the Sefwi Group in the Wassa mine area. They correspond to the Kumasi Group in the northeast (Akyem Basin) and to the Tarkwa group in the west. These metasediments do not exhibit the previously described D1 deformation. Deposition of the Akyem Basin (Kumasi Group) may be related to regional scale D2 extension according to Feybesse et al. (2006) and Perrouty et al. (2012). However, such D2 related extensional structures could not be identified in the Wassa mine area.

3.3.3.3 D3 (Eburnean)

The D3 deformation event is marked by a series of NE-SW oriented fold axes and a subvertical crenulation cleavage in both the Kumasi Group (Akyem Basin and the Tarkwa Group). In the Sefwi Group domain, the lack of outcrop outside of the Wassa mine means that the D3 structures are mostly interpreted at large scale from geophysical images. Rare small-scale

folds were observed in the southern part of the mine area and may be related to the D3 deformation stage (Fig. II-7B).

The second quartz vein generation (termed QV3 as they are D3-related) observed in the field occurs in both the Birimian and the Tarkwa groups and is not associated with mineralisation. These QV3 veins cross-cut the S1 cleavage and are subsequently folded by D4.

3.3.3.4 D4

The S0-S1 foliation varies from approximately NE-SW in the south of the mine to E-W further north (Fig. II-6). This variation of the S0-S1 direction suggests the presence of a kilometre scale F4 synform with a hinge centred on the Wassa mine, oriented ENE-WSW (Fig. II-6D). Numerous small scale F4 folds (< 1 m) can be observed (Fig. II-7B) throughout the mine. The fold axes plunge steeply to the SW with a plunge of around 60°. The folds have a subvertical axial surface, defined by crenulations of the earlier cleavages.

A third quartz veining event occurred during D4. Syn- to late-D4 veins (QV4) are composed of white quartz associated with rare sulphides. These veins are subvertical, slightly deformed and cross-cut the regional F4 folds (Fig. II-7C). During D4, earlier sulphides (and gold mineralisation) have been concentrated in the hinges of the small scale F4 folds by mechanical thickening of the hinges (Fig. II-9A).

3.3.3.5 D5 and D6

D5 deformation event shows a sub-horizontal crenulation cleavage associated with a series of symmetrical recumbent F5 folds with wavelength between 0.1 m and 1 m and variable amplitudes. F5 folds mostly affect the southern part of the mine area where the orientations of the S0-S1 fabric (subvertical, Fig. II-6B, Fig. II-6C) show favourable initial geometries to develop recumbent folds (Fig. II-7C, II-7D). In contrast, S0-S1 in the north of the mine presents intermediate dips (Fig. II-6A) that is less able to develop F5 fold although the S5 cleavage is clearly found. Some sulphides and thin quartz veins organised parallel to the S5 cleavage are observed in particular in the axial surface of those F5 folds with the largest amplitudes. The S5 is itself overprinted by a faint S6 subvertical crenulation (oriented NW-SE) sometimes re-working the S4 cleavage. Variations of about 40° of the F5 axis dip direction in the middle of the mine (F-shoot) suggest the presence of low amplitude F6 open folds. However, uncertainties on these measurements are large as a result of the shallow F5 fold axis plunge (< 15°, Fig. II-6E). Other evidence for a low amplitude F6 fold is suggested by an undulation of the S5 surface (or F5 axial surface).

Figure II-11   *Examples of mineralisation at the Wassa mine. A) Intensely foliated and mineralised "mafic volcanic" with foliation parallel veins and later folding. Drill hole NSADD006, 157-158m, 1.36 g/t Au. B) Isoclinal F1 folds defined by earlier foliation in contact with porphyry unit. Drill hole SED0027. C) Intensely foliated and mineralized "mafic volcanic" unit and early QV1 veins boundinaged along the foliation, a later stage thicker quartz carbonate vein is located at right hand side of figure (inferred QV4 vein set). Both veins sets are folded. Drill hole NSADD009 214-215m, 3.38 g/t Au. D) Mineralized and boudinaged QV1 veins with adjacent disseminated pyrite. The enlarged section highlights the pyrite is deformed within the S1 foliation and is therefore pre- to syn-D1. Drill hole NSADD009 212-213m 2.48 g/t Au. E) Disseminated pyrite adjacent to QV1 veins. Drill hole BSDD090.*
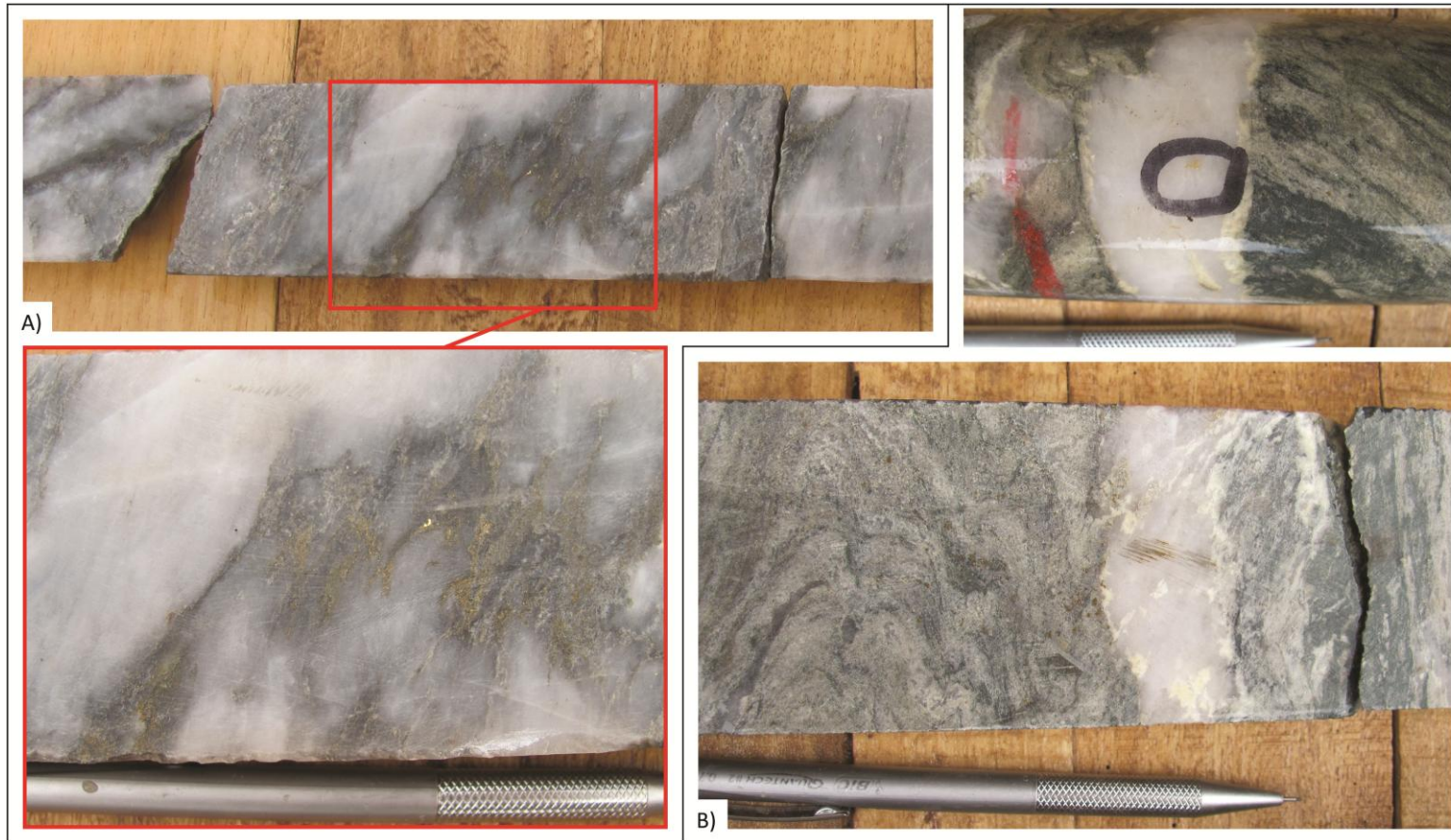
Figure II-12   *Examples of veins with visible gold at the Wassa mine. A) Folded QV1 quartz vein with visible gold. Note the folding increases the thickness of the vein. Drill hole 242DD029 180.6-181.6 66.8 g/t Au. B) QV5 quartz carbonate vein axial planar to an F4 fold - the figure shows a photograph of both sides of the drill core (i.e. the same vein is shown in top and bottom photograph). Visible gold is within black circle drawn onto drill core. The gold-bearing vein clearly cross cuts the S4 foliation (note top photograph). Drill hole SEDD025 164.7-165.3m 11.6 g/t Au.*

3.3.4 *Mineralisations*

The gold mineralisation within the Wassa deposit occurs within highly strained rocks within a sheared area that is hundreds of metres wide. It has been refolded several times with 5 phases of shortening recognized with three main phases of folding (D1, D4 and D5, summarized in Fig. II-10) and two main phases of crenulation (D4 and D5). This deposit setting is reflected in outcrop and drill core relationships with mineralisation occurring in intensely deformed rocks that have a strong foliation (termed S4) with boudinaged veins (Fig. II-11A). Earlier isoclinal F1 folds occur and indicate that a transposition of the stratigraphy may have occurred (Fig. II-11B). Later F4 and F5 folding of the dominant foliation occurs throughout the ore body (Fig. II-11A, Fig. II-11C).

The first hydrothermal event (QV1) linked to gold emplacement occurred during the first deformational phase (D1) and is inferred to be the main gold mineralising event, although gold is also associated with the later deformation events. This phase of mineralisation is associated with early QV1 veins that are commonly characterised by smoky to translucent quartz (Fig. II-11C, Fig. II-11D) with ankerite-calcite-pyrite alteration assemblages associated with local silicification and occasional tourmaline within the host rock. Other foliation-parallel veins are quartz-ankerite. Pyrite associated with the QV1 quartz veins is fine grained and stretched along the S4 foliation providing evidence for a pre to syn D4 emplacement of the sulphides (Fig. II-11D). In some areas the rocks are hightly pyritized adjacent to QV1 veins (Fig. II-11E). The boudinage, folding and transposition of the QV1 veins along the dominant S4 foliation affects the continuity of the individual QV1 veins along strike (this is also evidence in the grade distribution delineated from gold assays of drill core). F4 folding has also resulted in thickening of the QV1 veins at fold hinges (Fig. II-12A).

Mineralisation is also associated with quartz-carbonate veins (locally termed QV5 veins) that are milky-white to pinkish-white in color, associated with ankeritic, chloritic and potassic alteration assemblages within the host rock. Some QV5 veins are sub-parallel to the S5 crenulation and located in the axial plane of the F5 folds (Fig. II-12B), crosscutting S1 and S4 foliations (Fig. II-12B) as well as older QV1 and QV4 veins. A minor remobilisation of the main mineralisation associated with the late QV5 quartz veins in the Wassa mine is suspected to have occurred during D5 or D6. Euhedral pyrite and few chalcopyrite grains have been observed overprinting the S0-S1 and S4 cleavages (Fig. II-9B).

The gold distribution within the Wassa deposit is highly variable and visible gold is spatially associated with early QV1 veins (e.g. folded example in Fig. II-12A) and also later

QV5 veins which clearly cross cut the dominant foliation (Fig. II-12B). Assays of 1 to 3 g/t are common within rocks dominated by the ductile fabric (e.g. Fig. II-11A, Fig. II-11C, Fig. II-11D). However, there is not always a direct correlation between quartz and gold grade within a given drill hole intercept. This is inferred to not only reflect an original nuggetty grade distribution, but also the effects of subsequent boudinage and folding post the emplacement of the QV1 veins that affect grade continuity. This markedly complicates the resource modelling of the deposit. In the original 2003 feasibility study Wassa was assigned a reserve of 23 million tonnes at 1.4 g/t for over 1 million ounces of gold (Bourassa, 2003). However, in spite of the low grade assigned, the Wassa deposit has many areas with veins that assay in excess of an ounce gold (e.g. Fig. II-12A) and visible gold is a relatively common occurrence.

3.4 Structural geophysics

3.4.1 *Geophysical data*

Our field observations have mainly been carried out around the mine site where we got an excellent overview of the structures. Outside of the mined area, the thickness of the lateritic weathered layer approaches 15 meters, and the saprolite unit extends down to 50 m. Fresh rocks are only exposed in the open pits. As a consequence, to create a geological and structural map of the Wassa mine area, extensive use of geophysical data was required to extrapolate the mine observation and interpretation to a larger scale.

Geophysical data were acquired in 2004 in two separate helicopter surveys, for the northern and southern parts of the mine. Flight lines trending N135° were acquired with 75 m and 50 m spacing, respectively, for the two surveys (Fugro logistics report, 2004). The data were stitched and gridded together using a resolution of 25 m for both the radiometric and magnetic data.

The total magnetic intensity (TMI) grid was created and reduced to the pole (RTP) using Geosoft Oasis Montaj. The RTP was calculated using an amplitude correction to minimise visual artefacts (Fig. II-13A). Other filtering and processing techniques included the analytic signal (McLeod et al., 1993) which has been found to be particularly useful at low magnetic latitudes. The resulting grids were further processed to enhance high intensity magnetic bodies and structures, and to estimate the continuity of the structures at depth. The filters applied include the first vertical derivative (Fig. II-14) Gunn et al., 1997; Milligan et al., 1997), upward

continuation, vertical integration (Fig. II-13B) and tilt derivative (Fig. II-13C, Verduzco et al., 2004; Lahti et al., 2010)

The high resolution survey of the Wassa mine area also collected radiometric and radar topography data. Radiometric data are composed of four bands representing K, Th, U and total count proportions within the first half-meter of the ground. A ternary RGB image was produced by combining these three channels (Fig. II-15).

Using the different signals available including the RTP magnetic grid, the radiometric grids (K, Th, U and total count) and the digital elevation model, Principal Component Analysis (PCA) images (Richards et al., 1999) were produced using Envi-IDL. They show different homogenous domains and are interpreted to reflect lithological variations. The Wassa mine provides a very strong signature on all input data because of the exposure of fresh rocks, a highly varying topography and of course the mining equipment.

3.4.2 *Petrophysical data*

Magnetic susceptibility data were acquired during a regional study of Perrouty et al. (2012) to help to constrain the magnetic data interpretation. Magnetic susceptibilities within the Wassa mine have also been measured using a Geofyzika KT-5 Kappameter hand held susceptibility meter and a Kappabridge KLY-3 susceptibility meter. Susceptibility values show two distinct ranges (Fig. II-16): the first range with low susceptibility values corresponds to the phyllites and felsic porphyry units. The second one is related to highly susceptible diorite and metavolcanic rocks. The strongest magnetic response in the study area is found within the metavolcanic Sefwi group hosting the Wassa mine and corresponds to the BMU which exhibits magnetic susceptibility values 5 to 10 times higher than the host rocks with a mean value of 0.279 SI and anisotropies of up to 75 %. Bourassa et al, 2003 suggested that the magnetite could have an exhalative or chemical origin which is consistent with the observation that most if not all of the BMU occurrences seems to be parallel to bedding in the Wassa mine. This is confirmed by thin-section observations of BMU showing that the magnetite marks the S0-S1 fabric. The BMU was used as a marker horizon in the magnetic signal to interpret geology and structures from the processed magnetic data.

3.4.3 *Interpretations*

The magnetic, radiometric and Principal Component Analysis (PCA) images were used to constrain our interpretation of the main rock packages and to map out their boundaries. Aeromagnetic images show magnetic domains and sub-linear features. The magnetic domains are relatively homogenous areas in terms of magnetic intensity and texture. They are interpreted as corresponding to specific lithologies or groups of lithologies. Linear features are defined either by linear magnetic trends (e.g. BMU, dolerite dykes) or by discontinuities in the alignment of magnetic trends corresponding to the presence of faults or shear zones that control fluid flow leading to magnetite formation or destruction. Linear features can also have a sedimentary origin and reflect the magnetic stratigraphy. This mapping methodology was also used by Metelka et al. (2011) and Perrouty et al. (2012). Fig. II-17 is an interpretative map of both the lithologies and the structures in the Wassa mine area.

The area with the highest magnetic response in the middle of the magnetic survey is interpreted as the metavolcanic Sefwi group hosting the Wassa deposit (Fig. II-13). The low to moderate intensity magnetic zone in the western part of the images correlates with potassium poor Tarkwaian sandstones on the radiometric ternary image (Fig. II-15). In the south eastern part of the area, the potassium rich domain with a weak thorium and uranium signal correlates with a low response, uniform magnetic area. This is interpreted as a granodiorite intrusion which was observed at two outcrops. The contact between the granodiorite and the Sefwi Group is seen in the reduced to pole (RTP) image (Fig. II-13A). In contrast this contact cannot be clearly identified on the vertical integration image (Fig. II-13B) which shows a low and decreasing magnetic intensity towards the southeast. This suggests a possible very shallow dipping contact between the Sefwi Group and the granodiorite (Fig. II-14B).

From the magnetic data a few high magnetic intensity dykes are interpreted, cross-cutting all existing lithologies. The main N-S dyke observed on the eastern part of the magnetic maps (Fig. II-13) seems to intrude along an existing fault or shear zones as suggested by a kilometre of apparent displacement of the units across the dyke. According to previous regional mapping (Agyei Duodu et al., 2009), these dykes have a dolerite composition, extend over hundreds of kilometres and are less than 100 meters thick.
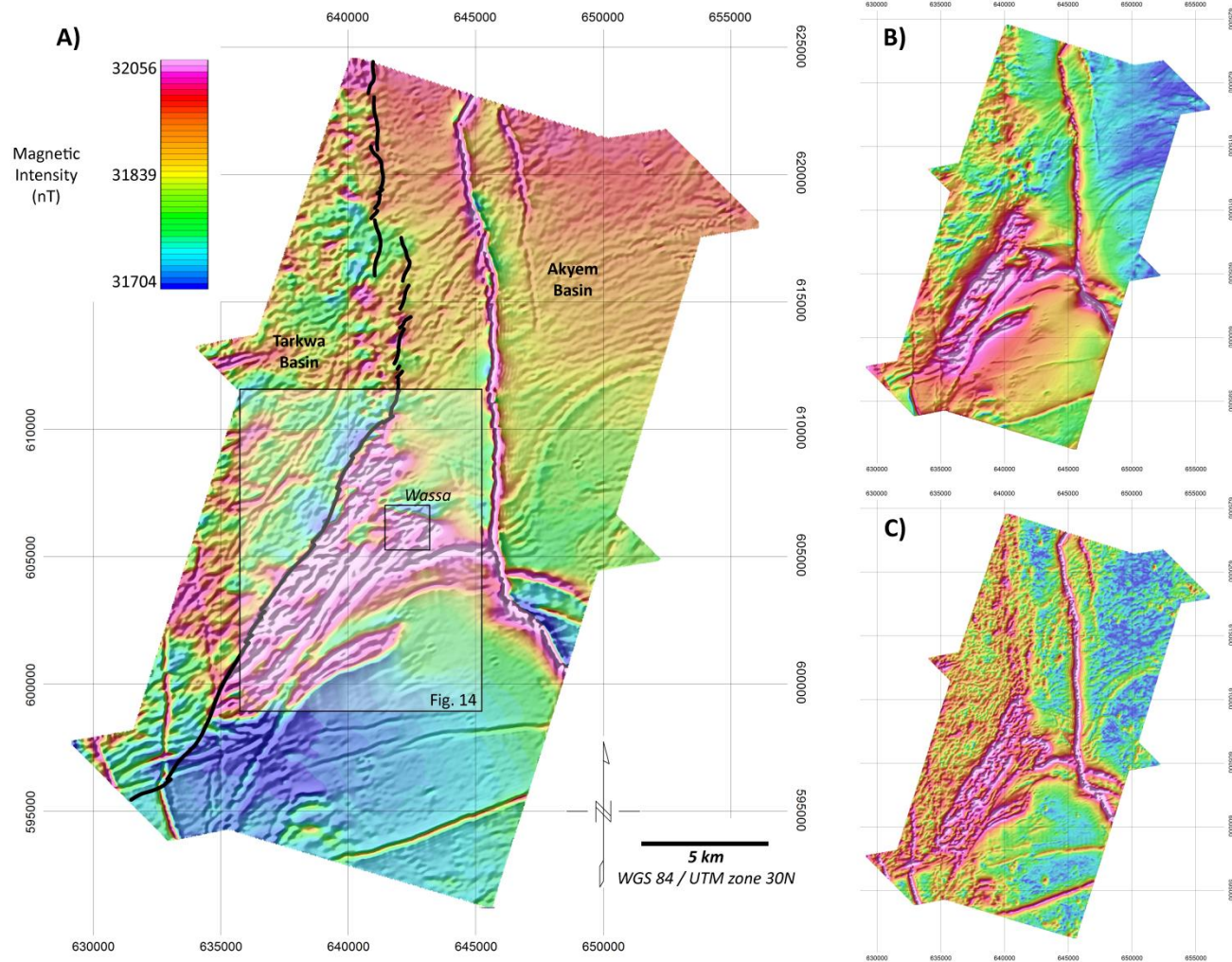
Figure II-13   *Examples of processed magnetic data. Pixel size is 25 metres. Rectangle shows the location of Figure II-14 and of the Wassa mine. A) Reduced to pole image (RTP) of the total magnetic intensity draped over the shaded first vertical derivative. B) Vertical Integration image calculated from the analytic signal. C) Tilt derivative calculated from the RTP image. Apart from the dolerite dykes, the strongest magnetic response in the middle of these images corresponds to the Sefwi Group hosting the Wassa deposit.*

111
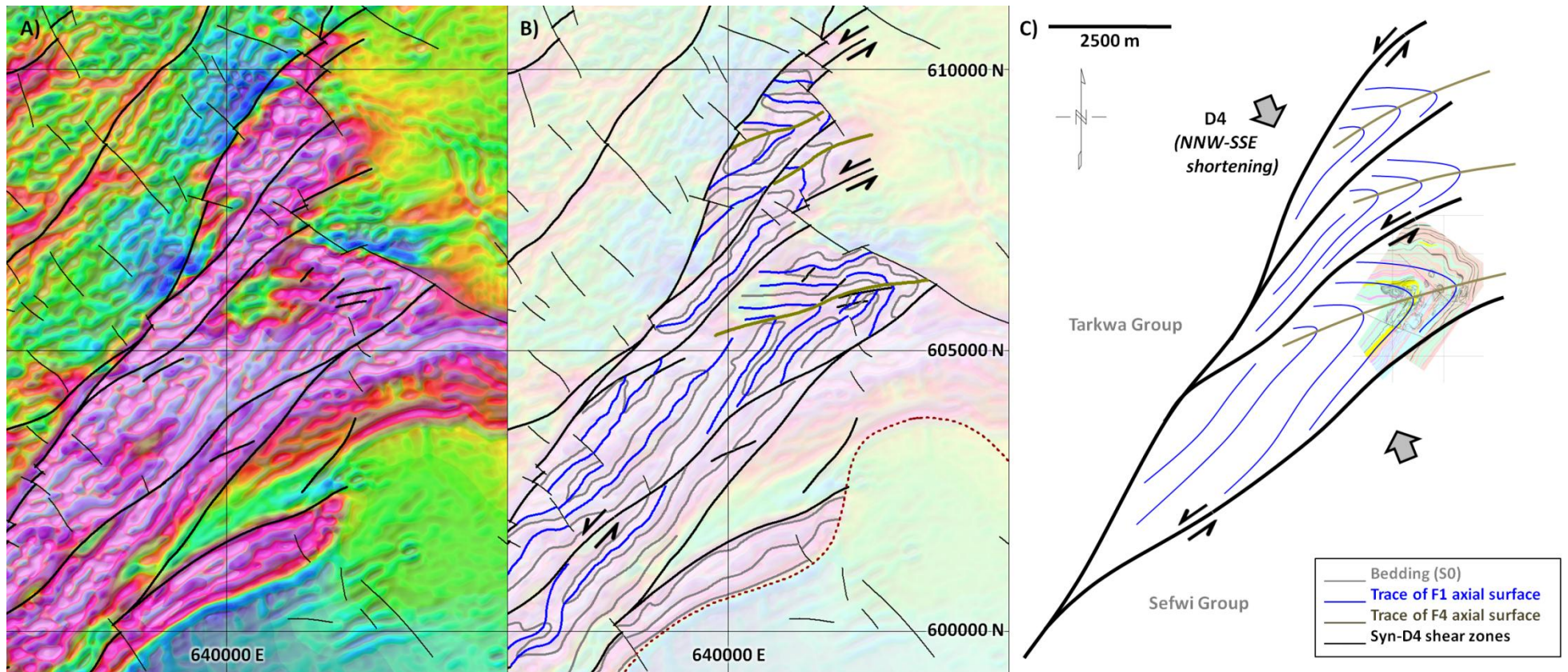
Figure II-14 *Detailed magnetic lineament interpretation in the Sefwi Group. The area is located on Figure II-13. A) The left image is the first vertical derivative after automatic gain control draped over the magnetic RTP image. This combination highlights subtle magnetic features and keeps an overview of the magnetic field amplitude. Black lines are interpreted faults. B) The middle image show our interpretation with the bedding folded by F1 and then refolded by F4 during D4 sinistral shearing. Brown dashed line on the south of the image represent the contact (dipping southeast) between the Sefwi Group metavolcanics and a granodiorite intrusion. C) The right image is a schematic interpretation of the D4 deformation in the Wassa mine area characterised by a NNW-SSE shortening. Kilometre-scale F4 folds in the Wassa mine area could have been formed to accommodate sinistral large scale shearing along the Sefwi Group/Tarkwa Group eastern contact.*
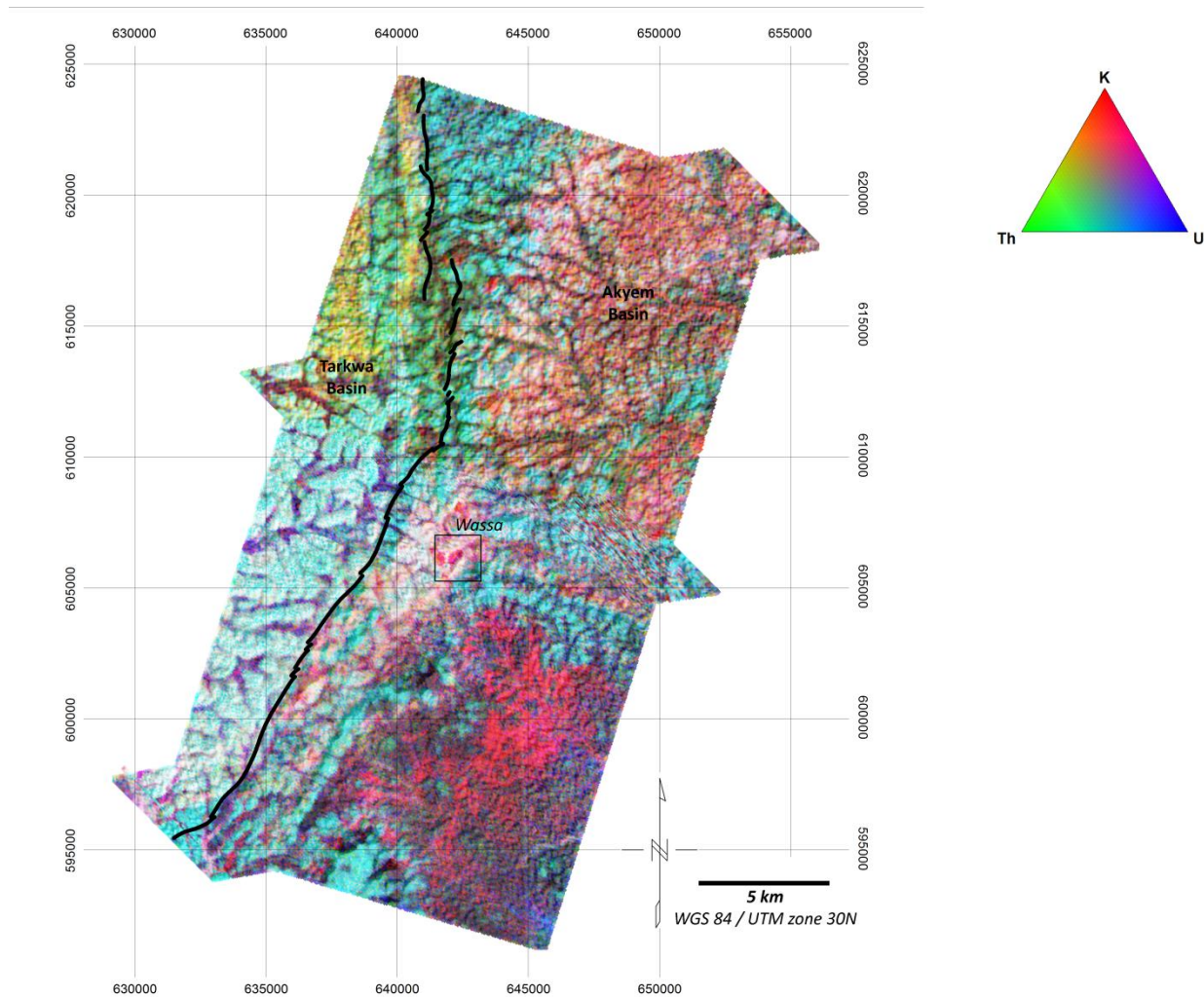
Figure II-15   *This image shows a combination of the K, Th and U bands as an RGB ternary draped over the shaded digital elevation model. The potassium-poor area in the western part of the image correlates with Tarkwaian metasediments. In contrast the potassium-rich domain in the southeast corresponds to a granodiorite intrusion. The Birimian supergroup from the northeast (Kumasi Group) to the south (Sefwi Group) shows intermediate K, Th and U proportions. Pixel size is 25 metres.*
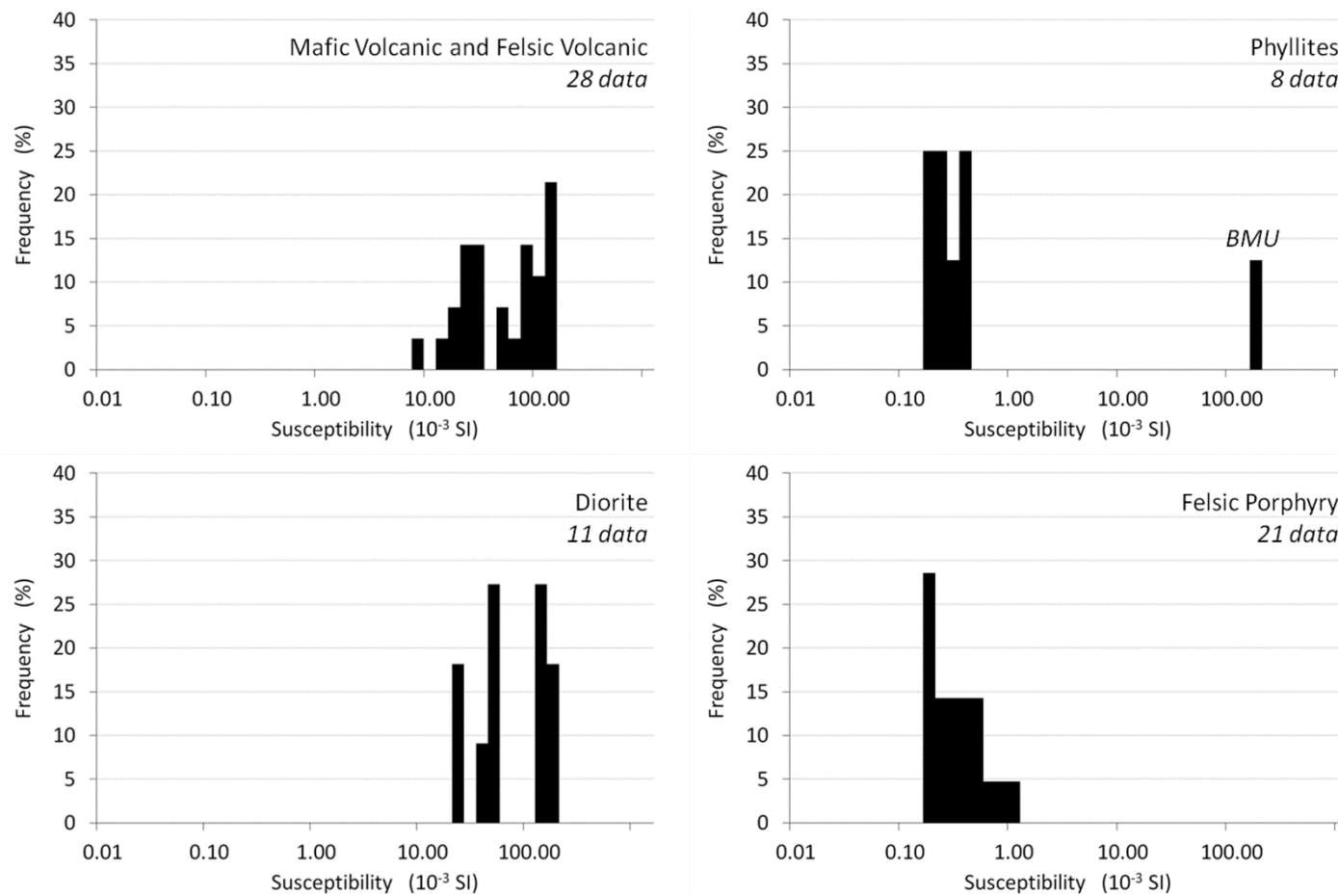
Figure II-16 *Histograms showing measured susceptibilities for each dominant lithology found in the Wassa mine area. The "Mafic volcanic", "felsic volcanic" and "metadiorite" display high susceptibility values. The "Phyllites" (excepting the BMU) and the "Felsic porphyry" are low susceptible.*
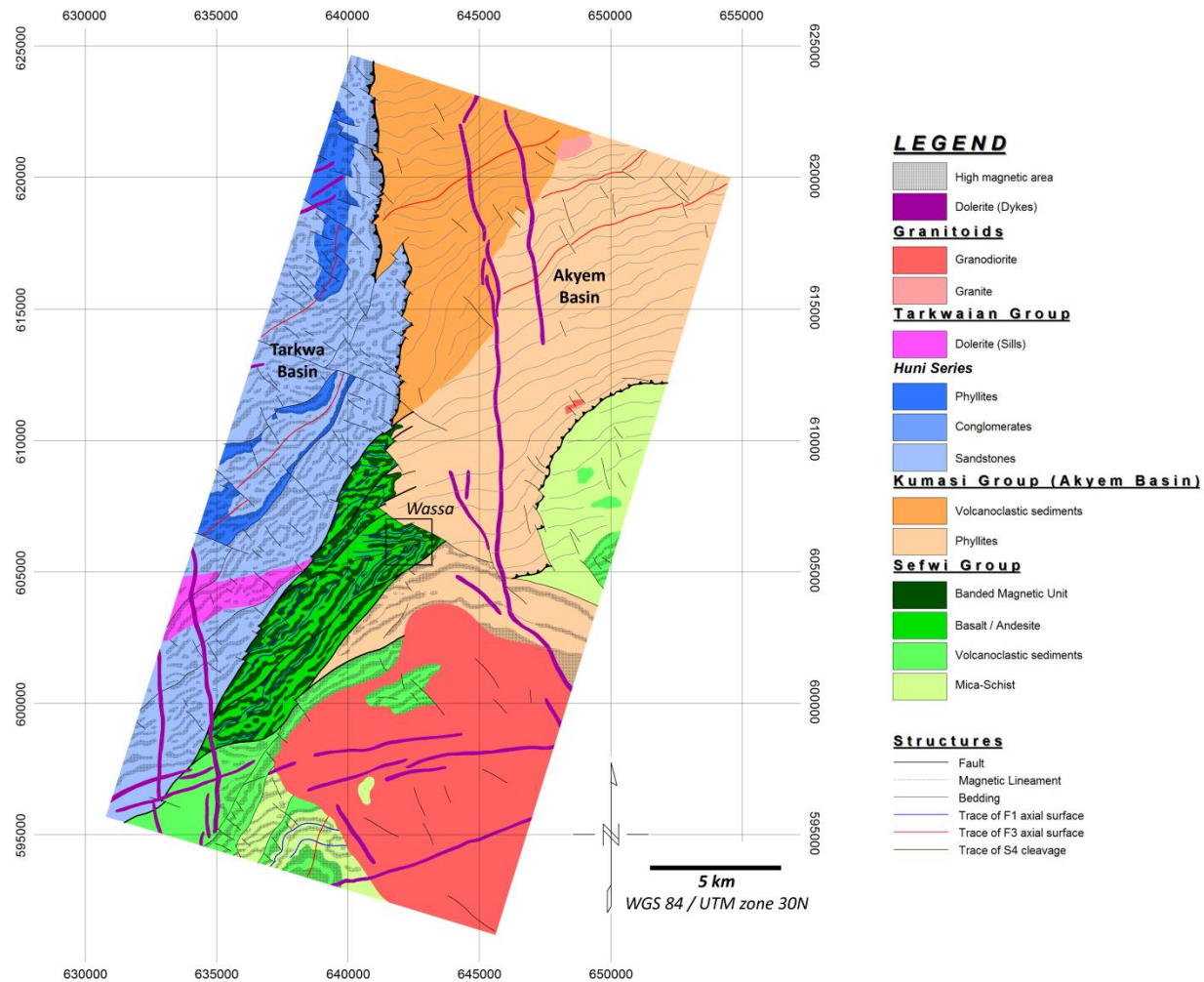
Figure II-17 *Lithological and structural interpretation of the Wassa mine region based on interpretation of airborne geophysical data and mine observations.*

In the Sefwi Group hosting the Wassa mine, the highly magnetic trends are interpreted to represent the orientation of the BMU layers with orientation assumed as equivalent to the S0-S1 cleavage. These highly magnetic BMU layers are deformed by large (100 m) scale F1 isoclinal folds that can be identified on the first vertical derivative image after Automatic Gain Control processing (AGC, Fig. II-14). The trace of these F1 folds axial surface are folded by a kilometre-scale F4 as observed in the magnetic image. The D4 shortening event also developed multiple sinistral strike-slip shear zones mostly located along the contact between the Birimian Supergroup and the Tarkwa Group. These shear zones are interpreted from the magnetic data and are evidenced by truncations with or without apparent displacement of magnetic trends (Fig. II-14) The magnetic gradients observed at the location of the shear zones suggest that they are sub-vertical or steeply dipping to the west.

3.5 Discussion

The structural interpretations integrating field observation and geophysical data around the Wassa mine mirror the regional Ashanti Belt Paleoproterozoic evolution (Perrouty et al., 2012). Although all of the regional deformation events have been identified, the D1, D4 and D5 events correspond to the most significant deformation events in the mine area (Table II-2). The Wassa mine appears to be a particular deposit in southwest Ghana in terms of Eoeburnean (2190 – 2140 Ma) timing for the main hydrothermal event. In contrast, the giant Obuasi gold deposit (60 million ounces) and the Damang deposit (8 million ounces) developed during the Eburnean phase (2130 – 2070 Ma). These three major deposits represent distinct examples of the different structural contexts of hydrothermal gold mineralisations in the southern Ashanti Belt. Their comparison (Table II-3) infers the relationship between deformation and mineralisation during the Eburnean Orogeny.

3.5.1 *Wassa-type mineralisations*

Deformation at Wassa was associated with formation of quartz veins (Fig. II-6, II-7, II-8), carbonates (ankerite and rare calcite) and sulphides (pyrite and rare chalcopyrite). The main hydrothermal event resulted in mostly low-grade gold mineralisation (Table II-2), characterised by gold-bearing pyrites elongated within the S0-S1 fabrics (Fig. II-8), folded by isoclinal F1 folds and then partially concentrated in F4 hinges (Fig. II-9A). 3D visualisation of Au assay data illustrates the distribution of mineralised horizons in the Wassa mine area (Fig. II-18). Gold mineralised layers follow a series of F1 folds refolded by the D4 event. These observations

suggest that the main hydrothermal event in the Wassa mine was associated with the early stage of the Eoeburnean D1 deformation, maybe in the form of bedding parallel veins, as has been reported in other fold related vein systems (Jessell et al., 1994).
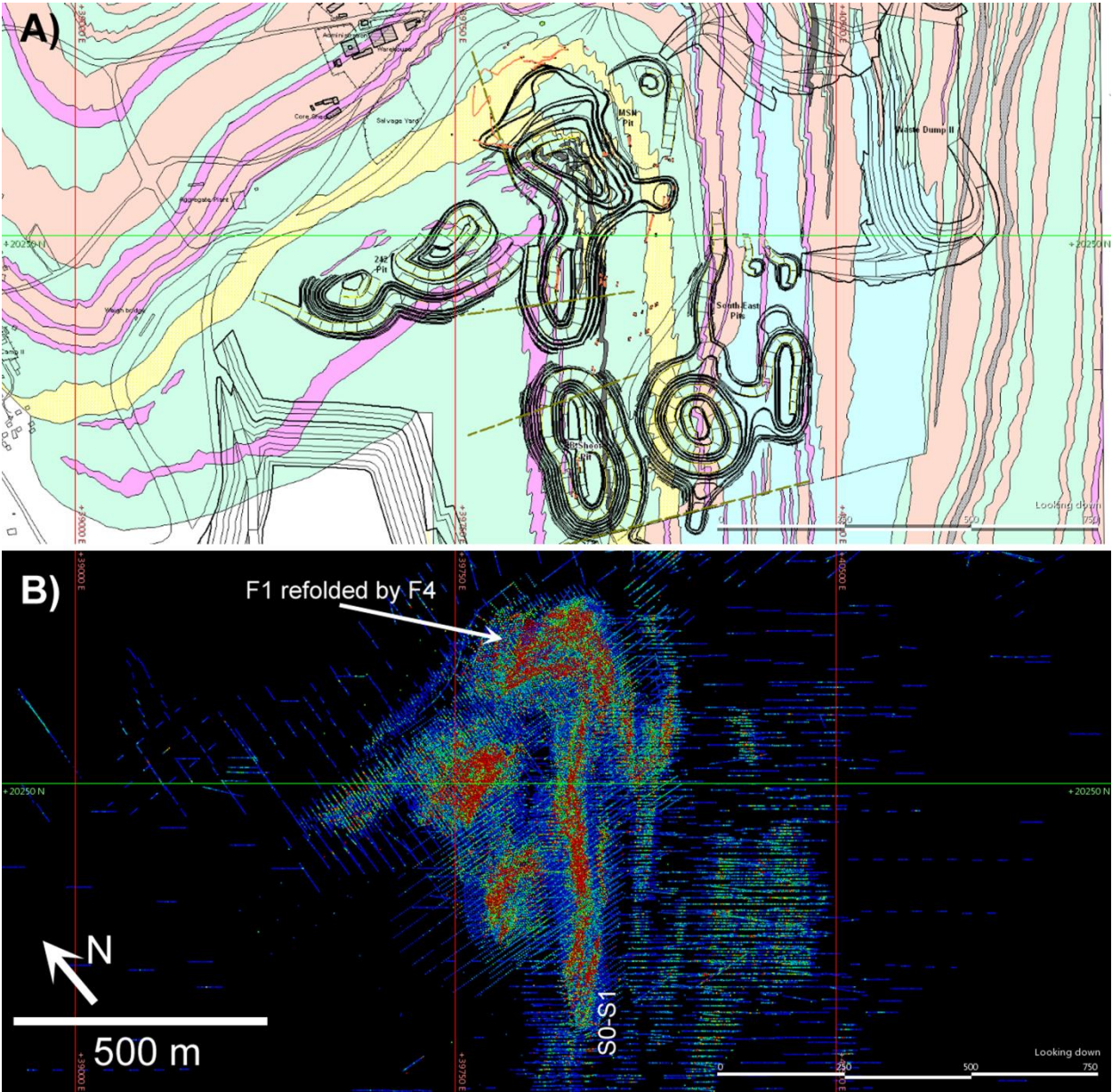
Figure II-18   *Spatial distribution of Au Assay data. A) Geological map of the Wassa mine (modified after Bourassa, 2003). B) 3D distribution of Au assays data viewed from above with gold grade > 0.5 g/t. Red color represent the highest gold grade, blue the lowest. The highest gold grade outlines specific horizons which have been preferentially mineralised and then folded by F1 and refolded around the large F4 fold hinge.*

Event	Regional kinematics (after Perrouty et al., 2012)	Structural observations	Veins, Alterations	Mineralisations, Average Au grade
D6	NE-SW shortening	Reverse fault oriented NW-SE (identified from geophysical data)	QV5 quartz-ankerite veins overprinting D4 Ankeritic, chloritic and potassic alteration	Euhedral pyrite and rare chalcopyrite Locally 10 g/t
D5	ESE-WNW shortening ?	Meter scale recumbent folds Subhorizontal S5 crenulation cleavage		
D4	NNW-SSE shortening *Sinitral shearing*	Shearing along the Tarkwa / Sefwi groups contact with kilometer scale F4 drag fold S4 crenulation cleavage	QV4 quartz veins cross-cutting F4	Non-mineralised
D3	NW-SE shortening *Major regional folds* *Tarkwa group sedimentation*	Kilometer scale open folds in both the Tarkwa and the Akyem basins Rare meter-scale folds in the Wassa mine	QV3 quartz veins folded by F4	Non-mineralised
D2	NW-SE Extension *(after Feybesse et al., 2006)* *Kumasi group sedimentation*	Akyem Basin	No data	No data
D1	N-S or NNW-SSE shortening *Major folds in the Sefwi Group*	F1 isoclinal folds S0-S1 foliation and associated lineation marked by chlorite / micas alignments	Smoky quartz and ankerite veins Ankerite, calcite and pyrite assemblages within the host rock	Gold-bearing deformed pyrites 1 to 3 g/t in the host rock Locally up to 70 g/t

Table II-2   *Summary of Wassa mine structural and hydrothermal evolution.*

		Wassa Mine (This Study)	Obuasi Mine (Allibone et al., 2002a)	Damang Mine (Tunks et al., 2004)
Eoeburnean 2140 - 2190 Ma		Sefwi Group stratigraphy **D1,** F1 Folding in the Sefwi Group Smoky QV1 quartz veins, folded by F1 Gold-bearing pyrite mineralisation	Volcanism Granitoids intrusion Regional metamorphism	
	D2	Kumasi Group (Akyem basin) sedimentation	D1 S1 parallel to bedding Flat-lying bedding parallel shearing	
Eburnean 2070 - 2130 Ma		**D3, NW-SE shortening** Tarkwa Group sedimentation Kilometre-scale folds in the Akyem Basin Rare F3 folds in the Wassa mine (Sefwi Group) S3 subvertical crenulation cleavage NE-SE QV3 quartz veins overprinting S0-S1 No mineralisation or remobilisation	D2, NW-SE shortening Isoclinal folds and thrust faults (Ashanti) Early-D2 quartz veins parallel to bedding with boudinage and possible gold mineralisation D3, NW-SE shortening Low dip axial surface folds S3 crenulation cleavage Final stage of D2 ?	D1, NW-SE shortening Kilometre scale folds Thrust faults (Damang)
		D4, NNW-SSE shortening Kilometre-scale F4 drag folds S4 crenulation cleavage ENE-WSW White QV4 quartz veins Pyrite (and gold) concentration in the hinges of F4 folds at all scale	D4, D5 NNW-SSE shortening Hectometre scale F4 folding Sinistral strike-slip D5 faults or shear zones Quartz veins in dilatant fractures in the F4 hinges or hosted by the D5 shear zones Gold mineralisation associated with sulphids	D2, NNW-SSE shortening Minor folds and faults
		D5, Metre scale recumbant folds Subhorizontal S5 crenulation cleavage - Euhedral pyrite mineralisations cross-cutting S4 Subhorizontal QV5 quartz veins Possible late D5 or syn-D6 event	Post or late D5 quartz veins Gold remobilisation in ore pods	D3, ESE-WNW shortening Open folds with sub-horizontal axial surfaces Shallow dipping quartz veins associated with thrust faults oriented NNE-SSW Pyrite and gold mineralisations Quartz veins cross-cutting D3 thrust
		D6, NE-SW shortening Low amplitude folds S6 crenulation cleavage Reverse faults oriented NW-SE		D4 Faults oriented NW-SE

Table II-3   *Summary of Wassa mine interpretation and its correlation with Allibone et al. (2002a) study in Obuasi mine and Tunks et al (2004) in Damang mine. Shaded cells indicate the main mineralisation events.*

3.5.2 Comparison with the Obuasi-type structures and mineralisations (Ashanti Belt)

The Obuasi mine is located along the Ashanti fault close to the contact between the Kumasi Group and the Tarkwa Group on the western side of the Ashanti Belt. According to Allibone et al. (2002a) five successive events deformed the Obuasi mine area during Eburnean stage (Table II-3). The D3 event (nomenclature of Perrouty et al., 2012) at Obuasi mine corresponds to the development of the Ashanti thrust fault and to a series of folds resulting from NW-SE shortening. These characteristics are in good agreement with F3 folding in the north (Kumasi Group metasediments in the Akyem Basin) and in the west (Tarkwa Group) of the Wassa mine and by a major fault marking the contact between these post-Eoeburnean metasedimentary groups.

The most significant structural correlation between the Wassa and Obuasi mines can be made for the D4 event. Allibone et al. (2002a) described hectometre scale F4 folds and a series of sinistral strike-slip shear zones. Most of these shear zones have been formed before the D4 event but are not folded by F4. They explain this contradiction with a possible continuing deformation developing both the folds and the shear zones. We interpret a similar relationship between folding and shearing at Wassa mine: the D4 event produces a series of sinistral shear zones in the Sefwi Group and along the eastern border of the Tarkwa Basin. This was followed by kilometric-scale folding resulting in NNW-SSE shortening. This shortening direction is in good agreement with a sinistral movement along the shear zones. We propose that the macro-scale F4 folding in the Wassa mine formed synchronously with sinistral shearing where drag folds developed locally to accommodate the displacement produced by the shear zones (Fig. II-12C).The Obuasi and Wassa mines are the two sites in the southern Ashanti Belt where F4 folding has been clearly identified, although D4 is expressed in numerous places as an S4 crenulation cleavage (Perrouty et al., 2012). The hypothesis of a local F4 folding event accommodating sinistral shearing is able to explain both the presence of these rare and isolated folds and their asymmetrical disposition, always on the east side of the shear zones in Wassa (Fig. II-12C).

Three major generations of quartz veins were observed in Obuasi mine by Allibone et al. (2002a). The first generation is bedding parallel, strongly boudinaged and has been produced early during the regional kilometre scale F3 folding. Allibone et al. (2002a) proposed that no major mineralisation was associated with these early veins. This first vein generation in Obuasi mine is contemporaneous of the non-mineralised QV3 quartz veins that have been observed around Wassa mine. The second quartz veins generation in Obuasi mine contains high grade of

gold and occurred in dilatant fractures in hectometre scale F4 folds during shearing. They correspond to the major gold and sulphide (mainly arsenopyrite) bearing hydrothermal event at Obuasi mine (Table II-3). In contrast, contemporaneous QV4 veins in Wassa mine are not linked with a major mineralisation event. The third generation of quartz veins presents only small amounts of gold and sulphides which could result from a late remobilisation of the pre-existing mineralisation in Obuasi mine (Allibone et al., 2002a). This last event could be synchronous with QV5 veining and with euhedral pyrite and chalcopyrite mineralisations overprinting S4 crenulation cleavage in Wassa mine.

3.5.3 *Comparison with the Damang-type structures and mineralisations*

The Damang mine is located on the eastern side of the Ashanti Belt close to the contact with the Sefwi group, and is entirely hosted in the Tarkwa metasedimentary group. Consequently, as for the Obuasi deposit, the host rocks of the Damang mine have been deformed only during the Eburnean stage. All of the corresponding deformation events found in the Wassa region are also expressed at the Damang mine (Table II-3). According to Tunks et al. (2004), the Damang major structures correspond to kilometre scale open to close folds resulting from a NW-SE shortening similar to our F3 folds observed in Kumasi and Tarkwa groups around Wassa mine. The next event in Damang mine (our D4) developed minor folds and faults under a NNW-SSE shortening.

Late deformation in Damang (our D5) is characterised by metre-scale open folds associated with a sub-horizontal crenulation cleavage, with NNE-SSW lineations and fold axis and with thrust faults oriented NNE-SSW (Table II-3). Tunks et al. (2004) described two quartz veins generations that have developed during and after this event. Their first set of veins is shallowly dipping and related to thrust fault development. They are associated with pyrite and main gold mineralisation. The second generation does not contain much mineralisation and cross-cuts the previous thrust faults.

The late timing of the mineralisation in the Damang mine contrasts with the other hydrothermal gold deposits of the Ashanti Belt. However, Tunks et al. (2004) proposed that the Damang mineralisation may consist of a remobilisation of gold and sulphides from an older hydrothermal source or from placers. Observation of late quartz veins that are also associated with a remobilisation of the main mineralisation, in the Obuasi mine (Table II-3, Allibone et al., 2002a) and in Wassa mine (QV5 veins and euhedral pyrite and chalcopyrite), suggest that these late Eburnean "remobilisations" occurred contemporaneously during D5 in many place in southwest Ghana.

3.5.4 *Implications for mineralisation at the regional scale*

The southern Ashanti Belt has been deformed during two main phases (Eoeburnean and Eburnean) associated with magmatism and with multiple mineralisation events, characterised by the Wassa-type (Eoeburnean age, hydrothermal), the Tarkwa-type (placer), the Obuasi-type (Eburnean age, hydrothermal) and the Damang-type (late Eburnean age, hydrothermal). Table II-3 summarizes the relative timing of deformation and of main mineralisation for the three hydrothermal type gold deposits. The major mineralisations occurred at different timing and structural context for these deposits and were always followed by some remobilisation during late deformation event.

3.5.4.1 Carbonate alteration

All of the hydrothermal deposits in southwest Ghana are associated with carbonate alteration of their host rocks. In the Wassa mine, a hydrothermal ankerite-calcite alteration is related to early quartz vein formation and primary gold mineralisation. Numerous ankerite veins stretched and boudinaged within the S1 foliation have also formed during this event. Mumin et al. (1995, 1996) correlate the carbonate alteration of the basalt with the sinistral strike-slip reactivation of the Ashanti fault (D4) followed by gold mineralisation in the Prestea and Bogoso mines or in the Obuasi mine (Allibone et al., 2002a). Damang syn-D5 mineralisation is also associated with sericite-calcite assemblages and with quartz veining (Tunks et al., 2004). These studies show that the systematic presence of important carbonate alterations of the host rocks developed in relation with the main gold mineralisations whatever the considered deposit in the Ashanti Belt.

3.5.4.2 A Wassa-type deposit source of the gold for the placers

The Eoeburnean Wassa-type gold mineralisation is a possible candidate for the source of the gold contained in the Tarkwa paleoplacer (over 40 Moz). (1) As deducted from field and thin-section observations the main gold mineralisation in Wassa mine formed very early in the tectonic evolution of the Ashanti Belt (Table II-2). (2) Sefwi Group lithologies at Wassa mine are characterised by chlorite, carbonates, magnetite (in the BMU), tourmaline and pyrite and by numerous quartz-ankerite veins. This mineral assemblage is consistent with studies by Sestini (1973) and Hirdes et al. (1994) that described the presence of tourmaline, carbonates, hematite, pyrite and chloritoids associated with the Tarkwaian quartz pebbles. Tarkwaian phyllites also show intense cross-bedding marked by magnetite. (3) The Wassa mine is considered to be a low gold grade deposit that is not usually favourable to make a source for placer. However, gold

distribution is very heterogeneous and some visible gold grain are present (nuggetty grade distribution of gold as shown on Fig. II-12A).

Considering the relative ages, mineral assemblages and gold grades observed in the hydrothermal Wassa deposit and in the Tarkwa placer, the Wassa-type Eoeburnean deposits hosted by the Sefwi Group could be a potential source of gold of the Tarkwa group placers.

3.6 Conclusions

This paper represents the first published structural interpretation integrating field observations and geophysical data of a major Eoeburnean gold deposit in southwest Ghana (Table II-2). The Wassa mine exhibits multiple deformation events which are consistent with those reported by Perrouty et al. (2012) at the regional scale. These deformation events are associated with multiple hydrothermal events that characterise the Wassa-type, the Obusai-type and the Damang-type quartz and carbonates veins, sulphide and gold mineralisation.

The Wassa Eoeburnean mineralisation is unusual in southwest Ghana as it developed very early in the structural evolution of the belt. Gold-bearing pyrites observed in the S0-S1 fabric were strongly deformed during D1 macro-scale folding (pre-Tarkwaian). By its early-timing and its associated mineral assemblage, this style of mineralisation constitutes a reasonable candidate for the source of the Tarkwa placer gold.

Mineralisation that occurred during the Eburnean phase was regionally controlled by major faults and shear zones with timing varying from syn-D4 in Obuasi to syn-D5 in Damang. In the Wassa mine these deformation events were associated with late quartz veins generations showing little mineralisation that may represent local remobilisation of earlier mineralisation.

3.7 Résumé du chapitre II

3.7.1 *Introduction*

La ceinture d'Ashanti héberge de nombreux gisements d'or hydrothermaux et de placers. Comme l'ont mentionné de précédentes études (Allibone et al., 2002a), la plupart des gisements hydrothermaux sont contemporains des grands cisaillements senestres (e.g. Faille d'Ashanti, gisements de Prestea, Bogoso, Obuasi) de la seconde phase de l'Orogénèse Éburnéenne de Bonhomme (1962). Toutefois, la présence de gisements de placers dans le bassin de Tarkwa,

plus anciens, nécessite la présence de minéralisations en or antérieures, d'âge Éoéburnéen. Bourassa (2003) suggère que les minéralisations comme celles observées dans le gisement de Wassa, potentiellement précoces, pourraient être à la source de l'or contenu dans les placers. Ce second chapitre a pour but de caractériser les événements de minéralisations à la mine de Wassa, de les inclure dans l'évolution structurale précédemment établie (cf. chapitre I) et d'établir des corrélations avec les autres gisements connus tel Obuasi (60 millions d'onces).

3.7.2 *La mine de Wassa*

La mine d'or de Wassa se situe à 30 km au nord-est de la ville de Tarkwa, à l'est de la ceinture d'Ashanti, dans le groupe de Sefwi. Au contraire de tous les autres gisements hydrothermaux connus le long de la ceinture d'Ashanti, celui de Wassa ne semble pas être localisé le long d'une zone de cisaillement majeure. Bourassa (2003) et McCandlish (2003) décrivent un contexte structural complexe, avec notamment un pli d'échelle hectométrique, dont la charnière est centrée sur la mine de Wassa. Ils mentionnent également la présence de plusieurs épisodes de minéralisations associés à la formation de veines de quartz et à la précipitation de sulfures.

3.7.3 *Observations de terrain*

Plusieurs lithologies peuvent être distinguées dans la mine de Wassa : des métabasaltes, des métaandésites, des métavolcanosédiments (phyllites) et des métadiorites. L'analyse minéralogique de ces lithologies indique des assemblages de quartz, de chlorite, de carbonates (ankerite et calcite) et de rares feldspaths plagioclases avec des proportions légèrement variables selon la roche considérée. De même, l'analyse géochimique montre une certaine similitude de composition, en éléments majeurs et traces, entre ces lithologies. Le site de Wassa est également parcouru de niveaux très enrichis en magnétite, appelés BMU (Banded Magnetic Unit). Ces niveaux semblent être subparallèles à la foliation S0 – S1.

Les observations structurales conduisent à l'identification des phases de déformations décrites à l'échelle régionale (cf. chapitre I). Les déformations dominantes à Wassa sont reliées aux évènements D1, avec le développement de grands plis isoclinaux, D4 avec un plissement majeur, de nombreux plis parasites, et une crénulation intense de la foliation S0 – S1, et D5, marqué par une crénulation subhorizontale du clivage S4 et par la mise en place de plis couchés d'amplitude et de longueur d'onde très variables suivant l'orientation des précédentes structures.

L'hydrothermalisme associé au début de la phase D1 (Éoéburnéenne) conduit à la formation de pyrite et d'or, au contact des veines de quartz. Ces veines et ces pyrites sont

transposées, boudinées et plissées le long de la foliation S0 − S1. Les minéralisations plus tardives, Éburnéennes, sont représentées par des pyrites et de rares chalcopyrites automorphes recoupant la crénulation S4. Cet évènement tardif dérive d'une possible remobilisation de la minéralisation principale à la mine de Wassa.

3.7.4 *Géophysique structurale*

L'interprétation des données géophysiques héliportées montrent clairement les relations entre les déformations D1 et D4. Notamment, les données magnétiques mettent en évidence les niveaux de BMU, supposés parallèles à la foliation S0 − S1. Ceux-ci sont plissés une première fois par les plis isoclinaux F1 puis replissés par le pli F4. Plusieurs zones de cisaillements D4 parcourent également la région de Wassa. La formation du pli F4 majeur observé à Wassa pourrait ainsi avoir été contrôlée par ces zones de cisaillement, pour accommoder le déplacement.

3.7.5 *Discussion*

Cette étude met en évidence un troisième épisode hydrothermal au sud-ouest du Ghana, caractérisé par le gisement d'or de Wassa. La minéralisation principale est associée à des veines de quartz formées au tout début de la déformation D1, avec des concentrations en or qui semblent être distribuées le long des plis isoclinaux F1. Il est suggéré que des minéralisations de type Wassa, développées durant la phase Éoéburnéenne, pourraient, de par leur précocité, avoir fourni l'or aux placers du bassin de Tarkwa. Les phases de minéralisations tardives sont représentées par les gisements de type Obuasi (Allibone et al., 2002a, 2002b) et de type Damang (Tunks et al., 2004). Les contextes structuraux de ces minéralisations Éburnéennes s'observent également à la mine de Wassa où ils sont associés avec des remobilisations locales de l'or précoce.

Chapitre III

Chapitre III

A new model for Paleoproterozoic crustal growth in southwest Ghana: an Eoeburnean crustal source for the younger Eburnean granites

<u>Abstract</u>

New whole rock geochemical data were acquired on samples of igneous and sedimentary rocks from the southern Ashanti Belt in southwest Ghana. Previously published dating and overprinting relationships permit us to establish the chronology of the analysed granitoid intrusions. New and published geochemical results supported by age data clearly show that two distinct magmatic episodes (Eoeburnean, 2190 - 2140 Ma, Eburnean, 2130 - 2070 Ma) occurred in southwest Ghana during the Eburnean Orogeny.

The first phase (Eoeburnean) produced calc-alkaline volcanism and numerous Paleoproterozoic TTGs (mostly tonalite and granodiorite) within the Birimian Sefwi Group. Rare Earth Element profiles show enrichment in LREE (high La/Sm and La/Yb ratios) and flat profiles for the HREE (Gd/Yb ratio close to 1). Positive Ba anomalies and negative Ta, Nb and Th anomalies are also observed. The second phase (Eburnean) formed more differentiated intrusions, with granodiorite, granite and leucogranite compositions, that are hosted by the entire Ashanti Belt (Sefwi, Kumasi and Tarkwa groups). These Eburnean granitoids contrast with the Eoeburnean intrusions by their strong depletion in HREE (high Gd/Yb ratio).

Our proposed geodynamic model starts with a first Eoeburnean magmatic phase in a subduction-related context (as has already been suggested by previous studies in West Africa) that was associated with a significant deformation of the Sefwi Group, according to ages and overprinting relationships. This magmatism and deformation caused thickening of the Eoeburnean crust and metamorphism at depth. Thermodynamic modelling shows that partial melting of garnet-bearing metamorphosed rocks with the composition of the Eoeburnean crust can produce melts depleted in HREE with Eburnean granitoid major element geochemistry. This mechanism of partial melting of a garnet-bearing metamorphosed lower crust may play an important role in the generation of Archean / Paleoproterozoic granitoid intrusions.

4.1 Introduction

The Paleoproterozoic Birimian and Tarkwaian units that comprise the Ashanti greenstone belt in southwest Ghana were deformed during the Eburnean Orogeny ($\approx$ 2.1 Ga, Bonhomme, 1962) and are intruded by numerous granitoids. The geochemistry of Birimian rock assemblages has been investigated by Dampare et al. (2008) in the Sefwi Group basalts, by Attoh et al. (2006) in ultramafic rocks and by Asiedu et al. (2004, 2009) in the Kumasi Group metasediments. Many studies performed geochemical analyses of the granitoids (Mauer, 1990, Loh et al.; 1999, John et al., 1999; Yao et al., 2000). Mauer (1990) and Loh et al. (1999) integrate their geochemical data into a regional scale interpretation and distinguish two types of granitoids: the belt-I-type and the basin-S-type, depending on their location and geochemical characteristics. Klein et al. (2005, 2008) highlight two phases of magmatism based on age correlations with the South American São Luís Craton (believed to be a small fragment of the West African Craton in northern Brazil). A classification based on geochemical and petrological evolution of granitoids with time rather than on the location within the belts or basins seems to be more appropriate according to the histogram of ages (Perrouty et al., 2012) that clearly indicates two phases of plutonism.

Most of the previous studies in southwest Ghana described the belt-type tonalites and granodiorites as Archean TTG analogue. However, although these Paleoproterozoic TTG display a mineralogy similar to the Archean TTG (Moyen and Martin, 2012), they also display different trace elements geochemistry patterns that clearly suggests a different geotectonic context for their formation. This paper characterises the geochemical signature of the two phases of granitoid magmatism, contributing to a better understanding of the magmatic evolution of the Ashanti Belt during the Eburnean Orogeny and possible mechanisms of the Paleoproterozoic continental crustal growth in West Africa.

Whole rock major and trace elements of various intrusions and their host lithologies were analysed in southwest Ghana. Ages of all the analysed samples of intrusive rocks are constrained by previously published geochronology as well as by the relative geochronology based on overprinting relationships. The new data combined with previously published data show that both the Eoeburnean and Eburnean (De Kock et al., 2011) phases of the Eburnean Orogeny of Bonhomme (1962) developed magmatism specific to their respective tectonic contexts.
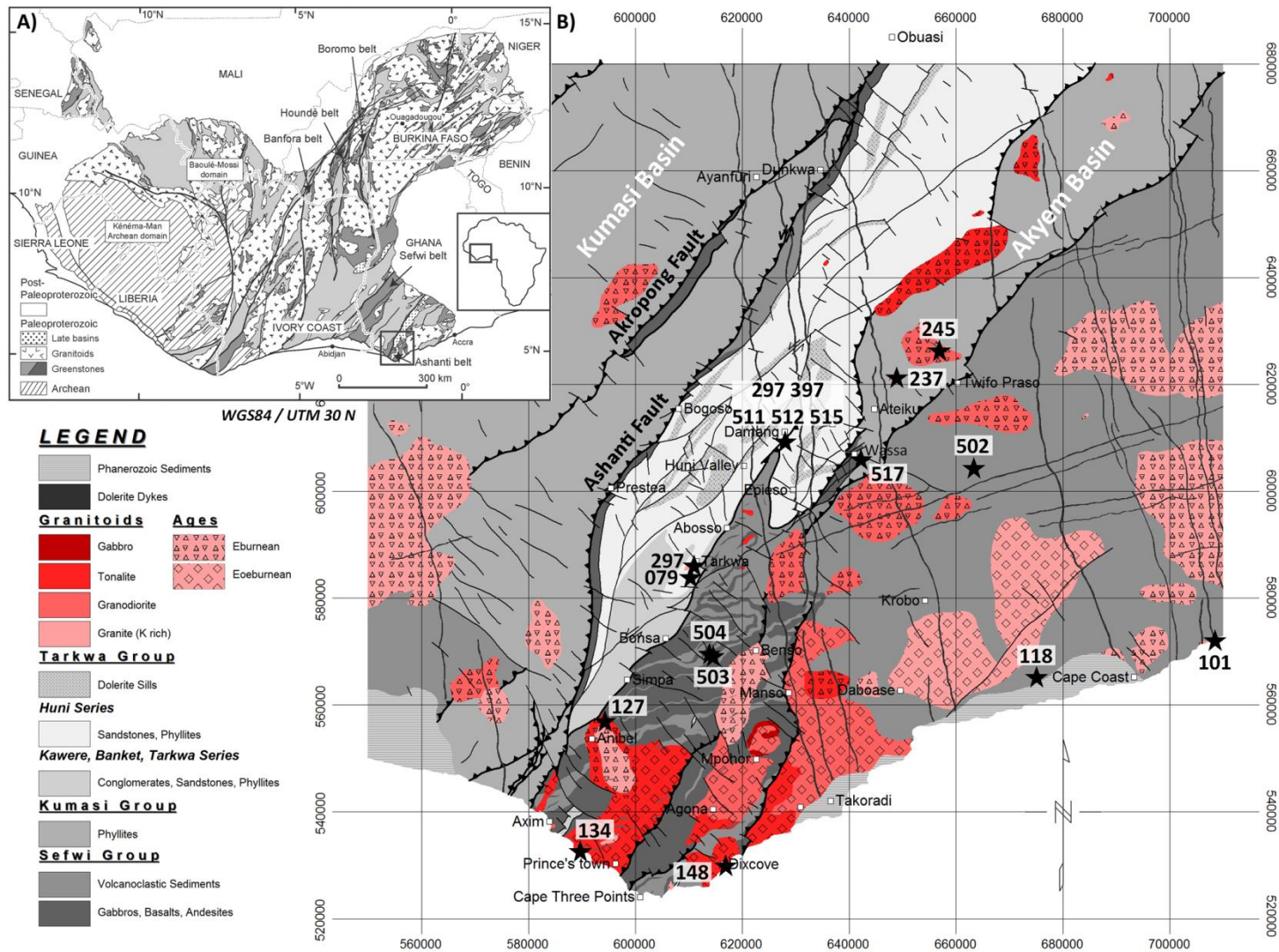
Figure III-1 *Map of the southern Ashanti Belt. Eoeburnean granitoids intruded the Sefwi Group in the south and southeast of the Ashanti Belt. Eburnean intrusions are found across the area with numerous intrusions found within the metasedimentary basins. Samples collected in the study are reported on the map.*
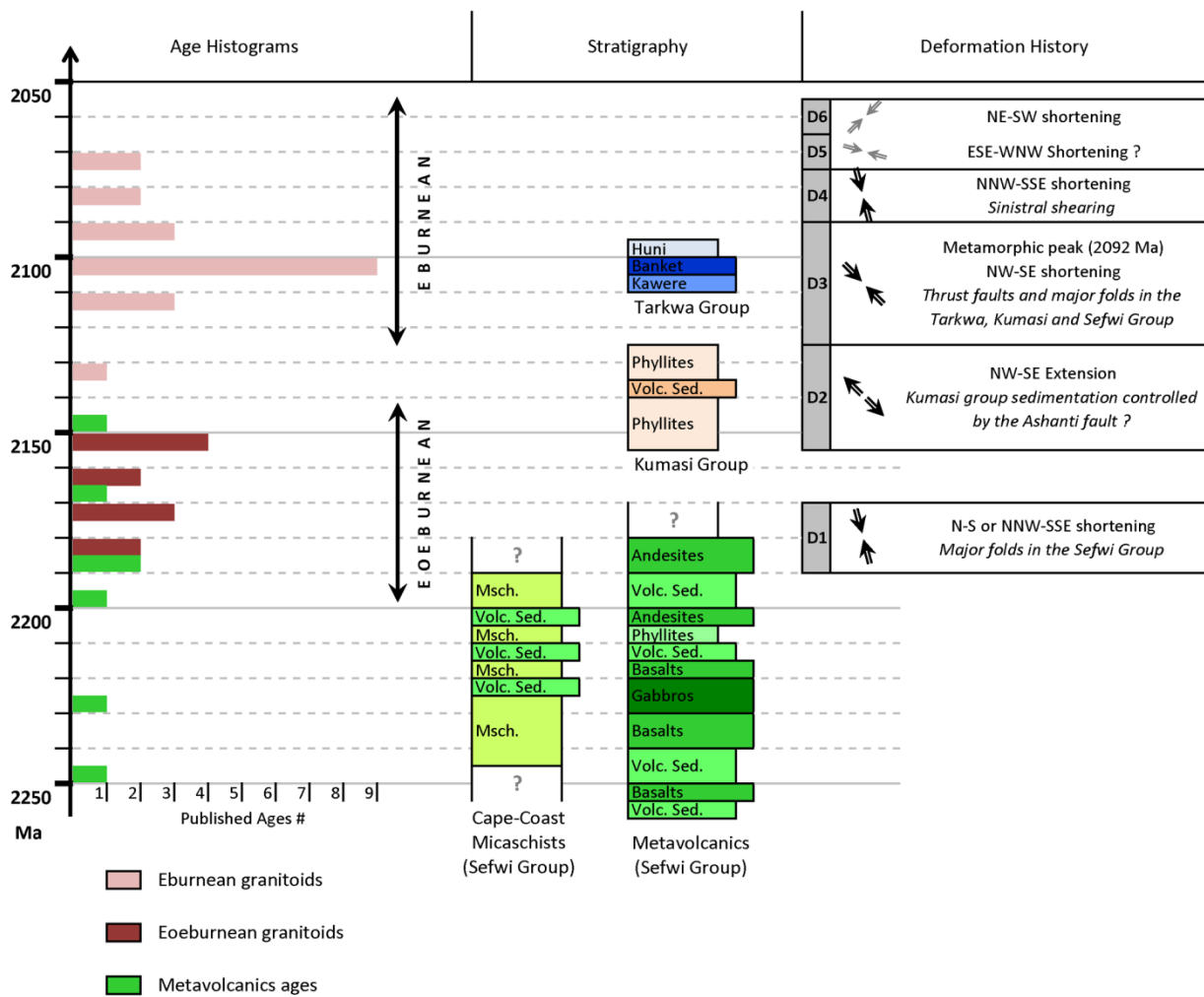
Figure III-2   *Summary of granitoid ages, metavolcanic rock ages and deformation phases in the southern Ashanti Belt.*

Figure III-3   *Photographs of granitoid outcrops: investigated granitoids were preferentially sampled in quarry (a) (c), along the coast (b) or in large scale outcrops (d). Samples from mine sites were collected as far as possible from the main mineralised zone. (a) GH127B Granite with tonalitic aureole and hosting numerous mafic xenoliths, overprint the D1 deformation of the Sefwi Group, Anibel village. (b) GH101 Granodiorite veins emplaced within the S3 foliation of the hosting garnet-bearing micaschist, east of Cape Coast. (c) GH118B Foliated granodiorite, northwest of Cape Coast. (d) GH237 Leuco-granite, any visible deformation, west of Twifo-Praso.*

4.2 Geological setting

4.2.1 *Geodynamic context*

The southwest of Ghana, in the southeastern West African Craton consists of a series of greenstone belts oriented NE-SW separated by metasedimentary basins. These paleoproterozoic terrains were strongly deformed and metamorphosed during the Eburnean Orogeny (2250 - 2050 Ma according to John et al., 1999, Ledru et al., 1994, Milesi et al., 1992, Bonhomme, 1962). The Ashanti Belt and the bordering Kumasi and Akyem basins (Fig. III-1) consist of three major stratigraphic groups known as the Sefwi, Kumasi and Tarkwa groups (Adadey et al., 2009). Major lithologies correspond to gabbros, basalts, andesites, volcanosediments, micaschists, phyllites, conglomerates and sandstones which have been intruded by numerous granitoids. The Sefwi and Kumasi groups form the Birimian Supergroup (Kitson, 1928).

Both the structural study in the Obuasi mine by Allibone et al. (2002) and the regional interpretation of Perrouty et al. (2012) separate the deformation events of the Eburnean Orogeny of Bonhomme (1962) into two broad phases at 2190-2150 Ma (Eoeburnean) and 2130-2070 Ma (Eburnean). These deformation phases correlate with two magmatic episodes as shown by the granitoid age distribution (Fig. 2, Taylor et al., 1992; Hirdes et al. 1992, 1994, 1998; Davis et al., 1994; Oberthür et al., 1998; Loh et al., 1999; Attoh et al., 2006; Feybesse et al., 2006; Agyei Duodu et al., 2009). A similar evolution was also identified in northern Ghana by De Kock et al. (2011).

The Eoeburnean and Eburnean phases correspond to six regional deformation (two Eoeburnean and four Eburnean) and developed minimum of four gold mineralisation events (Perrouty et al., 2012). The first deformation phase corresponds to a N-S shortening affecting only rocks of the Sefwi Group, developing a series of isoclinal F1 folds with a subvertical S1 cleavage defined by mica alignment. Only a few Eoeburnean granitoids were intruded during the D1 deformation (Loh et al. 1999).

The Kumasi Group sediments deposited during D2 extensional event related to a rifting phase in northwest Ghana between 2148 and 2125 Ma (De Kock et al., 2011). The Tarkwa Group sediments formed in response to the onset of D3 Eburnean shortening as proposed by Feybesse et al. (2006).

Eburnean deformation affected both the Birimian and Tarkwaian Groups. D3 corresponds to a NW-SE shortening event that developed large scale open folds with a subvertical crenulation cleavage and major thrust faults including the Ashanti Fault (Milési et al., 1992; Feybesse et al.,

2006). The peak of metamorphism occurred during the D3 deformation at 2092 ± 3 Ma (Oberthür et al., 1998) with temperature and pressure conditions reaching 500-650°C and 5-6 kbar, respectively (John et al., 1999; Schmidt Mumm et al., 1997). A second major Eburnean deformation event reactivated previous thrusts with a sinistral strike-slip movement (e.g. Ashanti Fault). This D4 shearing is associated with the development of hectometre scale folds (Allibone et al., 2002). These folds may locally accommodate the displacement induced by the shear zone. Most mineralisation takes place during D4 with a concentration of highest gold grade along the shear zones, such as along the Ashanti Fault. Perrouty et al. (2012) also described two late Eburnean deformation events, D5 and D6, which do not significantly affect the regional geometries.

4.2.1 *Sefwi metavolcanic group*

The southern and southeastern parts of the Ashanti Belt are dominated by the Sefwi Group (Adadey et al., 2009) and are composed of metavolcanic / metaplutonic rocks (basalts, andesites and gabbros) and of micaschists, alternating with phyllites and volcanosedimentary layers (Fig. III-2).

Dampare et al. (2008) and Attoh et al. (2006) geochemical studies agree with the stratigraphy proposed by Sylvester et al. (1992), corresponding to a unique thick volcanic sequence (3500 m of massive basalts with pillow lavas at the base) that overlay gabbros and ultramafic rocks. Two types of volcanic rocks can be distinguished in the southern Ashanti Belt. According to Dampare et al. (2008), type I basalts, found close to Cape Three Point, have a tholeiitic affinity close to the calc-alkaline field. They are derived from a depleted mantle melting and display Rare Earth Elements (REE) patterns enriched in light elements compared to those of the Mid-Ocean Ridge Basalt (MORB). Pillow basalts observed near Dixcove (Butre Beach, Loh et al., 1999) could also correspond to this type I. Type II volcanics consist of a calc-alkaline fractional crystallisation suite producing basalts and andesites in an Intra-Oceanic Island Arc context (Dampare et al., 2008). A few rhyolite occurrences mentioned by Loh et al. (1999) illustrate a relatively high degree of fractional crystallisation. Dampare et al. (2008) proposed that type I magma progressively evolved into type II from the east (Cape Three Point) to the west (Axim). The available U/Pb zircon ages of metavolcanic rocks range from 2266 ± 1 Ma (Loh et al., 1999) for the tholeiitic series to 2142 ± 24 Ma (Adadey et al., 2009) for the calco-alcaline series. Consequently, the Sefwi Group "type I" tholeiitic volcanism is anterior to the first plutonic phase identified in southwest Ghana (Eoeburnean) while the "type II" calco-alcaline volcanism seems to be synchronous.

Rare ultramafic Sefwi Group rocks (peridotite, pyroxenite, harzburgite, dunite) have been found in the northwest of Cape Three Point. This proposed ophiolitic suite was formed during Eoeburnean deformation (Attoh et al., 2006). The Sefwi Group stratigraphy with ultramafic rocks, gabbros, pillow basalts and volcanosediments may correspond to a pre-Eoeburnean oceanic crust or to an oceanic plateau fragment (Attoh et al., 2006).

4.2.2 *Kumasi metasedimentary group*

The Kumasi Group is composed of alternating phyllites and volcanosediments that were deposited within the Kumasi and the Akyem basins, either side of the Ashanti Belt. This metasedimentary group corresponds to the Lower Birimian series of Junner (1940) and Milési et al. (1992). U/Pb ages on detrital zircons indicate a maximum deposition age at 2154 ± 2 Ma (Oberthür et al., 1998) for the Kumasi Group. The end of Kumasi Group deposition is constrained by intrusions of Eburnean granitoids at 2136 ± 19 Ma (Adadey et al., 2009).

Geochemical analyses of the Kumasi Group metasediments from the Akyem Basin (Birim Diamond field, Asiedu et al., 2004) and the Kumasi Basin (Konongo region, Asiedu et al., 2009) have been conducted. These sediments are characterised by a ferromagnesian content higher than average Paleoproterozoic crust indicating an important mafic component in their source. Asiedu et al. (2004) suggest a local provenance for these sediments that probably derived from both the Sefwi Group metavolcanic rocks and the Eoeburnean granitoids that intrude the greenstone belts. Asiedu et al. (2004) also showed that the Kumasi Group have trace elements features typical of the Archean sedimentary rock (low Th/Sc ratios, high Cr/Sc ratios). They suggest that the Eoeburnean crust (Paleoproterozoic) of southwest Ghana which constitutes the source of these sediments displays significant similarities with the Archean crust.

4.2.3 *Tarkwa metasedimentary group*

The Tarkwaian metasediments are composed of conglomerates, sandstones and phyllites organised in four successive units known as the Kawere Group, the Banket Formation, the Tarkwa Phyllites and the Huni Sandstones (Whitelaw, 1929; Junner, 1940; Kesse, 1985) with a total thickness of more than 3000 metres. The Tarkwa Group is considered to have derived from surrounding Birimian rocks as suggested by Birimian quartz and metavolcanic pebbles found in the conglomerates (Hirdes et al., 1994). U/Pb and Pb/Pb ages obtained on detrital zircons (Davis et al., 1994, Hirdes et al., 1994, Pigois et al., 2003) give maximum deposition age around 2107 Ma after re-examination of all available zircon data (Perrouty et al., 2012). The minimum

estimated age for the Tarkwaian deposition is constrained by Eburnean granitoid intrusions at 2097 ± 2 Ma (Oberthür et al., 1998).

4.2.4 *Intrusive rocks*

Many granitoids intruded both the metavolcanic and the metasedimentary groups during the Eoeburnean and Eburnean orogenic phases (Fig. III-2). Their composition varies from gabbro/diorites to K-rich granites, although most of them correspond to tonalite and granodiorite. They commonly contain xenoliths of mafic rocks from the Sefwi Group.

Loh et al. (1999) classified these granitoids in two main categories called belt-type and basin-type, which are also called G2 and G1 respectively by Mauer (1990). The belt-type group includes the Prince's Town, Dixcove and Ketan (Sekondi) I-type plutons, located in the southern part of the Ashanti Belt. Dampare et al. (2005) suggested that these granitoids may have derived from partial melting of the Sefwi Group metamafic rocks in a volcanic arc context. In contrast, Mauer (1990) suggested a mantle source. Zircon dating give U/Pb ages around 2158.9 ± 3.6 Ma (Attoh et al., 2006), 2171 ± 2 Ma (Hirdes et al., 1992) and 2174 ± 2 Ma (Oberthür et al., 1998) for the three above mentioned plutons, respectively. According to Loh et al. (1999), the Ketan pluton displays a penetrative foliation, unlike the Dixcove and Prince's Town plutons, devoid of any visible deformation. All of them intruded the Sefwi Group metavolcanic rocks (explaining their initial 'belt-type' nomenclature) and are representative of Eoeburnean stage plutonism.

The basin-type granitoids mainly occurred in the Kumasi and Akyem basins. They display S-type characteristics (Loh et al., 1999). They are less mafic than the belt-type granitoids and display granodioritic and granitic compositions. The youngest intrusions are sometimes K-rich. Mauer (1990) proposed two formation models: (1) a formation in situ by partial melting of surrounding metasedimentary rocks, or (2) a formation by melting of metamafic rocks with significant contamination by the upper crustal metasediments. The ages of the basin-type granitoids correspond to the Eburnean orogenic episode, varying between 2136 ± 19 Ma (U/Pb age on zircon, Adadey et al., 2009) and 2072 ± 1 Ma (U/Pb age on zircon, Agyei Duodu et al., 2009).

4.3 Samples

Geochemical analyses were carried out on 21 samples of representative lithologies from the southeastern part of the Ashanti Belt (Fig. III-1, Fig. III-3).

4.3.1 *Intrusive rocks*

The intrusive rocks samples represent various compositions ranging from gabbro / diorite to leucogranite. They are related to both the Eoeburnean and Eburnean phases according to previous dating and overprinting relationships.

4.3.1.1 Eoeburnean intrusions

Seven samples of Eoeburnean intrusive rocks were analysed. The mineralogy of Eoeburnean granitoids consists of quartz, plagioclase, biotite, amphibole and rare clinopyroxene. Chlorite, epidote and few muscovites were found in deformed and metamorphosed samples (orthogneisses). **GH517B** is a small granodiorite intrusion located in the south of the Wassa mine. It shows a penetrative foliation sub-parallel to the S1 cleavage of the surrounding host rocks that attests to the Eoeburnean age of this intrusion. Many similar granodiorites and tonalites have been reported along the coast by Loh et al. (1999), John et al. (1999) and Dampare et al. (2005). **GH502** occurs in the Sefwi Group micaschists, 15 kilometres south of Twifo-Praso. It is a foliated orthogneiss with mica alignment (S1) related to D1 deformation event (Perrouty et al., 2012). **GH148** and **GH134** correspond to the Dixcove tonalite dated at 2171.6 ± 1.9 Ma (U/Pb on zircon, Hirdes et al., 1992) and to the Prince's Town granodiorite dated at 2158.9 ± 3.9 Ma (U/Pb on zircon, Attoh et al., 2006), respectively.

Sample **GH127B** is a granite found in the Biamankor Quarry, near Anibel village (Fig. III-1, Fig. III-3a). This granite is undeformed and has a tonalitic aureole overlain in the north by the Tarkwaian sediments. The Anibel granite cross-cuts the F1 folds and S1 cleavage and could correspond to a late Eoeburnean / early Eburnean intrusion (Perrouty et al., 2012).

4.3.1.2 *Eburnean intrusions*

Eburnean granitoids are abundant in the sedimentary basins of Kumasi and Akyem but only a few of them intruded the Sefwi Group metavolcanics. The three sampled Eburnean granitoids are hosted by the Sefwi Group "Cape Coast" micaschists. Their mineralogy is mostly quartz, plagioclase, K-feldspar, biotite and muscovite. The **GH101A** and **GH118B** granodiorites (Fig. III-3b, Fig. III-3c) were found to the east and to the northwest of Cape Coast. They correspond to massive granitoid veins and plutons crosscutting the S3 foliation (Perrouty et al., 2012) and slightly boudinaged. Similar granodiorites in Cape Coast area have been dated at 2072 Ma ± 1 (U/Pb on zircon, Agyei Duodu et al., 2009). **GH237** is a small (leuco)-granitic intrusion located 10 kilometres west of Twifo-Praso (Fig. III-3d). It does not display any visible

deformation and crosscuts the main S3 foliation of the hosting micaschists. This intrusion has not yet been dated but is likely to have a post-D3 Eburnean age.

4.3.2 *Metavolcanics and metasediments*

Two samples of metavolcanic rocks have been analysed. The mineralogy of these meta-andesites is mostly chlorite, biotite, amphibole, rare pyroxene and quartz. **GH503** has been sampled 10 kilometres west of Benso. It corresponds to an andesitic layer interbedded within Sefwi Group volcano-sediments. **GH245** is a 100m-scale xenolith of strongly deformed andesite in an undeformed Eburnean granodiorite intrusion hosted by the Kumasi Group metasediments of the Akyem Basin overlying the Sefwi Group 5 kilometres north of Twifo-Praso.

Sefwi Group metasediments were sampled in four locations in the southeast of the Ashanti Belt. **GH101B** is a garnet-bearing micaschist intruded by Eburnean granitoid and collected near Cape Coast. **GH504** and **GH515** correspond to volcano-sediments composed mostly of quartz, chlorite, biotite and scarce muscovite (Phyllites). Sample GH504 is weakly deformed and affected by syn-sedimentary normal faults. It is located 15 kilometres west of Benso. Sample GH515 was collected in the Damang mine.

Five samples of metasediments were collected in the Tarkwa Basin. **GH297**, **GH397** and **GH511** correspond to phyllitic layers with cross-bedding marked by magnetite concentrations. GH397 and GH511 come from the Damang gold mine. They were affected by contact metamorphism due to dolerite sill and dyke intrusions and are composed of quartz, staurolite, garnet, chlorite, biotite and muscovite mineral assemblage. In contrast, GH297 found near Tarkwa Town contains only quartz, chlorite, biotite and muscovite. **GH079** and **GH512** are sandstone samples taken in the Banket Formation near Tarkwa town and Damang mine, respectively.

4.3.3 *Analytical methods*

Geochemical compositions of the previously described rock samples were analysed at the A.L.S. Mineral laboratory, Sevilla, Spain. Analytical methods and detection limits are described on their website (www.alsglobal.com): whole rock measurements were performed using ICP-AES for major elements (ME-ICP06 and OA- GRA05 methods, ALS Minerals, 2006a) and base metal (ME-4ACD81, ALS Minerals, 2009); trace elements including Rare Earth Elements composition were measured by ICP-MS (ME-MS81 and ME-MS42 methods, ALS Minerals, 2009, 2006b). All geochemical data are presented in Table III-1.

	Eoeburnean Intrusions					Eburnean Intrusions			Analytical Method
	GH134	GH148	GH502	GH517B	GH127B	GH101A	GH118B	GH237	
In wt. %									
SiO2	72.00	55.00	75.90	67.9	72.0	69.4	68.9	71.2	ME-ICP06
TiO2	0.16	0.77	0.22	0.38	0.31	0.43	0.23	0.11	ME-ICP06
Al2O3	15.00	16.15	12.80	13.75	13.20	15.45	13.85	14.50	ME-ICP06
Fe2O3	1.68	9.02	2.47	2.73	3.51	2.41	1.51	0.72	ME-ICP06
MnO	0.04	0.15	0.10	0.04	0.06	0.02	0.01	0.01	ME-ICP06
MgO	0.74	4.13	0.41	1.34	0.29	0.83	0.48	0.21	ME-ICP06
CaO	2.29	6.59	1.12	2.66	1.53	2.09	1.54	1.36	ME-ICP06
Na2O	4.82	3.68	4.27	4.14	3.99	3.53	3.48	4.66	ME-ICP06
K2O	2.34	1.66	2.44	2.26	3.83	1.96	4.19	2.12	ME-ICP06
Cr2O3	<0.01	0.01	<0.01	<0.01	<0.01	<0.01	<0.01	<0.01	ME-ICP06
P2O5	0.05	0.27	0.02	0.10	0.05	0.16	0.04	0.03	ME-ICP06
SrO	0.08	0.11	0.02	0.03	0.02	0.09	0.05	0.07	ME-ICP06
BaO	0.09	0.09	0.14	0.13	0.17	0.19	0.16	0.13	ME-ICP06
LOI	0.70	2.20	0.80	5.00	0.78	1.68	0.90	2.38	OA-GRA05
Tot.	100.0	99.8	100.5	100.5	99.7	98.2	95.3	97.5	TOT-ICP06
In ppm									
C	0.04	0.03	0.08	1.07	0.03	0.04	0.08	0.35	C-IR07
S	0.01	0.07	0.13	0.03	<0.01	0.01	0.01	0.01	S-IR08
V	26	224	15	66	7	33	17	<5	ME-MS81
Cr	20	70	<10	10	<10	10	10	<10	ME-MS81
Co	96	48	66	40	70	19	105	38	ME-4ACD81
Ni	3	12	<1	10	5	6	1	<1	ME-4ACD81
Cu	9	75	64	32	13	31	5	<1	ME-4ACD81
Zn	28	92	70	23	65	46	31	45	ME-4ACD81
Ga	17.0	20.6	15.4	13.8	16.1	22.5	16.9	20.3	ME-MS81
As	0.1	0.7	<0.1	0.1	0.5	<0.1	<0.1	<0.1	ME-MS42
Se	<0.2	0.40	1.0	0.2	0.3	<0.2	<0.2	<0.2	ME-MS42
Rb	64.9	40.1	52.5	77.2	112.0	51.8	94.3	51.1	ME-MS81
Sr	724	933	158	192	139	736	395	572	ME-MS81
Y	4.9	20.8	44.6	11.8	36.5	4.7	3.2	2.1	ME-MS81
Zr	73	131	246	204	345	173	161	89	ME-MS81
Nb	2.8	4.6	6.9	7.1	9.6	5.5	3.2	1.6	ME-MS81
Mo	<1	<1	<1	2	1	<1	<1	<1	ME-4ACD81
Ag	<0.5	<0.5	0.6	<0.5	<0.5	0.7	<0.5	<0.5	ME-4ACD81
Cd	<0.5	<0.5	<0.5	<0.5	<0.5	<0.5	<0.5	<0.5	ME-4ACD81
Sn	<1	1.00	2	1	<1	<1	<1	1	ME-MS81
Sb	<0.05	0.21	<0.05	<0.05	<0.05	<0.05	<0.05	<0.05	ME-MS42
Te	<0.01	<0.01	0.05	0.03	<0.01	0.01	0.04	<0.01	ME-MS42
Cs	1.68	0.97	1.53	2.07	2.42	1.50	0.82	0.69	ME-MS81
Ba	816	858	1140	1040	1335	1460	1210	985	ME-MS81
La	9.5	25.8	30.1	27.0	39.7	39.4	28.0	11.0	ME-MS81
Ce	18.2	52.3	67.0	53.1	79.8	72.9	54.1	20.7	ME-MS81
Pr	2.13	6.99	8.11	5.38	9.66	8.13	5.83	2.67	ME-MS81
Nd	7.7	29.0	34.1	19.5	37.1	28.9	19.7	10.1	ME-MS81
Sm	1.38	5.86	7.59	3.14	7.11	4.20	2.93	1.80	ME-MS81
Eu	0.43	1.67	1.25	0.78	1.32	1.20	0.67	0.61	ME-MS81
Gd	0.98	4.45	6.49	2.02	6.77	3.33	2.39	1.30	ME-MS81
Tb	0.14	0.64	1.15	0.32	1.05	0.30	0.22	0.15	ME-MS81
Dy	0.75	3.62	7.82	2.03	7.10	1.20	0.87	0.50	ME-MS81
Ho	0.15	0.74	1.64	0.40	1.39	0.16	0.12	0.08	ME-MS81
Er	0.45	1.92	5.05	1.23	4.39	0.48	0.37	0.18	ME-MS81
Tm	0.06	0.28	0.77	0.18	0.54	0.04	0.03	0.03	ME-MS81
Yb	0.50	1.78	5.35	1.31	4.07	0.30	0.27	0.13	ME-MS81
Lu	0.08	0.28	0.84	0.21	0.54	0.03	0.03	0.03	ME-MS81
Hf	2.4	3.4	7.4	5.5	8.9	4.5	4.7	2.9	ME-MS81
Ta	0.2	0.3	0.5	0.7	0.6	0.3	0.2	0.1	ME-MS81
W	551	163	391	206	368	75	520	204	ME-MS81
Hg	0.53	0.15	0.396	0.240	0.275	0.061	0.473	0.147	ME-MS42
Tl	<0.5	<0.5	<0.5	<0.5	<0.5	<0.5	<0.5	<0.5	ME-MS81
Pb	11	6	7	4	19	14	23	5	ME-4ACD81
Bi	0.06	0.02	0.07	0.03	0.16	0.03	0.01	<0.01	ME-MS42
Th	4.44	2.21	4.82	5.25	7.37	8.10	11.75	1.51	ME-MS81
U	1.02	0.71	2.01	1.37	2.57	2.60	1.72	0.65	ME-MS81

Table III-1A

	Eoeburnean Mvolc.		Sefwi Group Metasediments			Tarkwa Group Metasediments				
	GH245	GH503	GH101B	GH504	GH515	GH297	GH397	GH511	GH079	GH512
In wt. %										
SiO_2	60.0	59.4	65.8	61.3	53.5	59.0	53.3	57.8	81.9	85.2
TiO_2	0.67	0.58	0.60	0.64	0.97	0.48	0.70	0.74	0.26	0.23
Al_2O_3	16.10	14.40	14.35	15.10	12.00	19.25	23.80	24.10	9.28	7.08
Fe_2O_3	7.78	8.08	6.20	7.25	9.74	7.96	9.30	8.17	3.13	2.07
MnO	0.11	0.10	0.07	0.10	0.09	0.13	0.07	0.07	<0.01	0.07
MgO	3.22	4.35	1.99	4.49	5.45	1.61	2.14	1.87	0.03	0.60
CaO	1.56	5.06	1.12	5.13	5.90	0.06	0.35	0.30	0.06	1.29
Na_2O	1.53	2.92	1.72	2.73	2.91	1.20	1.66	2.33	1.30	1.76
K_2O	3.35	1.13	3.15	1.36	1.12	2.96	2.64	3.18	0.69	1.05
Cr_2O_3	0.02	0.01	0.01	0.04	0.04	0.02	0.03	0.03	<0.01	0.01
P_2O_5	0.16	0.04	0.10	0.10	0.35	0.06	0.13	0.03	0.01	0.08
SrO	0.03	0.03	0.03	0.05	0.06	0.02	0.02	0.03	0.02	0.03
BaO	0.11	0.03	0.09	0.04	0.06	0.11	0.09	0.09	0.04	0.05
LOI	1.80	2.70	2.28	2.49	9.31	4.19	2.28	3.00	1.47	1.19
Tot.	96.4	98.8	97.5	101.0	101.5	97.1	96.5	101.5	98.2	100.5
In ppm										
C	0.19	0.01	0.39	0.04	1.99	0.03	0.03	0.02	0.03	0.31
S	0.01	0.02	0.07	0.04	0.03	<0.01	0.09	0.01	<0.01	<0.01
V	123	200	97	188	283	114	123	166	52	35
Cr	160	90	80	270	270	160	200	180	20	50
Co	50	48	23	35	48	26	49	25	74	120
Ni	58	47	31	89	58	71	69	52	6	18
Cu	51	250	54	78	159	28	43	15	1	19
Zn	42	81	42	88	98	91	64	24	2	25
Ga	20.2	16.3	17.7	17.9	14.6	25.7	32.7	31.4	10.7	8.7
As	<0.1	13.5	<0.1	<0.1	<0.1	0.8	0.1	0.2	0.3	1.6
Se	0.4	0.3	0.7	0.5	0.6	0.3	0.2	0.3	<0.2	0.3
Rb	147.0	32.3	90.8	39.4	35.3	118.5	112.5	130.5	13.6	36.1
Sr	232	276	252	410	525	164	196	255	185	205
Y	16.7	15.2	18.5	18.3	13.6	15.0	18.7	30.6	13.6	11.4
Zr	127	80	133	101	83	101	142	150	68	91
Nb	6.6	1.8	8.0	3.2	3.4	6.3	9.3	9.7	3.3	2.7
Mo	<1	<1	<1	<1	<1	<1	<1	<1	<1	<1
Ag	0.6	0.5	0.5	<0.5	0.7	<0.5	<0.5	<0.5	<0.5	<0.5
Cd	<0.5	<0.5	<0.5	<0.5	<0.5	<0.5	<0.5	<0.5	<0.5	<0.5
Sn	<1	1	<1	1	1	6	3	3	<1	<1
Sb	<0.05	0.09	<0.05	0.13	0.05	<0.05	0.13	0.25	<0.05	0.21
Te	0.06	0.01	0.07	0.04	0.05	<0.01	0.38	0.01	<0.01	0.02
Cs	5.91	1.25	4.27	1.59	4.13	5.38	9.19	9.52	0.45	2.01
Ba	809	260	730	376	565	866	708	792	298	386
La	12.9	10.0	22.2	12.8	9.0	30.7	36.4	42.4	32.4	22.1
Ce	38.3	23.7	47.1	25.4	21.3	73.3	70.6	87.0	66.1	45.5
Pr	3.34	2.99	5.57	3.47	2.81	7.95	8.77	9.95	7.60	5.14
Nd	13.5	13.7	21.9	15.4	13.1	29.5	34.0	39.5	29.0	18.9
Sm	2.67	3.18	4.02	3.57	3.22	5.56	6.48	7.60	4.95	2.96
Eu	0.97	0.85	1.08	1.05	0.83	1.29	1.48	1.53	1.25	0.75
Gd	2.70	2.82	3.73	3.37	2.67	4.63	5.39	5.34	4.07	2.47
Tb	0.43	0.42	0.53	0.51	0.41	0.64	0.72	0.83	0.53	0.33
Dy	3.18	2.73	3.57	3.22	2.54	3.39	4.04	5.41	3.11	2.00
Ho	0.62	0.56	0.70	0.66	0.48	0.66	0.71	1.04	0.55	0.40
Er	2.01	1.66	2.33	1.95	1.36	2.00	2.28	3.08	1.65	1.07
Tm	0.24	0.23	0.29	0.26	0.18	0.30	0.28	0.45	0.19	0.15
Yb	1.80	1.63	2.24	1.77	1.20	2.09	2.18	2.99	1.42	1.01
Lu	0.23	0.25	0.28	0.27	0.18	0.35	0.32	0.46	0.17	0.14
Hf	3.5	2.1	3.8	2.7	1.9	3.1	4.3	4.0	2.0	2.2
Ta	0.4	0.1	0.6	0.2	0.2	0.4	0.8	0.7	0.3	0.3
W	148	108	55	81	102	31	177	92	379	522
Hg	0.110	0.114	0.034	0.079	0.108	0.014	0.120	0.099	0.293	0.632
Tl	<0.5	<0.5	<0.5	<0.5	<0.5	0.50	<0.5	0.50	<0.5	<0.5
Pb	11	<2	13	4	4	18	19	24	11	9
Bi	0.12	0.02	0.21	0.05	0.02	0.06	0.36	0.07	0.01	0.10
Th	4.27	1.22	5.10	1.65	1.03	7.33	9.29	10.35	3.15	3.58
U	1.20	0.35	1.44	0.46	0.46	2.89	4.50	3.90	0.40	0.88

Table III-1B   *Geochemical data for (A) granitoid and (B) metavolcanic and metasedimentary samples from the southern Ashanti Belt.*

139

4.4 Geochemical results

4.4.1 *Metamorphism, hydrothermal alteration and weathering*

The Ashanti greenstone belt is known to have been significantly metamorphosed (greenschist facies, John et al., 1999) and hydrothermally altered. The intensity of this alteration is variable depending of the initial mineralogy (e.g. the alteration of our samples seems to mostly affect the mineralogy of the meta-andesites and of the metasediments while that of the granitoids has been less modified). The most altered rock samples present high loss-on-ignition (LOI) values (sometimes up to 20%) mostly caused by the presence of carbonates and hydrated minerals, such as chlorite. The focus of this study being the magmatic evolution of the investigated samples, we selected only samples with the lowest LOI proportion, thought to be the less altered. For this reason, we do not assess in the present work the effect of metamorphism and late (hydrothermal) alteration process on the investigated samples.

All southwest Ghana lithologies were affected by intense weathering resulting from warm and wet climatic conditions in the area. Samples used in this study were preferentially collected in mines (as far as possible from the main mineralisation zones), in quarries, in rivers or along the coast to minimize this alteration.

4.4.2 *Eoeburnean and Eburnean plutonism and volcanism*

Major element geochemistry indicates that the Eoeburnean plutonic rocks present heterogeneous compositions with SiO_2 varying from 49 wt. % to 76 wt. % (average value of 67 wt. %, Table III-2A, Fig. III-4) while the Eburnean intrusions are overall more acidic with SiO_2 range from 65 wt. % to 79 wt. % (average value of 71 wt. %). The more mafic Eoeburnean intrusions display whole rock geochemical compositions similar to those of the contemporaneous andesitic volcanism. Eoeburnean and Eburnean plutonism display either S-type (Peraluminous) or I-type (Metaluminous) characteristics on Shand's diagram (1943), irrespective of their ages or location within the southern Ashanti Belt (Fig III-5A).

The Eoeburnean intrusions vary from dioritic / tonalitic to granodioritic compositions. They show a decrease of Fe_2O_3, MgO, CaO, TiO_2 and P_2O_5 content with increasing SiO_2 content (Fig. III-4). Al_2O_3 versus SiO_2 proportions show a smaller decrease. Na_2O is not affected by SiO_2 variation while K_2O content seems to increase.
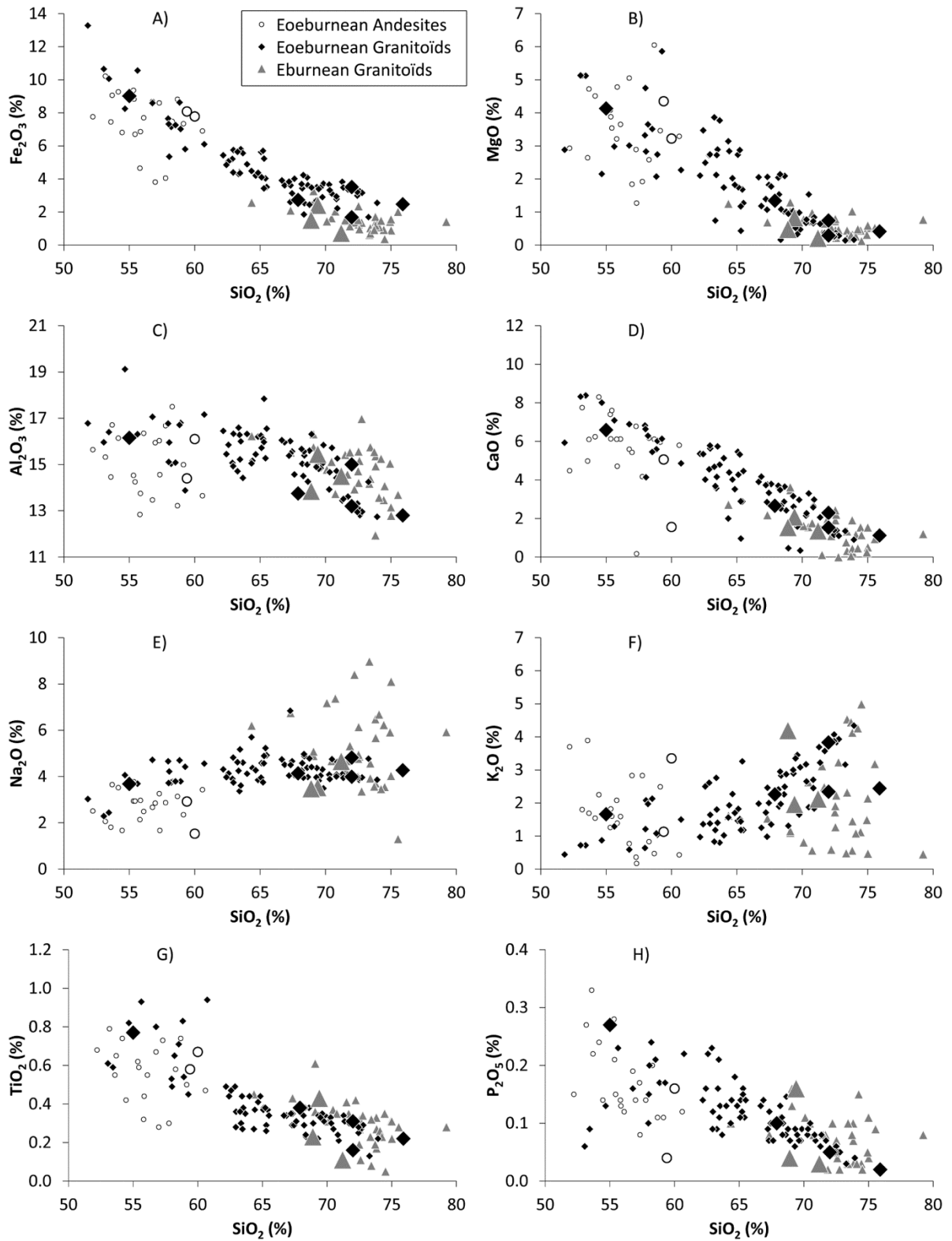
Figure III-4   *Major elements versus SiO2 diagrams for all southwest Ghanaian Eoeburnean and Eburnean igneous rock analyses from this study (large symbols) and from published data (small symbols) of John et al. (1999), Loh et al. (1999), Yao et al. (2000), Dampare et al. (2005, 2008), Attoh et al. (2006) and Adadey et al. (2009). Eoeburnean intrusions show differentiation series from diorite / tonalite to granodiorite end-members (see text for details). Eburnean granitoids are more homogenous with granodiorite, granite and leucogranite compositions.*
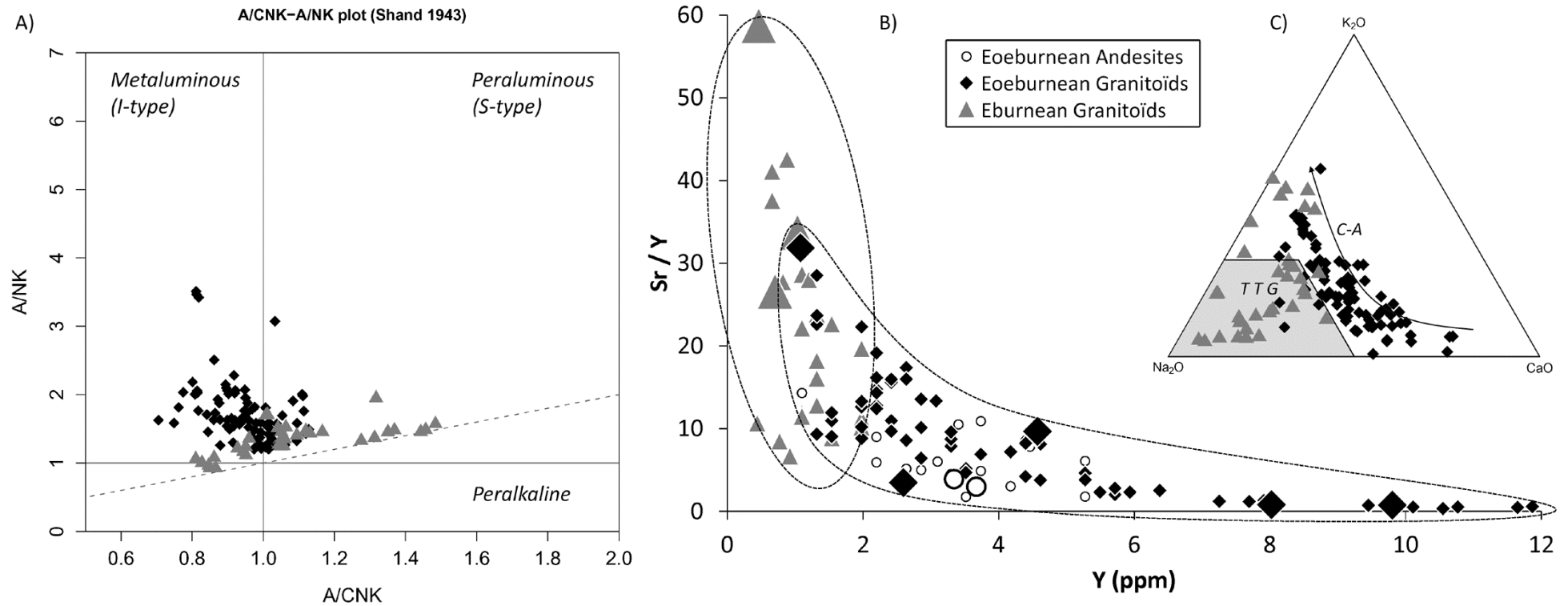
Figure III-5   *(A) A/NK versus A/CNK diagram of Shand (1943). Both Eoeburnean TTG and Eburnean granitoids present S-type and I-type characteristics. (B) Sr/Y versus Y diagram (Martin, 1999). Eoeburnean TTGs Sr and Y proportions are consistent with actual granitoid values while Eburnean granitoids are closely similar to the Adakite and Archean TTG with high Sr/Y ratios. C) Na2O, K2O, CaO ternary diagrams. Eoeburnean TTGs seem to follow a typical calc-alkaline trend (Barker and Arth, 1976) while most of the Eburnean granitoids are located in the TTG domain of Martin (1994).*
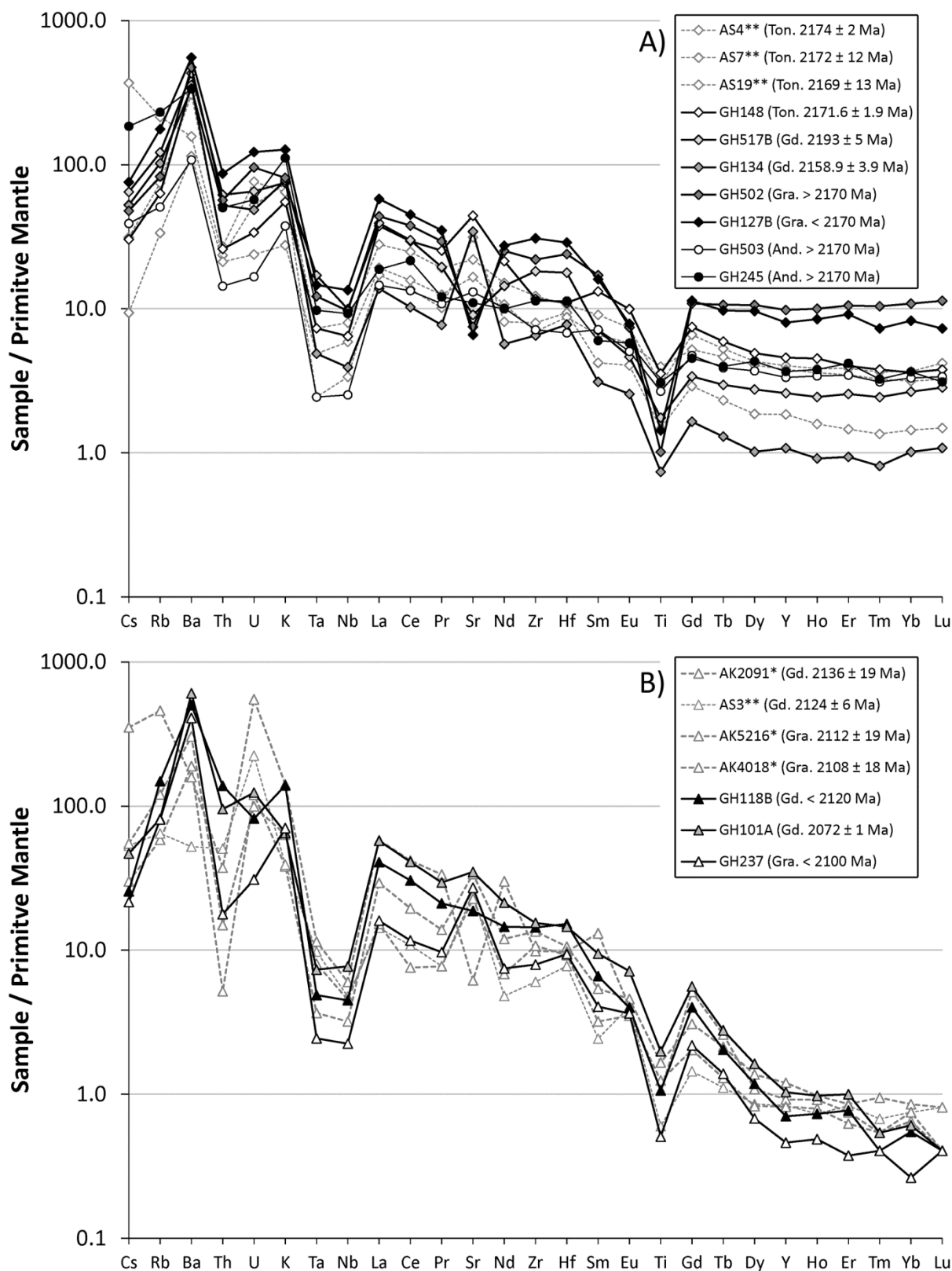
Figure III-6   *Trace element profiles for (A) the Eoeburnean TTGs and (B) the Eburnean granitoids normalised to primitive mantle (Sun and McDonough, 1989). * Analyses from Adadey et al. (2009), ** Analyses from Grenholm (2011), remainder of analyses from this study. Radiometric ages from Hirdes et al. (1992), Attoh et al. (2006), Oberthur et al. (1998), Adadey et al. (2009) and Scherstén (unpublished data referenced in Grenholm, 2011).*
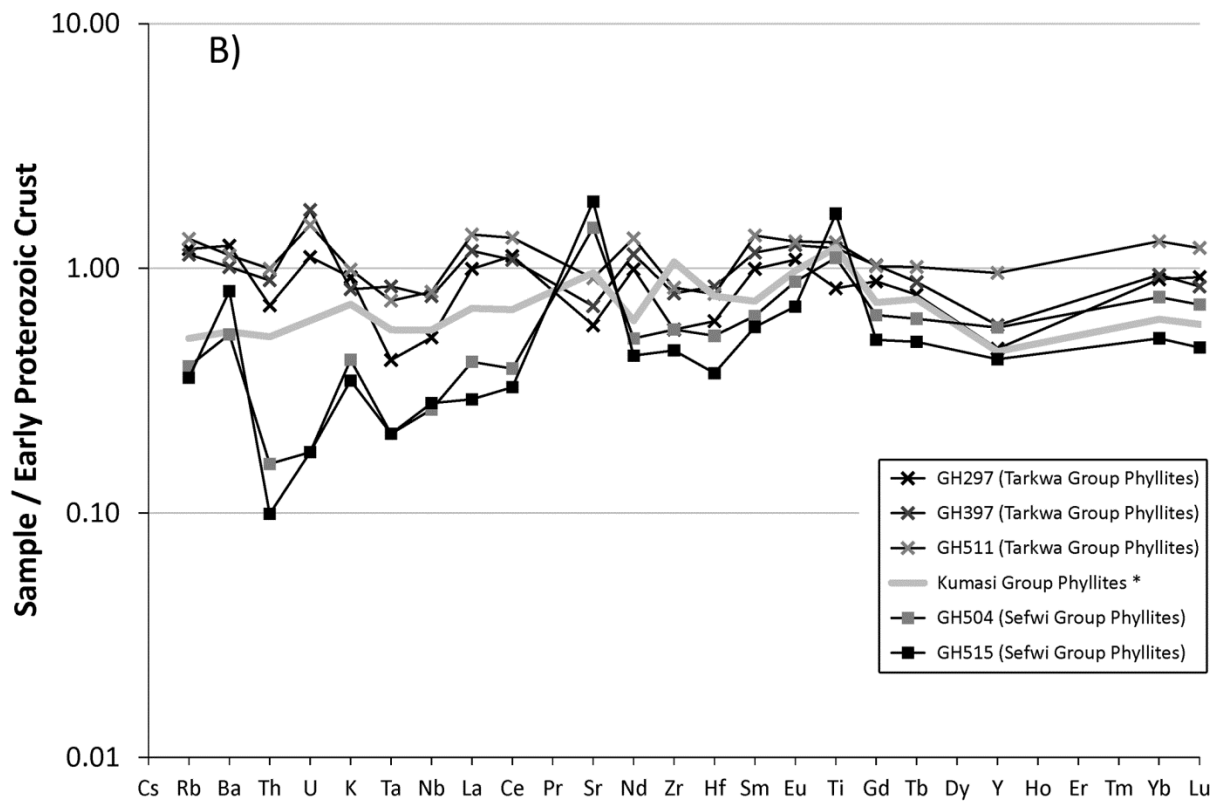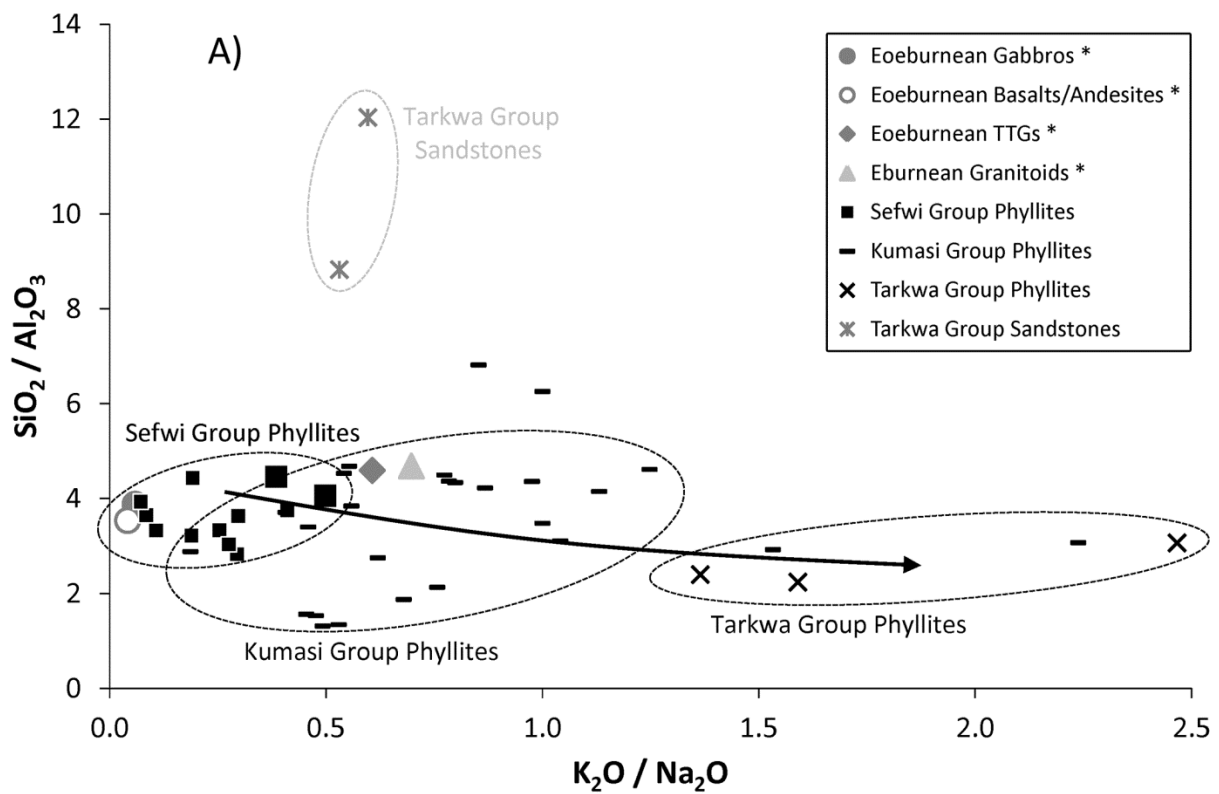
Figure III-7   *Metasediment geochemistry. (A) Plot of the K2O / Na2O ratio versus SiO2 /*
*Al2O3 ratio for Sefwi, Kumasi and Tarkwa group metasediments. * Average ratios.*
(B) Trace elements profiles for the Sefwi Group and Tarkwa Group phyllites
*normalised to the Early Proterozoic Crust (Condie, 1993). * Kumasi Group*
metasediments profile is an average calculated from geochemical analyses of Asiedu
et al. (2004, 2009).

Eburnean granitoids (Fig. 4) have more homogeneous compositions corresponding to granodiorite, granite and leucogranite which are very similar to those of the most differentiated Eoeburnean intrusions. However, they display different trace element compositions.

Primitive-Mantle-normalised (Sun and McDonough, 1989) multi-element profiles are useful to discriminate between the two groups of intrusions (Fig. III-6). The Eoeburnean TTGs and andesites are characterised by HREE (Heavy Rare Earth Element) flat profiles with enrichment levels depending on rock type (tonalites are less enriched than granodiorites) while the Eburnean granitoids are strongly depleted and fractionated in HREE. Both Eoeburnean and Eburnean granitoids are enriched in Light Rare Earth Elements (LREE) and display positive Ba anomalies and negative Ta, Nb, Th and Cs anomalies. The Sr anomalies do not seem to be linked with a specific phase of plutonism or with a specific granitoid composition.

The Sr/Y versus Y diagram (Fig. III-5B) is used to distinguish adakites and Archean TTGs from post-2.5 Ga granitoids (Martin, 1999, Moyen and Martin, 2012). Adakites and Archean TTGs usually present high Sr/Y values while the granitoids have lower Sr/Y ratios. In contrast, analysed Paleoproterozoic samples from SW Ghana display opposite trend, with low Sr/Y ratios for Eoeburnean TTGs and high ratios for the Eburnean granitoids. For our samples, a similar variation (not shown here) is also observed on a La/Yb versus Yb diagram (Martin, 1999, Moyen and Martin, 2012). On a K_2O-Na_2O-CaO diagram (Fig. III-5C), the Eoeburnean TTGs seem to follow a typical calc-alkaline trend (Barker and Arth, 1976) while most of the Eburnean granitoids are located in the TTG's domain of Martin (1994).

4.4.3 *Metasediments*

Metasedimentary rocks in southwest Ghana belong to the Sefwi, Kumasi and Tarkwa groups according to the stratigraphy of Adadey et al. (2009). Major element ratios show an evolution from a Na-rich / K-poor composition for the oldest (Sefwi Group) to a Na-poor / K-rich composition for the youngest (Tarkwa Group) metasedimentary groups (Fig. III-7A).

The multi-element profiles of these metasediments also show a compositional evolution (Fig. III-7B). Sefwi Group phyllites are depleted in the most imcompatible trace elements while the Tarkwa Group phyllites have composition more or less equivalent to the Early Proterozoic Crust (2.5 – 1.8 Ga) of Condie (1993). Kumasi Group metasediments (Asiedu et al., 2004, 2009) show intermediate composition. Sefwi Group phyllites are characterised by positive Ba, Sr and Ti anomalies. These peaks are also typical of the Sefwi Group metavolcanic rocks corroborating they might be the source of these sediments. In contrast these anomalies are less marked or even

inexistent in the younger Kumasi and Tarkwa groups. A more heterogeneous source needs to be considered for them (perhaps both the Sefwi Group rocks and the Eoeburnean TTGs).

4.5 Pseudosection modelling

4.5.1 *Methodology*

Pseudosections of rocks from the different terrains of the southwest Ghana were constructed using the Perple X software version 2007 (Connolly and Kerrick, 1987; Connolly, 2005, 2009), in the Na2O–CaO–K2O–FeO–MgO–MnO–Al2O3–TiO2–SiO2–H2O system, and using the thermodynamic database hp04 of Holland and Powell (1998, revised 2004). For solid solutions, we have used the internally consistent thermodynamic dataset termed solut_09.dat (available at www.perplex.ethz.ch/).The solution models used for the pseudosections are as follows: Bio(TCC) for biotite (Tajcmanová et al., 2009), Chl(HP) for chlorite (Holland et al, 1998), St(HP) for staurolite (Powell et al, 1998), Ctd(HP) for chloritoid (Holland and Powell, 1998), GlTrTsPg for amphibole (White et al, 2003 ; Wei et al, 2003), Gt(HP) for garnet (Holland and Powell, 1998), Ilm(WPH) for ilmenite (White et al., 2000), hCrd for cordierite, Pheng(HP) for phengite (Holland and Powell, 1998), MuPa for white micas (Chatterjee and Froese, 1975),melt(HP) (Holland and Powell, 2001), Pl(h) for plagioclase feldspar (Newton et al., 1980), Kf for potassic feldspar (Waldbaum and Thompson, 1968), Opx(HP) for orthopyroxene (Holland and Powell, 1996), Cpx(HP) for clinopyroxene (Holland and Powell, 1996), O(HP) for olivine (Holland and Powell, 1998) and MF for magnesioferrite/magnetite. Pseudosections were built using the bulk rock composition of each sample (Table III-2A) for H2O saturation conditions corresponding to the LOI (loss on ignition) values.

Pseudosections built with fixed bulk rock compositions are widely used to estimate peak pressure-temperature conditions where equilibrium can be assumed. However, this condition is not fully achieved in metamorphic rocks undergoing phase fractionation during their prograde or retrograde evolution. To solve this problem, it is useful to compute the initial stable assemblage for the specified bulk composition [Start : 300°C] and increment the system's conditions along the pressure and temperature path (Connolly, 2009). After each increment the program adapts the composition of the system to simulate fractionation by removing the newly crystallised phases and recalculates the new stable phase assemblage [Peak: 900°C]. The absolute molar composition (mol) output at 900°C is particularly useful in fractionation calculations because the difference between the final and initial compositions specified for the problem gives the

integrated composition of the fractionated phase. Such fractionation calculations are relevant where the extraction of melt during burial of partially molten rocks is thought to have taken place.

Here we propose to characterize the composition of melt produced by rocks at 900°C, the temperature at which we expect a reasonable degree of partial melting of each considered lithology regardless of the depth). The composition of melt corresponds to the sum of melt increments released by the partially molten rocks, from the solidus up to 900°C. The melt fractionation was depicted as a function of depth increase along two contrasted geothermal gradients of 15 and 25°C/Km that would correspond to subduction and crustal thickening environments, respectively (Table III-2B). A lithostatic pressure of 3.5-3.6 km per kilobar (Spear, 1993) was used, accounting for the mafic and felsic composition of the Birimian crust, and rocks of differing compositions were considered (i.e. sediment, granitoid, basalt and gabbro).

4.5.2 Modelling results

Fig. III-8 show the modal distribution of garnet for each Eoeburnean lithology depicted as a function of pressure and temperature. This pseudosection modelling shows that all Eoeburnean rock compositions can contain garnet before the start of partial melting considering the probable range of geothermal gradients ($< 30°C/Km$). Consequently, melts produced from each of these lithologies will be depleted in HREE (Martin, 1994).

Calculation of the major elements compositions of these melts (Table III-2B) indicates that partial melting of any one of the Eoeburnean lithologies results in melt compositions unable to fit those of the Eburnean granitoids (e.g. melts produced from gabbros and basalts are deficient in K_2O, those from granitoids in CaO and those from sediments in MgO, compared to the Eburnean granitoids composition, Table III-2). Consequently, mixing between melts sourced from all of these Eoeburnean lithologies need to be considered.

Melting of the metamorphosed Eoeburnean lithologies produced a large proportion of H_2O (more than 25 %, see hydrous melts calculated composition, Table III-2B). H_2O is the most "incompatible element" which may have been exsolved from the melt and then have percolated through the rocks during the early stage of melting. Removing a large amount of this water from the system during melting process, or before cooling and granite crystallisation, is a necessary condition to get reasonable magma composition and to approach the composition (close to anhydrous melt, Table III-2B) of the Eburnean intrusions (Table III-2A).

Average whole rocks geochemistry							
	Eoeburnean gabbros	Eoeburnean granitoids	Eoeburnean basalts	Eoeburnean micaschists	Eburnean granitoids		
	wt %	wt %	wt %	wt %	wt %	mol %	mol % (Anhydrous)
SiO$_2$	50.05	66.73	49.655	65.8	71.29	72.62	79.11
Al$_2$O$_3$	12.90	14.53	14.038	14.35	15.21	9.13	9.95
Fe$_2$O$_3$	6.40	4.24	11.65	6.2	1.63	1.39	1.51
MgO	14.25	1.63	7.878	1.99	0.62	0.95	1.03
CaO	12.80	3.27	8.868	1.12	1.65	1.80	1.96
Na$_2$O	0.68	4.16	2.365	1.72	4.10	4.05	4.41
K$_2$O	0.04	2.52	0.10	3.15	2.86	1.86	2.03
H$_2$0	1.55	2.17	3.89	2.28	2.35	8.20	0.00

Table III-2A

Global melt compositions extracted at 900°C									
Composition	100 % metagabbros		100 % granitoids		100 % metabasalts		100 % metasediments		50 % mgab., 30 % TTG, 10 % mbas., 10 % msed.*
Geothermal gradient	15°C/Km	25°C/km	15°C/Km	25°C/km	15°C/Km	25°C/km	15°C/Km	25°C/km	25°C/km
Hydrous melt (mol %)									
SiO$_2$	46.67	52.46	57.52	58.49	45.26	52.48	49.15	54.95	54.52
Al$_2$O$_3$	6.00	6.15	6.21	6.37	5.93	6.52	6.67	6.42	6.28
Fe$_2$O$_3$	0.00	0.41	0.33	2.12	0.20	0.93	0.24	0.21	0.96
MgO	0.67	0.82	0.00	0.47	0.00	0.31	0.00	0.00	0.58
CaO	1.33	1.64	0.33	0.24	0.40	0.62	0.73	0.63	1.02
Na$_2$O	4.00	3.28	2.61	2.83	5.34	5.28	3.40	2.84	3.30
K$_2$O	0.00	0.00	3.27	3.54	0.20	0.31	2.31	2.32	1.32
H$_2$O	41.33	35.25	29.74	25.94	42.69	33.54	37.50	32.63	32.02
Anhydrous melt (mol %)									
SiO$_2$	79.54	81.02	81.86	78.98	78.97	78.97	78.64	81.56	80.20
Al$_2$O$_3$	10.23	9.49	8.84	8.60	10.35	9.81	10.68	9.53	9.24
Fe$_2$O$_3$	0.00	0.63	0.47	2.87	0.34	1.40	0.39	0.31	1.41
MgO	1.14	1.27	0.00	0.64	0.00	0.47	0.00	0.00	0.86
CaO	2.27	2.53	0.47	0.32	0.69	0.93	1.17	0.94	1.49
Na$_2$O	6.82	5.06	3.72	3.82	9.31	7.94	5.44	4.22	4.86
K$_2$O	0.00	0.00	4.65	4.78	0.34	0.47	3.69	3.44	1.95

Table III-2B *(A) Average values of major element compositions for the Sefwi Group metagabbros, metabasalts, metasediments and Eoeburnean TTGs. (B) Global melt compositions extracted at 900°C for these lithologies (See text for details). *Best mix to produce melts with the composition of the Eburnean granitoids.*
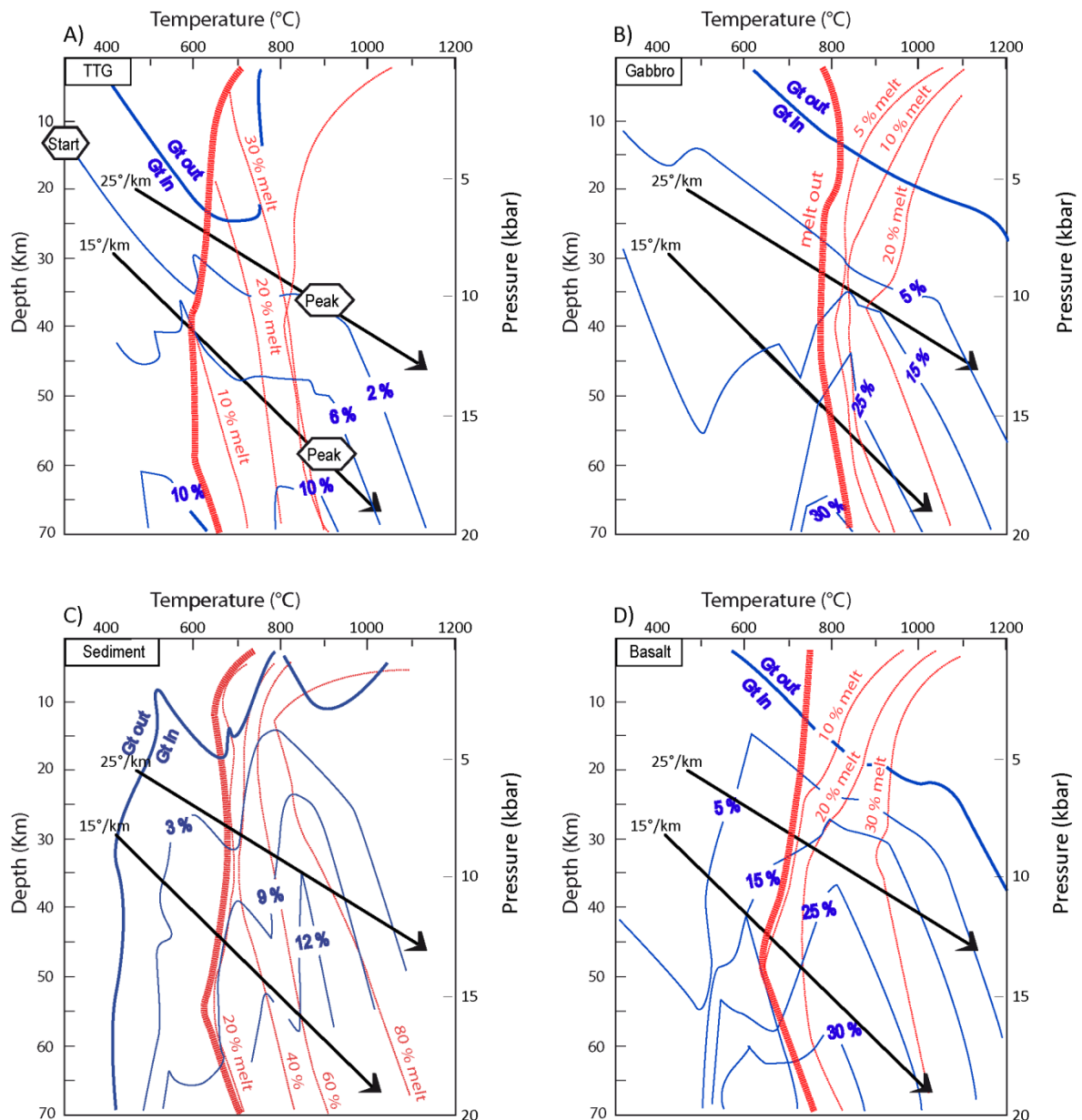
Figure III-8   *Evolution of garnet proportion in different lithologies as a function of pressure and temperature (blue lines, wt. %). Pseudosections were computed on typical (A) foliated granitoid (TTGs), (B) gabbro, (C) sediments and (D) basalt sampled in the southern Ashanti belt region (Ghana). This diagram shows that all of the analysed Eoeburnean lithologies can form garnet before reaching the solidus (thick red line) whatever the considered geothermal gradient. Thin red lines represent the percentage of melt. Calculations are for a CaTiMnNKFMAS system and for H2O saturation conditions corresponding to the LOI (loss on ignition) values. See text for details of model parameters.*
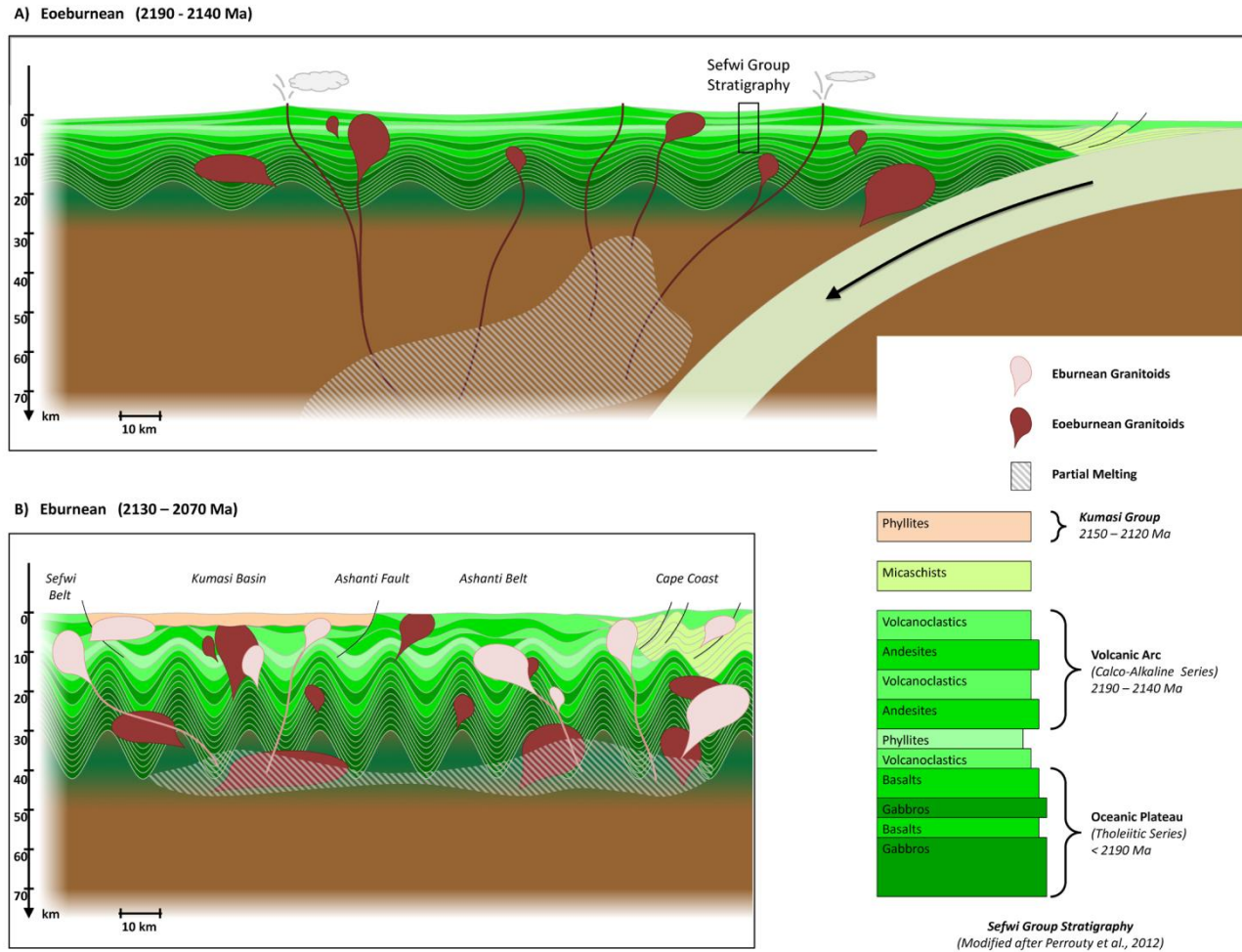
Figure III-9   *Schematic model of the evolution of the Paleoproterozoic crust in southwest Ghana. (A) During the first phase (Eoeburnean), the initial basement (that may consist of an oceanic plateau) was deformed and intruded by the Eoeburnean granitoids in a subduction context. Synchronous calc-alkaline volcanism built the upper layers of the Sefwi Group stratigraphy. (B) During the second phase (Eburnean), this thickened crust was deformed and intruded by numerous granitoids. According to our geochemical analyses, these granitoids may results from partial melting of a metamorphosed lower crust that is composed of both the mafic rocks and the Eoeburnean intrusions.*

4.6 <u>Discussion</u>

Previous structural mapping (Perrouty et al., 2012) described two distinct phases of deformation during the Eburnean Orogeny defined by Bonhomme (1962). These two phases can be correlated with the Eoeburnean and Eburnean phases of magmatism (De Kock et al., 2011). Compilation of a range of granitoid geochemical data from southwest Ghana (John et al., 1999, Loh et al., 1999, Yao et al., 2000, Dampare et al., 2005, Adadey et al., 2009, Grenholm, 2011) suggests that the belt-I-type and basin-S-type classification of Loh et al (1999) is not appropriate to discuss the magmatic evolution of the intrusive lithologies (Fig. III-5A). This nomenclature could be also confusing because of the occurrence of 'basin' S-type intrusions within the belts. Interpretation and correlation of granitoid whole rock geochemistry as a function of their ages provide new insights into the possible magmatic evolution of the Ashanti Belt.

4.6.1 Earliest Paleoproterozoic magmatism

The metamorphosed mafic series forming the base of the Sefwi Group are composed of ultramafic rocks (the ophiolite suite of Attoh et al., 2006), gabbros and basalts. According to Dampare et al. (2008) this series (their type I) corresponds to tholeiitic magmatism in a back-arc basin setting resulting from the partial melting of a depleted mantle. This early magmatism could equally have initiated growing as an oceanic plateau as proposed by Abouchami et al. (1990) and Boher et al. (1992).

4.6.2 *Eoeburnean phase*

The Eoeburnean intrusions show a large range of major elements compositions (Fig. 4). Their Fe_2O_3, MgO and CaO versus SiO_2 ratios are typical of differentiation series from diorite / tonalite to granodiorite end-members. However, these variations can also be explained by different degrees of partial melting at the source of the intrusions. The associated decrease of TiO_2 and P_2O_5 along the differentiation suite can be explained by early crystallisation of ilmenite and apatite minerals in the melt (Duchesne, 1999). A shallow decreasing trend (Fig. III-4C) is observed for Al_2O_3 which could result from a possible accumulation of plagioclase. Plagioclase crystallisation can also explain the lack of correlation between Na_2O and K_2O contents (Fig. III-4G, III-4H) for the Eoeburnean TTGs.

Considering their trace elements profiles (Fig. III-6), the Sr/Y versus Y diagram (Fig. III-5B) and the K_2O-Na_2O-CaO diagram (Fig. III-5C), the Eoeburnean TTGs clearly presents different characteristics, and therefore formation context, compared to actual adakites (Martin, 1999) and to Archean TTGs (Moyen and Martin, 2012).

Eoeburnean TTGs show calc-alkaline characteristics already identified for the Eoeburnean Prince's Town granodiorite by Dampare et al. (2005) who proposed a Cordilleran-type origin for this intrusion. Trace element concentration (Fig. III-6A) displays positive Ba anomalies and negative Ta, Nb and Th anomalies in both intrusions and coeval andesitic vocanic rocks that also is consistent with subduction-related calc-alkaline magmatism (Wilson, 1989). Similar granitoid ages and compositions were observed in the São Luís Craton in northern Brazil. According to Klein et al. (2005, 2008) the calc-alkaline Tromaí intrusive suite are highly enriched in LREE and HREE compared to the primitive mantle and their zircon ages vary between 2168 ± 4 Ma and 2149 ± 4 Ma. These geochronological and geochemical characteristics are remarkably similar to those identified in the Eoeburnean intrusive suites of southern Ghana.

A possible geodynamic context for the Eoeburnean plutonism would be a subduction zone interacting with oceanic crust/plateau segments leading to the progressive growth and accretion of volcanic island arcs (Fig. III-9A) as already suggested by several previous studies (Sylvester et al., 1992; Feybesse et al., 2006, Baratoux et al., 2011). The expected magma composition generated in this model, with partial melting of the mantle wedge above the subducted plate, is consistent with the calc-alkaline signature of the Eoeburnean magmatism. Similar major and trace element compositions of calc-alkaline metabasalt and meta-andesites (type II) of Dampare et al. (2008) and the less differentiated members of the Eoeburnean granitoids illustrate a possible similar origin (Fig. III-4).

According to the magmatic rock ages (Fig. III-2), the subduction zone may have been active from approximately 2190 Ma to 2140 Ma (andesite units within the Kumasi Group sediments dated at 2142 ± 24 Ma, U/Pb on zircon, Adadey et al., 2009), corresponding to the D1 deformation phase (Fig. III-2). During this D1 deformation phase, the Eoeburnean plutonism, the contemporaneous volcanism and a significant degree of shortening (oriented N-S according to Perrouty et al., 2012) led to thickening of the original oceanic lithosphere. By the end of the Eoeburnean stage, a thickened proto-continental crust was built. It represents the Sefwi Group basement for overlying Kumasi and Tarkwa basin formation. Asiedu et al. (2004, 2009) suggest that these sedimentary basins formed by the erosion of the Sefwi Group. The volume of Eoeburnean TTGs that reached the surface and was eroded increased with time, resulting in higher K proportions in the later adjacent sediments (Kumasi and Tarkwa groups, Fig. III-7).

4.6.3 *Eburnean phase*

Eburnean intrusions correspond to granodiorite and granite batholiths that intrude both the metasedimentary basins and the greenstone belts in southwest Ghana. Their major element

geochemistry do not show significant evidence of a differentiation series (Fig. III-4). Trace element geochemistry shows a strong depletion in HREE (Fig. III-6B) that suggests a derivation from partial melting of a garnet-bearing source (Martin, 1994). The Negra Velha granite that intruded the Tromaí suite in the São Luís Craton around 2070 Ma displays similar patterns with strong depletion in HREE (Klein et al., 2008). High Sr/Y ratios (Fig III-5B) usually characterise adakites and Archean TTGs (Martin, 1999). The context of the formation of such rocks is still a matter of debate. Some authors (Martin, 2005, Moyen, 2011) argue that most of the adakites and Archean TTGs derive from partial melting of a subducted oceanic crust (Hypothesis 1, see below). Other authors such as Smithies (2000), propose that Archean TTGs could be produced by partial melting of a garnet-bearing lower metamafic crust previously thickened by orogenic processes (Hypothesis 2, see below). These two hypotheses have also been proposed for Andean adakites (Kay et al., 2002). In southern Tibet, Chung et al. (2003) show that adakites were formed after melting of eclogites or garnet-amphibolites at the base of the continental crust.

Based on the steep HREE profiles of the Eburnean granitoids, partial melting of their source must occur under metamorphic conditions where garnet was stable. Eoeburnean lithologies in southwest Ghana correspond to metabasalts, metagabbros, metasediments of the Sefwi Group and TTG intrusions. Their average compositions are given in Table III-2A. All of these lithologies may have been buried during the late Eoeburnean or early Eburnean phases and thus could constitute the lower crust of the Eburnean Orogeny. The modal distribution of garnet within these chemically contrasted lithologies was first depicted as a function of pressure and temperature, using pseudosection calculations (Fig. III-8). These P-T diagrams show that all of these compositions produce garnet before the start of partial melting at geothermal gradients varying between 15°C/km and 25°C/km. These gradients were obtained by P-T thermodynamic modelling on Birimian metasediments in Ghana (Schmidt Mumm et al., 1997, John et al., 1999) Burkina Faso, Niger and Senegal (Ganne et al., 2012) and are thus considered to be representative of the Paleoproterozoic domain of the Leo-Man Craton. Table III-2B shows possible melt compositions extracted from these lithologies at 900°C along geothermal gradient at 15°C/km (that characterised subduction context) and at 25°C/km (that characterise melting of thickened crust).

Hypothesis 1: subducted oceanic plate melting. In the case of subduction (geothermal gradient of 15°C/km), the calculated melts at 900°C (Table III-2B) are highly deficient in iron whatever the composition of the subducted crust. Other element proportions agree with the composition of the Eburnean granitoids, including the potassium proportion assuming the subducted slab is composed of 10 % metasediments. A subducted crust composed of

metagabbros, metabasalts and sparse metasediments is not able to produce average composition of Eburnean granitoids.

Hypothesis 2: lower continental Eoeburnean crust melting (Fig. III-9B). Calculated melts using geothermal gradients of 25°C/km show compositions that agree with the Eburnean granitoids assuming mixing of melts derived from different lithologies. Magnesium and calcium were provided by metagabbro melting, iron by both the Eoeburnean TTGs and the metabasalts and potassium by Eoeburnean granitoids and metasediments. The best estimate of bulk melt composition obtained by magma mixing corresponds to 50% of melt issued from metagabbro, 30% from Eoeburnean TTGs, 10% from metabasalts and 10% from metasediments (Table III-2B). According to the percentage of partial melt at 900°C for each modelled lithology (Fig. III-8), the source rock of this melt would have approximately the following composition: 67% of metagabbro, 20% of Eoeburnean TTGs, 9% of metabasalts and 4% of metasediments. These proportions are consistent with the composition of the Eoeburnean deformed crust that was mainly composed of metafragments of the older tholeiitic oceanic crust (or oceanic plateau), of Eoeburnean TTG intrusions overlain by calc-alkaline metavolcanic rocks and of Birimian metasediments.

Consequently, partial melting of the garnet-bearing base of the thickened Eoeburnean lower crust could generate magma depleted in HREE with the composition of the Eburnean granitoids. In that case, the positive Ba anomalies and negative Ta, Nb and Th anomalies, typical of subduction context, could be inherited from the previous Eoeburnean magmatism. Melting temperatures of 900°C before extraction of melt corresponds to a depth of 30-40 km for a geothermal gradient of 25°C/km. These minimum depth values for lower crustal melting are slightly lower than the minimum of 50 km proposed for adakites in southern Tibet (Chung et al., 2003) and comparable to the 40 km for adakites in northern China (Xu et al., 2002).

4.7 Conclusions

According to new and previously published geochemical analyses, magmatism of the southern Ashanti Belt evolved in two phases associated with previously defined deformation events (Perrouty et al., 2012). The Eoeburnean TTGs and contemporaneous volcanic rocks displays trace elements concentrations (normalised to primitive mantle) characterised by significant enrichment in LREE, flat HREE profiles, positive Ba anomalies and negative Ta, Nb and Th anomalies suggesting subduction-related calc-alkaline magmatism (Wilson, 1989).

The Eburnean phase formed numerous intrusions of granodiorite and granite depleted in HREE with primitive mantle-normalised geochemical patterns characteristic of subduction, possibly inherited from Eoeburnean magmatism. They also have fractionated normalised HREE patterns and high Sr/Y ratios. This geochemistry is consistent with residual garnet in the source (Martin, 1999). Thermodynamic modelling shows that partial melting of an Eoeburnean thickened crust, composed mainly of metamafic rocks and Eoeburnean TTGs, could produce melts with a geochemical composition corresponding to those observed for the Eburnean intrusions.

Sediment composition varies from low-K composition for the Sefwi Group to medium and high K for the Kumasi and Tarkwa groups. The enrichment in potassium reflects changes in the Eoeburnean crust with increasing amounts of granitoid rocks exposed and eroded into the sedimentary basins with time.

4.8 <u>Résumé du chapitre III</u>

4.8.1 *Introduction*

Les granitoïdes du sud-ouest du Ghana furent longtemps classés en deux groupes : type-I-ceinture et type-S-bassin (Mauer, 1990, Loh et al., 1999) suivant leur localisation, sans prise en compte des âges de ces intrusions. Les études de Klein et al. (2008) menées sur des granitoïdes du craton de São Luís, au nord du Brésil (qui est supposé être un fragment du craton du Ghana) semblent mettre en évidence une variation de la composition des intrusions en fonction de leur âge. L'objectif de ce troisième chapitre est de caractériser les phases de magmatisme Éoéburnéenne et Éburnéenne (De Kock et al., 2011) via la collection de nouvelles données géochimiques complétées par les analyses et datations disponibles dans la bibliographie. Cette étude propose un nouveau mécanisme de construction de la croûte continentale Paléoprotérozoïque par la compréhension de l'évolution magmatique du sud-ouest du Ghana au cours de l'Orogénèse Éburnéenne (Bonhomme, 1962).

4.8.2 *Contexte géologique*

La géologie du sud-ouest du Ghana se compose de trois groupes stratigraphiques d'âge Paléoprotérozoïque (Sefwi, Kumasi et Tarkwa), formés de roches métavolcaniques et métasédimentaires pénétrées par d'abondants granitoïdes. Cette stratigraphie fut intensément

déformée en six évènements développant des plis d'échelle régionale et des zones de cisaillement le long desquelles se concentrent les minéralisations (cf. chapitre I).

4.8.3 *Échantillons*

21 échantillons de roche représentatifs de la diversité présente au sud-ouest du Ghana furent analysés : 10 granitoïdes, 2 métaandésites, 4 métasédiments du groupe de Sefwi et 5 métasédiments du groupe de Tarkwa. Les compositions en éléments majeurs et en éléments traces ont, toutes deux, été mesurées.

4.8.5 *Résultats*

Les granitoïdes reliés à la phase Éoéburnéenne, d'une composition de type TTG (Tonalite, Trondhjemite, Granodiorite) présentent des spectres enrichis en terres rares légères (LREE) et des spectres plats pour les éléments lourds (HREE), après normalisation par rapport au manteau primitif. Bien qu'ils montrent également un enrichissement en terres rares légères, les granodiorites et granites de la phase Éburnéenne sont caractérisés par des spectres très appauvris en éléments lourds (HREE) et par de forts rapports Sr/Y. Granitoïdes et roches métavolcaniques possèdent également des anomalies positives en Ba et négatives en Ta, Nb et Th.

L'analyse géochimique des métasédiments montre une évolution de la proportion de potassium au cours du temps, avec de faibles teneurs pour les métasédiments du groupe de Sefwi contrastant avec de plus fortes valeurs pour les métasédiments Tarkwaiens. Les métasédiments du groupe de Kumasi, affichent des teneurs en potassium (et des âges) intermédiaires.

4.8.4 *Modélisation thermodynamique*

Basées sur les compositions moyennes des lithologies caractéristiques de la croûte Éoéburnéenne, plusieurs pseudo-sections furent calculées afin de mettre en évidence l'apparition du grenat en fonction des conditions de température et de pression. Considérant des gradients géothermiques raisonnables (15°/km et 25°/km), les compositions de magmas produits lors de la fusion partielle de ces lithologies, à 900°C, ont été calculées afin d'estimer quelles seraient les proportions respectives en éléments majeurs pour un granitoïde produit.

4.8.6 *Discussion*

Les nouveaux résultats associés aux données de la littérature montrent que les deux phases de l'Orogénèse Éburnéenne ont formé un magmatisme distinct au sud-ouest du Ghana. La

première phase correspond à un magmatisme calco-alcalin typique des zones de subduction (Wilson 1989) avec un volcanisme intense en surface et de nombreuses intrusions de TTGs, entre approximativement 2190 Ma et 2140 Ma. Ce magmatisme, associé à une déformation majeure au sud de la ceinture d'Ashanti, a contribué à un épaississement significatif de la croûte Éoéburnéenne et a entraîné la formation de grenat dans les lithologies profondes comme le montre la modélisation thermodynamique.

La fusion partielle de la base de cette croûte préalablement épaissie et métamorphisée peut donc générer des magmas fortement appauvris en terres rares lourdes (Martin, 1999), avec un héritage des signatures de subduction (Wilson, 1989). Les magmas produits sont de composition similaire à celle des granitoïdes Éburnéens, si l'on considère un gradient géothermique de 25°/km, en accord avec une croûte continentale épaissie et avec les données métamorphiques du sud-ouest du Ghana. Ce mécanisme de fusion de la base de la croûte a pu jouer un rôle important dans la génération de granitoïdes, à l'Archéen et au Paléoprotérozoïque, contribuant ainsi à la croissance des croûtes continentales.

Chapitre IV

Chapitre IV

3D modelling of the Ashanti Belt, southwest Ghana, and lithostructural control on gold occurrences within the Sefwi Group

Abstract

A new 3D model of the southern Ashanti belt was build using Geomodeller and Gocad software and inverted by VPmg. This hybrid method allows to preserve the advantage of each software: Geomodeller helps us to build a 3D geological model based on stratigraphic relationships and bedding orientations, Gocad allows to easily enhance and complete the Geomodeller-modelled surfaces, and VPmg allows us to invert for basin depth. Input data for modelling include regional geological and structural map, geophysically constrained cross-sections and petrophysical data (Perrouty et al., 2012).

The calculated base of the Tarkwa Basin displays an asymmetric profile being the deepest close to the contact with the Ashanti Fault and most shallow on the eastern side of the syncline. The north of the basin is also deeper than the south, a feature corroborated by field observations and mapping. The average depth of the basin is around 3400 m, significantly deeper than previous estimates.

The 3D modelling also highlights the lithostructural control on the location of gold mineralisation within the Sefwi Group in the southeastern part of the Ashanti Belt. 85 % of the gold mineralisation in this area is located less than 1500 m from one specific tholeiitic metabasalt horizon in the stratigraphy which itself represents only 10 % of the Sefwi Group by volume. All of the gold occurrences in the area are simultaneously located close (with an average of 4 km) to a major fault (defined as being more than 50 km long). This 300 m thick metabasaltic layer, more competent than the surrounding metasediments, may have controlled secondary fracturing and acted as a focus for gold mineralisation near the major faults along which the mineralising fluid were transported.

5.1 <u>Introduction</u>

The Ashanti greenstone belt in the southwest of Ghana is of significant economic interest as it hosts numerous gold mines. These deposits formed during the Eburnean Orogeny (Bonhomme, 1962): a major tectonic event affecting the West African Craton during the Paleoproterozoic. Gold deposits are mainly located along faulted or sheared contacts between the major stratigraphic groups (Birimian Sefwi and Kumasi groups, Tarkwa Group), such as the Ashanti Fault that hosts the Obuasi giant gold deposit (over 60 million ounces of gold).

The base of the Tarkwa metasedimentary basin may be the focus of mineralisation as suggested by observations of mineralisation on both sides. Knowledge of the shape and depth of the base of this basin could present a significant economic importance in southwest Ghana. Hasting (1982) and Barritt and Kuma (1998) estimate Tarkwa Basin thicknesses between 1500 m and 2500 m depending on the location of their profiles. However, in their model they considered the old and inverse stratigraphy of the Birimian Supergroup that disagrees with modern dating and structural relationships (Adadey et al., 2009). Specifically they modelled a low density metasedimentary group (Lower Birimian) below high density metavolcanics (Upper Birimian). As a consequence, they may underestimate the depth of the Tarkwaian basin and some granitoids geometries.

Many gold occurrences (and several deposits, Griffis et al., 2002) have been described in the southeastern part of the Belt, within the Birimian Sefwi Group (Adadey et al., 2009). This area where recently studied by Perrouty et al. (2012) who proposed a new stratigraphy of the Sefwi Group. Using their new map, structural measurements and petrophysical data, we have built a new three-dimensional model of the southern Ashanti Belt that was refined by inversions based on both the gravity and the aeromagnetic data using the package VPmg (Fullagar et al, 2000, 2008). 3D modelling provides a means of exploring the sub-surface geometries of the gold-rich faulted contacts and represents an aid to mineral exploration.

5.2 <u>Geological setting</u>

5.2.1 *Stratigraphy*

The Ashanti Belt is composed of three Paleoproterozoic stratigraphic groups and by granitoids intrusions that are overlaid along the coast by Phanerozoic sediments. The Sefwi Group (Adadey et al., 2009) consists of metamorphosed Birimian volcanics rocks interbedded

with volcanosediments, phyllites and micaschists. The Kumasi Group corresponds to Birimian metasedimentary rocks (mainly phyllites) deposited in the Kumasi and Akyem Basins (Fig. IV-1). The Tarkwa Basin is a metasedimentary sequence located on top of the Sefwi Group and represents the bulk of the Ashanti Belt. It is composed of four sub-units known as the Kawere Group, the Banket Formation, the Tarkwa Phyllites and the Huni Sandstones (Junner, 1940). Granitoids intrusions occurred in two stages called Eoeburnean (2200 - 2150 Ma, De Kock et al., 2011) and Eburnean (2130 - 2000 Ma). These two sequences related to the Eburnean Orogeny (Bonhomme, 1962) were linked with significant deformation of the host rocks. Granitoids have mafic to felsic compositions varying from typical tonalite trondhjemite granodiorite suites to granite. In the southern part of the belt, the Mpohor Intrusive Complex is characterised by a gabbro/diorite/granodiorite assemblage related to the end of the Eoeburnean magmatism.

5.2.2 *Mineralisations*

Over a hundred gold occurrences and deposits are hosted by the Paleoproterozoic rocks that form the southern Ashanti Belt (Fig. IV-1). Most of the hydrothermal mineralisation is located along the major Akropong and Ashanti faults to the northwest of the Tarkwaian metasediments and are related to a sinistral strike-slip shear reactivation of the faults (Allibone et al., 2002). Others, such as the hydrothermal deposits of Damang (Tunks et al., 2004), are located along the eastern margin of the Tarkwa Basin. Perrouty et al. (2012) suggested that the whole contact at the base of this basin may be mineralised. The Tarkwa Group also hosts some gold placer deposits such as the Tarkwa placer (over 40 million ounces of gold).

Both structural and geochemical controls on gold mineralisation have been suggested for deposits located along the Ashanti Fault (Prestea, Bogoso and Obuasi gold mines). These deposits are hosted by the Birimian Kumasi Group phyllites and by the Birimian Sefwi Group metabasalts. The initial modifications of the host lithologies correspond to greenschist facies metamorphism related to the D3 shortening of Perrouty et al. (2102). Further circulation of hydrothermal CO_2 rich fluids along the Ashanti Fault and changes in the pressure-temperature conditions are thought to have resulted in the formation of carbonate in the host rocks (Mumin et al., 1996). Geochemical reaction occurred between sulphur form transported by these fluids and Fe rich mineral in the host rock resulting in precipitation of pyrite and arsenopyrite. At the same time, the loss in sulphur in the fluids caused a decrease of Au solubility (William-Jones et al., 2009) resulting in precipitation of primary "invisible" gold (Mumin et al., 1994). A further D4 deformation event produce significant fracturing allowing remobilisation of the gold particles

and their further concentration. According to Allibone et al. (2002), D4 shear zones are the major structures controlling the gold mineralisation localised along dilatational jogs at the Obuasi gold mine.

5.3 Mapping of the Birimian geology beneath the Tarkwa metasedimentary basin

The recent structural study of Perrouty et al. (2012) produced a new stratigraphy of the Birimian Sefwi Group. These units were affected by significant deformation before the Tarkwa Group deposition. This previous work highlighted some buried structures observed in this Sefwi Group, below the Tarkwa basin. Adding possible geological constraints at depth is a great aid in building deeper 3D models of the Birimian and of the overlying Tarkwa Basin. Consequently, a new map of the possible buried geology of the Sefwi Group has been produced (Fig. IV-1C). The mapping methodology is similar to that used in Metelka et al. (2011) and Perrouty et al. (2012), however, only magnetic images were used for mapping. Mapped "magnetic susceptibility domains" were linked with geology away from the Tarkwa Basin by correlation with regional geology mapping.

Several 3D modelling tests were conducted using the Noddy package (Jessell, 1981, 2001; Jessell and Valenta, 1996) which showed that the Sefwi Group structures below the basin can be mapped using magnetic data assuming a reasonable (5 times) increase in susceptibility between the basement lithologies and the Tarkwa Basin metasediments (Perrouty et al., 2012).

5.4 Geophysical datasets

5.4.1 *Aeromagnetic data*

Aeromagnetic data were acquired between 1994 and 1996 for the Geological Survey of Ghana. The flight height of the survey is 80 m above ground, striking 135° with 200 meters line spacing. The total magnetic intensity (TMI) data used for modelling and inversion was gridded with a resolution of 100 meters. The Earth's magnetic intensity at the time of the survey was around 31699 nT with inclination of -14.5° and declination of -6.5°. These values were used to reduce the data to the pole (RTP) using amplitude correction to avoid artefacts and to produce interpretable image for mapping. Multiple processing of the magnetic RTP grid such as the low pass filtering and upward continuation were performed to highlight deep structures and to help mapping of the Sefwi Group geology below the Tarkwa Basin.
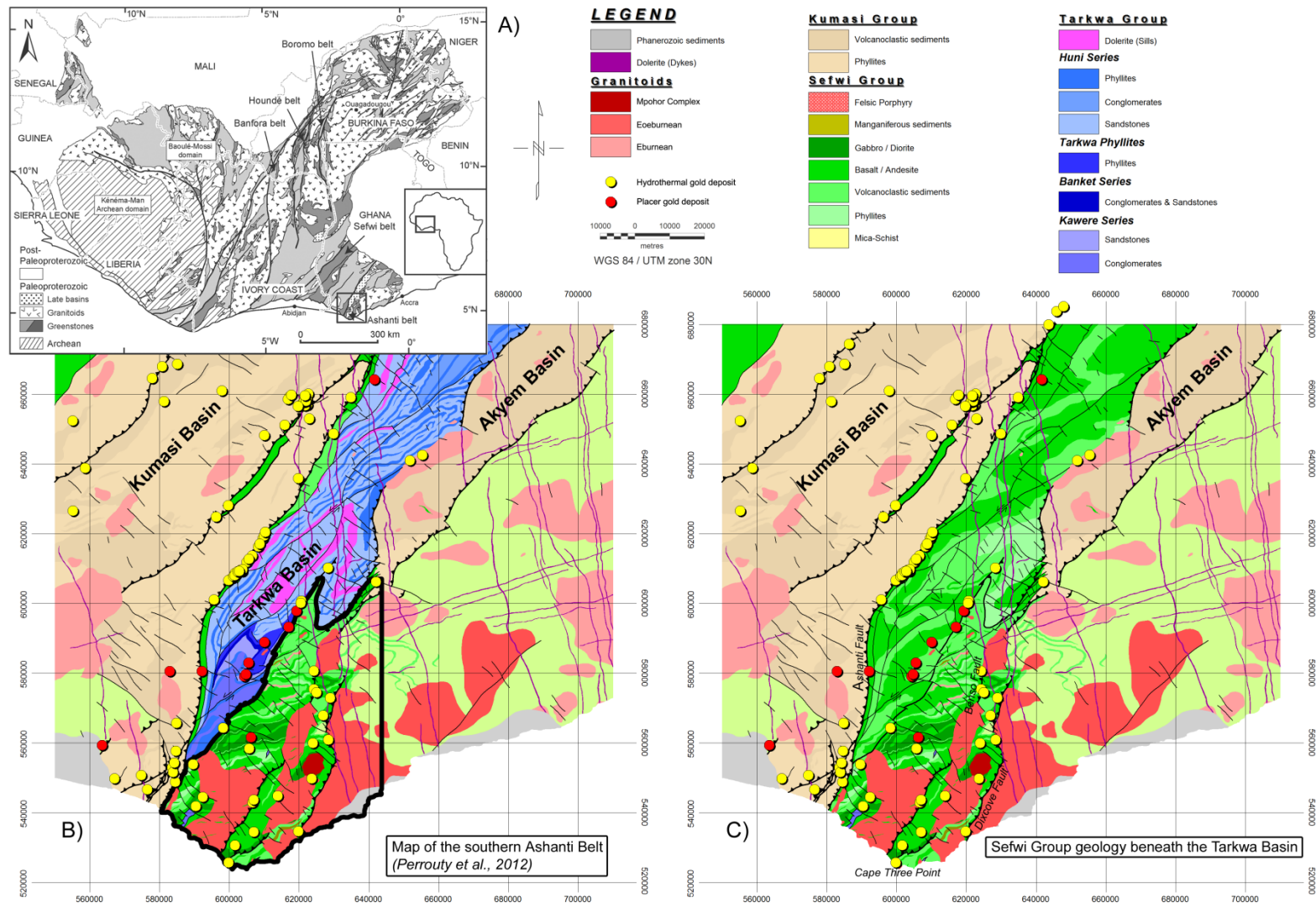
Figure IV-1 *A) West African Craton with the location of the study area. B) Map of the southern Ashanti Belt with the location of the major faults and of the gold deposits. Black line outlines deposits hosted by the Sefwi Group that are detailed on Figure IV-8 and on Table IV-4. C) New map of the Sefwi Group geology beneath the Tarkwa Basin.*
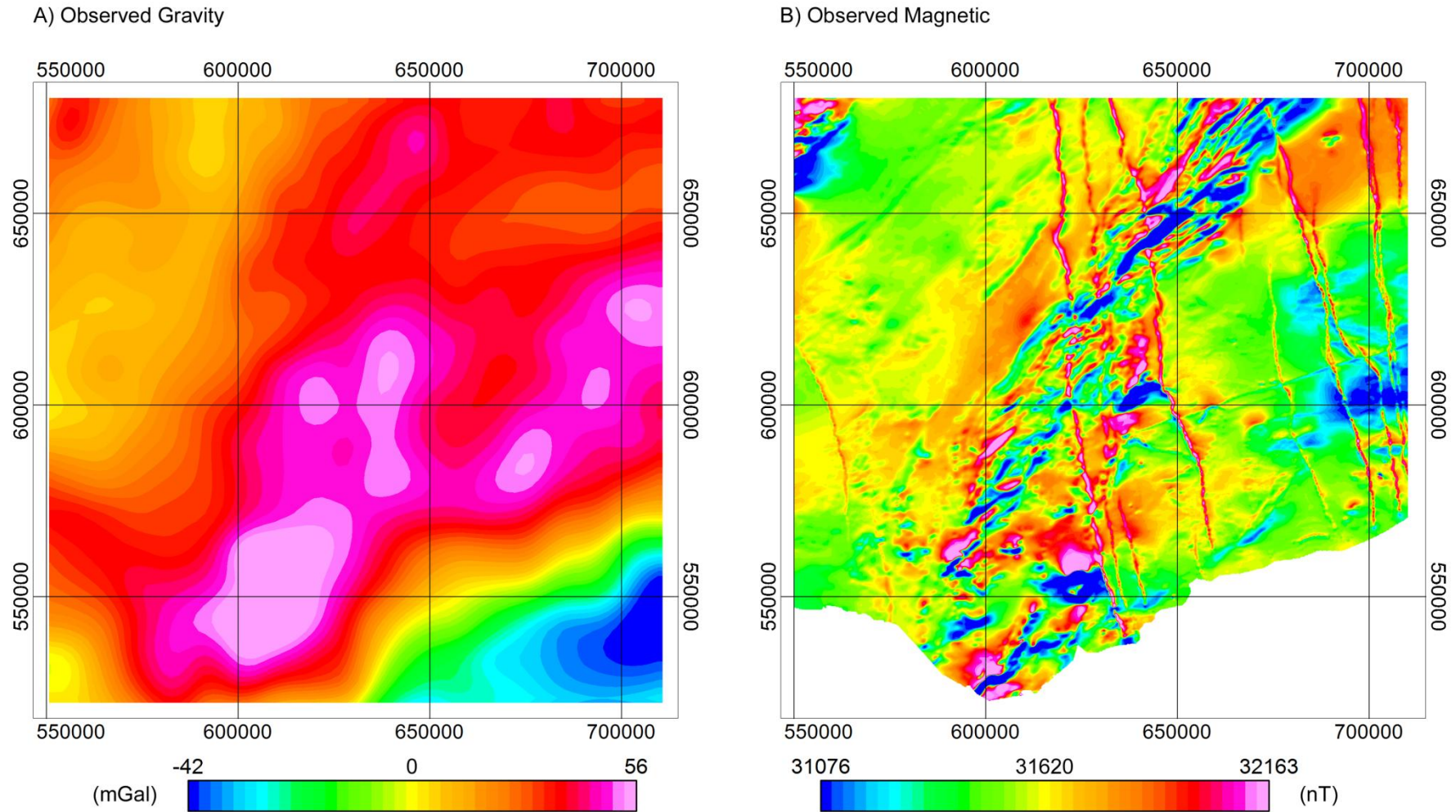
Figure IV-2   *Images of the free air gravity anomalies and of the total magnetic intensity data of the southern Ashanti Belt. A) The observed free air gravity image (A) has a resolution of 2.5 arc minute per pixel (4.6 km). B) Total magnetic intensity image were gridded with a resolution of 100 m. Coordinates are in UTM (WGS 84), zone 30N.*

The TMI image displays two major magnetic domains (Fig. IV-2B). The metasediments from the Kumasi Basin on the northwest and the Sefwi Group micaschists on the southeast present low intensity features with long wavelength variations. In contrast, the Ashanti Belt (the Sefwi Group metavolcanics and the Tarkwa Basin) is characterised by intense magnetic variations. Other significant magnetic objects are the NS dolerite dykes that extend across the image and the Mpohor Mafic Complex in the south.

5.4.2 *Gravity data*

Gravity data have been sourced from the International Gravimetric Bureau (BGI, http://bgi.omp.obs-mip.fr/) as a Free Air anomaly grid. This grid had already been processed using the Pavlis et al. (2008) and Fullea et al. (2008) computation methods by the BGI. The spatial resolution is 2.5 arc-minutes (approximately 4.6 km) per pixel. Many datasets were combined to build this grid including Getech ground gravity data (African Gravity Project 1986-1988, http://www.getech.com/history.htm), BGI ground and marine gravity data and satellite data.

The Free Air anomaly image (Fig. IV-2A) show two main domains: the strong positive anomaly on the centre to the northeast of the map correlates with the presence of thick high-density metavolcanic units (Sefwi Group) in the Ashanti Belt. The homogenous area without anomaly in the northwest part of the map correlates with the presence of Kumasi Basin metasediments. The major gravity gradient between these zones coincides with the Ashanti Fault marking the western border of the Ashanti Belt. The remarkable density contrast between the two sides of the fault has been previously modelled in 2D sections by Barritt and Kuma (1998). Hasting (1982) suggested the presence of a tectonic contact with massive post-sedimentation vertical movement to explain this gravity contrast. However, kilometric scale movement along the Ashanti Fault is contradicted by the absence of a jump in metamorphic grade between the two sides of the fault (Allibone et al., 2002). Consequently, the depositional context can more easily explain the regional geometry of the Kumasi Group than deformation can.

5.4.3 *Petrophysical data*

Previous studies published petrophysical measurements of density, magnetic susceptibility and remanence for southwest Ghanaian lithologies (Perrouty et al., 2012; Hasting, 1978). We make use of magnetic susceptibility values acquired in the field using a Geofyzika KT-5 Kappameter hand-held susceptibility meter resulting in a database of over 300 analyses (Perrouty et al. 2012). Natural remanent magnetization (NRM) was measured on two samples of

dolerite using an AGICO JR5A spinner magnetometer, mounted within Helmholtz coil systems, at the GET Magnetism Laboratory (Toulouse). Density values were measured on 26 small (≈ 5 cm^3) samples representative of rocks from the Ashanti Region after weighing in air and in water at 24.5°C (Perrouty et al., 2012). Their resulting density are in good agreement with ranges get in southwest Ghana (Hasting, 1978, on 150 kg of rocks), in Burkina Faso (Baratoux et al., 2011) and with usual standard values established for equivalent lithologies (Milsom, 2003).
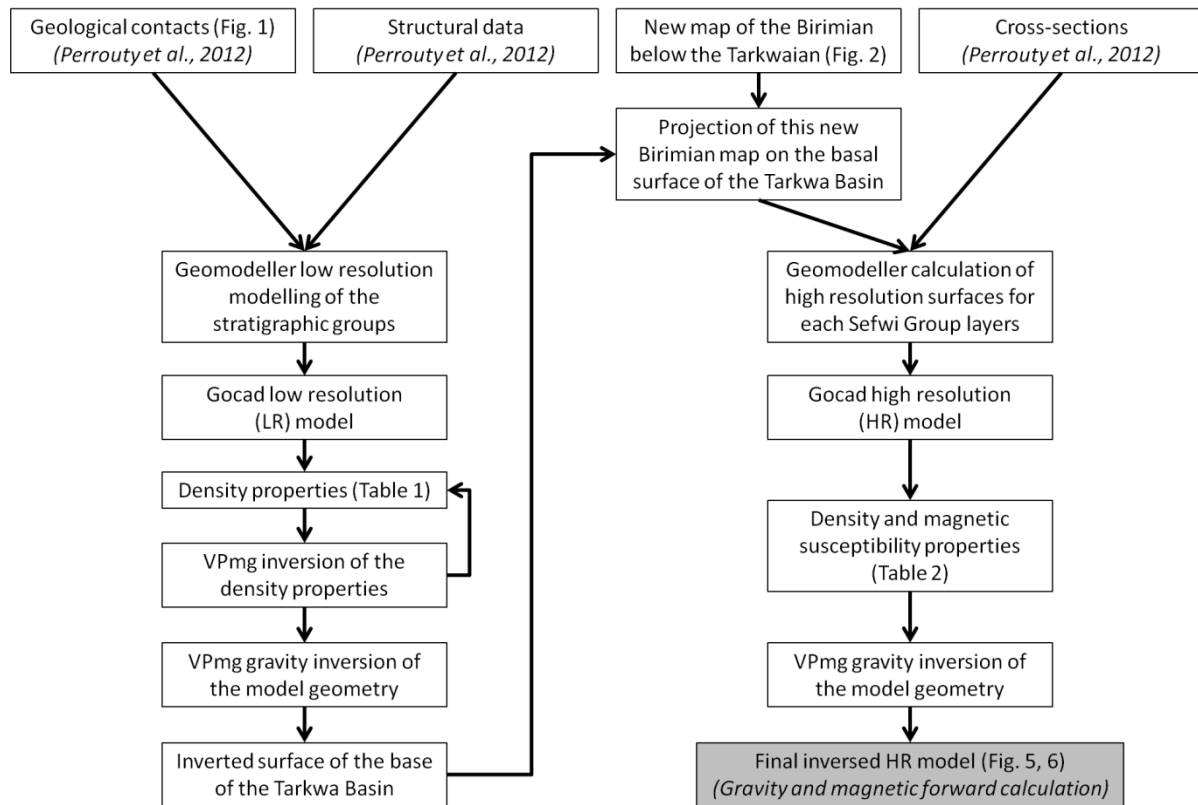
Figure IV-3   *Schematic diagram showing the different steps used for the 3D modelling of the Ashanti Belt (see text for details).*

5.5 3D modelling of the Ashanti Belt

The geological 3D model of the southern Ashanti Belt was built in several steps (Fig. IV-3): (1) an initial low resolution (LR) model representing each stratigraphic unit was built and was inverted using gravity data to estimate the approximate geometry of the Tarkwa Basin. (2) The new map of the possible Birimian geology beneath the Tarkwa Basin was projected down onto the newly calculated base of the Tarkwa Basin. (3) The projected lithologies contacts were used to build a new model with higher resolution (HR) that includes all

the layers mapped in the Sefwi Group and the dolerite dykes. (4) This HR model was then inverted using gravity data.

The forward 3D model of the Ashanti Belt is an hybrid model built using two modelling systems: Geomodeller (www.geomodeller.com) and Gocad (http://www.pdgm.com). Gravity/magnetic inversions of the base of the Tarkwa Basin were run using VPmg (http://www.mirageoscience.com).

5.5.1 *Modelling packages*

5.5.1.1 Geomodeller

The potential field method is used by 3D Geomodeller to calculate geological interfaces as implicit surfaces (Lajaunie et al., 1997). This method determines what the potential is of a point in the model volume belonging to a specific geological unit. Geological interfaces can be determined by finding where the potential for one unit exceeds that of another, forming the contact between the geological units (Calcagno et al. 2008). Three sources of geological information are required before model calculation can take place: the location of geological contacts for the units being modelled; strike and dip measurements describing the orientation of the geological interface and a stratigraphic column. Faults can be calculated using the potential field method if contact and orientation information are provided. Each modelled fault can be attributed to stop on, or to cross-cut other faults and geological units.

5.5.1.2 Gocad

Gocad uses the discrete smooth interpolation method (DSI, Mallet, 1992). Each explicitly modelled surface is determined by node locations with a resolution depending on the number of these nodes. The surfaces are displayed by triangular facets linking neighbour nodes. Input data to build a Gocad model can be: surfaces already created by other modelling software (e.g. Geomodeller); point sets (e.g. elevation data) or curves (e.g. trace of dolerite dykes) interpolated to make surface. Surfaces bordering geological regions were used to define the 3D model. Geological/Geophysical properties were then assigned to each modelled volume. In this work we used Gocad to enhance the model by adding some geological details that haven't been modelled in Geomodeller.

5.5.1.3 VPmg

The VPmg model is based on previously calculated Gocad modelled volumes that are discretised into vertical rectangular prisms matching the topography on their top faces (Fullagar,

2000, 2008). The size of the prisms depends on the resolution of the model. Each prism preserve the geophysical (density or susceptibility and remanence) properties of the Gocad volume.

VPmg proposes two mode of inversion to minimise the difference between observed and calculated geophysical data (Fullagar, 2008). The first style inverts the petrophysical properties of the modelled rectangular prisms (heterogenous inversion) or to the whole model (homogenous inversion) keeping their respective geometry. The second style of inversion affects the size of each prism (along Z axis) preserving the petrophysical properties within the prism. Consequently, this geometry inversion modifies the shape of the surfaces defined by the base and the top of each modelled geological prism.

5.5.2 *Low resolution model of the Ashanti Belt*

5.5.2.1 Geological modelling

The LR geological model of the Ashanti Belt covers an area of 160 by 160 kilometres to a depth of 14 kilometres. Input data for Geomodeller are lithological contacts from the recent mapping of the area (Perrouty et al., 2012) and bedding orientation measurements acquired in the field. The general modelling methodology is described in Calcagno et al. (2008).

Surfaces representing the base of each modelled stratigraphic unit and granitoids were imported into Gocad and used as input data to build a voxet model of the same area with a voxel size of 1000 metres for the X and Y axes and 200 metres in the Z direction. Voxels from the upper surface (from 0 to -200 m) were prolonged to fit the topography. The topography used is a digital elevation model at 90 m resolution from the SRTM (Shuttle Radar Topographic Mission). It has been re-gridded to match the model resolution. In southwest Ghana, the topography varies between 0 and 470 m with less than 3 % of the area above 200 m.

5.5.2.2 Geophysical modelling

Input density values were calculating from samples density measurements of Perrouty et al. (2012), Hasting (1978) and Baratoux et al. (2011). A homogenous mean density value was assign to each modelled stratigraphic unit. These input densities were then refined by a first inversion sequence using VPmg (Fullagar et al., 2008). Both homogenous and heterogeneous density inversions were run for each modelled unit. This confirmed that the input ranges of density were consistent with the values needed to fit the gravity data assuming constant initial model geometry.

Modelled lithology (LR Model)	Measured density ranges for southwest ghanaian rocks (g/cc)		Input density values (estimated from samples measurements)		VPmg calculated density and ranges	
	Perrouty et al., 2012	Hasting, 1978*	d (g / cc)	ranges (g/cc)	d (g / cc)	ranges (g / cc)
1- Phanerozoic Sediments	no data	no data	2.500	2.40 - 2.60	2.541	2.44 - 2.64
2 - Eburnean granitoids	2.58 - 2.75	2.41 - 2.76	2.680	2.58 - 2.75	2.740	2.66 - 2.75
3 - Eoeburnean granitoids	2.76 - 2.89	2.41 - 2.76	2.820	2.76 - 2.89	2.773	2.76 - 2.85
4 - Mpohor Mafic Complex (gabbro, diorite)	2.65 - 3.03	no data	2.860	2.65 - 3.03	2.840	2.82 - 2.86
5 - Tarkwa Group (conglomerates, quartzites, phyllites)	2.68 - 2.99	2.45 - 2.84	2.710	2.68 - 2.99	2.701	2.68 - 2.74
6 - Kumasi Group (Birimian phyllites)	2.69 (1 data)	2.71 - 2.74	2.690	2.59 - 2.79	2.717	not calculated
7 - Sefwi Group (Birimian metavolcanics)	2.70 - 3.01	2.74 - 3.00	2.800	2.70 - 3.01	2.779	2.70 - 3.01
8 - Sefwi Group (Birimian, Cape Coast micaschists)	2.65 (1 data)	no data	2.650	2.50 - 2.80	2.766	not calculated

Table IV-1   *Input and Calculated density values for the low resolution (LR) model compared to the published density ranges of Perrouty et al. (2012) and Hasting (1978, *unpublished report referenced in Barritt and Kuma, 1998).*

Resulting gravity values and ranges of density calculated after inversion show some correlations with the ranges of measured values (Table IV-1). However, significant differences are observed for the Sefwi Group. The Cape Coast micaschists show higher density estimation than the input value. Densities for this unit were based on only one measurement that may not be representative of the mean density of the whole area covered by this lithology. Therefore, the value calculated by homogenous inversion was assumed to be a more accurate estimation of the density of this unit and was used for further inversions. Heterogeneous density calculations in the Sefwi Group (metavolcanic) suggests the presence of a minimum of 3 lithologies with following distribution: 4% below 2.7 g/cm^3, 5% above 3 g/cm^3 and the rest around 2.78 g/cm^3 (peak of density histogram). This distribution agrees with the regional mapping of the Sefwi Group (Perrouty et al., 200) that found many metabasalts layers that alternate with volcanosediments, rare phyllites layers (lower density) and gabbros bodies (higher density).

Using homogenous-inverted density values as the new input petrophysical data, a geometry inversion of the LR model was run using VPmg to refine the shape of the base of the Tarkwa Basin.

5.5.3 *High resolution model of the Ashanti Belt*

5.5.3.1 High resolution modelling

The HR model was built by adding the detailed geology of the Sefwi Group and highly magnetic dolerite dykes to the LR model, and taking into account the new shape of the base of

the Tarkwa Basin. The new interpretation of the Sefwi Group beneath the Tarkwa Basin was also use as input data for modelling. Mapped lithological contacts in the Sefwi group (Fig. IV-1) were sampled with one point each 1000 meters and then geometrically projected on the inverted surface defining the base of the Tarkwa Basin. Geometry inversion of the LR model using gravity data indicates mean depths of the Tarkwa Basin around 2100 m which is compatible with the modelling of the Sefwi Group structures. However, a few areas are deeper. Based on tests using Noddy (Perrouty et al., 2012), mapping of the Sefwi Group is possible at 3000 m depth assuming magnetic susceptibility contrast of 5 times or more between the Tarkwa Group and the Sefwi Group lithologies. Only contacts projected at less than 3000 m depth were taking into account and imported as 3D data into Geomodeller software.

After model computation using Geomodeller and importing of the modelled surfaces into Gocad, a voxet model was created using a cubic voxel size of 200 metres for the X, Y and Z axes. This HR model covered the same area as the LR one (160 per 160 km for a depth of 14 km). The use of Gocad allows us to significantly enhance the resolution of the voxel model by faster calculation processes than Geomodeller and as a consequence, to be able to add some thin geological bodies including dolerite dykes (assuming a thickness close to 200 m). We wanted to include these dolerite dykes in the model because of their very strong signature in the aeromagnetic data. Forward calculation or inversion of magnetic data is not possible without taking the dykes into account. In contrast with regards to the low resolution of the gravity data (5 km) the 200 m dykes thickness makes them negligible for gravity calculations using the LR model.

5.5.3.2 VPmg forward-modelling

Petrophysical data has been added to this model using previously calculated homogenous values for the large modelled units and measured mean densities for the different modelled layers of the Sefwi Group and dolerite dykes. Susceptibility was added using measured mean values for each lithology. We also take into account the magnetic remanence of the dolerite dykes (measured in Perrouty et al., 2012). Table IV-2 summarizes the petrophysical data used in the HR model. The geometry of the HR model was then inverted using gravity data. The final inverted HR model of the Ashanti Belt is shown in Fig. IV-4. Fig. IV-5 displays horizontal sections of the model at depth of 0, 1000, 2000 and 5000 m. These images show that some parts of the Tarkwa Basin are still present at 5000 m depth. The geometry of the Sefwi group is mostly constrained by bedding orientation data close to the surface and by gravity data inversions at depth.

RMS errors between this final model and the gravity data were calculated over a square of 140 km centred on the model area. The surface area was cropped by 10 km to avoid border artefacts. Gravity modelling presents RMS of 5.41 mgal. The calculated gravity signature of the model gives intensity of Free Air anomalies comparable to the data (Fig. IV-6). However, the low resolution of the data (2.5 arc minute) can't reproduce the short-wavelength gravity signal. The Free Air gravity image calculated from the model displays some correlation with the topography (that also correlates with lithologies in southwest Ghana). For more effective comparison, the calculated gravity map was re-sampled at the location of ground gravity data and then re-gridded to the resolution of the BGI map (Fig. IV-6). The total magnetic intensity of the model was also calculated and compared to the data (Fig IV-7).

5.6 Results

5.6.1 *Geometry of the Tarkwa Basin*

The LR initial 3D model was built assuming a mean depth of 1700 m for the Tarkwa Basin in agreement with previous estimations. Geometry inversion suggests a mean depth of 2100 m for the LR model which increases to 3400 m for the HR model. The 2D gravity-constrained cross-sections of Barritt and Kuma (1998) suggest that the Tarkwa Basin geometry correspond to an approximately "half-cylinder". This hypothesis was also used for the LR density model building. In contrast, the modelled surface after inversion, which represents the base of the Tarkwaian basin, displays an asymmetric profile which is deeper close to the contact with the Ashanti Fault and shallower on the eastern side (Fig. IV-5). Minimum depths are observed to the south of the Tarkwa town where the Kawere conglomerates (the basal unit of the Tarkwaian metasediments) are outcropping. Conversely the deeper areas correlate with the presence of the Huni Sandstones (the upper Tarkwaian metasedimentary unit, Junner, 1940) on the surface, even though the different sub-units of the Tarkwa Group haven't been modelled. The highly mineralised Damang antiform and Epieso synform folds areas show maximum depths less than 1500 m in a perimeter of more than 3 km from the Tarkwa Group / Sefwi Group contact. A possible shift of around 1000 m height seems to be correlated with the Bogoso non-mineralised shear zone striking N45 and cross-cutting the whole Tarkwa Basin. The Tarkwa Basin shows depths that generally increase from the south to the north and from the east to the west over the whole study area.

Layer ID (HR model)	Modelled Stratigraphy	Input Density	Input Susceptibility
01 - Phanerozoic	Phanerozoic sediments	2.550	0.002
02 - DNS	Dolerite dykes (oriented N-S)	3.000	0.010*
03 - DEW	Dolerite dykes (oriented E-W)	3.000	0.010
	Eburnean Intrusions		
04 - Mpohor	Gabbro, diorite - Mpohor Mafic Complex	2.840	0.050
05 - Eburnean	Eburnean granitoids	2.740	0.002
06 - DoSills	Paleoproterozoic dolerite sills	3.000	0.010
	Tarkwa Group		
07 - Tarkwa	Conglomerates, quartzites, phyllites	2.700	0.005
	Birimian Kumasi Group		
08 - Akyem	Phyllites	2.710	0.001
09 - Kumasi	Phyllites	2.710	0.001
	Eoeburnean Intrusions		
10 - Eoeburnean	Eoeburnean granitoids	2.780	0.005
	Birimian Sefwi Group		
11 - BVSefwi	Metavolcanics rocks of the eastern Sefwi Belt	2.810	0.005
12 - BV6	Metavolcanics	2.760	0.005
13 - BVC5	Metavolcanosediments	2.720	0.001
14 - BV5	Metavolcanics	2.810	0.020
15 - BVC4	Metavolcanosediments	2.720	0.001
16 - BV4	Metavolcanics	2.810	0.020
17 - BVS	Phyllites	2.710	0.001
18 - BVC3	Metavolcanosediments	2.720	0.001
19 - BV3	Metavolcanics	2.810	0.020
20 - BG	Metagabbro	2.890	0.010
21 - BV2	Metavolcanics	2.810	0.020
22 - BVC2	Metavolcanosediments	2.720	0.001
23 - BV1	Metavolcanics	2.810	0.020
24 - BVC1	Metavolcanosediments	2.720	0.001
25 - Basement	Micaschist	2.760	0.005

Table IV-2 *Petrophysical data used in the high resolution (HR) model. S.G., Sefwi Group (Birimian). * remanence data of the Neoproterozoic dolerite dykes oriented NS were also includes in the model with remanence value of 3 A/m, inclination of -18° and declination of 59°.*
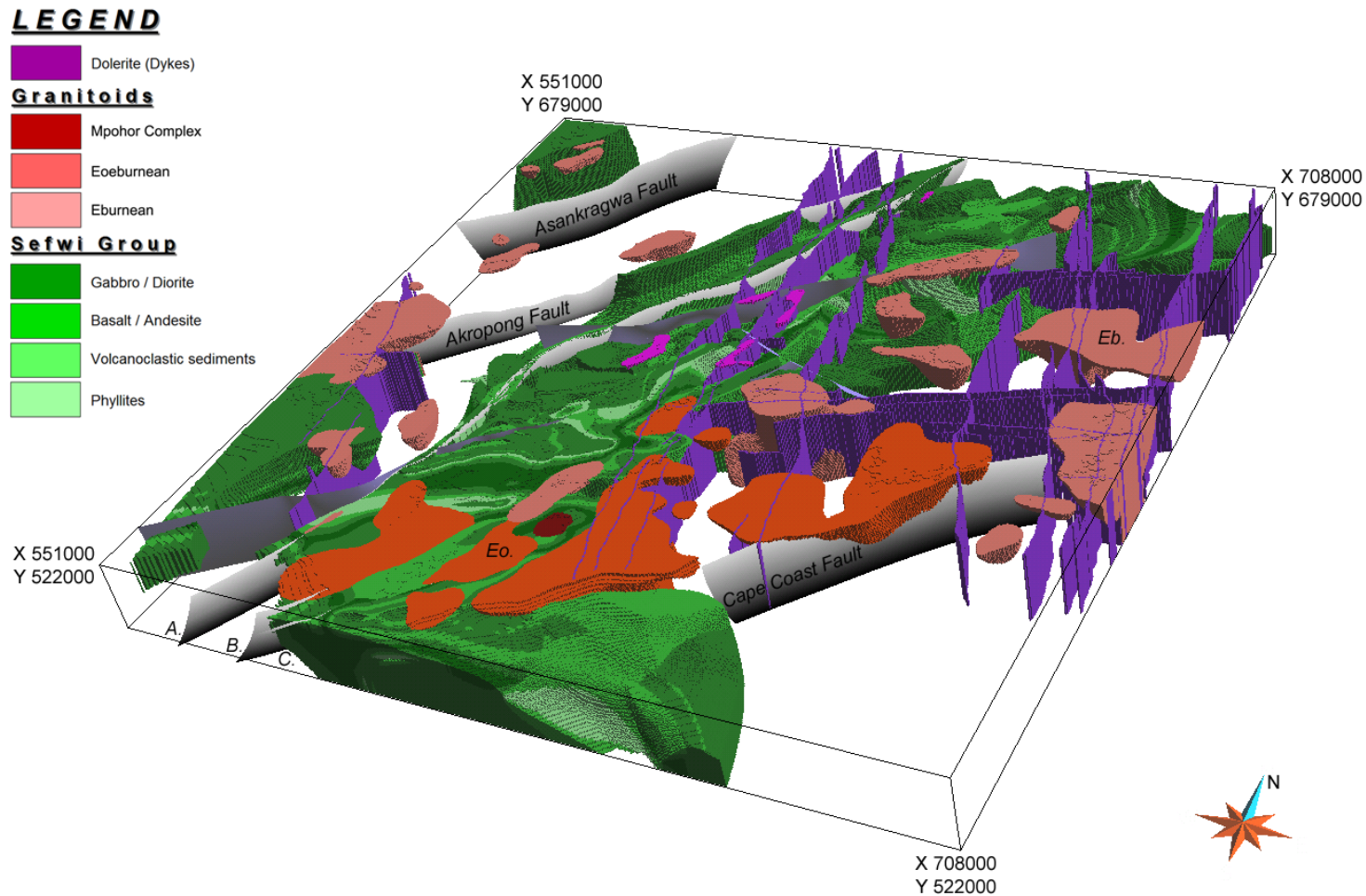
Figure IV-4   *High resolution (HR) three dimensional model of the studied area after gravity inversions and recalculation using Geomodeller. Only the Sefwi Group, the intrusive rocks and the major faults (grey) are shown. Eo. Eoeburnean granitoids, Eb. Eburnean granitoids, A. Ashanti Fault, B. Benso Fault, C. Cape Three Point Fault. Coordinates are in UTM (WGS 84), zone 30N.*

175
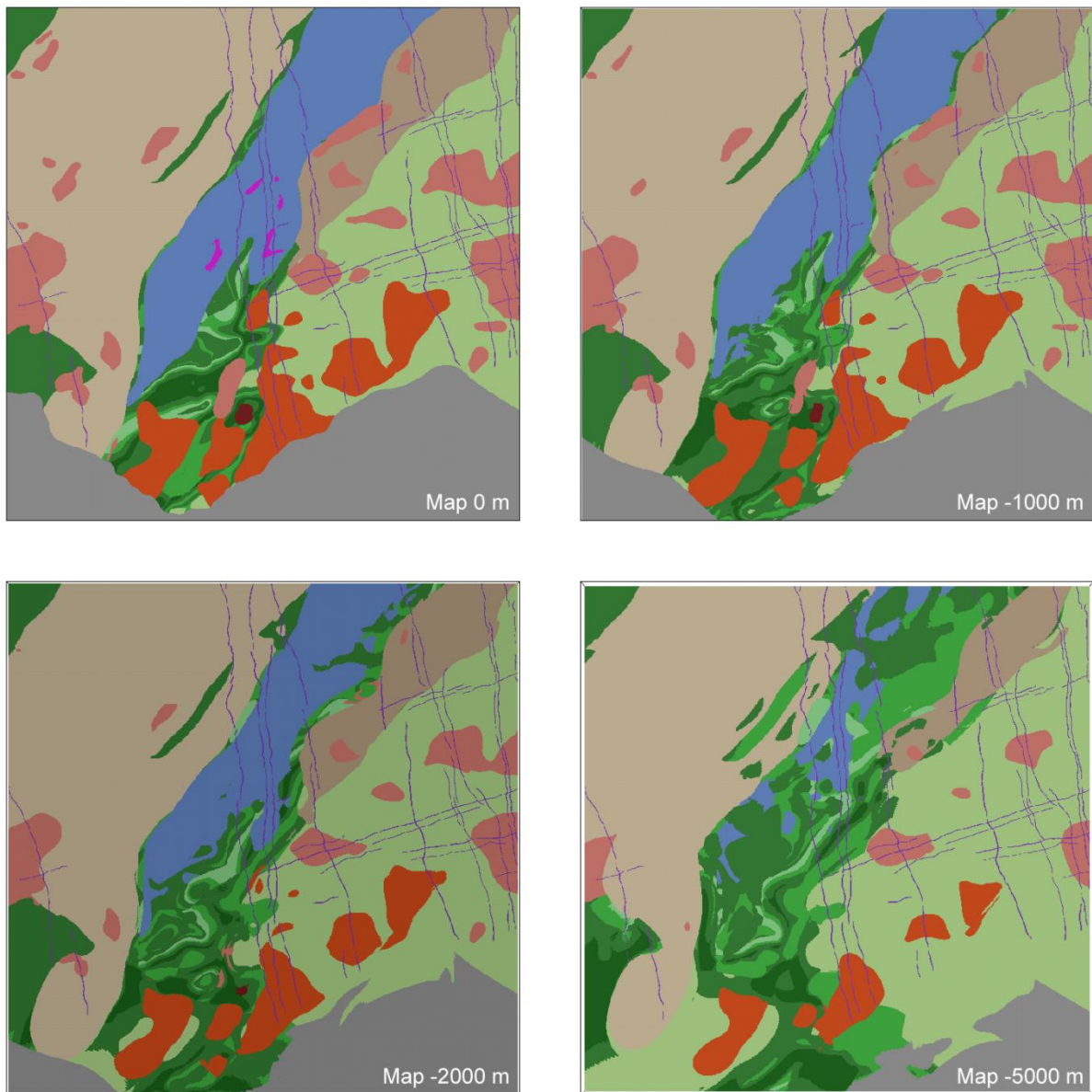
Figure IV-5   *Horizontal sections (maps) of the 3D HR model built at various depth. They show clearly the asymmetric shape of the Tarkwa basin with maximum depths reached on the northwestern part along the Ashanti fault. The geometry of the Birimian Sefwi group is constrained by bedding orientation data close to the surface and by gravity data inversions at depth.*

A) Observed Free Air Gravity   B) Calculated Free Air Gravity   C) Residual Free Air Gravity

-42   0 (mgal)   56
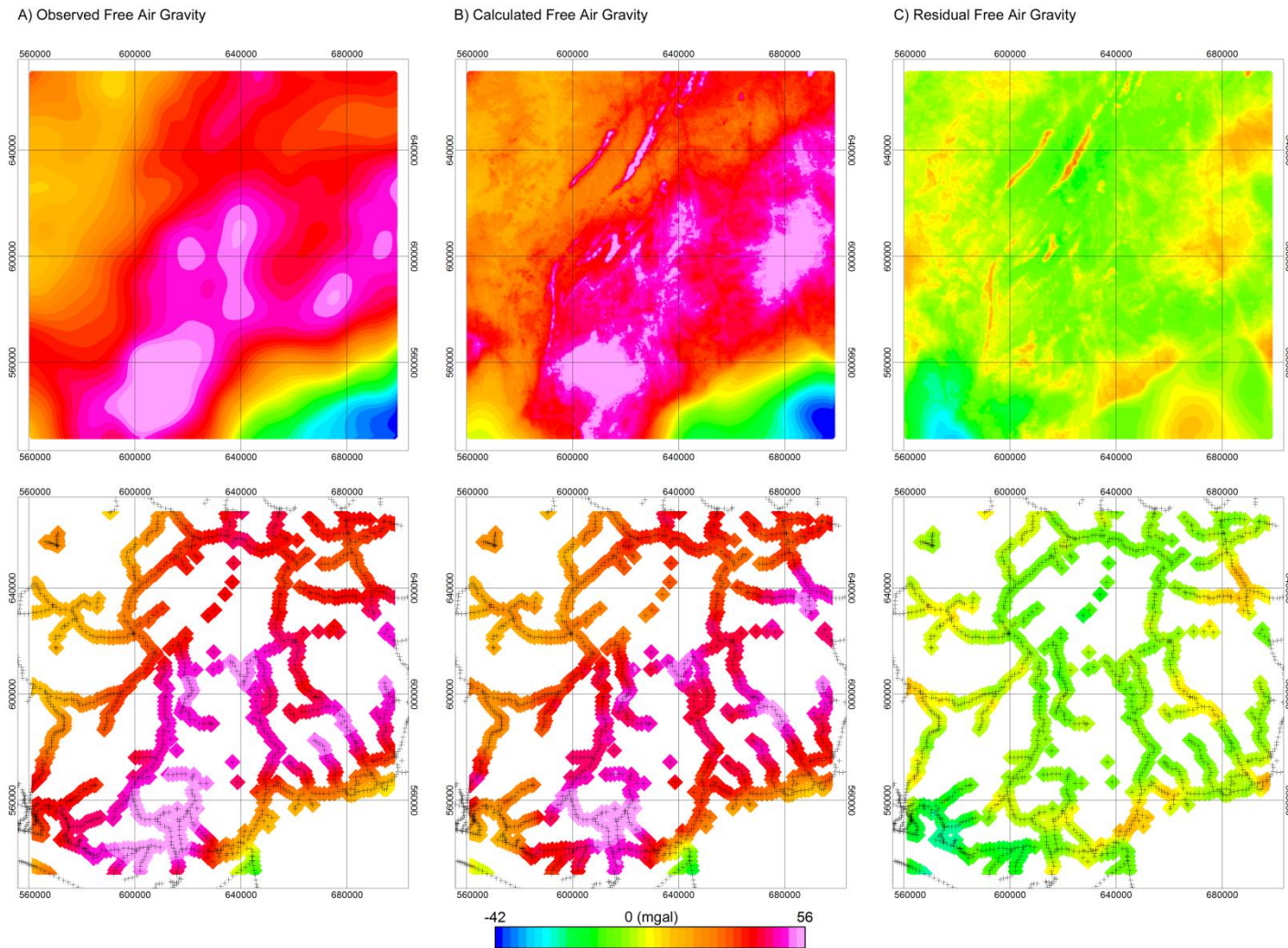
Figure IV-6   *Observed (A), Calculated (B) and Residual (C) free air gravity map calculated after inversion of the 3D HR model. Lower images represent Free Air gravity after sampling of the grids at the location of the ground gravity data point (BGI). These images show that the HR model is geophysically consistent with the gravity data.*

177
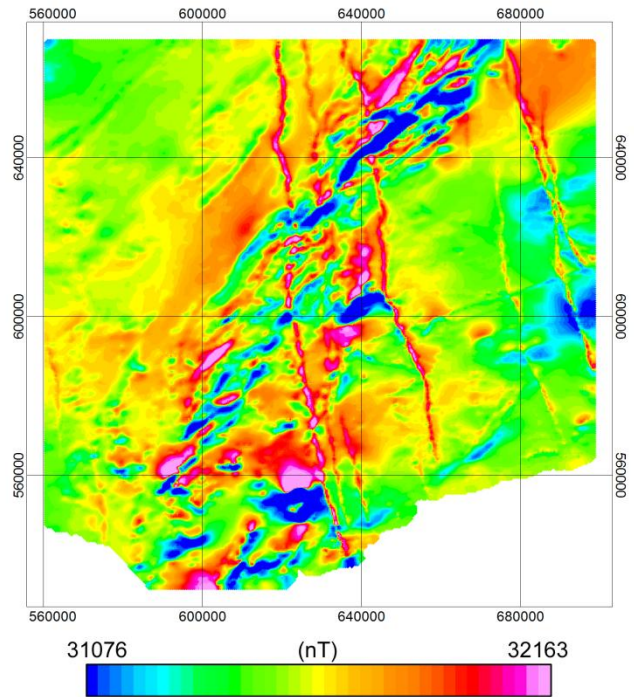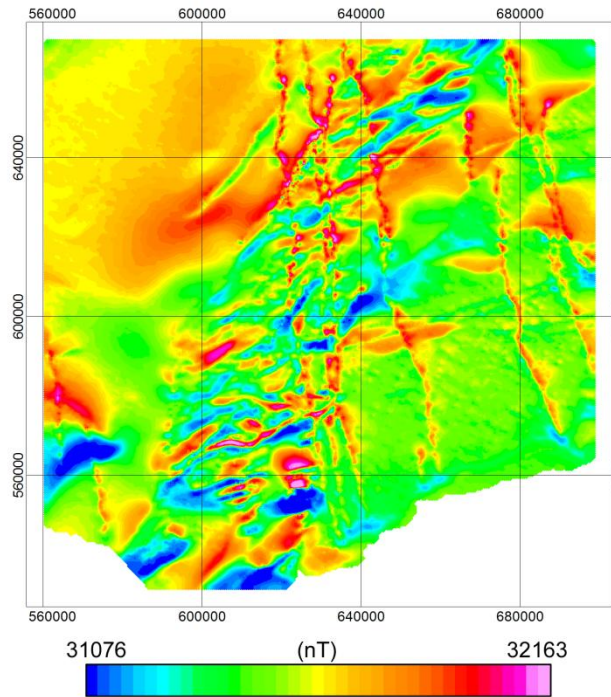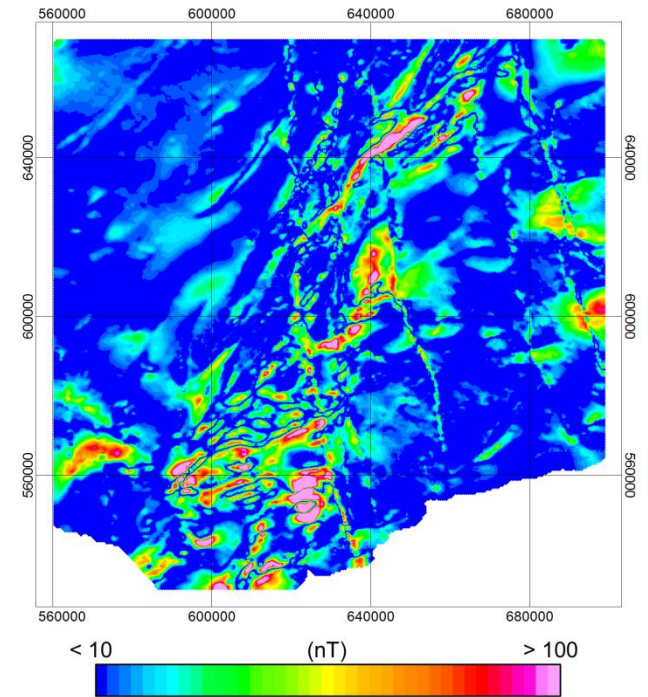
Figure IV-7   *Observed (A), Calculated (B) and Residual (C) total magnetic intensity map calculated from the 3D HR model. The absence of remanence data for the intrusive rocks (with the exception of the dolerite dykes) explains most of the difference between the observed and the calculated images. However, most of the residual anomalies represent less than 10 % (< 100 nT) of the intensity range (≈ 1000 nT).*

5.6.2 *Correlation between the gold deposit locations and the modelled lithologies*

The HR model includes all lithological details of the Sefwi Group on the southeast of the Tarkwa Basin, using the stratigraphy proposed by Perrouty et al. (2012). The fault network in this part of the belt is composed by three major interconnected strike-slip faults: the Ashanti (over 200 km long); the Benso and the Cape Three Point faults (over 50 km long). Numerous secondary faults were also developed in this highly deformed area. 21 hydrothermal gold occurrences hosted by the Sefwi Group are referenced (Griffis et al., 2002) in the southeast of the Ashanti Belt (Fig. IV-1, Fig. IV-8).

Using Gocad, we measured the shortest distance between each gold occurrence and each of the modelled surfaces, both stratigraphic contacts and the major faults, in order to characterise their spatial relationships. Over 85 % of the gold occurrence and deposits can be correlated with the presence at short distance (< 1500 m) of the modelled location of a specific metabasalt horizon which represents only 10 % by volume of the Sefwi Group (Fig. IV-8, Table IV-3). This layer (called BV1) is one of the deepest units of the Sefwi Group according to Perrouty et al. (2012) stratigraphy. Average distance between the gold occurrences and this BV1 layer is 550 m considering the 85 % of occurrences in a radius of 1500 m. This average distance increases to 1090 m considering all of the gold occurrences in the area (Table IV-4). These gold occurrences are also located at an average distance of 4300 m from one of the major regional-scale faults.

Proportion of gold deposits related to each modelled unit is shown on Fig. IV-9 and on Table IV-3. A peak (18/21) is marked for the BV1 metabasalts and the number of deposits decreases progressively for the upper layers of the stratigraphic pile. The modelled units located deeper than the BV1 metabasalts do not host any gold deposits.

Layer ID (HR model)	Main lithology (Sefwi Group)	Average thickness (m) (Perrouty et al., 2012)	Volume (km^3) (% of the Sefwi Group)	Nb (%) of gold occurrences at distance < 1500 m
12-BV6, 13-BVC5, 14-BV5, 15-BVC4	Upper Sefwi Group Layers	> 1300	44750.8 (45.6)	0 (0 %)
16-BV4	Calco-alcaline metabasalts (Axim unit)	300	5054.2 (5.1)	1 (5 %)
17-BVS	Phyllites	300	6910.8 (7.0)	3 (14 %)
18-BVC3	Metavolcanosediments	200	2468.1 (2.5)	5 (24 %)
19-BV3	Metabasalts	400	3618.7 (3.7)	6 (29 %)
20-BG	Intrusive gabbro body	700	10739.2 (10.9)	10 (48 %)
21-BV2	Tholeiitic metabasalts (Cape Three Point unit)	600	4418.7 (4.5)	11 (52 %)
22-BVC2	Metavolcanosediments	500	7830.1 (8.0)	13 (62 %)
23-BV1	Tholeiitic metabasalts (Dixcove / Butre unit)	300	9344.3 (9.5)	18 (86 %)
24-BVC1	Metavolcanosediments	200	3100.7 (3.2)	4 (19 %)
25-Basement	Micaschist, gneiss, metabasalts, metagabbros	Unknown	Unknown	5 (24 %)

Table IV-3   *Correlations between the Sefwi Group modelled geologynd the gold occurrences in the southeast of the Ashanti Belt. The BV1 layer (shaded line) represents 10 % of the volume and 7 % of the thickness of the Sefwi Group. More than 85 % of the gold occurrences are located at less than 1500 m of this BV1 layer.*
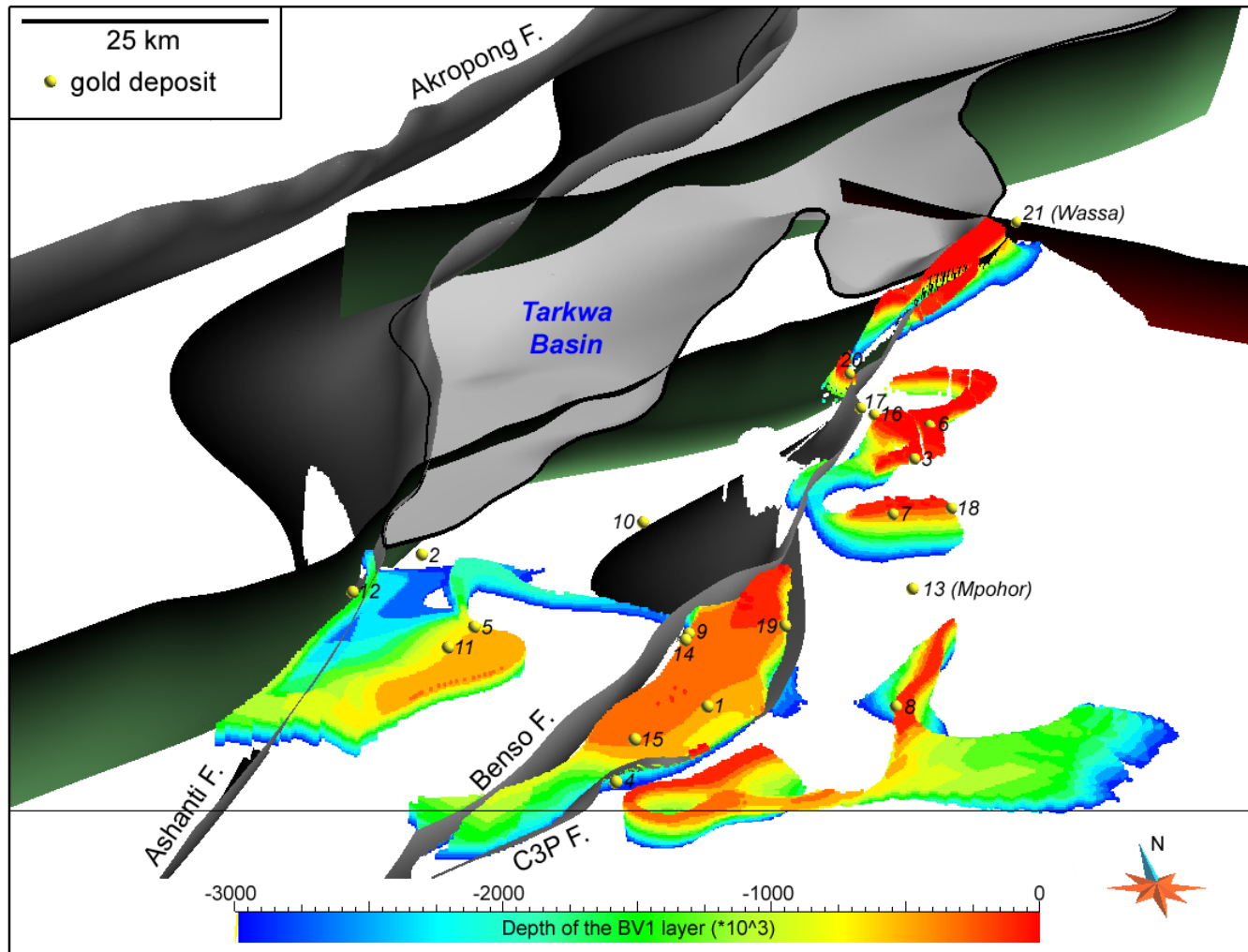
Figure IV-8   *3D view of the BV1 layer (tholeiitic metabasalts) and major faults with the location of the gold occurrence in the southeast of the Ashanti Belt. The BV1 layer is displayed down to 5000 m depth. Coordinates are in UTM (WGS 84), zone 30N. All deposits listed in Table IV-4 are located on this figure.*
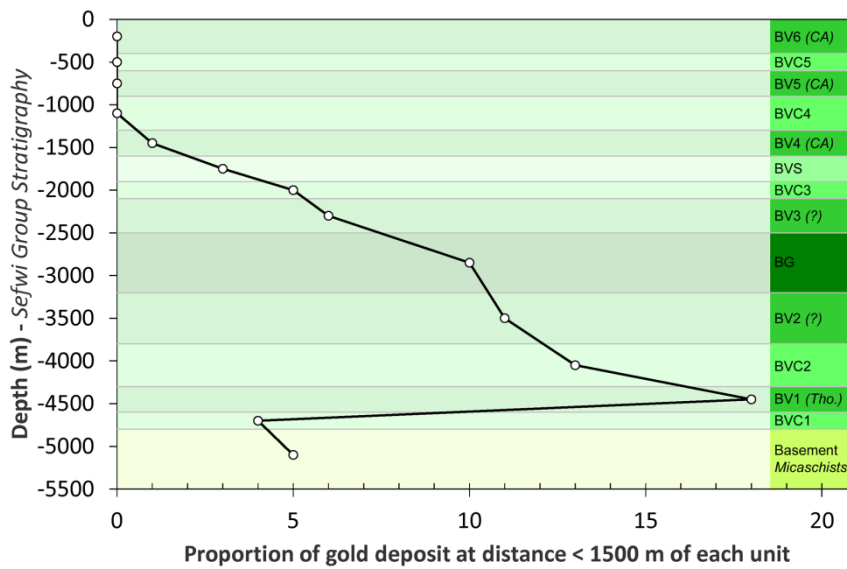
Figure IV-9   *Proportion of gold deposit at distance < 1500m from each modelled units. 18/21 gold deposits are located at short distance from the BV1 metabasalts layer. This proportion decreases progressively for the upper stratigraphic layers.*
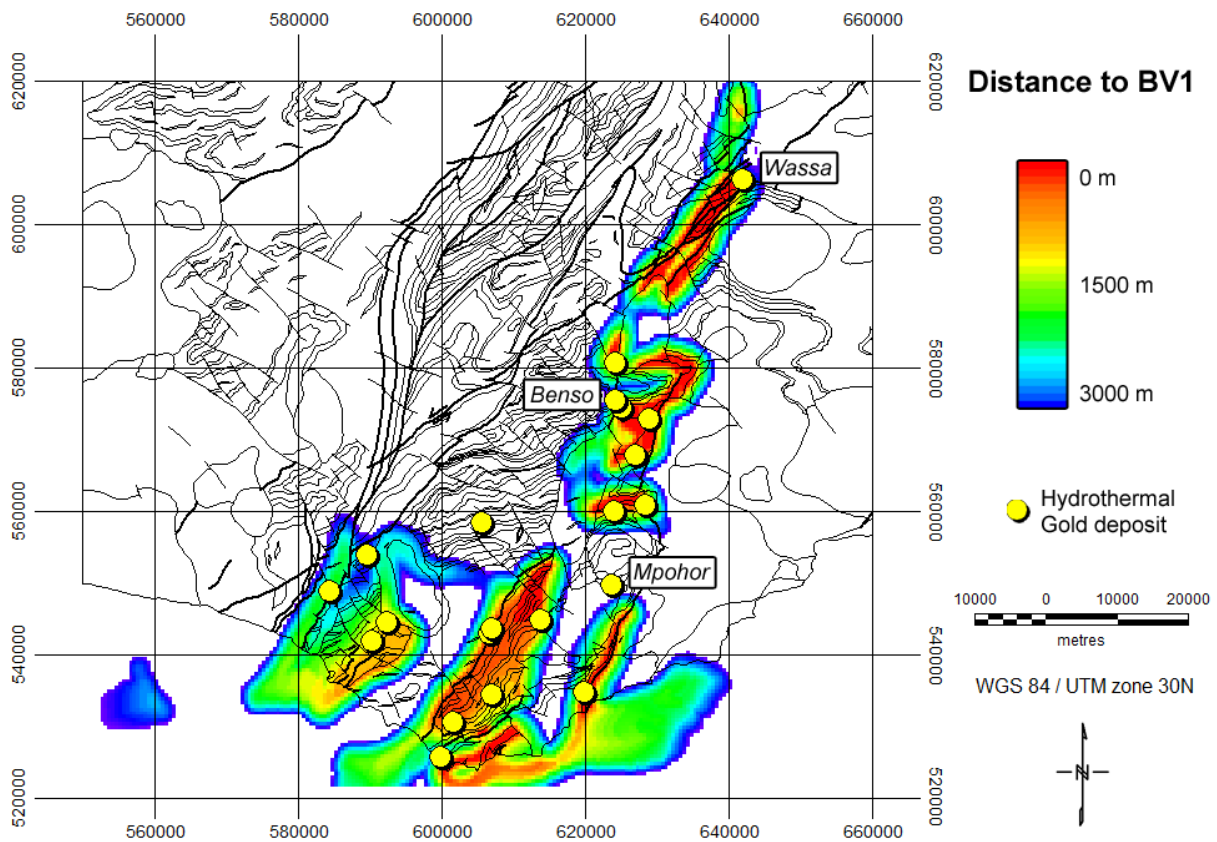
Figure IV-10 *Map of the distance between the topography and the BV1 metabasaltic layer. This distance is displayed up to 3000 m.*

	Site and Status	X	Y	Z	Distance to BV1	Unit	Host Rock	Structural data and Mineralisation (after Junner, 1935 and Griffis et al., 2002)
1	Akanoe (Old prospect)	607191	534317	142	0	BV1 / BVC2	Metavolc.	NE fault or shear zone (2 km long), high grade pyrite quartz veins (30 g/T)
2	Akoko (Asheba) (Old mine, 29000 oz)	589794	553715	19	2520	BV3	Metavolc.	NNE fault or shear zone, high grade thin quartz veins (15-30 g/T)
3	Amantin (Old prospect)	627095	567701	110	300	BVC1 / BV1	Metased. (interbed-ded metavolc.)	NNE shear zone, visible gold in quartz veins, abundant pyrite
4	Atinchin (Old artisanal mine)	599995	525463	36	1321	BG / BVC2	Metased. ?	Cape Three Point shear zone, Gold occurrence
5	Avrebo (Abredini) (Old artisanal mine)	592577	544309	19	491	BV2 / BVC2	Metavolc., Metased. (porphyry intrusions)	N-S shear zone (1 m wide), 2 sets of quartz veins : NE quartz veins, ENE carbonates quartz mineralised veins (1-25 g/t)
6	Bippo Achil (Old prospect)	629118	572680	95	0	BV1 / BVC1	Metavolc. (interbed-ded metased.)	NNE shear zone, weakly mineralised quartz veins
7	Breminsu (Krobo) (Prospect)	624153	559772	77	593	BV2	Metavolc.	N-S fault or shear zones, E-W quartz veins, soil anomaly (> 200 ppb Au)
8	Butre (Old prospect)	620000	534500	50	0	BV1	Metavolc.	ENE quartz veins, gold occurrence
9	Essuadai (Edubia) (Old artisanal mine)	607178	543531	52	0	BV1	Metavolc.	NNE fault or shear zone, thin quartz veins, soil anomaly (> 300 ppb Au)
10	Kanyankaw (Old mine, 5000 oz)	605863	558158	152	6105	BV3	Metavolc.	NNE fault or shear zone, NNE-45°W mineralised quartz veins (< 0.5 m wide)
11	Mame (Intiri Esikaim) (Old mine, 35 oz ?)	590548	541666	26	496	BV2	Metavolc.	NE ? shear zone, N-S pyrite quartz veins (en-echelon, 1-10 g/T)

Table IV-4

183

Site and Status	X	Y	Z	Distance to BV1	Unit	Host Rock	Structural data and Mineralisation (after Junner, 1935 and Griffis et al., 2002)
12 Mamponso (Old artisanal mine)	584626	548660	46	1487	Kumasi	Metased.	Ashanti shear zone, NNE pyrite arsenopyrite gold quartz veins (< 0.6 m wide, 30 g/T)
13 Mpohor (Dabokrom) (Active mine,> 1 Moz)	623786	549606	52	4288	Mpohor	Gabbro, Diorite, Granodiorite	Mpohor Mafic Complex, mineralisation related to felsic dyke intrusion
14 Satin (Old artisanal mine)	606840	567701	42	0	BV1	Metavolc.	NNE fault or shear zone (4 km long), thin quartz veins, erratic gold grade
15 Sefwi (Old prospect)	601836	530440	56	0	BV1	Metavolc.	Pyrite quartz veins (1-10 g/T)
16 Subriso East (Benso) (Active mine,> 1 koz)	625215	574250	82	304	BV2	Metavolc. (porphyry intrusions)	N-S Shear zones, pyrite and arsenopyrite along minor fractures, quartz veins (2-10 g/T)
17 Subriso West (Benso) (Active mine,> 1 koz)	624375	575266	72	1446	BG / BV3	Metavolc. Porphyry intrusions	Benso shear zone, contact metabasalt / porphyry intrusion, pyrite chlorite quartz veins, locally high grade (20-100 g/T)
18 Supome (Prospect)	628586	560702	86	349	BVC2	Metased. Granodiorite	(Faulted ?) contact between the granodiorite and the metasediments, thin quartz veins, soil anomaly (> 200 ppb Au)
19 Tetrim (Fankoba) (Artisanal mine)	614014	544646	48	370	Eoeburnean	Granodiorite Metavolc.	(Faulted ?) contact between the granodiorite and the metavolc., NNE-vertical high grade pyrite quartz veins (< 0.6 m wide, 30 g/T)
20 Wasidumi (Prospect)	624362	580441	84	4	BVC2	Metased.	Benso shear zone, mineralised quartz veins (0.9 m wide)
21 Wassa (Active mine,> 1 Moz)	642198	606065	120	0	BV1	Metavolc., Metased. (porphyry intrusions)	Km scale F4 fold, multiple mineralisation events (or remobilisation), main event and visible gold within early deformed veins

Table IV-4   *List of the 21 gold occurrences and deposits known to be hosted by the Sefwi Group in the southeast of Ashanti Belt (after Griffis et al., 2002). See Figure IV-8 for their location. Structural context and the distance to the BV1 metabasaltic layer are also shown.*

5.7 <u>Discussion</u>

5.7.1 *Depth of the Tarkwa Basin*

The geometry of the Tarkwa basin calculated by inversion indicates that the depth of the Tarkwa basin may locally be much deeper than the published estimations from field observation (Whitelaw, 1929, Junner, 1940, Kesse, 1985, Pigois 2003) which suggest depths between 2000 m and 3000 m and estimation from 2D geophysical modelling (Hasting, 1982, Barritt and Kuma, 1998) giving depths between 1500 m and 2500 m. At the location of their profiles, our 3D inversions indicate depths to the base of Tarkwa Basin are twice as deep. These authors underestimate the depth of the Tarkwaian basin by modelling a low density metasedimentary group (Lower Birimian) below high density metavolcanics (Upper Birimian), considering the old and inverse stratigraphy of the Birimian Supergroup. The constrained cross-section of Perrouty et al. (2012) also displays depth around 2500m. However their profiles are located in the southern part of the Tarkwa Basin where it is less deep according to our 3D modelling (Fig. IV-5).

5.7.2 *Possible lithostructural control on gold mineralisation*

The BV1 layer is composed by tholeiitic metabasalts from the Dixcove suite (Loh et al., 1999) that alternate with rare and thin volcanosedimentary layers. Sometime pillow-lavas were observed within this layer as on the Butre beach. The origin of the metavolcanics tholeiitic rocks in southeastern Ghana is still debate. Some authors (Sylvester and Attoh, 1992, Feybesse et al., 2006) argue that the metavolcanics results from volcanic arc accretion that precedes the Eburnean Orogeny. Other Abouchami et al. (1990) and Boher et al. (1992) suggest that most of the metavolcanics rocks derived from ancient oceanic plateau that collide during the Eburnean Orogeny. Attoh et al (2006) proposed that the metavolcanic rocks from southwest Ghana represent a fragment of an old oceanic lithosphere. Many studies (Groves, 2003) shown that metavolcanic rocks are often hosting gold deposits in Archean and in Paleoproterozoic terranes.

As shown on Table IV-4, most of the gold deposits hosted by the Sefwi Group are located within metabasaltic layers and were developed in relation with shear zones. The apparent correlation between the location of the gold occurrence and the BV1 layer suggests that both the tholeiitic BV1 metabasalt layer and the major faults have controlled the location of the gold mineralisation in the southeastern part of the Ashanti Belt. This control may consist (1) in a source of gold or (2) in a trap for mineralisations or both.

(1) The BV1 layer can be a source of gold that have been then mineralised within upper stratigraphic layers. This hypothesis help to explain the distribution of the gold deposits within the stratigraphy with a peak at short distance to the BV1 metabasalts, the absence of deposits for the lower stratigraphic layers and the progressive decreasing of the gold deposit proportion for the upper ones (Fig. IV-9) considering reasonable upward fluid transport.

(2) The BV1 layer could also be a trap for gold mineralisation. This thin (300 m) tholeiitic metabasalt layer bordered by metavolcanosediments, that are less competent, could give both a structural control on the mineralisation by developing secondary faults and a chemical control as was proposed at the Ashanti Fault contact between metabasalts and metasediments (Mumin et al, 1996). Higher proportion of gold deposit related with this BV1 layer may result from its location, close to the basement of the Sefwi Group stratigraphy (the deepest metabasaltic unit according to Perrrouty et al., 2012).

Assuming that the BV1 metabasalts effectively control the location of the gold mineralisation within the Sefwi Group, a predictive map of the distance between actual topography and the BV1 layer can be built (Fig. IV-10). Areas closer to the BV1 layer may present higher probability to host gold deposits.

5.7.3 *Limits of the Ashanti Belt 3D modelling*

The 3D models built in this study are based on regional mapping and structural measurements and geophysically constrained cross-sections (Perrouty et al., 2012). Complex geology modelling using Geomodeller is strongly limited by the software calculation process. Geomodeller software on our systems had a maximum limit to the number of nodes it could account for, and generating models with resolution above 3 million nodes was not possible. This represents a spatial resolution of 500 meters for the southern Ashanti Belt HR model with 320 nodes along X and Y axis and 30 nodes along Z axis). For this reason, Geomodeller surfaces were built in several stages and imported into Gocad to create the whole model. In addition, some details of the 3D model that were not modelled using Geomodeller were added to the HR model using Gocad such as the dolerite dykes.

The Geomodeller model generating process is an implicit system which places restrictions on the amount of data that can be sensibly used, based on the frequency content defined by the spatial resolution of the model. Particularly structural data in a given area are often simplified and only one mean orientation is kept. Bedding orientations in southwest Ghana depends on numerous folds generation and the use of mean orientation is often not the best way

to model these complex geology. It was necessary to delete some of the field data to keep bedding orientations that defines only the major structures. At the same time, the addition of artificial structural data at the border of the model was needed to force the model in some areas and to avoid unconstrained artefact bodies that don't reflect the observed geometries.

Gravity inversions of the Tarkwa Basin suggest depths that are much deeper than previous 2D modelling (Hasting, 1982, Barritt and Kuma, 1998). According to Junner (1940) the base of the Tarkwaian stratigraphy is formed by more than 300 m of conglomerates from the Kawere Group that are composed of granitoid, Birimian rock and quartz pebbles (average size around 5 cm, Hirdes and Nunoo, 1994). Density of the conglomerates bodies hasn't been measured for evident problem of sampling. It is possible that the conglomerates density could be lower or higher than the rest of the Tarkwaian units. The modelled base of the Tarkwa Basin also displays greater depths, up to 9000 m close to the Ashanti fault. More than 20% of the Tarkwa Group is below 5000 m depth after geometric inversion of the HR model. Possible Tarkwaian lithologies and density at these deep areas are unknown. Consequently, Tarkwaian depth estimations may be assumed to have error bars of ± 1000 m (15 %) assuming reasonable density ranges.

The calculated Total Magnetic Intensity map calculated displays some significant differences with the data although general overview of the image is similar (Fig. IV-7). This is mostly caused by the presence of magnetic remanence in most of the model units that are not be take into account for this modelling work (with the exception of the intense remanence values of the dolerite dyke). High to medium remanence values probably need to be considered for some of the Eburnean granitoids intrusions in the Cape Coast micaschists. Other major differences are observed in the Kumasi Basin where magnetic properties are also less constrained. These areas displays thick weathered cover and no major gold mine that limit the possibility of oriented sampling of fresh rocks, needed for remanence measurements.

5.8 Conclusion

Based on regional geological mapping (Perrouty et al., 2012), on geophysically constrained cross-section and on new mapping of Birimian geology beneath the Tarkwa Basin (Fig. IV-1), a 3D model of the southern Ashanti Belt have been build using Geomodeller and Gocad software. Multiple gravity inversions using VPmg were run to enhance the model geometry. The final model (Fig. IV-5, IV-6) shows that the Tarkwa Basin could be locally twice

as deep as the previous estimation of Junner (1940) and of Barritt and Kuma (1998). The thicknesses of the Tarkwa Group increase from the east to the west with deepest areas located close to the contact with the Ashanti fault in the northwestern part of the study area.

The 3D modelling allows us to establish a correlation between the location of gold occurrences in the southeast of the Ashanti Belt and a specific metabasaltic layer in the lower part of the Sefwi Group. The 300 m thick BV1 layer and the major faults may have determined the location of gold mineralisation as suggested by the presence of 79 % of the gold mineralisation at less than 1500 m of the layer with an average distance of 565 m. This tholeiitic metabasalt layer is probably more competent than the metavolcanosediments located on its both side. Consequently it may have preferentially controlled secondary fracturing and gold mineralisation with the major faults acting as the primary conduits of the transportation of mineralising fluids.

5.9 Résumé du chapitre IV

5.9.1 *Introduction*

Ce dernier chapitre présente un modèle tridimensionnel du sud de la ceinture d'Ashanti, réalisé de manière hybride au moyen des logiciels Geomodeller et Gocad, puis affiné par VPmg, via l'inversion des données de gravité.

La cartographie régionale (cf. chapitre I) indique une répartition des gisements d'or le long des contacts entre le bassin de Tarkwa et son socle Birimien. Il est supposé que l'ensemble de la base des métasédiments Tarkwaiens pourrait être minéralisé (cf. chapitre I), d'où l'intérêt de connaître sa géométrie. Les études précédentes montrent que le groupe de Sefwi consiste en une stratigraphie complexe et déformée le long de la phase Éburnéenne. Plusieurs sites minéralisés y sont référencés (Griffis et al., 2002). Établir des corrélations entre la localisation de ces minéralisations, les lithologies du groupe de Sefwi et les emplacements des failles majeures, via leur modélisation, représenterait une aide capitale pour de futures explorations.

5.9.2 *Contrôles sur les minéralisations Éburnéennes*

Parmi les nombreux gisements hydrothermaux du sud-ouest du Ghana, seuls ceux localisés le long de la Faille d'Ashanti furent étudiés de manière approfondie (Allibone et al., 2002A). Ces travaux montrent que des contrôles chimiques et structuraux ont permis leur formation. Les fluides minéralisateurs circulant le long des failles majeures ont réagi avec

l'encaissant métabasaltique, résultant en la précipitation de sulfures et d'or primaire (Mumin et al., 1994, 1996), qui fut remobilisé et concentré dans les fractures secondaires formées suite aux grands cisaillements D4 (Allibone et al., 2002a).

5.9.3 *Cartographie du Groupe de Sefwi sous le Bassin de Tarkwa*

Il a précédemment été montré que la cartographie géologique du Birimien sous le bassin de Tarkwa était possible, considérant une épaisseur de bassin inférieure à 3000 m pour un contraste de susceptibilité d'au moins 5 fois, en accord avec les données pétrophysiques (cf. chapitre I). Basée sur les données magnétiques aéroportées, après traitements pour faire apparaître les structures profondes, de grande longueur d'onde, une carte de ces lithologies enfouies a été réalisée afin d'apporter des informations complémentaires utiles à la modélisation du groupe de Sefwi.

5.9.4 *Données géophysiques*

Des données de gravité (fournies par le Bureau Gravimétrique International) et des données aéromagnétiques (acquises pour le Service Géologique du Ghana) furent utilisées lors de cette étude pour la cartographie et les inversions des modèles.

5.9.5 *Modélisation*

La modélisation s'est effectuée en plusieurs étapes, via les logiciels Geomodeller, Gocad et VPmg. La méthodologie utilisée par ces logiciels est décrite par Lajaunie et al. (1997) et Calcagno et al. (2008) pour Geomodeller, Mallet (1992) pour Gocad et Fullagar (2000, 2008) pour VPmg.

Le modèle 3D du sud de la ceinture d'Ashanti fut réalisé en plusieurs étapes. Dans un premier temps, un modèle basse résolution (LR 1000 m par voxel), formé des principaux groupes stratigraphiques et des granitoïdes a été construit, puis inversé au moyen des données de gravité, afin d'obtenir une approximation de la forme de la base du bassin de Tarkwa. Dans un second temps, la nouvelle carte du Birimien fut projetée sur cette surface basale (à l'exception des parties à plus de 3000 m de profondeur), puis importée dans Geomodeller, pour être ajoutée aux autres données géologiques et structurales. Les interfaces générées entre unités géologiques furent exportées vers Gocad, et complétées par l'ajout des dykes de dolérites, afin de construire un nouveau modèle 3D haute résolution (HR, 200 m par voxel), intégrant la stratigraphie détaillée du groupe de Sefwi. La géométrie de ce modèle HR fut finalement améliorée par inversion des données de gravité, sous VPmg.

5.9.6 Résultats

La surface calculée de la base du bassin de Tarkwa affiche un profil asymétrique avec de fortes profondeurs à proximité du contact avec la Faille d'Ashanti et de faibles profondeurs sur sa partie est. Le secteur nord du Bassin est aussi plus profond que la partie sud, comme cela est aussi suggéré par les observations de terrain et la stratigraphie (Junner, 1940). La profondeur moyenne du bassin est autour de 3400 m, soit près de deux fois plus profond que les hypothèses des études antérieures (Hasting, 1982 ; Barritt et Kuma, 1998).

La modélisation 3D souligne un possible contrôle lithostructural sur la localisation des minéralisations en or dans le groupe de Sefwi, au sud-est de la Ceinture d'Ashanti : 85 % des minéralisations en or dans ce secteur sont localisés à moins de 1500 m (moyenne de 550 m) d'une des couches modélisées. Celle-ci se compose de métabasaltes tholéiitiques sur une épaisseur d'environ 300 m et ne représente que 10 % du volume modélisé du groupe de Sefwi. Chacun de ces sites minéralisés se situe à proximité (moyenne de 4 km) de l'une des trois failles majeures (de plus de 50 km long) mises en évidence par la cartographie. Il est proposé que ce fin niveau de métabasaltes, plus compétent que les métasédiments environnants, pourrait avoir contrôlé la formation d'une fracturation secondaire pendant la déformation et, ainsi, la formation de minéralisations en or à faible distance des failles majeures, le long desquelles les fluides furent transportés.

5.9.7 Limites de la modélisation

Les données géologiques et structurales collectées à l'échelle régionale ainsi que les cartes et coupes réalisées (cf. chapitre I) furent utilisées pour la modélisation avec Geomodeller. Cependant, les processus de calculs utilisés par ce logiciel ne permettent pas la prise en compte de l'intégralité des données (notamment les mesures structurales autres que celles relatives au litage S0) et limitent la résolution des modèles générés. Pour s'affranchir du problème de résolution, les interfaces entres unités modélisées furent générées séparément et ensuite assemblées avec Gocad.

L'inversion VPmg des données de gravité suggère que le bassin de Tarkwa est localement plus profond que ce qui était préalablement estimé. Les lithologies Tarkwaiennes profondes et leur densité sont inconnues, ce qui entraine une incertitude de l'ordre de 1000 m (15 %) sur la profondeur maximale du bassin, si l'on considère une gamme de densités raisonnables pour des métasédiments.

Bien que la signature magnétique du modèle ait pu être calculée, l'inversion VPmg des données magnétiques n'a pas été possible, suite à l'absence d'information sur les propriétés de rémanence des roches intrusives et en raison de temps de calculs par itération trop élevés.

Conclusions et Perspectives

Conclusions

Malgré de nombreuses précédentes études de la géologie sud-ouest du Ghana, certains aspects de l'évolution Paléoprotérozoïque de la ceinture minéralisée d'Ashanti demeuraient obscurs, en dépit de leur importance fondamentale pour la compréhension de la genèse des gisements aurifères de cette région. Notamment, les déformations antérieures au bassin de Tarkwa, et les possibles gisements d'or qui leur sont associés, ne furent jamais caractérisées par les études antérieures, bien qu'ils fussent mentionnés par plusieurs auteurs comme éventuelle source de l'or des placers Tarkwaiens.

Au cours de ce travail, il a été montré que l'Orogénèse Éburnéenne telle que décrite par Bonhomme (1962) ne se limite pas à une simple phase orogénique s'étendant sur près de 200 Ma mais peut être subdivisée en deux phases, Éoéburnéenne et Éburnéenne (De Kock et al., 2011). L'étude structurale du sud de la ceinture d'Ashanti a mis en évidence 6 événements de déformation distincts, via les observations de terrains et l'interprétation des données géophysiques : aéromagnétiques, aéroradiométriques, gravité et radar. La première phase de déformation identifiée (D1) s'est produite avant la formation des bassins Birimiens de Kumasi et Akyem. Caractérisée par un raccourcissement N-S, elle développa des plis d'échelle kilométrique dans le groupe de Sefwi (Adadey et al, 2009). Ce groupe principalement composé de roches métavolcaniques Birimiennes, a ensuite été partiellement recouvert par le groupe de Kumasi pendant la phase d'extension D2 et par le bassin de Tarkwa, formé au début du raccourcissement D3 (NW-SE). La formation de ces bassins fut contrôlée par les failles majeures telle la Faille d'Ashanti. Suite à la réinterprétations des âges des zircons détritiques du bassin de Tarkwa (Pigois et al., 2003), l'âge de celui-ci a été précisé à 2107 – 2097 Ma. L'étude de terrain a également permis une redéfinition de la stratigraphie du Groupe de Sefwi, mettant en évidence une alternance des niveaux de métabasaltes et de métavolcanosédiments.

À une échelle plus locale, l'analyse des déformations et des minéralisations à la mine de Wassa indique que ces événements de déformation régionaux sont associés à plusieurs événements hydrothermaux majeurs caractérisés par la formation de veines à quartz et la précipitation d'arséniosulfures, de sulfures et d'or dans les roches hôtes. La principale phase de minéralisation à la mine de Wassa se développa au début de la déformation D1 (Éoéburnéenne). L'étude de terrain ainsi que la répartition des concentrations en or montrent que les minéralisations se répartissent majoritairement le long des plis isoclinaux F1, avec lesquels elles

sont associées. De par leur précocité, les gisements de type Wassa, formés dans le groupe de Sefwi puis érodés, pourraient avoir fourni l'or contenu dans les placers du bassin de Tarkwa. Les phases suivantes de minéralisation, d'âge Éburnéen, furent largement étudiées par le passé (Allibone et al., 2002a). Certaines sont régionalement contrôlées par les zones de cisaillements majeurs comme la Faille d'Ashanti, le long desquelles elles sont mises en place durant la déformation D4 (Mines de Prestea, Bogoso, Obuasi, etc.). D'autres sont reliées à des déformations tardives (D5-D6) comme à la mine de Damang (Tunks et al., 2004). À la mine de Wassa, ces minéralisations Éburnéennes, bien qu'observées, ne présentent que des concentrations mineures en or et résultent d'une remobilisation de la minéralisation Éoéburnéenne.

Les phases Éoéburnéenne et Éburnéenne précédemment mentionnées sont toutes deux associées à un magmatisme intense au sud-ouest du Ghana. Les campagnes de terrain ont permis un échantillonnage précis des différents plutons, datés par de précédentes études, pour analyses géochimiques des éléments majeurs et traces. Les TTGs Éoéburnéens sont caractérisés par un important enrichissement en terres rares légères (LREE) et par des spectres plats pour les terres rares lourdes (HREE). Les anomalies positives en Ba et négatives en Ta, Nb et Th observées à la fois pour ces TTGs et pour les roches volcaniques contemporaines suggèrent un magmatisme calco-alcalin de zone de subduction (Wilson, 1989). Les intrusions de granodiorites et de granites Éburnéens montrent un appauvrissement en éléments lourds (HREE) et des rapports Sr/Y élevés, typiques des magmas adakitiques et des TTGs archéens (Martin, 1999). Cette géochimie indique la présence de grenat dans les roches sources de ces granitoïdes. La modélisation thermodynamique de la formation de grenats dans une croûte de composition Éoéburnéenne montre que ceux-ci apparaissent avant le franchissement du solidus, quelle que soit la lithologie, si l'on considère un gradient géothermique raisonnable de 25°/km. Ainsi, il a été montré que la fusion partielle des roches métamafiques et des TTGs Éoéburnéens en base de croûte pouvait produire des magmas de composition similaire à celle des granitoïdes Éburnéen, avec un héritage de la signature géochimique de subduction.

Pour terminer cette étude, l'ensemble des données collectées au cours des campagnes de terrain a permis la réalisation d'un modèle tridimensionnel du sud de la ceinture d'Ashanti, et, plus particulièrement, du groupe de Sefwi. Ce modèle 3D, basé sur la cartographie géologique et structurale régionale (Perrouty et al., 2012), sur l'interprétation de structures Birimiennes enfouies sous le bassin de Tarkwa et sur des coupes géologiques en accord avec les données de géophysique, a été réalisé via l'utilisation des logiciels de modélisation Geomodeller et Gocad et d'inversion VPmg. La modélisation du bassin de Tarkwa, dont la base serait entièrement

minéralisée, montre qu'il pourrait être localement près de deux fois plus profond que cela ne fut estimé par les études stratigraphiques de Junner (1940). En ce qui concerne le groupe de Sefwi, la modélisation suggère une possible corrélation entre la localisation des gisements d'or au sud-est de la ceinture d'Ashanti et une unité de métabasaltes tholéiitiques, avec 85 % des sites minéralisés localisés à moins de 1500 m de cette couche, pour une distance moyenne de 550 m. Ce niveau de métabasaltes de 300 m d'épaisseur, plus compétent que les métavolcanosédiments situés de part et d'autre, aurait pu contrôler la formation de fracturation secondaire et la formation des minéralisations à partir des fluides transportés le long des failles majeures.

Perspectives

L'analyse structurale ainsi que l'identification des phases de magmatisme au sud-ouest du Ghana a permis de répondre à de nombreuses questions concernant l'évolution Paléoprotérozoïque de la ceinture d'Ashanti. Dans un même temps, cette étude a mis en évidence d'autres points à éclaircir pour une compréhension plus globale de la géotectonique précambrienne du craton d'Afrique de l'Ouest.

Ainsi, si l'évolution du magmatisme illustre de possibles mécanismes de construction de la croûte continentale, les interprétations de cette étude restent limitées au sud-ouest du Ghana. Étendre l'analyse géochimique des granitoïdes à la partie Paléoprotérozoïque du Ghana, puis à l'ensemble du craton d'Afrique de l'Ouest permettrait de vérifier si ces interprétations locales s'appliquent également à grande échelle, avec de nouvelles implications pour la genèse des croûtes continentales Précambriennes.

Un autre point intéressant à élucider concerne la couche de métabasaltes tholéiitiques, dans le groupe de Sefwi, dont le possible lien avec la localisation des minéralisations a été mis en évidence par la modélisation 3D. Une étude plus approfondie de cette unité, via sa cartographie précise et son échantillonnage, confirmerait ou infirmerait son contrôle sur les minéralisations de cette région. La compréhension des relations structurales (et chimiques) entre ce niveau de métabasaltes, les failles majeures et les minéralisations, fournirait une piste intéressante pour de futures explorations.

Parallèlement à cette étude, un échantillonnage des différentes lithologies à l'affleurement a été réalisé afin d'apporter de nouvelles informations sur l'évolution du métamorphisme régional durant la phase Éburnéenne. Les assemblages chlorites / micas blancs suggèrent des conditions maximales de pressions de l'ordre de 5 kbar pour l'ensemble des échantillons analysés (cf. annexe 2). Les assemblages staurotide / grenat indiquent des conditions de pression similaires mais des températures plus élevées. Ces valeurs sont en accord avec les précédentes études métamorphiques (Schmidt Mumm et al., 1997 ; John et al., 1999). En conséquence, il semblerait que le pic de pression soit uniforme sur l'ensemble de la région, avec de locales variations de température suite aux intrusions de granitoïdes Éburnéens. Ceci implique l'absence de mouvement vertical significatif le long des failles (supérieur à 1.5 km, soit 0.5 kbar d'incertitude sur les analyses) après le maximum de métamorphisme (à 2092 ± 3 Ma selon Oberthur et al. 1998). Les données d'inclusions fluides indiquent des conditions

d'homogénéisation autour de 200°C, 2 kbar lors des minéralisations de Damang (Schmidt Mumm et al., 1997), datées autour de 2063 ± 9 Ma (Pigois et al., 2003). Il semblerait donc que l'ensemble du sud-ouest Ghana se soit soulevé de manière homogène d'environ 10 à 12 km (3 kbar) en 30 Ma, puis très peu au cours des 2 milliards d'années suivantes. Ces premiers résultats de l'étude métamorphique suggèrent que les déformations Éburnéennes du Ghana sont principalement exprimées par des grandes zones de cisaillements (e.g. Ashanti Fault) avec des mouvements verticaux réduits.

Références

Références

Abouchami, W., Boher, M., Michard, A., Albarède, F., 1990, "A major 2.1 Ga event of mafic magmatism in West Africa, an early stage of crustal accretion", Journal of Geophysical Research, B, Solid Earth and Planets, 95, 17605-17629

Adadey, K., Clarke, B., Théveniaut, H., Urien, P., Delor, C., Roig, J.Y., Feybesse, J.L., 2009, Geological map explanation - Map sheet 0503 B (1:100 000), CGS/BRGM/Geoman, Geological Survey Department of Ghana (GSD). No MSSP/2005/GSD/5a

Agyei Duodu, J., Loh, G.K., Boamah, K.O., Baba, M., Hirdes, W., Toloczyki, M., Davis, D.W., 2009, Geological Map of Ghana 1:1,000,000, Geological Survey of Ghana, Map 1:1M

Allibone, A., MacCuaig, T.C., Harris, D., Etheridge, M., Munroe, S., Byrne, D., 2002, Structural Controls on Gold Mineralization at the Ashanti Gold Deposit, Obuasi, Ghana, Society of Economic Geologists, Special Publication, 9, 65-93

Allibone, A., Teasdale, J., Cameron, G., Etheridge, M., Uttley, P., Soboh, A., Appiah-Kubi, J., Adanu, A., Arthur, R., Mamphey, J., Odoom, B., Zuta, J., Tsikata, A., Pataye, F., Famiyeh, S., Lamb, E., 2002, Timing and Structural Controls on Gold Mineralization at the Bogoso Gold Mine, Ghana, West Africa, Economic Geology, 97, 949-969

ALS Minerals, 2006a, ME-ICP06 and OA-GRA05 Analysis of Major Oxides by ICP- AES Method, www.alsglobal.com, 2p.

ALS Minerals, 2006b, MEMS41 Aqua Regia ICP AES ICPMS Multielement Method, www.alsglobal.com, 2p.

ALS Minerals, 2009, ME-MS81 Lithium Metaborate fusion-ICP-MS Multi-element Method, www.alsglobal.com, 3p.

Asiedu, D.K., Dampare, S.B., Asamoah Sakyi, P., Banoeng-Yakubo, B., Osae, S., Nyarko, B.J.B., Manu, J., 2004, Geochemistry of Paleoproterozoic metasedimentary rocks from the Birim diamondiferous field, southern Ghana: Implications for provenance and crustal evolution at the Archean-Proterozoic boundary, Geochemical Journal, 38, 215-228

Asiedu, D.K., Kutu, J.M., Manu, J., Hayford, E.K., 2009, Geochemistry and provenance of metagreywackes from the Konongo Area, Southwestern Ghana, African Journal of Science and Technology (AJST), Science and Engineering Series, 10 (1), 37-44

Attoh, K., Corfu, F., Nudec, P.M., 2007, U-Pb zircon age of deformed carbonatite and alkaline rocks in the Pan-African Dahomeyide suture zone, West Africa, Precambrian Research, 155, 251-260

Attoh, K., Dallmeyer, R.D., Affaton, P., 1997, Chronology of nappe assembly in the Pan-African Dahomeyide orogen: evidence from 40Ar/39Ar mineral ages, Precambrian Research, 82, 153-171

Attoh, K., Evans, M.J., Bickford, M.E., 2006, Geochemistry of an ultramafic-rodingite rock association in the Paleoproterozoic Dixcove greenstone belt, southwestern Ghana, Journal of African Earth Sciences, 45, 333-346

Baer, P., Riegel, W., 1980, Les microflores des séries Paléozoiques du Ghana (Afrique occidentale) et leurs relations paléofloristiques, Bulletin Sciences Géologiques, 27, 39-58

Baratoux, L., Metelka, V., Naba, S., Jessell, M.W., Gregoire, M., Ganne, J., 2011, Juvenile Paleoproterozoic crust evolution during the Eburnean orogeny (?2.2–2.0 Ga), western Burkina Faso, Precambrian Research, 191, 18-45

Barker, F., Arth, J.G., 1979, Generation of trondhjemitic-tonalitic liquids and Archean bimodal trondhjemite-basalt suites, Geology, 4, 596-600

Barritt, S.D., Kuma, J.S., 1998, Constrained gravity models and structural evolution of the Ashanti Belt, southwest Ghana, Journal of African Earth Sciences, 26 (4), 539-550

Batchelor, R.A., Bowden, P., 1985, Petrogenetic Interpretation of Granitoid Rock Series Using Multicationic Parameters, Chemical Geology, 48, 43-55

Bermúdez-Lugo, O., 2008, The Mineral Industry of Ghana, Mineral Yearbook, 2006, U.S. Geological Survey, 5 p.

Blenkinsop, T.G., Schmidt Mumm, A., Kumi, R., Sangmor, S., 1994, Structural Geology of the Ashanti Gold Mine, Geologisches Jahrbuch, D 100, 131-153

Boher, M., Abouchami, W., Michard, A., Albarède, F., Arndt, N.T., 1992, Crustal growth in West Africa at 2.1 Ga, Journal of Geophysical Research, B, Solid Earth and Planets, 97, 345-369

Bonhomme, M., 1962, Contribution à l'étude géochronologique de la plate-forme de l'Ouest Africain, Annales de la Faculté des Sciences, Université de Clermont-Ferrand, Géologie, Minéralogie, 5, 62 p.

Bourassa, Y., 2003, Wassa Geology Report, Golden Star Resources Ltd, 34p.

Bourman, R.P., 1993, Perennial problems in the study of laterite: A review, Australian Journal of Earth Sciences, 40, 387-401

Bowell, R.J., Foster, R.P., Stanley, C.J., 1990, Telluride mineralization at Ashanti gold mine, Ghana, Mineralogical Magazine, 54, 617-627

Buah, F.K., 1998, A History of Ghana, Revised and Updated, MacMillan Education, Oxford, 259 p.

Caen-Vachette, M., Vialette, Y., Bassot, J.P., Vidal, P., 1988, Apport de la géochronologie isotopique à la connaissance de la géologie gabonaise, Chronique Recherche Minière, 491, 35-54.

Calcagno, P., Chilès, J.P., Courrioux, G., Guillen, A., 2008, Geological modelling from field data and geological knowledge, Part I – Modelling method coupling 3D potential-field interpolation and geological rules, Physics of the Earth and Planetary Interiors, 171, 147-157

Chaloner, W.G., Mensah, M.K., Crane, M.D., 1974, Non-vascular land plants from the Devonian of Ghana, Palaeontology, 17 (4), 925–947

Chatterjee, N. D., Froese, E. , 1975, A thermodynamic study of the pseudobinary join muscovite-paragonite in the system KAlSi3O8-NaAlSi3O8-Al2O3-SiO2-H2O, American Mineralogist, 60, 985-993

Chung, S.L., Liu, D., Ji, J., Chu, M.F., Lee, H.Y., Wen, D.J., Lo, C.H., Lee, T.Y., Qian, Q., Zhang, Q., 2003, Adakites from continental collision zones: Melting of thickened lower crust beneath southern Tibet, Geology, 31 (11), 1021-1024

Clark, D.A., 1997, Magnetic petrophysics and magnetic petrology: aids to geological interpretation of magnetic surveys, AGSO Journal of Australian Geology & Geophysics, 17 (2), 83-103

Condie, K.C., 1993, Chemical composition and evolution of the upper continental crust: contrasting results from surface samples and shales, Chememical Geology, 104, 1-37

205

Condie, K.C., 2005, High field strength element ratios in Archean basalts: a window to evolving sources of mantle plumes, Lithos, 79, 491-504

Connolly, J.A.D., 2005, Computation of phase equilibria by linear programming. A tool for geodynamic modeling and its application to subduction zone decarbonation, Earth and Planetary Science Letters, 236, 524-541.

Connolly, J.A.D., 2009, The geodynamic equation of state: what and how, Geochemistry, Geophysics, Geosystems, 10, Q10014

Connolly, J.A.D., Kerrick, D.M., 1987, An algorithm and computer program for calculating composition phase diagrams, CALPHAD, 11, 1-55

Crow, A.T., 1952, The rocks of the Sekondi Series of the Gold Coast, Gold Coast Geological Survey, Bulletin, 18, 68 p.

Dampare, S., Shibata, T., Asiedu, D., Osae, H., 2005, Major-element geochemistry of Proterozoic Prince's Town granitoid from the southern Ashanti volcanic belt, Ghana, Earth Science Report, 12, 15-30

Dampare, S.B., Shibata, T., Asiedu, D.K., Osae, S., Banoeng-Yakubo, B., 2008, Geochemistry of Paleoproterozoic metavolcanic rocks from the southern Ashanti volcanic belt, Ghana: Petrogenetic and tectonic setting implications, Precambrian Research, 162, 403-423

Davis, D.W., Hirdes, W., Schaltegger, U., Nunoo, E.A., 1994, U-Pb age constraints on deposition and provenance of Birimian and gold-bearing Tarkwaian sediments in Ghana, West Africa, Precambrian Research, 67, 89-107

De Kock, G.S., Armstrong, R.A., Siegfried, H.P., Thomas, E., 2011, Geochronology of the Birim Supergroup of the West African craton in the Wa-Bolé region of west-central Ghana: Implications for the stratigraphic framework, Journal of African Earth Sciences, 59, 1-40

Dickson, B.L., Scott, K.M., 1997, Interpretation of aerial gamma-ray surveys - adding the geochemical factors, AGSO Journal of Australian Geology & Geophysics, 17 (2), 187-200

Duchesne, J.C., 1999, Fe-Ti deposits in Rogaland anorthosites (South Norway): geochemical characteristics and problems of interpretation, Mineralium Deposita, 34, 182-198

Eisenlohr, B.N., 1992, Conflicting evidence on the timing of mesothermal and paleoplacer gold mineralisation in early Proterozoic rocks from southwest Ghana, West Africa, Mineralium Deposita, 27, 23-29

Eisenlohr, B.N., Hirdes, W., 1992, The structural development of the early Proterozoic Birimian and Tarkwaian rocks of southwest Ghana, West Africa, Journal of African Earth Sciences, 14 (3), 313-325

Ennih, N., Liégeois, J.-P, 2008, The boundaries of the West African craton, with special reference to the basement of the Moroccan metacratonic Anti-Atlas belt, In: Ennih, N., Liégeois, J.-P. (Eds.), The Boundaries of the West African Craton, Special Publications, Geological Society, London, 297, 1-17.

Eriksson, K.A., Krapez, B., Fralick, P.W., 1994, "Sedimentology of Archean greenstone belts, signatures of tectonic evolution", Earth-Science Reviews, 37, 1-88

Feybesse, JL., Billa, M., Guerrot, C., Duguey, E., Lescuyer, JL., Milési, JP., Bouchot, V., 2006, The paleoproterozoic Ghanaian province: Geodynamic model and ore controls, including regional stress modeling, Precambrian Research, 149, 149-196

FUGRO Logistics Report, 2004, Helicopter Borne Magnetic Horizontal Gradient (MIDAS™) And Radiometric Geophysical Survey over the Wassa Project Area, Damang, Ghana, Golden Star Resources Ltd, 89 p.

Fullagar, P.K., Hughes, N.A., Paine, J., 2000, Drilling constrained 3D gravity inversion, Exploration Geophysics, 31, 17-23

Fullagar, P.K., Pears, G., MacMonnies, B., 2008, Constrained inversion of geologic surfaces - pushing the boundaries, The Leading Edge, 27 (1), 98-105

Fullea, J., Fernandez, M., Zeyen, H., 2008, FA2BOUG - A FORTRAN 90 code to compute Bouguer gravity anomalies from gridded free-air anomalies: Application to the Atlantic-Mediterranean transition zone, Computers & Geosciences, 34 (12), 1665-1681

Ganne, J., De Andrade, V., Weinberg, R., Vidal, O., Dubacq, B., Kagambega, N., Naba, S., Baratoux, L., Jessell, M.W., Allibon J., 2011, Modern-style plate subduction preserved in the PalaeoproterozoicWest African craton, Nature Geoscience, 5, 60-65

Grenholm, M., 2011, Petrology of Birimian granitoids in southern Ghana - petrography and petrogenesis, Bachelor thesis, Lund University, 41 p.

Griffis, R.J., Barning, K., Agezo, F.L., Akosah, F.K., 2002, Gold Deposits of Ghana, Minerals Commission, Accra, Ghana, 438 p

Groves, D.I. , Goldfarb, R.J. , Robert, F., Hart, C.J.R., 2003, Gold Deposits in Metamorphic Belts: Overview of Current Understanding, Outstanding Problems, Future Research, and Exploration Significance, Economic Geology, 98, 1-29

Gunn, P.J., Maidment, D., Milligan, P.R., 1997, Interpreting aeromagnetic data in areas of limited outcrop, AGSO Journal of Australian Geology & Geophysics, 17 (2), 175-185

Hastings, D.A., 1978, The southwest Ghana gravity survey, with West African regional correlations and implications, Ghana Geological Survey, Unpublished Report, 202 p.

Hastings, D.A., 1982, On the tectonics and metallogenesis of West Africa: A model incorporating new geophysical data, Geoexploration, 20, 295-327

Hein, K.A.A., 2010, Succession of structural events in the Goren greenstone belt (Burkina Faso): Implications for West African tectonics, Journal of African Earth Sciences, 86, 77-89

Hilson, G., 2002, Harvesting mineral riches: 1000 years of gold mining in Ghana, Resources Policy, 28, 13-26

Hirdes, W., Davis, D.W., 1998, First U-Pb zircon age of extrusive volcanism in the Birimian Supergroup of Ghana/West Africa, Journal of African Earth Sciences, 27 (2), 291-294

Hirdes, W., Davis, D.W., Eisenlohr, B.N., 1992, Reassessment of Proterozoic granitoid ages in Ghana on the basis of U/Pb zircon and monazite dating, Precambrian Research, 56, 89-96

Hirdes, W., Nunoo, B., 1994, The Proterozoic Paleoplacers at Tarkwa Gold Mine, SW Ghana: Sedimentology, Mineralogy, and Precise Age Dating of the Main Reef and West Reef, and Bearing of the Investigations on Source Area Aspects, Geologisches Jahrbuch, D 100, 247-311

Holland, T., Baker, J., Powell, R., 1998, Mixing properties and activity–composition relationships of chlorites in the system $MgO–FeO–Al_2O_3–SiO_2–H_2O$, European Journal of Mineralogy, 10, 395-406

Holland, T., Powell, R, 1996, Thermodynamics of order-disorder in minerals. 2. Symmetric formalism applied to solid solutions, American Mineralogist, 81, 1425-1437

Holland, T., Powell, R., 2001, Calculation of phase relations involving haplogranitic melts using an internally consistent thermodynamic dataset, Journal of Petrology, 42, 673-683

Holland, T.J.B., Powell, R., 1998, An internally consistent thermodynamic data set for phases of petrological interest, Journal of Metamorphic Geology, 16, 309-343

Hong, H., Li, Z., Xiao, P., 2009, Clay mineralogy along the laterite profile in Hubei, South China: mineral evolution and evidence for eolian origin, Clays and Clay Minerals, 57 (5), 602-615

Hünken, U., Klemd, R., Olesch, M., 1994, Fluid Inclusions in Quartz-Pebbles of Proterozoic Tarkwaian Conglomerates in Ghana, Geologisches Jahrbuch, D 100, 313-341

Jessell, M.W., 1981, Noddy - an interactive map creation package, M.Sc. Thesis, University of London, England, 49 p.

Jessell, M.W., 2001, Three-dimensional geological modelling of potential-field data, Computers & Geosciences, 27, 147-157

Jessell, M.W., Valenta, R.K., 1996, Structural geophysics: integrated stuctural and geophysical mapping, In: DePaor, D. (Ed.), Structural Geology and Personal Computers, Elsevier, Oxford, 303-324

Jessell, M.W., Willman, C.E., Gray, D.R., 1994, Bedding parallel veins and their relationship to folding, Journal of Structural Geology 16 (6), 753-767

John, T., Klemb, R., Hirdes, W., Loh, G., 1999, The metamorphic evolution of the Paleoproterozoic (Birimian) volcanic Ashanti belt (Ghana, West Africa), Precambrian Research, 98, 11-30

Junner, N.R., 1935, Gold in the Gold Coast, Gold Coast Geological Survey, Memoir 4, 76 p.

Junner, N.R., 1940, Geology of the Gold Coast and Western Togoland, Gold Coast Geological Survey, Memoir 11, 40 p.

Kalsbeek, F., Frei, D., Affaton, P., 2008, Constraints on provenance, stratigraphic correlation and structural context of the Volta basin, Ghana, from detrital zircon geochronology: An Amazonian connection?, Sedimentary Geology, 212, 86-95

Kay, R.W., Kay, S.M., 2002, Andean adakites: Three ways to make them, Acta Petrologica Sinica, 18, 303-311

Kesse, G.O., 1985, The Mineral and Rock Resources of Ghana, A.A. Balkema Publishers, Book, 610 p.

Kitson, A.E., 1918, Annual Report for 1916/17, Gold Coast Geological Survey, Accra, Ghana

Kitson, A.E., 1928, Provisional geological map of the Gold Coast and Western Togoland, with brief descriptive notes thereon, Gold Coast Geological Survey, Bulletin 2

Klein, E.L., Luzardo, R., Moura, C.A.V., Armstrong, R., 2008, Geochemistry and zircon geochronology of paleoproterozoic granitoids: Further evidence on the magmatic and crustal evolution of the São Luís cratonic fragment, Brazil, Precambrian Research, 165, 221-242

Klein, E.L., Moura, C.A.V., Pinheiro, B.L.S., 2005, Paleoproterozoic Crustal Evolution of the Sao Luis Craton, Brazil: Evidence from Zircon Geochronology and Sm-Nd Isotopes, Gondwana Research, 8 (2), 177-186

Kleinschrot, D., Klemd, R., Brocker, M., Okrusch, M., Franz, L., Schmidt, K., 1993, The Nsuta manganese deposit, Ghana: geological setting, ore-forming process and metamorphic evolution, Zeitschfirt fuer Angewandte Geologie, 39, 135-155

Kleinschrot, D., Klemd, R., Brocker, M., Okrusch, M., Franz, L., Schmidt, K., 1994, Protores and country rocks of the Nsuta manganese deposit, Neues Jahrbuch Mineral, 168, 67-108

Klemd, R., Hirdes, W., Olesch, M., Oberthür, T., 1993, Fluid inclusions in quartz-pebbles of the gold-bearing Tarkwaian conglomerates of Ghana as guides to their provenance area, Mineralium Deposita, 28, 334-343

Kutu, J.M., 2003, Structure, Deformation and Mineralization of Konongo Mines in the Ashanti Gold Belt of Ghana, PhD. Thesis, Univeristy of Ghana

Lahti, I., Karinen, T., 2010, Tilt derivative multiscale edges of magnetic data, The Leading Edge, 23 (2), 116-118

Lajaunie, C., Courrioux, G., Manuel, L., 1997, Foliation Fields and 3D Cartography in Geology: Principles of a Method Based on PotentialInterpolation, Mathematical Geology, 29 (4), 571-584

Ledru, P., Johan, V., Milési, J.P., Tegyey, M., 1994, Markers of the last stages of the Palaeoproterozoic collision: evidence for a 2 Ga continent involving circum-South Atlantic provinces, Precambrian Research, 69, 169-191

Leube, A., Hirdes, W., Mauer, R., Kesse, G.O., 1990, The Early Proterozoic Birimian Supergroup of Ghana and Some Aspects of its Associated Gold Mineralization, Precambrian Research, 46, 139-165

Loh, G., Hirdes, W., Anani, C., Davis, D.W., Vetter, U., 1999, Explanatory Notes for the Geological Map of Southwest Ghana 1 : 100,000, Geologisches Jahrbuch, Reihe B, Heft 93, 150 p.

MacCandlish, K., 2003, Qualifying Report for the First Disclosure of a Resource Estimate on a Material Property Wassa Mine, Southwest Ghana, Golden Star Resources Ltd, 54 p.

MacLeod, I.N., Jones, K., Fan Dai, T., 1993, 3-D Analytic Signal in the Interpretation of Total Magnetic Field Data at Low Magnetic Latitudes, Exploration Geophysics, 24, 679-688

Mahar, E.M., Baker, J.M., Powell, R., Holland, T.J.B., Howell, N., 1997, The effect of Mn on mineral stability in metapelites, Journal of Metamorphic Geology, 15, 223–238

Mallet, J.L., 1992, Discrete smooth interpolation in geometric modelling, Computer Aided Design, 24 (4), 178-191

Martin, H., 1994, The Archean grey gneisses and the genesis of continental crust, Precambrian Geology, 11, 205-259

Martin, H., 1999, The adakites: modern analogs of Archaean granitoids, Lithos, 46, 411-429

Martin, H., Smithies, R.H., Rapp, R., Moyen, J.F., Champion, D.C., 2005, An overview of adakite, tonalite–trondhjemite–granodiorite (TTG), and sanukitoid: relationships and some implications for crustal evolution, Lithos, 79, 1-24

Mauer, R., 1990, Petrographische und geochemische Untersuchungen tier präkambrischen (Birimian) Granitoide Ghana, Dissertation, Technische Universität Berlin, 202 p.Mensah, M., 1973, On the question of the age of the Sekondi Series, Upper Devonian or Lower Carboniferous rocks of Ghana, Ghana Journal of Sciences, 13, 134–139

Metelka, V., Baratoux, L., Naba, S., Jessell, M.W., 2011, A geophysically constrained litho-structural analysis of the Eburnean greenstone belts and associated granitoid domains, Burkina Faso, West Africa, Precambrian Research, 190, 48-69

Milesi, J.P., Ledru, P., Ankrah, P., Johan, V., Marcoux, E., Vinchon, C., 1991, The metallogenic relationship between Birimian and Tarkwaian gold deposits in Ghana, Mineralium Deposita, 26, 228-238

Milési, J.P., Ledru, P., Feybesse, JL., Dommanget, A., Marcoux, E., 1992, Early Proterozoic ore deposits and tectonics of the Birimian orogenic belt, West Africa, Precambrian Research, 58, 305-344

Milligan, P.R., Gunn, P.J., 1997, Enhancement and presentation of airborne geophysical data, AGSO Journal of Australian Geology & Geophysics, 17 (2), 63-75

Milsom, J., 2003, Field Geophysics, The geological field guide series, Third edition, J. Wiley, 249 p.

Moyen, J.F., 2011, The composite Archaean grey gneisses: Petrological significance, and evidence for a non-unique tectonic setting for Archaean crustal growth, Lithos, 123, 21-36

Moyen, J.F., Martin, H, 2012, Forty years of TTG research, Lithos 148, 312-336

Mumin, A.H., Fleet, M.E., 1995, Evolution of gold mineralization in the Ashanti Gold Belt, Ghana: evidence from carbonate compositions and parageneses, Mineralogy and Petrology, 55, 265-280

Mumin, A.H., Fleet, M.E., Chryssoulis, S.L., 1994, "Gold mineralization in As-rich mesothermal gold ores of the Bogosu-Prestea mining distric of the Ashanti Gold Belt, Ghana: remobilization of ""invisible"" gold", Mineralium Deposita, 29, 445-460

Mumin, A.H., Fleet, M.E., Longstaffe, F.J., 1996, Evolution of Hydrothermal Fluids in the Ashanti Gold Belt, Ghana: Stable Isotope Geochemistry of Carbonates, Graphite, and Quartz, Economic Geology, 91, 135-148

Newton, R.C., Charlu, T.V., Kleppa, O.J., 1980, Thermochemistry of the high structural state plagioclases, Geochimica et Cosmochimica Acta, 44 (7), 933-941

Nomade, S., Che, Y., Pouclet, A., Féraud, G., Théveniaut, H., Daouda, B.Y., Vidal, M., Rigolet, C., 2003, The Guiana and theWest African Shield Palaeoproterozoic grouping: new palaeomagnetic data for French Guiana and the Ivory Coast, Geophysical Journal International, 154, 1-18

Ntiamoah-Agyakwa, Y., 1979, Relationship between gold and manganese mineralizations in the Birimian of Ghana, West Africa, Geological Magazine, 116, 345-352

Nyame, F.K., Kase, K., Yamamoto, M., 1998, Spessartine Garnets in a Manganiferous Carbonate Formation from Nsuta, Ghana, Resource Geology, 48 (1), 13-22

Oberthür, T., Vetter, U., Davis, D.W., Amanor, J.A., 1998, Age constraints on gold mineralization and Paleoproterozoic crustal evolution in the Ashanti belt of southern Ghana, Precambrian Research, 89, 129-143

Oberthür, T., Vetter, U., Schmidt Mumm, A., Weiser, T., Amanor, J.A., Gyapong, W.A., Kumi, R., Blenkinsop, T.G., 1994, The Ashanti Gold Mine at Obuasi, Ghana: Mineralogical, Geochemical, Stable Isotope and Fluid Inclusion Studies on the Metallogenesis of the Deposit, Geologisches Jahrbuch, D 100, 31-129

Oberthür, T., Weiser, T., Amanor, J.A., Chryssoulis, S.L., 1997, Mineralogical siting and distribution of gold in quartz veins and sulfide ores of the Ashanti mine and other deposits in the Ashanti belt of Ghana: genetic implications, Mineralium Deposita, 32, 2-15

Pavlis, N.K., Holmes, S.A., Kenyon, S.C., Factor J.K., 2008, An Earth Gravitational Model to Degree 2160: EGM2008, EGU General Assembly 2008, Vienna, Austria

Perrouty S., Aillères L., Jessell M., Baratoux L., Bourassa Y., Crawford B., 2012, New Field and Geophysical Evidence of Pre-Tarkwaian Deformation in the Southern Ashanti Belt, Ghana – Implications for Gold Mineralisation, Precambrian Research, 204-205, 12-39

Pigois, J.P., Groves, D.I., Fletcher, I.R., MacNaughton, N.J., Snee, L.W., 2003, Age constraints on Tarkwaian palaeoplacer and lode-gold formation in the Tarkwa-Damang district, SW Ghana, Mineralium Deposita, 38, 695-714

Powell, R., Holland, T.J.B., Worley, B., 1998, Calculating phase diagrams involving solid solutions via non-linear equations, with examples using THERMOCALC, Journal of Metamorphic Geology, 16, 577-588

Schmidt Mumm, A., Oberthür, T., Vetter, U., Blenkinsop, T.G., 1997, High CO2 content of fluid inclusions in gold mineralisations in the Ashanti Belt, Ghana: a new category of ore forming fluids ?, Mineralium Deposita, 32, 107-118

Schwartz, M.O., Oberthür, T., Amanor, J., Gyapong, W.A., 1992, Fluid inclusion re-equilibration and P-T-X constraints on fluid evolution in the Ashanti gold deposit, Ghana, European Journal of Mineralogy, 4, 1017-1033

Sestini, G., 1973, Sedimentology of a Paleoplacer: The Gold-bearing Tarkwaian of Ghana, Ores in Sediments, International Union of Geological Sciences, Series A, 3, 275-305

Shand, S.J., 1943, Eruptive rocks. Their genesis, composition, classification, and their relations to ore-deposits, Wiley, New York, 444 p.

Smithies, R.H., 2000, The Archaean tonalite-trondhjemite-granodiorite (TTG) series is not an analogue of Cenozoic adakite, Earth and Planetary Science Letters, 182, 115-125

Spear, F.S., 1993, Metamorphic Phase Equilibria and Pressure-Temperature-Time Paths, Mineralogical Society of America, Washington, D. C., 799 p.

Sun, S.S., MacDonough, W.F., 1989, Chemical and isotopic systematics of oceanic basalts: implication for mantle composition and processes, In: Saunders, A.D., Norry, M.J. (Eds.), Magmatism in Ocean Basins, 42, Geological Society of London Special Publication, 313-345

Sylvester, P.J., Attoh, K., 1992, Lithostratigraphy and composition of 2.1 Ga greenstone belts of the West African Craton and their bearing on crustal evolution and the Archean-Proterozoic boundary, Journal of Geology, 100, 377-393

Tajcmanová, L., Connolly, J.A.D., Cesare, B., 2009, A thermodynamic model for titanium and ferric iron solution in biotite, Journal of Metamorphic Geology, 27, 153-164

Talwani, M.,Worzel, J.L., Landisman, M., 1959, Rapid gravity computations for twodimensional bodies with application to the Mendochino submarine fracture zone, Journal of Geophysical Research, 64, 49-59

Talwani. M., Heirtzler, J. R., 1964, Computation of magnetic anomalies caused by two-dimensional bodies of arbitrary shape, In Parks. G. A., Ed., Computers in the mineral industries, Part 1: Stanford Univ. Pub., Geological Sciences, 9, 464-480.

Taylor, P.N., Moorbath, S., Leube, A., Hirdes, W., 1992, Early Proterozoic crustal evolution in the Birimian of Ghana: constraints from geochronology and isotope geochemistry, Precambrian Research, 56, 97-111

Tevendale, W. B., 1950, Annual Report 1948-49, Gold Coast Geol. Survey, 32 p.

Thompson, J.B., Waldbaum, D.R., 1968, Mixing properties of sanidine crystalline solutions. 2. Calculations based on volume data, American Mineralogist, 53, 811-838

Trompette, R., 1980, La chaîne panafricaine des Dahomeyides et le Bassin des Volta (bordure sud-est du craton ouest-africain), In: Bessoles, B., Trompette, R. (Eds.), Géologie de l'Afrique. Mémoires du Bureau de Recherches Géologiques et Minières, 92, 9-62

Trompette, R., 1994, Geology of Western Gondwana (2000–500 Ma) Panafrican-Brasiliano Aggregation of South America and Africa, Balkema, Rotterdam, 366 p.

Tshibubudze, A., Hein, K.A.A., Marquis, P., 2009, The Markoye Shear Zone in NE Burkina Faso, Journal of African Earth Sciences, 55, 245-256

Tunks, A.J., Selley, D., Rogers, J.R., Brabham, G., 2004, Vein mineralization at the Damang Gold Mine, Ghana: controls on mineralization, Journal of Structural Geology, 26, 1257-1273

Verduzco, B., Fairhead, J.D., Green, C.M., 2004, New insights into magnetic derivatives for structural mapping, The Leading Edge, 29 (1), 24-29

Wei, C.J., Powell, R., Zhang, L.F., 2003, Eclogites from the south Tianshan, NW China: petrological characteristic and calculated mineral equilibria in the Na2O-CaO-FeO-MgO-Al2O3-SiO2-H2O system, Journal of Metamorphic Geology, 21, 163-180.

White, R.W., Powell, R., Holland, T.J.B., Worley, B.A., 2000, The effect of TiO2 and Fe2O3 on metapelitic assemblages at greenschist and amphibolites facies conditions: mineral equilibria calculations in the system K2O–FeO–MgO–Al2O3–SiO2–H2O–TiO2–Fe2O3., Journal of Metamorphic Geology, 18, 497-511

White, R.W., Powell, R., Phillips, G. N., 2003, A mineral equilibria study of hydrothermal alteration in mafic greenschist facies rock at Kalgoorlie, Western Australia, Journal of Metamorphic Geology, 21, 455-468

Whitelaw O.A.L., 1904, Geological map of the Tarkwa-Abosso goldfield, 1:50000, Gold Coast Geological Survey, Memoir 1

Whitelaw, O.A.L., 1929, The Geological and Mining Features of the Tarkwa-Abosso Goldfield, Gold Coast Geological Survey, Memoir 1, 46 p.

Wille, S.E., Klemd, R., 2004, Fluid inclusion studies of the Abawso gold prospect, near the Ashanti Belt, Ghana, Mineralium Deposita, 39, 31-45

Williams-Jones, A.E., Bowell, R.J., Migdisov, A.A., 2009, Gold in Solution, Elements, 5, 281-287

Wilson, M., 1989, Igneous Petrogenesis, Unwin Hyman, London, 457 p.

Winchester, J.A., Floyd, P.A., 1977. Geochemical discrimination of different magma series and their differentiation products using immobile elements. Chemical Geology 20, 325-343.

Xu, J.F., Shinjo, R., Defant, M.J., Wang, Q., Rapp, R.P., 2002, Origin of Mesozoic adakitic intrusive rocks in the Ningzhen area of east China: Partial melting of delaminated lower continental crust?, Geology, 30 (12), 1111-1114

Yao, Y., Murphy, P.J., Robb, L.J., 2001, Fluid Characteristics of Granitoid-Hosted Gold Deposits in the Birimian Terrane of Ghana: A fluid Inclusion Microthermometric and Raman Spectroscopic Study, Economic Geology, 96, 1611-1643

Yao, Y., Robb, L.J., 2000, Gold mineralization in Palaeoproterozoic granitoids at Obuasi, Ashanti region, Ghana: Ore geology, geochemistry and fluid characteristics, South African Journal of Geology, 103, 255-278

Listes des Tables et des Figures

Liste des Tables

Liste des Figures

223

Annexes

Annexe 1 : Données d'affleurements et cartes

Les données d'affleurements (localisations, mesures structurales, numéros d'échantillons), les mesures de susceptibilité magnétique, les mesures de densité, les analyses géochimiques, la liste des lames minces, ainsi que les cartes et modèles géoréférencés produits durant ces travaux de recherche, sont disponibles en format numérique (cf. DVD ci-joint).

Annexe 2 : Métamorphisme, premiers résultats
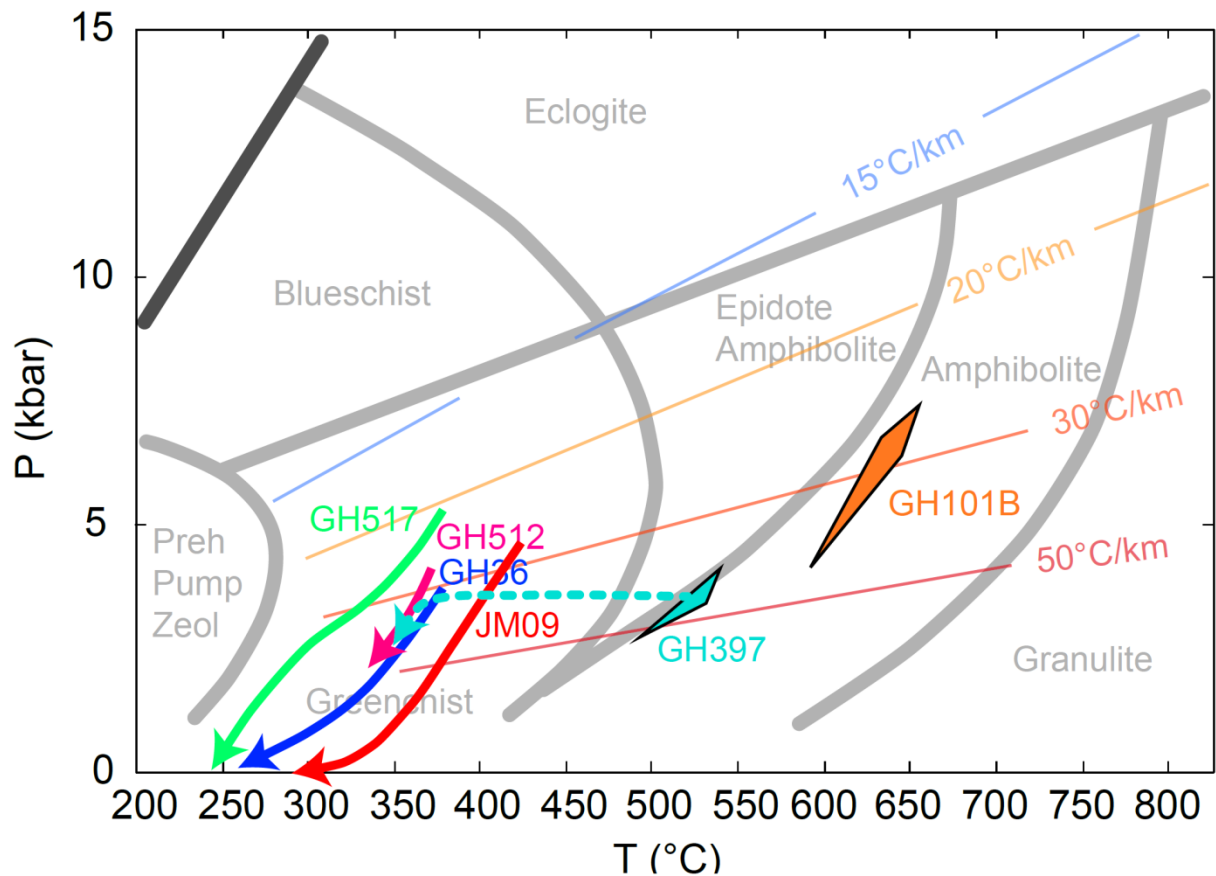
Chemins pression-température obtenus, pour différents échantillons du sud-ouest du Ghana, par analyse des assemblages Chlorites / Micas Blancs (JM09, phyllites Birimiennes, groupe de Kumasi, mine de Pampe, GH36, phyllites Birimiennes, groupe de Kumasi, mine de Bogoso, GH512, quartzites Tarkwaiennes, mine de Damang, GH517, phyllites Birimiennes, groupe de Sefwi, mine de Wassa) et des assemblages Staurotides / Grenats (GH101B, paragneiss, groupe de Sefwi, Cape Coast, GH397, phyllites Tarkwaiennes, mine de Damang). Ces échantillons, ainsi que les analyses de la littérature (Ledru et al., 1994, John et al., 1999 Kleinschrot et al., 1994), suggèrent tous des pressions maximales autour de 5 kbar et des températures très variables, probablement controlées par les intrusions de granitoïdes Éburnéens.

Annexe 3 : Liste de publications associées à cette thèse

Revised Eburnean geodynamic evolution of the gold-rich southern Ashanti Belt, Ghana, with new field and geophysical evidence of pre-Tarkwaian deformations, *Stéphane Perrouty, Laurent Aillères, Mark W. Jessell, Lenka Baratoux, Yan Bourassa, Brenton Crawford*, Precambrian Research, 2012, 204-205, 12-39, http://dx.doi.org/10.1016/j.precamres.2012.01.003

The tectonic context of the Eoeburnean Wassa gold mine - Implications for relative timing of mineralising events in southwest Ghana, *Stéphane Perrouty, Mark W. Jessell, John Miller, Yan Bourassa, Daniel Apau, Luc Siebenaller, Germán Velásquez, Laurent Aillères, Didier Beziat, Stefano Salvi, Lenka Baratoux*, Submitted to Precambrian Research

A new model for Paleoproterozoic crustal growth in southwest Ghana: an Eoeburnean crustal source for the younger Eburnean granites, *Stéphane Perrouty, Lenka Baratoux, Jérôme Ganne, Michel Grégoire, Mathieu Benoit, T. Campbell McCuaig, Mark W. Jessell, Laurent Aillères*, Submitted to Lithos

3D modelling of the Ashanti Belt, southwest Ghana, and lithostructural control on gold occurrences within the Sefwi Group, *Stéphane Perrouty, Mark D. Lindsay, Mark W. Jessell, Laurent Aillères, Roland Martin, Yan Bourassa*, In preparation

AUTEUR : **Stéphane Perrouty**

TITRE : **Évolution Structurale de la Ceinture Minéralisée d'Ashanti, SO Ghana**

DIRECTEUR DE THÈSE : **Dr. Mark W. Jessell (I.R.D.), Dr. Laurent Aillères (Monash University)**

LIEU ET DATE DE SOUTENANCE : **Mardi 19 Juin 2012, Observatoire Midi-Pyrénées, Toulouse**

RESUMÉ EN FRANÇAIS :

La ceinture Paléoprotérozoïque d'Ashanti, au sud-ouest du Ghana, est l'hôte de nombreux gisements d'or, de classe mondiale, tels les gisements d'Obuasi (60 million d'onces) et de Tarkwa (40 millions d'onces). La caractérisation de l'évolution structurale et magmatique régionale permet d'éclaircir le contexte géotectonique de formation de ces gisements et ainsi fournir des pistes pour de futures explorations. Ainsi, au cours de ces travaux de thèse, ont été réalisés : (1) une nouvelle carte géologique et structurale de la région, en accord avec les observations de terrains et les données de géophysique aéroportée, (2) une étude détaillée du gisement d'or précoce de la mine de Wassa, (3) une étude de l'évolution du magmatisme au cours de l'Orogénèse Éburnéenne et (4) un modèle tridimensionnel de la ceinture d'Ashanti mettant en évidence un possible contrôle litho-structural sur la localisation des minéralisations.

MOTS-CLÉS : **Afrique de l'Ouest, Ghana, Paléoprotérozoïque, Birimien, Tarkwaien, Éburnéen, Minéralisations, Or, Granitoïdes, Interprétations Géophysiques, Modélisation 3D**

DISCIPLINE ADMINISTRATIVE : **Sciences de la Terre et des Planètes Solides**

LABORATOIRE : **Géosciences Environnement Toulouse (G.E.T.), UMR 5563, UR234**
Obs. Midi-Pyrénées, 14 Av. Edouard Belin, 31400 Toulouse, France